

Understanding and Improving Gas Phase Capture of Organic Vapors by Carbonaceous Adsorbents

by

Masoud Jahandar Lashaki

A thesis submitted in partial fulfillment of the requirements for the degree of

Doctor of Philosophy

in

Environmental Engineering

Department of Civil and Environmental Engineering

University of Alberta

© Masoud Jahandar Lashaki, 2015

ABSTRACT

Vehicle painting booths are among the major sources of volatile organic compounds (VOCs) emissions in the auto manufacturing sector. A challenge with controlling VOCs by adsorption onto activated carbon (AC) is the occurrence of strongly, or even permanently, adsorbed species. Irreversible adsorption (aka heel formation) prevents complete regeneration of the sorbent, decreasing its capacity and lifetime. A better understanding of the factors enhancing the irreversible adsorption is instructive in finding ways to decrease heel buildup and eventually increasing the lifetime of the adsorbent. The adsorption capacity of AC for VOCs is also of concern for the design of a reliable adsorption system. Experimentally determining the adsorption capacity of AC needs considerable effort, time, and cost. Hence, there is interest in developing reliable models to predict the adsorption capacity of adsorbents. The objective of this dissertation, therefore, is to understand and improve gas phase capture of VOCs by carbon-based adsorbents. This research was conducted in two parts, 1) enhancing the prediction of the adsorption capacity of VOCs on carbonaceous adsorbents, and 2) studying the reason and mechanism for irreversible adsorption of VOCs on AC adsorbents, and subsequent use of these results to improve process know-how.

In the first part, the effect of the kinetic diameter (KD) of the reference adsorbate on the accuracy of the Dubinin-Radushkevich (D-R) equation for predicting the adsorption isotherms of organic vapors on microporous AC was investigated (Chapter 3). Adsorption isotherms for 13 VOCs on microporous beaded activated carbon (BAC) were experimentally measured, and predicted using the D-R model and affinity coefficients. Choosing a reference adsorbate with a KD similar to that of the test adsorbate resulted in better prediction of the adsorption isotherm.

The proposed hypothesis was also used to explain reports of inconsistent findings among published articles.

In the second part, the effect of operational parameters such as adsorption and regeneration temperature (Chapter 4), BAC's surface oxygen groups (Chapter 5), desorption purge gas oxygen impurity (Chapter 6), and BAC's pore size distribution (PSD; Chapter 7) on the irreversible adsorption of a mixture of organic compounds typically emitted from automobile painting operations was explored. Results indicated that increasing the adsorption temperature from 25 to 45 °C increased heel buildup on BAC by about 30% irrespective of the regeneration temperature possibly due to chemisorption. Conversely, increasing the regeneration temperature from 288 to 400 °C resulted in 61% reduction in the heel at all adsorption temperatures, possibly due to more effective desorption of chemicals from narrow micropores. PSD and pore volume reduction confirmed that the heel was mainly formed in narrow micropores, which can be occupied or blocked by some of the adsorbates. Microporous BAC was treated with hydrogen to remove oxygen groups or treated with nitric acid to add oxygen groups. Derivative thermogravimetric (DTG) results showed heel formation due to physisorption for heat-treated and hydrogen-treated BACs, and weakened physisorption combined with chemisorption for nitric acid-treated BAC. Microporous BAC was also regenerated using different concentrations of oxygen ($\leq 5 - 10,000$ ppm_v) in the nitrogen desorption purge gas. With increasing O₂ concentration, mass balance cumulative heel increased by up to 35% and the fifth cycle adsorption capacity decreased by up to 55% relative to baseline scenario (≤ 5 ppm_v O₂ in N₂). DTG analysis showed heel formation due to physisorption for ≤ 5 ppm_v O₂ and a combination of physisorption and chemisorption for other samples. Finally, five BAC samples with varying PSDs but similar elemental compositions were tested. Heel formation was linearly correlated

with BAC micropore volume. Meanwhile, first cycle adsorption capacities and breakthrough times correlated linearly with BAC total pore volume. Overall, results showed that highly microporous adsorbents turn a higher portion of adsorbed species into heel due to higher share of high energy adsorption sites in their structure.

In summary, it was found that high adsorption temperature, low regeneration temperature, high levels of surface oxygen groups on adsorbents, oxygen impurities in desorption purge gas, and high adsorbent microporosity may increase heel formation. Some of the outcomes of this research have been implemented in full scale adsorbers controlling VOC emissions from automobile painting operations, resulting in longer adsorbent lifetime and lower solid waste generation.

PREFACE

The research completed in this dissertation was planned, designed, conducted, analyzed, interpreted, and compiled by myself, and was fully reviewed and supervised by Dr. Zaher Hashisho in the Department of Civil and Environmental Engineering at the University of Alberta. My colleagues in the Air Quality Characterization Lab in the Department of Civil and Environmental Engineering at the University of Alberta, and collaborators from our industrial sponsor, Ford Motor Company, assisted me in the following areas:

Chapter 2:

- Mr. Mohammadreza Fayaz assisted me in compiling parts of the literature review.
- Dr. John Atkinson contributed to manuscript edits.

Chapter 3:

A version of this chapter has been published as: Jahandar Lashaki, M.; Fayaz, M.; Niknaddaf, S.; Hashisho, Z. Effect of the adsorbate kinetic diameter on the accuracy of the Dubinin-Radushkevich equation for modeling adsorption of organic vapors on activated carbon. *Journal of Hazardous Materials* **2012**, 241–242, 154–163.

- Mr. Mohammadreza Fayaz assisted me in obtaining some of the adsorption isotherms.
- Mr. Saeid Niknaddaf helped me in finding the physical properties of the organic adsorbates.

Chapter 4:

A version of this chapter has been published as: Jahandar Lashaki, M.; Fayaz, M.; Wang, H.; Hashisho, Z.; Phillips, J.H.; Anderson, J.E.; Nichols, M. Effect of adsorption and regeneration temperature on irreversible adsorption of organic vapors on beaded activated carbon. *Environmental Science and Technology* **2012**, 46, 4083–4090.

- Mr. Mohammadreza Fayaz and Dr. Haiyan (Helena) Wang helped me in conducting some of the 5-cycle adsorption/regeneration experiments.
- Mr. John Phillips, Dr. James Anderson, and Dr. Mark Nichols, all from Ford Motor Company, contributed to manuscript edits.

Chapter 5:

A version of this chapter was published as a conference paper: Jahandar Lashaki, M.; Atkinson, J.D.; Hashisho, Z.; Phillips, J.H.; Anderson, J.E.; Nichols, M. Effect of surface oxygen

groups on the irreversible adsorption of organic vapors. *In proceedings of 107th Air & Waste Management Association Annual Conference and Exhibition*, Long Beach, CA, 2014.

- Dr. John Atkinson assisted me in the treatment and characterization of activated carbon samples as well as conducting some of the 5-cycle adsorption/regeneration experiments. He also contributed to manuscript edits.
- Mr. John Phillips, Dr. James Anderson, and Dr. Mark Nichols, all from Ford Motor Company, contributed to manuscript edits.
- Dr. James Sawada from the Department of Chemical and Materials Engineering at the University of Alberta helped out with the thermogravimetric analysis-mass spectrometry.

Chapter 6:

A version of this chapter has been published as: Jahandar Lashaki, M.; Atkinson, J.D.; Hashisho, Z.; Phillips, J.H.; Anderson, J.E.; Nichols, M.; Misovski, T. Effect of desorption purge gas oxygen impurity on irreversible adsorption of organic vapors. *Carbon* **2015**, doi:10.1016/j.carbon.2015.12.037.

- Dr. John Atkinson assisted me in conducting some of the 5-cycle adsorption/regeneration experiments. He also contributed to manuscript edits.
- Dr. Mark Nichols and Mr. Tony Misovski, both from Ford Motor Company, completed the 50-cycle adsorption/regeneration experiments and sent the samples to us for analysis.
- Mr. John Phillips, Dr. James Anderson, and Dr. Mark Nichols, all from Ford Motor Company, contributed to manuscript edits.

Chapter 7:

A version of this chapter was presented at a conference: Jahandar Lashaki, M.; Atkinson, J.D.; Hashisho, Z.; Phillips, J.H.; Anderson, J.E.; Nichols, M. The impact of activated carbon's pore size distribution on heel formation during adsorption of organic vapors. *In proceedings of American Institute of Chemical Engineers Annual Meeting*, Salt Lake City, UT, 2015.

- Dr. John Atkinson assisted me in conducting some of the 5-cycle adsorption/regeneration experiments. He also contributed to manuscript edits.
- Mr. John Phillips, Dr. James Anderson, and Dr. Mark Nichols, all from Ford Motor Company, contributed to manuscript edits.

I dedicate this dissertation to my beloved family.

A special gratitude to my loving parents, Ardeshir and Behjat, for their invaluable support throughout my life and encouraging me to pursue higher education.

This dissertation is also dedicated to my lovely wife, Sara, for her patience, understanding, support, and encouragement.

Last but not least, I dedicate this dissertation to my son, Surena, who has grown into a wonderful 2 year old in spite of his father spending so much time away from him working on this research work.

ACKNOWLEDGEMENTS

First and foremost, I would like to express my deepest appreciation to my supervisor, Dr. Zaher Hashisho, for his continuous guidance, generous support, and invaluable comments and feedbacks during my PhD studies. This work could not be accomplished without his experience, knowledge, and passion. He has been a great supervisor and friend, and he is an excellent example to follow.

I would like to acknowledge financial support from Ford Motor Company and the Natural Sciences and Engineering Research Council (NSERC) of Canada as well as infrastructure and instruments grants from Canada Foundation for Innovation, NSERC of Canada, and Alberta Advanced Education and Technology.

I am grateful to my funders, including but not limited to, Air & Waste Management Association (Dave Benferado Scholarship and Air Quality Study and Research Scholarship), Canadian Prairies and Northern Section of the Air & Waste Management Association (Scholarship Award and Graduate Student Travel Award), the Faculty of Graduate Studies and Research at the University of Alberta (Dissertation Fellowship, Andrew Stewart Memorial Graduate Prize, Lehigh Inland Cement Graduate Scholarship in Environmental Studies, and Mary Louise Imrie Graduate Student Award), the Graduate Students Association at the University of Alberta (Graduate Student Principal Instructor Teaching Award and Professional Development Award), and the Department of Civil and Environmental Engineering at the University of Alberta (Gordon R. Finch Memorial Graduate Scholarship in Environmental Engineering) for their financial support.

I also acknowledge my defense committee members, Dr. George Sorial, Dr. Selma Guigard, Dr. Ian Buchanan, and Dr. Natalia Semagina as well as my former committee members, Dr. Ania Ulrich and Dr. Tayfun Babadagli, for their contributions to this work.

I highly appreciate the contribution of my co-authors: Dr. Zaher Hashisho, Dr. John Atkinson, John Phillips, Dr. James Anderson, Dr. Mark Nichols, Mohammadreza Fayaz, Dr. Haiyan (Helena) Wang, Dereje Tamiru Tefera, Pooya Shariaty, Samineh Kamravaei, Saeid Niknaddaf, and Tony Misovski.

I would also like to express my gratitude to the postdoctoral fellows of our research group: Dr. John Atkinson and Dr. Haiyan (Helena) Wang for their support, comments, recommendations, and availability.

Thank you to a number of technicians in the Department of Civil and Environmental Engineering for their support and availability: Chen Liang, Elena Dlusskaya, Yupeng (David) Zhao, Jela Burkus, and Maria Demeter.

Special thanks to Mohammadreza Fayaz and Dr. John Atkinson for the help they provided, and more importantly their friendship.

I am very thankful to my friends and colleagues in Air Quality Characterization Lab: Saeid Niknaddaf, Dereje Tamiru Tefera, Pooya Shariaty, Samineh Kamravaei, Abedeh Gholidoust, and Monisha Alam.

TABLE OF CONTENTS

1.	CHAPTER 1. INTRODUCTION AND RESEARCH OBJECTIVES.....	1
1.1	General Introduction	1
1.2	Problem Statement	3
1.3	Research Objectives and Originality.....	3
1.3.1	Adsorption Capacity Prediction.....	3
1.3.2	Irreversible Adsorption	4
1.4	Organization of Thesis	4
1.5	References	8
2	CHAPTER 2. LITERATURE REVIEW.....	11
2.1	Adsorption Capacity Prediction	11
2.1.1	Definition of Adsorption Isotherm.....	11
2.1.2	Adsorption Isotherm Models	11
2.1.2.1	Langmuir Isotherm Model	11
2.1.2.2	Freundlich Isotherm Model.....	12
2.1.2.3	Dubinin-Radushkevich Isotherm Model	12
2.1.2.4	Brunauer-Emmett-Teller Isotherm Model	13
2.2	Irreversible Adsorption	13
2.2.1	Mechanisms for Irreversible Adsorption	13
2.2.1.1	Chemisorption	15
2.2.1.2	Oxidative Coupling	16
2.2.1.3	Adsorbate Decomposition	17
2.2.2	Impacts of Adsorption Conditions on Irreversible Adsorption.....	17
2.2.2.1	Adsorption Environment.....	17

2.2.2.2	Adsorption Temperature	19
2.2.2.3	Adsorption Duration.....	20
2.2.3	Impacts of Adsorbate Properties on Irreversible Adsorption	21
2.2.3.1	Single Adsorbates.....	22
2.2.3.2	Mixture of Adsorbates.....	30
2.2.4	Impacts of Adsorbent Properties on Irreversible Adsorption	32
2.2.4.1	Pore Size Distribution	32
2.2.4.2	Surface Functional Groups.....	35
2.2.4.3	Effect of Metals and Metal Oxides	37
2.2.5	Impacts of Regeneration Conditions on Irreversible Adsorption	37
2.2.5.1	Regeneration Environment.....	37
2.2.5.2	Regeneration Temperature	38
2.2.5.3	Regeneration Heating Rate.....	39
2.2.6	Characterizing Irreversible Adsorption.....	39
2.2.6.1	Heat of Adsorption	40
2.2.6.2	Thermal Analysis	41
2.2.6.3	Nitrogen Adsorption Isotherm	43
2.3	References	44
3	CHAPTER 3. EFFECT OF THE ADSORBATE KINETIC DIAMETER ON THE ACCURACY OF THE DUBININ-RADUSHKEVICH EQUATION FOR MODELING ADSORPTION OF ORGANIC VAPORS ON ACTIVATED CARBON.....	53
3.1	Introduction	53
3.2	Materials and Methods.....	58
3.2.1	Adsorbent.....	58
3.2.2	Adsorbates.....	59

3.2.3	Reference Adsorbates	61
3.2.4	Adsorption Experiments	61
3.2.5	Relative Error Calculation	61
3.3	Results and Discussion.....	62
3.3.1	Reference Compounds	62
3.3.2	Affinity Coefficients	63
3.3.3	Adsorption Isotherms.....	67
3.3.4	Effect of Adsorbate Kinetic Diameter	71
3.3.5	Explanation of Previously Published Contradictory Results	75
3.4	Conclusions	76
3.5	References	78
4	CHAPTER 4. EFFECT OF ADSORPTION AND REGENERATION TEMPERATURE ON IRREVERSIBLE ADSORPTION OF ORGANIC VAPORS ON BEADED ACTIVATED CARBON.....	82
4.1	Introduction	82
4.2	Materials and Methods.....	84
4.2.1	Adsorbent and Adsorbate.....	84
4.2.2	Experimental Setup and Methods	86
4.2.3	BAC Characterization.....	89
4.2.3.1	Thermo-Gravimetric Analysis.....	89
4.2.3.2	Micropore Surface Analysis.....	89
4.3	Results and Discussion.....	90
4.3.1	Breakthrough Curves	90
4.3.2	Adsorption and Regeneration Temperature	92
4.3.3	BET Surface Area and Pore Size Distribution.....	95

4.4	Conclusions	99
4.5	References	101
5	CHAPTER 5. THE ROLE OF BEADED ACTIVATED CARBON'S SURFACE OXYGEN GROUPS ON IRREVERSIBLE ADSORPTION OF ORGANIC VAPORS	105
5.1	Introduction	105
5.2	Materials and Methods	107
5.2.1	Adsorbent Preparation	107
5.2.2	Adsorbates	108
5.2.3	Setup and Methods	109
5.2.4	BAC Characterization	110
5.3	Results and Discussion	112
5.3.1	BAC Characterization	112
5.3.2	Cyclic Adsorption/Regeneration	117
5.3.3	Regenerated BAC Characterization	118
5.3.3.1	DTG Analysis of 5-Cycle Samples	118
5.3.3.2	DTG Analysis of 1-Cycle Samples	120
5.3.3.3	Heel Formation Mechanism for 5-Cycle Samples	124
5.3.3.4	TGA-MS of 5-Cycle Samples	125
5.3.3.5	XPS of 5-Cycle Samples	125
5.3.3.6	Micropore Surface Analysis of 5-Cycle Samples	126
5.4	Conclusions	127
5.5	References	129
6	CHAPTER 6. EFFECT OF DESORPTION PURGE GAS OXYGEN IMPURITY ON IRREVERSIBLE ADSORPTION OF ORGANIC VAPORS	134
6.1	Introduction	134

6.2	Materials and Methods	136
6.2.1	Adsorbent	136
6.2.2	Adsorbates	136
6.2.3	Setup and Methods	139
6.2.4	BAC Characterization	141
6.3	Results and Discussion	142
6.3.1	Adsorption Breakthrough Curves of 5-cycle BAC samples	142
6.3.2	Mass Balance Heel of 5-Cycle BAC Samples	144
6.3.3	Adsorption Capacity of 5-Cycle BAC Samples	145
6.3.4	Characterization of 5-Cycle BACs	146
6.3.5	Effect of Long-Term Exposure to Oxygen	154
6.4	Conclusions	157
6.5	References	158
7	CHAPTER 7. THE ROLE OF BEADED ACTIVATED CARBON'S PORE SIZE DISTRIBUTION ON HEEL FORMATION DURING CYCLIC ADSORPTION/DESORPTION OF ORGANIC VAPORS	162
7.1	Introduction	162
7.2	Materials and Methods	165
7.2.1	Adsorbents	165
7.2.2	Adsorbate	165
7.2.3	Setup and Methods	166
7.2.4	BAC Characterization	167
7.3	Results and Discussion	169
7.3.1	Characterization of Virgin BACs	169
7.3.2	Adsorption/Regeneration Cycles	172

7.3.3 Characterization of Regenerated BACs.....	178
7.4 Conclusions	183
7.5 References	184
8 CHAPTER 8. CONCLUSIONS AND RECOMMENDATIONS.....	188
8.1 Dissertation Overview	188
8.2 Summary of Findings	188
8.3 Significance of the Research	190
8.4 Recommendations for Future Work.....	190
BIBLIOGRAPHY	193
APPENDIX A: SUPPLEMENTARY DATA FOR CHAPTER 3	212
APPENDIX B: SUPPLEMENTARY DATA FOR CHAPTERS 4 TO 7	229

LIST OF TABLES

Table 2-1. Adsorption conditions used to investigate irreversible adsorption.	18
Table 2-2. Single adsorbates used to investigate irreversible adsorption.	22
Table 2-3. Adsorbate mixtures used to investigate irreversible adsorption.	31
Table 2-4. Adsorbents used to investigate irreversible adsorption of organic compounds.....	33
Table 2-5. Techniques used to characterize irreversible adsorption.	40
Table 3-1. List of the adsorbates with their kinetic diameters (references provided in the table) and physical properties.	59
Table 3-2. Affinity coefficients and corresponding relative errors considering different relative pressure ranges (compounds with similar kinetic diameter to that of the reference adsorbate are marked in bold).	63
Table 4-1. Composition of the test mixture.....	85
Table 5-1. Physical and chemical properties of virgin, treated, and regenerated BACs before and after adsorption/regeneration cycling.	113
Table 6-1. Composition of test mixtures.....	138
Table 6-2. Physical and chemical properties of virgin, blank, and regenerated (5-cycle and 50-cycle) Kureha BACs.	151
Table 7-1. Physical and chemical properties of BACs before and after cycling.	170

LIST OF FIGURES

Figure 2-1. Two-state adsorption model.	21
Figure 3-1. Pore size distribution of the beaded activated carbon.	58
Figure 3-2. Flow chart for prediction of the adsorption capacity.	62
Figure 3-3. Measured and predicted, gravimetric adsorption isotherms for (a) 1-butanol, (b) toluene, (c) THF, and (d) <i>o</i> -xylene using <i>n</i> -hexane (KD=4.3 Å) as reference adsorbate and for (e) 1-butanol, (f) toluene, (g) THF, and (h) <i>o</i> -xylene using acetone (KD=4.4 Å) as the reference adsorbate.	68
Figure 3-4. Measured and predicted, gravimetric adsorption isotherms for (a) 1-butanol, (b) toluene, (c) THF, and (d) <i>o</i> -xylene using benzene (KD=5.85 Å) as reference adsorbate and for (e) 1-butanol, (f) toluene, (g) THF, and (h) <i>o</i> -xylene using <i>m</i> -xylene (KD=6.8 Å) as the reference adsorbate.	70
Figure 3-5. Total mean relative errors when predicting the adsorption isotherms of all 13 adsorbates, adsorbates with similar ($ KD_{\text{reference}} - KD_{\text{test}} \leq 0.6 \text{ Å}$) and non-similar ($ KD_{\text{reference}} - KD_{\text{test}} > 0.6 \text{ Å}$) kinetic diameters for $0.01 \leq P/P_o \leq 0.9$ and $0.01 \leq P/P_o \leq 0.1$	72
Figure 3-6. Mean relative error versus absolute difference in the kinetic diameter between the reference and test adsorbates ($ KD_{\text{reference}} - KD_{\text{test}} $).	73
Figure 3-7. Comparison between modeled and measured adsorption capacities for adsorbates with similar ($ KD_{\text{reference}} - KD_{\text{test}} \leq 0.6 \text{ Å}$) and non-similar ($ KD_{\text{reference}} - KD_{\text{test}} > 0.6 \text{ Å}$) kinetic diameters.	75
Figure 4-1. Schematic diagram of the adsorption/regeneration setup.	87
Figure 4-2. Breakthrough curves for adsorption on BAC at 35 °C and regeneration at (a) 288 °C and (b) 400 °C.	91
Figure 4-3. Reduction in breakthrough time ($t_{5\%}$) with mass balance cumulative heel for all adsorption and desorption temperatures.	92
Figure 4-4. Effect of adsorption temperature on adsorption capacity on virgin BAC.	93
Figure 4-5. Heel percentages as determined by mass balance and TGA for BAC adsorbed with tested mixture and regenerated at 288 or 400 °C. Legends are labeled as Mass balance- or TGA-x where x corresponds to the regeneration temperature in °C.	94

Figure 4-6. Relationship between mass balance cumulative heel on BET surface area and pore volume of regenerated BAC. Values for virgin BAC are presented for comparison.	96
Figure 4-7. Effect of adsorption and regeneration temperature on pore size distribution of BAC. Legends are labeled as x-y where x and y correspond to the adsorption and regeneration temperatures in °C, respectively.	97
Figure 4-8. Relationship between mass balance cumulative heel and pore volume reduction....	99
Figure 5-1. Pore size distributions (a) and DTG analysis (b) of unused treated BACs.	114
Figure 5-2. Contribution of various SOGs based on Boehm titration.	115
Figure 5-3. TGA-MS results of BAC samples.....	116
Figure 5-4. Mass balance cumulative heel after 5 adsorption/regeneration cycles.	117
Figure 5-5. DTG analysis of: (a) BAC-O-5C, BAC-V-5C, and BAC-H-5C, (b) BAC-O, BAC-O-5C, and BAC-O-Blank-5C, (c) BAC-V and BAC-V-5C, and (d) BAC-H and BAC-H-5C.....	119
Figure 5-6. DTG analysis of treated BACs loaded with single adsorbates.....	124
Figure 5-7. PSD of: (a) BAC-O-5C, BAC-V-5C, and BAC-H-5C, (b) BAC-O and BAC-O-5C, (c) BAC-V and BAC-V-5C, and (d) BAC-H and BAC-H-5C.	127
Figure 6-1. Adsorption breakthrough curves for 5-cycle BAC samples exposed to different concentrations of O ₂ in the desorption purge gas.	143
Figure 6-2. (a) Cumulative (5 cycles) and first cycle mass balance heel of 5-cycle BAC samples (b) Adsorption capacity of 5-cycle BAC samples for first and fifth cycles. Data labels are presented as $x \pm y$ where x and y correspond to mean and standard deviation (n=2), respectively.	145
Figure 6-3. DTG analysis of 5-cycle BAC samples regenerated by different levels of O ₂ in N ₂ (after 5 cycles).....	147
Figure 6-4. Percent of cumulative heel removed during DTG analysis (up to 800 °C) of different 5-cycle BACs. Data labels are presented as $x \pm y$ where x and y correspond to mean and standard deviation (n=2), respectively.	148
Figure 6-5. Pore size distributions of 5-cycle BACs.	153
Figure 6-6. DTG analysis of 50-cycle BACs regenerated with N ₂ purge gas with two O ₂ concentrations.	155
Figure 7-1. PSD analysis of BACs: (a) micropore (≤ 20 Å) and (b) mesopore (20-500 Å) regions.....	170

Figure 7-2. DTG analysis of different virgin BACs.	171
Figure 7-3. Boehm titration of different virgin BACs.	172
Figure 7-4. Breakthrough curves of different BACs.....	173
Figure 7-5. Mass balance cumulative heel after 5 successive adsorption/regeneration cycles: (a) Comparison of different BACs, (b) Correlations to micropore and total pore volumes of the virgin BAC. Data labels are presented as $x \pm y$ where x and y correspond to mean and standard deviation (n=2), respectively.	175
Figure 7-6. First cycle adsorption capacity and breakthrough time: (a) Comparison of different BACs, (b) Correlations with micropore and total pore volumes of the virgin BAC. Data labels are presented as $x \pm y$ where x and y correspond to mean and standard deviation (n=2), respectively.	177
Figure 7-7. DTG analysis of different regenerated BACs. Note same scale as Figure 7-2.	178
Figure 7-8. Percent heel removal during DTG analysis of regenerated BACs. Data labels are presented as $x \pm y$ where x and y correspond to mean and standard deviation (n=2), respectively.	180
Figure 7-9. Pore size distribution of virgin and regenerated BACs.	182

LIST OF ACRONYMS

AC	Activated Carbon
ACC	Activated Carbon Cloth
BAC	Beaded Activated Carbon
BAC-H	Hydrogen-Treated BAC
BAC-O	Oxygen Functionalized BAC
BAC-V	Heat-Treated BAC
BET	Brunauer-Emmett-Teller
COP	Critical Oxidation Potential
DAC	Data Acquisition and Control
DFT	Density Functional Theory
DO	Dissolved Oxygen
D-R	Dubinin-Radushkevich
DTG	Derivative Thermo-Gravimetric
GAC	Granular Activated Carbon
GC-MS	Gas Chromatography-Mass Spectrometry
HOMO	Highest Occupied Molecular Orbital
KD	Kinetic Diameter
LUMO	Lowest Unoccupied Molecular Orbital
MFC	Mass Flow Controller
MS	Mass Spectrometry
PAC	Powdered Activated Carbon
PID	Photoionization Detector
pH _{PZC}	pH Value of the Point of Zero Charge
PSA	Pressure Swing Adsorption
PSD	Pore Size Distribution
QSDFE	Quenched Solid Density Functional Theory
RMSEP	Root-Mean-Square Error of Prediction
SCCM	Standard Cubic Centimeter per Minute
SFG	Surface Functional Group

SOG	Surface Oxygen Group
SLPM	Standard Liter per Minute
TGA	Thermo-Gravimetric Analysis
TGA-MS	Thermo-Gravimetric Analysis-Mass Spectrometry
TPD	Temperature Programmed Desorption
USEPA	United States Environmental Protection Agency
VOC	Volatile Organic Compound
XPS	X-Ray Photoelectron Spectroscopy

CHAPTER 1. INTRODUCTION AND RESEARCH OBJECTIVES

1.1 General Introduction

Volatile organic compounds (VOCs) are defined as liquids (at ambient temperatures) with low boiling points and high vapor pressures, and are commonly emitted from industries that handle paints, varnishes, chemical cleaners, solvents, lubricants, and liquid fuels (Khan and Ghoshal, 2000). The United States Environmental Protection Agency (USEPA) defines VOC as “any compound of carbon excluding carbon monoxide, carbon dioxide, carbonic acid, metallic carbides or carbonates, and ammonium carbonate, which participate in atmospheric photochemical reaction” (USEPA, 2009). VOCs are among the most common environmental contaminants (Khan and Ghoshal, 2000; Parmar and Rao, 2009). They can negatively impact human health and are precursors to photochemical smog (Parmar and Rao, 2009; Kim, 2011). Exposure to VOCs can cause headaches, eye, nose, and throat irritations, nausea, dizziness, memory loss, and damages to the liver, central nervous system, and lungs (Leslie, 2000; Kampa and Castanas, 2008). In 2013, a total of 2.1 megatonnes of VOCs were emitted in Canada, with oil and gas sector, industries handling paints and solvents, and agricultural activities being the largest contributors (31, 15, and 12%, respectively) (Environment Canada, 2015). Increasingly stringent regulations on VOC emissions warrant continuous research to develop more effective technologies to mitigate emissions of these pollutants.

On average, 6.58 kg of VOCs is used as paint solvents per vehicle in typical car manufacturing plants in North America (Kim, 2011). Automotive painting operation is a major source of VOC emissions from car manufacturing sector (Papasavva et al., 2001). These

emissions consist of a mixture of low and high molecular weight compounds from different organic groups including aromatic hydrocarbons, aliphatic hydrocarbons, alcohols, ketones, esters, ethers, polyaromatic hydrocarbons, etc. (Kim, 2011). Since VOCs can adversely affect public health, VOC laden streams need to be treated before discharging to the atmosphere.

Mitigation techniques such as adsorption, absorption, oxidation, biofiltration, condensation, and membrane separation are used to control VOCs (Parmar and Rao, 2009). Adsorption is widely used to remove organic compounds from gas (Shonnard and Hiew, 2000; Gupta and Verma, 2002; Lapkin et al., 2004; Hung and Bai, 2008; Ramos et al., 2010) and aqueous systems (Pelekani and Snoeyink, 1999; Dabrowski et al., 2005; Efremenko and Sheintuch, 2006) systems because it is inexpensive, flexible, efficient, and effective even at low contaminant concentrations. It also provides the potential for adsorbent reuse, adsorbate recovery, and multi-pollutant control (Shonnard and Hiew, 2000; Gupta and Verma, 2002; Lapkin et al., 2004).

Activated carbon (AC) is one of the most frequently used adsorbents in air and water treatment due to its cost effectiveness and large surface area (Kawasaki et al., 2004; Alvarez et al., 2005; Aktas and Cecen, 2006). AC is inexpensive and can have high adsorption capacity for organic compounds (Popescu et al., 2003; Kawasaki et al., 2004; Alvarez et al., 2005; Dabrowski et al., 2005; Hashisho et al., 2005, 2008; Aktas and Cecen, 2006, 2007). AC is also available in many physical forms including fibers, powders, beads, monoliths, and granules, implying that it can be used in nearly any shape or size reactor. It is resistant to acidic and basic conditions, can have tailored physical and chemical properties, can be regenerable, is thermally stable in anoxic conditions, and is inexpensive (Yang, 2003).

1.2 Problem Statement

The adsorption capacity of AC is of concern for the design of a reliable adsorption system. Experimentally determining the adsorption capacity of AC needs considerable effort, time, and cost especially at low concentrations (Hung and Lin, 2007). Hence, there is interest in developing reliable models to predict the adsorption capacity of adsorbents (Wu et al., 2002).

A challenge with controlling organics by adsorption onto AC is the occurrence of strongly, or even permanently, adsorbed species. Irreversible adsorption, which can also be described as heel formation, prevents complete regeneration of the sorbent, decreasing its capacity and lifetime and therefore removing a key advantage of using AC. This increases operation and maintenance costs because more frequent replacement of the adsorbent is necessary to maintain a high adsorption capacity. A better understanding of the factors enhancing the irreversible adsorption is instructive in finding ways to decrease heel buildup and eventually increasing the lifetime of the adsorbent.

1.3 Research Objectives and Originality

1.3.1 Adsorption Capacity Prediction

One objective of this research is to enhance the prediction of the adsorption capacity of organic vapors on carbonaceous adsorbents. For this purpose, the impact of the reference adsorbate kinetic diameter (KD) on the accuracy of the organic compounds adsorption capacity prediction is probed (Chapter 3). It is hypothesized that the accuracy of the Dubinin-Radushkevich (D-R) equation would increase if the reference and test adsorbates have similar kinetic diameters. To the best of our knowledge, no report has investigated this hypothesis.

1.3.2 Irreversible Adsorption

Adsorbent lifetime can be maximized and operating conditions can be optimized if factors promoting irreversible adsorption are better understood. Adsorption reversibility is exhaustively investigated in *aqueous solutions* (Dabrowski et al., 2005 and references therein). To the best of our knowledge, however, there is little or no information about the irreversible adsorption of organic compounds from *air* onto AC, particularly novel forms of AC such as beaded activated carbon (BAC). Oxidative coupling is the main contributor to *aqueous phase* irreversible adsorption (Dabrowski et al., 2005). Since this phenomenon has not been reported in the *gas phase*, results cannot be expected to directly transfer to the *gas phase*. In addition, previous investigations mainly focused on irreversible adsorption of phenols (Dabrowski et al., 2005 and references therein) while heel buildup during adsorption of non-phenolic organic compounds is also important, warranting scientific investigation.

The main objective of this study, therefore, is to study the reason and mechanism for irreversible adsorption of organic vapors on AC adsorbents. The impact of various operational parameters on the irreversible adsorption of a mixture of organic compounds commonly found in many environmental systems particularly vehicle painting operations is investigated. The effect of various operational parameters such as adsorption and regeneration temperature (Chapter 4), adsorbent's surface oxygen groups (Chapter 5), desorption purge gas oxygen impurity (Chapter 6), and adsorbent's pore size distribution (PSD; Chapter 7) are evaluated.

1.4 Organization of Thesis

This dissertation consists of eight chapters. General overview of VOC adsorption onto AC, problem statement, research objectives and originality, and organization of thesis are provided in Chapter 1. Chapter 2 contains a literature review of available models for predicting

adsorption capacity of adsorbents as well as influential parameters on irreversible adsorption of organic compounds and relevant techniques for characterizing this phenomenon. The experimental methodologies, and the results and discussion of this study are presented in Chapters 3 to 7.

Chapter 3 investigated the effect of the KD of the reference adsorbate on the accuracy of the D-R equation for predicting the adsorption isotherms of organic vapors on microporous AC. Adsorption isotherms for 13 organic compounds on microporous BAC were experimentally measured, and predicted using the D-R model and affinity coefficients. The affinity coefficients calculated based on molar volumes, molecular polarizabilities, and molecular parachors were used to predict the isotherms based on four reference compounds ($4.3 \leq K_D \leq 6.8 \text{\AA}$). The proposed hypothesis was also used to explain reports of inconsistent findings among published articles.

The effect of adsorption and regeneration temperature on the irreversible adsorption of a mixture of organic compounds was investigated in Chapter 4. A bench-scale adsorption/regeneration system was built and cyclic adsorption of the organic vapors mixture onto microporous BAC and regeneration of the saturated BAC were completed under different adsorption and regeneration temperatures. The BAC was analyzed for irreversible adsorption in terms of the amount of accumulated adsorbates and changes in adsorption capacity. Thermogravimetric analysis (TGA) and micropore surface analysis were also used to characterize irreversible adsorption.

In Chapter 5, the effect of AC's surface oxygen groups (SOGs) on irreversible adsorption of organic vapors was investigated. BAC was treated with hydrogen to remove oxygen groups or treated with nitric acid to add oxygen groups. Micropore surface analysis, X-ray photoelectron

spectroscopy (XPS), point of zero charge measurements (pH_{PZC}), derivative thermo-gravimetric (DTG) analysis, Boehm titration, and thermo-gravimetric analysis-mass spectrometry (TGA-MS) were used to assess differences in the physical and chemical properties of these adsorbents. The samples had similar physical properties but different chemical characteristics, allowing for isolating the contribution of AC's SOGs to heel buildup. Samples were tested for 5 consecutive adsorption/regeneration cycles using a mixture of nine organic compounds. Regenerated samples were then characterized using micropore surface analysis, XPS, DTG analysis, and TGA-MS to assess the changes in the physical and chemical properties of the adsorbent as a result of irreversible adsorption.

The effect of desorption purge gas oxygen impurity on irreversible adsorption of organic vapors was studied in Chapter 6. BAC was tested for 5 adsorption/regeneration cycles using a mixture of nine organic compounds representing industrially-relevant organic groups. Different concentrations of oxygen ($\leq 5 - 10,000 \text{ ppm}_v$) were used in the nitrogen desorption purge gas. Micropore surface analysis, XPS, and DTG analysis were used to assess the changes in the physical and chemical properties of the adsorbent as a result of irreversible adsorption.

Chapter 7 explored the effect of AC's PSD on heel formation during adsorption of organic vapors. Five BACs were used for this purpose. Micropore surface analysis, XPS, Boehm titration, and DTG analysis were used to assess differences in the physical and chemical properties of these adsorbents. The samples had similar chemical characteristics but different physical properties, allowing for isolating the contribution of AC's porosity to heel formation. The samples were tested for 5 consecutive adsorption/regeneration cycles using a mixture of nine organic compounds representing different organic groups. The regenerated samples were then

characterized using micropore surface analysis, XPS, and DTG analysis to evaluate the changes in the physical and chemical properties of the adsorbent due to irreversible adsorption.

Finally, dissertation overview, summary of findings, significance of the research, and recommendations for future work are presented in Chapter 8.

1.5 References

- Aktas, O.; Cecen, F. Effect of type of carbon activation on adsorption and its reversibility. *J. Chem. Technol. Biot.* **2006**, *81*, 94–101.
- Aktas, O.; Cecen, F. Competitive adsorption and desorption of a bi-solute mixture: Effect of activated carbon type. *Adsorption* **2007**, *13*, 159–169.
- Alvarez, P.M.; Garcia-Araya, J.F.; Beltran, F.J.; Masaa, F.J.; Medina, F. Ozonation of activated carbons: Effect on the adsorption of selected phenolic compounds from aqueous solutions. *J. Colloid Interf. Sci.* **2005**, *283*, 503–512.
- Dabrowski, A.; Podkoscielny, P.; Hubicki, Z.; Barczak, M. Adsorption of phenolic compounds by activated carbon-A critical review. *Chemosphere* **2005**, *58*, 1049–1070.
- Efremenko, I.; Sheintuch, M. Predicting solute adsorption on activated carbon: phenol. *Langmuir* **2006**, *22*, 3614–3621.
- Environment Canada (2015); Volatile organic compound emissions; www.ec.gc.ca/indicateurs-indicators/default.asp?lang=en&n=64B9E95D-1.
- Gupta, V.K.; Verma, N. Removal of volatile organic compounds by cryogenic condensation followed by adsorption. *Chem. Eng. Sci.* **2002**, *57*, 2679–96.
- Hashisho, Z.; Rood, M.J.; Botich, L. Microwave-swing adsorption to capture and recover vapors from air streams with activated carbon fiber cloth. *Environ. Sci. Technol.* **2005**, *39*, 6851–6859.
- Hashisho, Z.; Emamipour, H.; Rood, M.J.; Hay, K.J.; Kim, B.J.; Thurston, D. Concomitant adsorption and desorption of organic vapor in dry and humid air streams using microwave and direct electrothermal swing adsorption. *Environ. Sci. Technol.* **2008**, *42*, 9317–9322.
- Hung, H.; Lin, T. Prediction of the adsorption capacity for volatile organic compounds onto activated carbons by the Dubinin–Radushkevich–Langmuir model. *J. Air Waste Manage. Assoc.* **2007**, *57*, 497–506.
- Hung, C.; Bai, H. Adsorption behaviors of organic vapors using mesoporous silica particles made by evaporation induced self-assembly method. *Chem. Eng. Sci.* **2008**, *63*, 1997–2005.

- Kampa, M.; Castanas, E. Human health effects of air pollution. *Environ. Pollut.* **2008**, *151*, 362–367.
- Kawasaki, N.; Kinoshita, H.; Oue, T.; Nakamura, T.; Tanada, S. Study on adsorption kinetic of aromatic hydrocarbons onto activated carbon in gaseous flow method. *J. Colloid Interface Sci.* **2004**, *275*, 40–43.
- Khan, F.I.; Ghoshal, A.K. Removal of volatile organic compounds from polluted air. *J. Loss Prev. Process Ind.* **2000**, *13*, 527–545.
- Kim, B.R. VOC emissions from automotive painting and their control: A review. *Environ. Eng. Res.* **2011**, *16*, 1–9.
- Lapkin, A.; Joyce, L.; and Crittenden, B. Framework for evaluating the “Greenness” of chemical processes: Case studies for a novel VOC recovery technology. *Environ. Sci. Technol.* **2004**, *38*, 5815–5823.
- Leslie, G.B. Health risks from indoor air pollutants: Public alarm and toxicological reality. *Indoor Built Environ.* **2000**, *9*, 5–16.
- Papasavva, S.; Kia, S.; Claya, J.; Gunther, R. Characterization of automotive paints: An environmental impact analysis. *Prog. Org. Coat.* **2001**, *43*, 193–206.
- Parmar, G.R.; Rao, N.N. Emerging control technologies for volatile organic compounds. *Cri. Rev. Environ. Sci. Technol.* **2009**, *39*, 41–78.
- Pelekani, C.; Snoeyink, V.L. Competitive adsorption in natural water: role of activated carbon pore size. *Water Res.* **1999**, *33*, 1209–1219.
- Popescu, M.; Joly, J. P.; Carre, J.; Danatoiu, C. Dynamical adsorption and temperature-programmed desorption of VOCs (toluene, butyl acetate and butanol) on activated carbons. *Carbon* **2003**, *41*, 739–748.
- Ramos, M.E.; Bonelli, P.R.; Cukierman, A.L.; Ribeiro Carrott, M.M.L.; Carrott, P.J.M. Adsorption of volatile organic compounds onto activated carbon cloths derived from a novel regenerated cellulosic precursor. *J. Hazard. Mater.* **2010**, *177*, 175–182.
- Shonnard, D.R.; Hiew, D.S. Comparative environmental assessments of VOC recovery and recycle design alternatives for a gaseous waste stream. *Environ. Sci. Technol.* **2000**, *34*, 5222–5228.
- US Environmental Protection Agency (2009); Definition of volatile organic compounds (VOC); www.epa.gov/ttn/naaqs/ozone/ozonetech/def_voc.htm.

- Wu, J.; Stromqvist, E.; Claesson, O.; Fangmark, I.E.; Hammarstrom, L.G. A systematic approach for modeling the affinity coefficient in the Dubinin–Radushkevich equation. *Carbon* **2002**, *40*, 2587–2596.
- Yang, R.T. *Adsorbents: Fundamentals and Application*; John Wiley & Sons, Inc.: Hoboken, NJ, USA, 2003.

CHAPTER 2. LITERATURE REVIEW

2.1 Adsorption Capacity Prediction

2.1.1 Definition of Adsorption Isotherm

Adsorption isotherm describes the equilibrium relationship between adsorbate and adsorbent at a certain temperature (El-Khaiary, 2008). Adsorption capacity of AC for any adsorbate can be found from the corresponding adsorption isotherm (Foo and Hameed, 2010). Some of the most widely used adsorption isotherm models are described in the following section.

2.1.2 Adsorption Isotherm Models

2.1.2.1 Langmuir Isotherm Model

The Langmuir adsorption isotherm model describes the adsorption of gases on solid sorbents (Langmuir, 1916). Adsorption is assumed to occur in monolayer and on a certain number of homogenous sites with no lateral interaction and steric hindrance (Foo and Hameed, 2010). The Langmuir adsorption isotherm model can be presented as (Tefera et al., 2013a):

$$q_e = \frac{q_m bc}{1 + bc}$$

and

$$b = b_0 \exp\left(\frac{-\Delta H_{ad}}{RT}\right)$$

where q_e is the adsorbent equilibrium capacity, q_m the adsorbent maximum equilibrium capacity, b the temperature-dependent Langmuir affinity coefficients, c the gas phase concentration, b_0 the pre-exponential constant, ΔH_{ad} the heat of adsorption, R the ideal gas constant, and T the temperature.

2.1.2.2 Freundlich Isotherm Model

The Freundlich adsorption isotherm model is an empirical model and describes non-ideal and reversible adsorption (Freundlich, 1906). Adsorption may occur in multilayer and on heterogeneous sites with various affinities and heats of adsorption given that adsorption occurs on strong sites first (Foo and Hameed, 2010). This model suffers from lack of thermodynamic basis and does not approach to Henry's law constant at low concentrations (Foo and Hameed, 2010). Freundlich adsorption isotherm model can be presented as (Foo and Hameed, 2010):

$$q_e = K_f C_e^{\frac{1}{n}}$$

where q_e is the adsorbent equilibrium capacity, C_e the equilibrium concentration of adsorbate in solution, and K_f and n are constants for a given adsorbate and adsorbent at a particular temperature. n is between 0 and 1 and indicates surface heterogeneity (Haghseresht and Lu, 1998).

2.1.2.3 Dubinin-Radushkevich Isotherm Model

D-R adsorption isotherm model is an empirical model and was initially developed for adsorption of vapors onto microporous adsorbents with heterogeneous surface (Dubinin and Radushkevich, 1947). The model successfully predicts adsorption capacities at intermediate and high concentrations but fails to approach to Henry's law constant at low concentrations (Foo and Hameed, 2010). D-R adsorption isotherm model can be presented as (Foo and Hameed, 2010):

$$W = W_o \exp\left(-k \frac{\varepsilon^2}{\beta^2}\right)$$

and

$$\varepsilon = RT \ln \frac{P_o}{P}$$

where W is the volume of adsorbed adsorbate per gram of adsorbent, W_0 the limiting pore volume of the adsorbent, k a constant related to the adsorbate as well as adsorbent, β the affinity coefficient which permits the comparison of the adsorption potential of the test adsorbate to that of a reference adsorbate, R the ideal gas constant, T the temperature, P_0 the saturated vapor pressure of the test adsorbate at test temperature, and P the equilibrium vapor pressure of the test adsorbate.

2.1.2.4 Brunauer-Emmett-Teller Isotherm Model

Brunauer-Emmett-Teller (BET) adsorption isotherm model is a theoretical model and applicable to gas-solid systems (Brunauer et al., 1938). The model covers multilayer adsorption with relative pressures between 0.05 and 0.3 (Foo and Hameed, 2010). The model can be presented as (Foo and Hameed, 2010):

$$q_e = \frac{q_s C_{BET} C_e}{(C_s - C_e) \left[1 + (C_{BET} - 1) \left(\frac{C_e}{C_s} \right) \right]}$$

where C_{BET} is the ratio of monolayer and multilayer heats of adsorption, C_s the adsorbate monolayer saturation concentration, q_s the theoretical isotherm saturation capacity, and q_e the equilibrium adsorption capacity. Since C_{BET} is significantly larger than unity, the model can be simplified as (Foo and Hameed, 2010):

$$q_e = \frac{q_s}{1 - \left(\frac{C_e}{C_s} \right)}$$

2.2 Irreversible Adsorption

2.2.1 Mechanisms for Irreversible Adsorption

Adsorption can be reversible or irreversible (Aktas and Cecen, 2007). Reversible adsorption is often attributed to physical interactions, such as van der Waals' forces, between the

adsorbate and the adsorbent (Yonge et al., 1985; Lowell and Shields, 1991; Khan and Ghoshal, 2000; Aktas and Cecen, 2007). Popescu et al. (2003) stated that, as a general rule, the heat of desorption resulting from physical adsorption, or physisorption, is similar to or slightly greater than the heat of vaporization. In most cases, physisorption is reversible due to its low heat of adsorption (20 – 70 kJ/mol) (Ruthven, 1984; Khan and Ghoshal, 2000; Ramirez et al., 2005). Van der Waals' forces may be strong enough to prevent desorption under the selected regeneration parameters. This scenario may be associated with adsorbates with high boiling point and/or molecular weight, or adsorbates with molecular diameters that are very close to that of the adsorbent's pore width. In this case, strong dispersive forces acting on adsorbate molecules in narrow micropores makes regeneration difficult due to overlapping attractive forces from opposing pore walls. These non-desorbed physisorbed species decrease the capacity of the adsorbent in subsequent adsorption cycles.

Adsorbates that are irreversibly adsorbed to carbon cannot be removed with a selected regeneration technique, and often cannot be removed without destroying the carbon adsorbent. Most of the previous research on irreversible adsorption of organic compounds focused on their removal from aqueous solutions, and similar studies in gas phase are limited. Since adsorption fundamentals are similar in gas and aqueous phases, the outcomes of irreversible aqueous phase adsorption of organic compounds have also been reviewed to help identify the relevant operational parameters in gas phase capture of VOCs.

Three scenarios can result in irreversible adsorption: 1) strong interactions between adsorbent and adsorbate, often associated with bonding between the species (chemisorption), 2) adsorbate coupling leading to higher molecular weight/boiling point compounds that are difficult to desorb due to their large size (trapping of molecules within the narrow pores due to coupling

reactions catalyzed by the activated carbon – small molecules enter the narrow pores and react to form larger molecules with new dimensions that prevent desorption), or 3) adsorbate decomposition during regeneration, resulting in coke deposition inside the pores of adsorbent.

2.2.1.1 Chemisorption

Chemisorption occurs when the adsorbate and adsorbent are united by chemical bonds, especially covalent bonds (Yonge et al., 1985; Lowell and Shields, 1991; de Jonge et al., 1996b; Ha and Vinitnantharat, 2000; Aktas and Cecen, 2007). Hence, the heat of adsorption is high (up to 400 kJ/mol), approaching the energy of chemical bonds (Lowell and Shields, 1991; Wark et al., 1998). Chemisorption is associated with an activation energy related to bond formation (Lowell and Shields, 1991). Gases or liquids react with carbon's surface functional groups (SFGs), or with the carbon itself, to form chemical bonds. Unlike physical adsorption, which relies on carbon's accessible pore volume, chemisorption relies on carbon's accessible adsorption sites. When an active site bonds to an adsorbate molecule, it is deactivated and the adsorption potential decreases (Langmuir, 1918). Because chemisorption requires surface reactions, adsorbates can only form a monolayer on the adsorbent – a key difference between physical and chemical adsorption (Langmuir, 1918). Increased surface area only enhances chemisorption if there is an associated increase in the number of adsorption sites accessible to the contaminant (Langmuir, 1918). By varying the chemistry of the surface, the extent of chemical adsorption can change. Increased temperatures and reduced pressures that do not degrade the adsorbent or adsorbate may not be sufficient to break the bonds formed via chemical adsorption. This can increase operational costs, but may also increase selectivity. As such, chemical adsorption occurs most frequently for removing trace contaminants. Environmental applications include mercury removal via surface functionalized ACs (Liu and Vidic, 1998) and

adsorptive removal of chlorine (Tobias and Soffer, 1985). Chemical adsorption may also occur through additives added to the adsorbent (e.g. sulfur for adsorbing mercury) (Liu and Vidic, 1998). Chemisorption results in diminished adsorption capacity in successive adsorption cycles and a shorter lifetime of the adsorbent (Goto et al., 1986).

2.2.1.2 Oxidative Coupling

In the aqueous phase, oxidative polymerization of phenolic compounds also contributes to irreversible adsorption (de Jonge et al., 1996b; Vinitnantharat et al., 2001; Soto et al., 2011). Several studies show that irreversible adsorption of phenols can be attributed to oxidative coupling (Vidic et al., 1990, 1992, 1993, 1997; Vidic and Suidan, 1991, 1992; Nakhla et al., 1992; Abuzaid and Nakhla, 1994, 1997; Cooney and Xi, 1994; Abuzaid et al., 1995; Uranowski et al., 1998; Garner et al., 2001). Upon losing a hydrogen atom, a phenol molecule is converted to a phenoxy radical that can oligomerize with others. The reaction can occur at room temperature in an activated carbon pore – the carbon functions as an oxidation catalyst (Vidic et al., 1993; Cooney and Xi, 1994). Oxidative coupling promotes irreversible adsorption because the larger compounds have higher boiling points. Additionally, if coupling occurs in a larger void space accessible only through narrow channels, the oligomers can become trapped. Several factors, including the chemical properties and pore size distribution of the adsorbent (Sorial et al., 1993; Vidic et al., 1993, 1997; de Jonge et al., 1996a, 1996b; Vinitnantharat et al., 2001; Lu and Sorial, 2004a, 2004b, 2007; Aktas and Cecen, 2006), the presence of oxygen in adsorption medium (de Jonge et al., 1996b; Dabrowski et al., 2005), and, to a lesser extent, the presence of metals and metal oxides on adsorbent's surface (Grant and King, 1990; Leng and Pinto, 1997; Kilduff and King, 1997; Terzyk, 2003) can affect oxidative coupling. Oxidative coupling of

phenols has been documented many times in aqueous phase applications, but, to the best of our knowledge, has not been reported in gas phase adsorption applications.

2.2.1.3 Adsorbate Decomposition

Organic adsorbates may decompose during regeneration due to exposure to high temperature, resulting in coke formation inside the pores of the AC, which subsequently decreases the performance of AC adsorbents (Ania et al., 2007; Niknaddaf et al., 2016). Suzuki et al. (1978) performed one of the very first comprehensive studies on the behavior of adsorbates during thermal regeneration. Using TGA, they showed that adsorbed phenols decompose to form carbon deposits inside the pores of the AC, which remain there even at 800 °C (Suzuki et al., 1978). The carbon deposits may be removed when heated at temperatures > 600 °C under oxidizing environments such as steam (Liu et al., 1987). Adsorbate decomposition results in diminished adsorption capacity during successive adsorption/regeneration cycles and a shorter lifetime of the adsorbent (Niknaddaf et al., 2016).

2.2.2 Impacts of Adsorption Conditions on Irreversible Adsorption

Adsorption conditions, including adsorption environment, adsorption temperature, and adsorption duration, affect the irreversible adsorption of organic compounds. It is important to identify conditions that promote or hinder irreversible adsorption so that its industrial occurrence can be understood and minimized (Table 2-1).

2.2.2.1 Adsorption Environment

Dissolved oxygen (DO) increases activated carbon's adsorption capacity for aqueous phase phenols due to increased oxidative coupling and, consequently, increases irreversible adsorption (Grant and King, 1990; Vidic and Suidan, 1991; Chatzopoulos et al., 1993; de Jonge et al., 1996b; Vinitnantharat et al., 2001; Alvarez et al., 2005; Dabrowski et al., 2005; Aktas and

Cecen, 2007; Terzyk, 2007). De Jonge et al. (1996b) found that oxic conditions enhanced adsorption of o-cresol (a phenolic compound) but had no impact on adsorption of 3-chlorobenzoic acid (a non-phenolic compound). A linear relationship between the consumption of DO and irreversibly adsorbed phenols has been shown (Vidic et al., 1993).

Table 2-1. Adsorption conditions used to investigate irreversible adsorption.

Adsorption Medium	Temperature (°C)	Reference(s)
Water (oxic)	25	Yonge et al., 1985; Alvarez et al., 2005
Water (oxic and anoxic)	35	Vidic et al., 1990
Water (oxic and anoxic)	21	Vidic et al., 1993, 1997; Abuzaid and Nakhla, 1994
Water (oxic and anoxic)	21 and 35	Vidic and Suidan, 1991
Water (oxic and anoxic)	23	Abuzaid et al., 1995; Lu and Sorial, 2004a, 2004b, 2007
Water (oxic and anoxic)	25, 53, and 80	Grant and King, 1990
Water (oxic)	20, 30, and 40	Garcia-Araya et al., 2003
Water (oxic)	5, 25, and 50	Ravi et al., 1998
Air	30	Park and Lee, 1993

During oxic phenol adsorption from neutral water at 21°C, adsorption kinetics and capacity are limited by the adsorbate's polymerization rate, not by the physisorption rate (Vidic

et al., 1994a). DO increased carbon's capacity for o-cresol and 4-nitrophenol, and, more generally, oxidizing conditions increased adsorption of phenols (Vidic et al., 1994a).

Oxidative coupling of phenols under oxic conditions decreases the regeneration efficiency of the loaded adsorbent during solvent extraction (Vidic et al., 1997). For activated carbon loaded with 2-methylphenol, regeneration (extraction) efficiencies were 100% and 10 – 30% under anoxic and oxic conditions, respectively (Vidic et al., 1994b). With oxygen present, adsorbate polymerization caused irreversible adsorption. Nakhla et al. (1994) confirmed these results, showing regeneration efficiencies for phenol-loaded carbon of 80% and 25% in anoxic and oxic conditions, respectively. All the aforementioned studies investigated the effect of oxygen on aqueous phase adsorption of phenols. To the best of our knowledge, however, no previous report has explored the effect of oxygen on gas-phase irreversible adsorption of organic compounds.

2.2.2.2 Adsorption Temperature

Adsorption of organics onto activated carbon is exothermic; increasing adsorption temperature decreases adsorption capacities (Garcia-Araya et al., 2003; Das et al., 2004; Kawasaki et al., 2004; Ramirez et al., 2004; Dabrowski et al., 2005). Furthermore, providing additional thermal energy increases the likelihood of polymerization reactions (Mattson et al., 1969; Grant and King, 1990; Ravi et al., 1998), decreases diffusion limitations (Costa et al., 1989; Chiang et al., 2001; Das et al., 2004), and increases bond-forming chemisorption (Magne and Walker, 1986; Schnelle and Brown, 2002). Clearly, temperature is a crucial parameter for determining the occurrence of irreversible adsorption.

In the liquid phase, contradictory results have been reported for temperature's impact on polymerization of adsorbed phenols. Grant and King (1990) and Nakhla et al. (1994) reported

higher adsorption capacities and more irreversible adsorption at higher adsorption temperatures due to increased polymerization and chemisorption. It is recommended, therefore, that adsorption of phenols occur at the lowest possible temperature (Magne and Walker, 1986; Grant and King, 1990; Nakhla et al., 1994). Vidic and Suidan (1991), however, found that polymerization was independent of adsorption temperature. While no explicit explanation was provided for this counter-intuitive result, it may be notable that the temperature range tested by Vidic and Suidan (1991) was 21 – 35 °C, while Grant and King (1990) tested a wider range, 25 – 80 °C. The impact of adsorption temperature on the irreversible adsorption of VOCs in the gas phase has not yet been described in the literature.

2.2.2.3 Adsorption Duration

Aqueous phase irreversible adsorption of phenols increases when more adsorption time is provided (Yonge et al., 1985; Grant and King, 1990). To justify these observations, Tamon et al. (1996) proposed a two-state adsorption model that includes an energy barrier between a precursor and an irreversible state (Figure 2-1). The initial energy barrier is higher for electron-attracting compounds, so they cannot proceed to the irreversible state. The barrier is weaker for electron-donating compounds, allowing them to more readily become irreversibly adsorbed. In order to obtain the needed activation energy, the electron-donating compounds need a long contact time with the adsorbent (Tamon et al., 1996).

Wang et al. (2012) investigated gas-phase irreversible adsorption of a mixture of 8 organic compounds on BAC, using gas chromatography-mass spectrometry (GC-MS) analysis of the effluent gas during adsorption and regeneration. At the beginning of breakthrough, the outlet gas consisted of low boiling point compounds, including 1-butanol and *n*-butylacetate (Wang et al., 2012). The authors attributed this to displacement by high boiling point compounds due to

competitive adsorption (Wang et al., 2012). Smaller, low boiling point compounds adsorb weakly compared to the heavier compounds. Since the heavier compounds have a higher tendency to accumulate on the surface of the carbon, irreversible adsorption increases as adsorption continues past breakthrough (Wang et al., 2012). While it may not be industrially practical to continue adsorption past breakthrough, these results are fundamentally important, providing evidence to justify the role of adsorbate properties on irreversible adsorption, which is discussed later in this chapter.

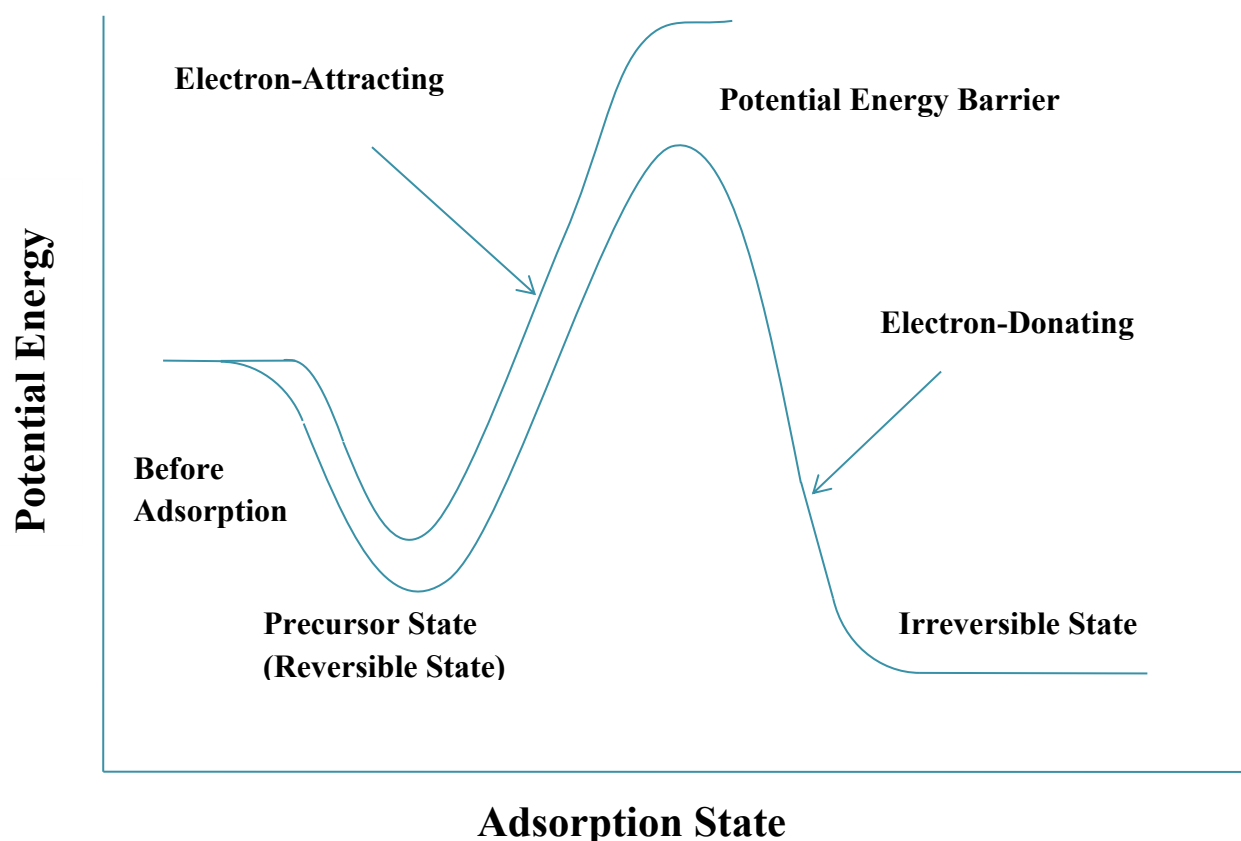


Figure 2-1. Two-state adsorption model (Tamon et al., 1996; reproduced with permission from Elsevier).

2.2.3 Impacts of Adsorbate Properties on Irreversible Adsorption

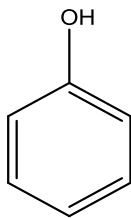
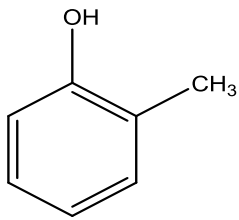
An adsorbate's properties, including its molecular size, boiling point, molecular weight, and functional groups, impact its proclivity to irreversibly adsorb. It is important to identify these

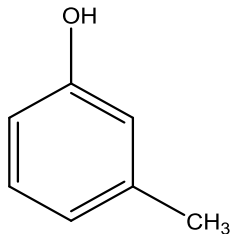
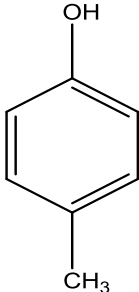
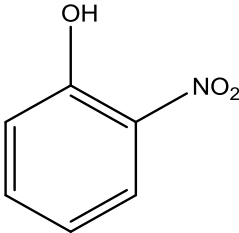
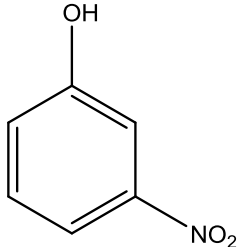
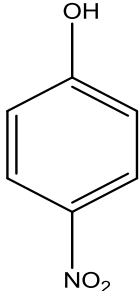
properties and quantify their relevance to irreversible adsorption, and researchers have investigated a wide range of single adsorbates (Table 2-2) as well as mixtures of adsorbates (Table 2-3) to discern these trends.

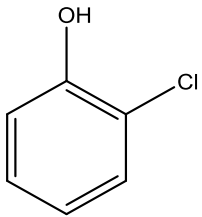
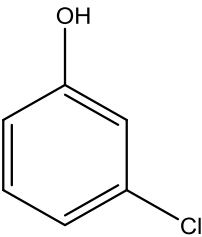
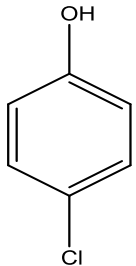
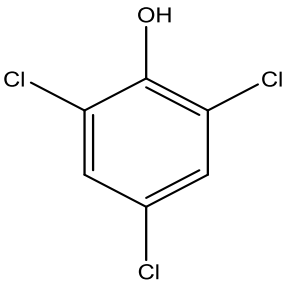
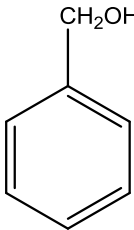
2.2.3.1 Single Adsorbates

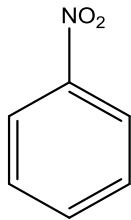
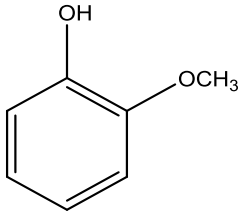
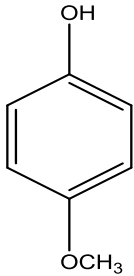
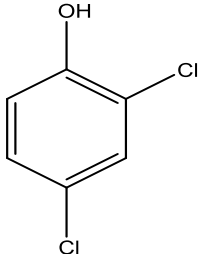
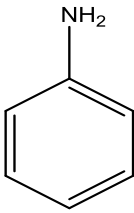
Adsorbates with electron-donating groups (Grant and King, 1990; Tamon et al., 1990, 1996; Tamon and Okazaki, 1996; Tanthapanichakoon et al., 2005), and high molecular weight and/or boiling point (Fayaz et al., 2011) are most likely to irreversibly adsorb. It is well-established that, in the aqueous phase, phenols adsorb irreversibly on activated carbon (Suzuki et al., 1978; Grant and King, 1990).

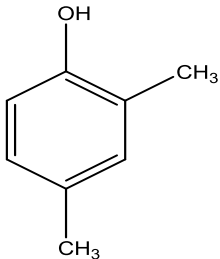
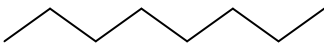
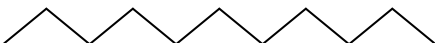
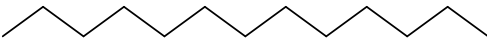
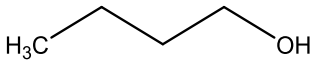
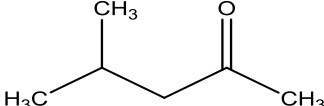
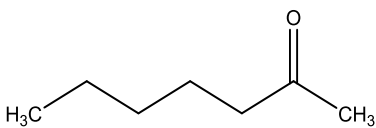
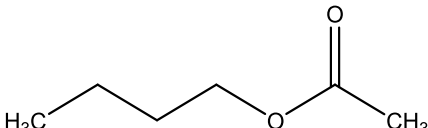
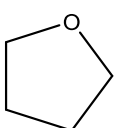
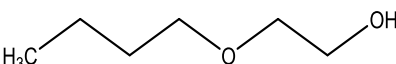
Table 2-2. Single adsorbates used to investigate irreversible adsorption.

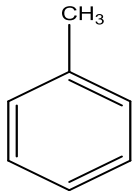
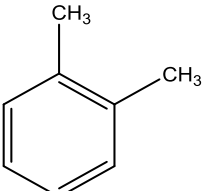
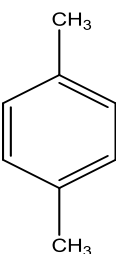
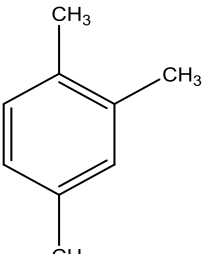
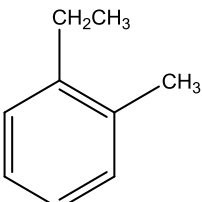
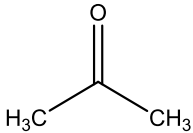
Adsorbate (phase)	Chemical Structure	Reference(s)
phenol (aqueous)		Yonge et al., 1985; Grant and King, 1990; Vidic et al., 1990, 1993; Vidic and Suidan, 1991; Abuzaid and Nakhla, 1994; Abuzaid et al., 1995; Lu and Sorial, 2004a, 2007; Ravi et al., 1998; Alvarez et al., 2005
2-methylphenol (aqueous)		Yonge et al., 1985; Vidic et al., 1990, 1993, 1997; Vidic and Suidan, 1991; Abuzaid and Nakhla, 1994; Abuzaid et al., 1995; Ravi et al., 1998; Lu and Sorial, 2004a, 2004b, 2007

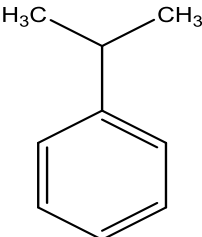
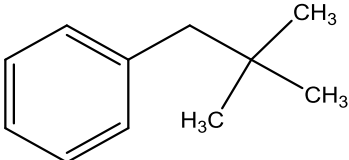
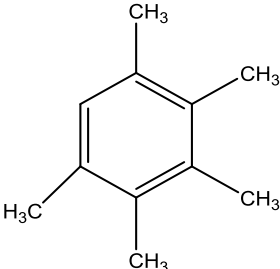
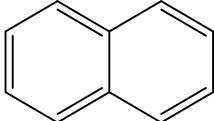
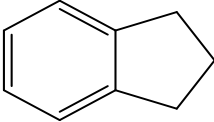
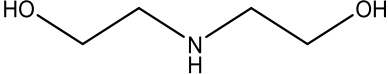
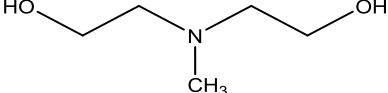
Adsorbate (phase)	Chemical Structure	Reference(s)
3-methylphenol (aqueous)		Vidic et al., 1993; Ravi et al., 1998
4-methylphenol (aqueous)		Vidic et al., 1993; Ravi et al., 1998
2-nitrophenol (aqueous)		Vidic et al., 1993; Lu and Sorial, 2007
3-nitrophenol (aqueous)		Vidic et al., 1993
4-nitrophenol (aqueous)		Grant and King, 1990; Vidic et al., 1993; Abuzaid et al., 1995; Alvarez et al., 2005; Lu and Sorial, 2007

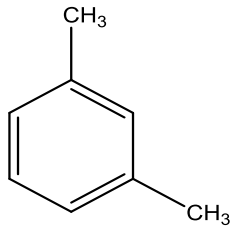
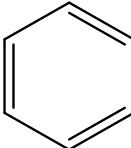
Adsorbate (phase)	Chemical Structure	Reference(s)
2-chlorophenol (aqueous)		Vidic and Suidan, 1991; Vidic et al., 1993, 1997; Lu and Sorial, 2007
3-chlorophenol (aqueous)		Vidic et al., 1993
4-chlorophenol (aqueous)		Grant and King, 1990; Vidic et al., 1993; Alvarez et al., 2005; Lu and Sorial, 2007
methyl iodide (gas)	$\text{H}_3\text{C}-\text{I}$	Park and Lee, 1993
2, 4, 6-trichlorophenol (aqueous)		Vidic et al., 1993
benzylalcohol (aqueous)		Ravi et al., 1998

Adsorbate (phase)	Chemical Structure	Reference(s)
nitrobenzene (aqueous)		Grant and King, 1990
2-methoxyphenol (aqueous)		Yonge et al., 1985
4-methoxyphenol (aqueous)		Grant and King, 1990
2, 4-dichlorophenol (aqueous)		Vidic et al., 1993
aniline (aqueous)		Grant and King, 1990; Vidic et al., 1993

Adsorbate (phase)	Chemical Structure	Reference(s)
2,4-dimethylphenol (aqueous)		Grant and King, 1990; Vidic et al., 1993
<i>n</i> -heptane (gas)		Fayaz et al., 2011
<i>n</i> -decane (gas)		Fayaz et al., 2011
<i>n</i> -dodecane (gas)		Fayaz et al., 2015a
1-butanol (gas)		Fayaz et al., 2011
methylisobutylketone (gas)		Fayaz et al., 2011
2-heptanone (gas)		Fayaz et al., 2011
<i>n</i> -butylacetate (gas)		Fayaz et al., 2011
tetrahydrofuran (gas)		Fayaz et al., 2011
2-butoxyethanol (gas)		Fayaz et al., 2011, 2014

Adsorbate (phase)	Chemical Structure	Reference(s)
toluene (gas)		Fayaz et al., 2011
<i>m</i> -xylene (gas)		Fayaz et al., 2011
<i>p</i> -xylene (gas)		Fayaz et al., 2011
1,2,4-trimethylbenzene (gas)		Fayaz et al., 2011, 2014, 2015b; Niknaddaf et al., 2014, 2016
1-ethyl-2-methylbenzene (gas)		Fayaz et al., 2011
acetone (gas)		Fayaz et al., 2011

Adsorbate (phase)	Chemical Structure	Reference(s)
cumene (gas)		Fayaz et al., 2011
2,2-dimethylpropylbenzene (gas)		Fayaz et al., 2011
pentamethylbenzene (gas)		Fayaz et al., 2011
naphthalene (gas)		Fayaz et al., 2011
indan (gas)		Fayaz et al., 2011
diethanolamine (gas)		Fayaz et al., 2011
methyldiethanolamine (gas)		Fayaz et al., 2011

Adsorbate (phase)	Chemical Structure	Reference(s)
<i>o</i> -xylene (gas)		Fayaz et al., 2011
benzene (gas)		Fayaz et al., 2011

The potential for oxidative coupling on activated carbon depends on the adsorbate's critical oxidation potential (COP), which controls polymerization of phenols and subsequent irreversible adsorption. Electron withdrawing groups (e.g. nitro and chloro) increase COP (and decrease irreversible adsorption) by making it harder for the compound to lose a hydrogen atom (Grant and King, 1990; Lu and Sorial, 2004a, 2004b). Electron donating groups (e.g. methyl and ethyl) decrease COP (and increase irreversible adsorption). A trend for liquid phase irreversible adsorption on activated carbon has been established for the following compounds: *p*-methoxyphenol > 2,4-dimethylphenol = *p*-chlorophenol > phenol > aniline > *p*-nitrophenol = *p*-hydroxybenzaldehyde (Grant and King, 1990). Electron donating substituents have similarly been ranked based on their potential to promote oxidative coupling: OCH₃ > CH₃ > Cl > H > COOH > CHO > NO₂ (Osei-Twum et al., 1996). Tamon et al. (1996) compared aqueous adsorption of electron-donating (phenol, aniline, L-phenylalanine, L-tyrosine) and electron-attracting (*p*-nitroaniline and nitrobenzene) compounds on activated carbon. In the presence of electron-donating groups (e.g. -NH₂ and -OH), irreversible adsorption occurs, while in the presence of electron-attracting groups (e.g. -NO₂) adsorption is reversible (Tamon et al., 1996).

Tamon and Okazaki (1996) evaluated desorption of 11 aromatic compounds from activated carbon: phenol, benzaldehyde, aniline, β -naphthol, p-nitroaniline, m-cresol, nitrobenzene, p-nitrophenol, p-cresol, p-nitrobenzoic acid, and p-chlorophenol. Consistent with the group's previous studies, irreversible adsorption occurred for compounds with electron-donating groups (phenol, aniline, β -naphthol, m-cresol, p-cresol, and p-chlorophenol) and reversible adsorption occurred for compounds with electron-attracting groups. The authors suggested that the energy difference between the adsorbate's highest occupied molecular orbital (HOMO) and the adsorbent's lowest unoccupied molecular orbital (LUMO) contributes to reversibility. Adsorption is most likely to be reversible when this difference is large. To promote reversible adsorption, therefore, the authors used wet oxidation of the activated carbon to decrease the carbon's LUMO (Tamon and Okazaki, 1996). Since the adsorbate's HOMO, which represents its electron donating ability, is fixed, it cannot be adjusted to promote reversibility. Another study ranked the HOMO for 4 organic adsorbates: aniline > phenol > benzoic acid > nitrobenzene (Koh and Nakajima, 2000). This order is consistent with the adsorbate's likelihood to irreversibly adsorb on activated carbon.

Tanthapanichakoon et al. (2005) explored activated carbon prepared from waste tires and a commercial activated carbon as adsorbents for dilute phenol and reactive dyes (Black 5 and Red 31). They found, similar to previous reports, that electron-donating hydroxyl groups promote irreversible adsorption on activated carbon (Tanthapanichakoon et al., 2005).

2.2.3.2 Mixture of Adsorbates

Lu and Sorial (2004a) studied aqueous phase irreversible adsorption of binary (phenol/2-methylphenol) and ternary (phenol/2-methylphenol/2-ethylphenol) mixtures. For both scenarios, no irreversible adsorption was observed. The authors attributed this to decreased oligomerization

resulting from the adsorbent's narrow pore width (< 0.8 nm), which is comparable to the molecular size of the considered adsorbates, preventing adjacent adsorption of two adsorbate molecules. In another study, the same authors found that oxidative coupling was less likely in mixtures compared to individual compounds, again attributing the differences to decreased oligomerization (Lu and Sorial, 2004b). Oxidative coupling occurs when the same adsorbate is adsorbed on adjacent sites, which is less likely in mixtures due to competition for adsorption sites.

Table 2-3. Adsorbate mixtures used to investigate irreversible adsorption.

Mixture	Reference(s)
Binary mixture of phenol and 2-methylphenol	Lu and Sorial, 2004a
Binary mixture of 2-ethylphenol and 2-methylphenol	Lu and Sorial, 2004a, 2004b
Binary mixture of 2-ethylphenol and phenol	Lu and Sorial, 2004a, 2007
Ternary mixture of 2-ethylphenol, 2-methylphenol, and phenol	Lu and Sorial, 2007
Binary mixture of 2-methylphenol and 2-chlorophenol	Lu and Sorial, 2007
Binary mixture of 2-methylphenol and 2-nitrophenol	Lu and Sorial, 2007
Binary mixture of <i>n</i> -decane and <i>n</i> -heptane	Wang et al., 2012
Mixture of <i>n</i> -decane, 1-butanol, 2-heptanone, <i>n</i> -butylacetate, 2-butoxyethanol, 1,2,4-trimethylbenzene, indan, and 2,2-dimethylpropylbenzene	Wang et al., 2012

Wang et al. (2012) investigated gas-phase irreversible adsorption of a binary mixture of *n*-heptane and *n*-decane. As time elapsed during adsorption, *n*-heptane was displaced by *n*-decane. Irreversible adsorption increased as a result of this displacement, because *n*-decane is larger, heavier, and has a higher boiling point than *n*-heptane. The same study then used a mixture of 8 organic compounds and found that competitive adsorption results in additional irreversible adsorption due to accumulation of heavy, strongly-adsorbed compounds (Wang et al., 2012).

These results are important because most of the polluted aqueous or gaseous streams contain a mixture of organic compounds. Furthermore, the stark differences between gas and aqueous phase multi-component adsorption are notable. In the gas phase, irreversible adsorption is enhanced with mixtures, while only the opposite trends have been reported in the liquid phase.

2.2.4 Impacts of Adsorbent Properties on Irreversible Adsorption

Table 2-4 lists activated carbons used to investigate irreversible adsorption of organic compounds in the literature. GAC, BAC, PAC, and ACC represent granular activated carbon, beaded activated carbon, powdered activated carbon, and activated carbon cloth, respectively. BET surface area is also included in Table 2-4 to provide more information about the physical properties of the adsorbents.

2.2.4.1 Pore Size Distribution

The pore size distribution of AC, which is influenced by the organic starting material and the activation method and conditions, has a critical role in its adsorption behavior (Lillo-Rodenas, 2005; Li et al., 2011). Previous studies showed that narrow pore sizes hamper oxidative coupling of phenolics, decreasing irreversible adsorption (Lu and Sorial, 2004a, 2004b, 2004c, 2007, 2009; Yan and Sorial, 2011). Other studies show that narrow pore sizes promote

adsorption energy, increasing irreversible adsorption (Qin et al., 2009). Lu and Sorial (2004b) studied adsorption of o-cresol and 2-ethylphenol under oxic and anoxic conditions using four ACCs (ACC-10, ACC-15, ACC-20, ACC-25) and one GAC (Filtrisorb 400) to test the effects of pore size on irreversible adsorption. They found significantly higher regeneration efficiency (about 3-fold) and reversible adsorption for ACC-10 compared to other adsorbents. They attributed this behavior to the smaller pore width of ACC-10 compared to the other ACCs tested (Lu and Sorial, 2004b), concluding that small pores hamper oligomerization.

Table 2-4. Adsorbents used to investigate irreversible adsorption of organic compounds.

Adsorbent	Supplier	BET Surface Area (m²/g)	Reference(s)
AQ40 GAC	Chemvicon Carbon	864	Alvarez et al., 2005
SA4 PAC	Norit	800	de Jonge et al., 1996b; Aktas and Cecen, 2006
CA1 PAC	Norit	1400	de Jonge et al., 1996b; Aktas and Cecen, 2006
PKDA GAC	Norit	850	Aktas and Cecen, 2006
CAgran GAC	Norit	1400	Aktas and Cecen, 2006
Filtrisorb 400 GAC	Calgon Carbon Corp.	993	Yonge et al., 1985; Vidic et al., 1990, 1993; Vidic and Suidan, 1991; Abuzaid and Nakhla, 1994; Nakhla et al., 1994; Abuzaid et al., 1995; Lu and Sorial, 2004a, 2004b, 2007; Alvarez et al., 2005
ACC-10	Nippon Kynol	900	Lu and Sorial, 2004a, 2004b, 2007; Niknaddaf et al., 2014, 2016

Adsorbent	Supplier	BET Surface Area (m²/g)	Reference(s)
ACC-15	Nippon Kynol	1137	Lu and Sorial, 2004a, 2004b, 2007; Niknaddaf et al., 2014, 2016
ACC-20	Nippon Kynol	1456	Lu and Sorial, 2004b; Niknaddaf et al., 2014, 2016
ACC-25	Nippon Kynol	2014	Lu and Sorial, 2004b
Columbia GAC	Witco Chemical Co.	900	Grant and King, 1990
Filtrisorb 100 GAC	Calgon Carbon Corp.	800	Grant and King, 1990
Norit Row 0.8s GAC	American Norit Co.	650	Grant and King, 1990
Supersorb GX031 GAC	Amoco Research Corp.	2350	Grant and King, 1990
Witcarb 950 GAC	Witco Chemical Co.	1050	Grant and King, 1990
Filtrisorb 300 GAC	Calgon Carbon Corp.	970	Chatzopoulos et al., 1993, 1994; Chatzopoulos and Varma, 1995
Hydraffin P110 GAC	Donan Carbon GmbH & Co.	967	Garcia-Araya et al., 2003
Coconut-based activated carbon	Sam Chul Ri Carbon Co. Ltd.	1483	Park and Lee, 1993
SGL	Calgon Carbon Corp.	950-1050	Chakma and Meisen, 1989
DARCO	Norit	600-650	Chakma and Meisen, 1989

Lu and Sorial (2007) also investigated adsorption of phenol, 2-methylphenol, 2-ethylphenol, 2-chlorophenol, 2-nitrophenol, 4-chlorophenol, and 4-nitrophenol using GAC

(F400) and ACC (ACC-10 and ACC-15). For ACC-10, < 3% difference in adsorption capacity was observed for 2-ethylphenol, 2-chlorophenol, 2-nitrophenol, 4-chlorophenol, and 4-nitrophenol under oxic and anoxic conditions (Lu and Sorial, 2007). For these five adsorbates, the narrow pore widths of ACC-10 hampered oxidative coupling, preventing irreversible adsorption of the contaminants (Lu and Sorial, 2007). For the two smallest adsorbates, phenol and 2-methylphenol, there were notable differences in capacity under oxic and anoxic conditions (Lu and Sorial, 2007). These adsorbates are small enough to penetrate into the narrow pores of ACC-10 and oligomerize in the presence of oxygen, leading to higher adsorption capacities (> 15%) compared to anoxic conditions (Lu and Sorial, 2007). Similar results have been noted for adsorbate mixtures, where competitive adsorption also contributes to decreases in oligomerization (Lu and Sorial, 2009). Similar studies investigating adsorbent's porosity impacts on irreversible adsorption have not been completed for gas phase applications. Differences between the two phases are expected because oxidative coupling has not been reported in the gas phase.

2.2.4.2 Surface Functional Groups

Edge-site carbon atoms are saturated with heteroatoms, including O and N. These atoms contribute to SFGs, which are important to understand because of their impact on the activated carbon's adsorption properties (Lillo-Rodenas, 2005; Li et al., 2011). The effect of SFGs on irreversible adsorption of organics, especially aqueous phase phenolic compounds, has been described (Vidic et al., 1993, 1997; Tessmer et al., 1997; Terzyk, 2003; Lu and Sorial, 2007). Terzyk (2007) reported that oxidative coupling was proportional to the inverse of the carboxylic group concentration. That is to say, an acidic activated carbon resulting from carboxylic group was less likely to cause oxidative coupling. Conversely, saturated SFGs (e.g. methyl, ethyl,

methoxy) enhance the phenomenon, causing increased irreversible adsorption (Yonge et al., 1985). Acidic SFGs decrease irreversible adsorption of phenols by hindering oxidative coupling (Magne and Walker, 1986). This can be attributed to the hydration of the SFGs, where higher water adsorption reduces the possibility of oxidative coupling (Coughlin and Ezra, 1968).

Alvarez et al. (2004) showed that acidic functional groups on AC impact phenol adsorption by: 1) decreasing dispersive interactions during π -electron removal from carbon, 2) forming water clusters in pores to prevent phenol diffusion, 3) preventing irreversible adsorption of phenol on activated carbon under oxic conditions by preventing oxidative coupling reactions, 4) promoting phenol chemisorption on carbonyl groups through donor-acceptor mechanisms, and 5) promoting phenol chemisorption on carboxylic groups via esterification. The net impact of these five mechanisms is expected to be a decrease in overall irreversible adsorption because the main contributor, oxidative coupling, is hampered.

Leng and Pinto (1997) found that aqueous phenol adsorption on AC proceeded via physisorption and surface polymerization. Interactions between phenol and carbon's basal planes and surface oxygen groups control physisorption. Adsorption capacity decreased with increased carboxylic groups because dispersion interactions with basal planes weakened. Surface polymerization occurred under oxic conditions, but could be suppressed by increasing the number of acidic oxygen groups on AC. Basic oxygen groups catalyzed polymerization, increasing irreversible adsorption. Similar studies investigating functional group impacts on irreversible adsorption have not been completed for gas phase applications. Differences between the two phases are expected because SOG hydration is not necessarily relevant in the gas phase.

2.2.4.3 Effect of Metals and Metal Oxides

Previous studies suggest that ash content (typically consisting of trace metals and mineral content) diminishes the regeneration efficiency of activated carbon after aqueous phase irreversible adsorption of organic compounds (Suzuki et al., 1978; Grant and King, 1990; Kilduff and King, 1997; Soto et al., 2011). Grant and King (1990) found that regeneration efficiency of KMnO_4 -treated activated carbon was significantly decreased compared to non-treated activated carbon (Grant and King, 1990). There is also evidence suggesting that metals promote phenol polymerization (Leng and Pinto, 1997). Conversely, Vidic et al. (1997) found no significant relationship between irreversible adsorption and ash and/or metal content of activated carbon. These contradictory conclusions might be attributable to different metal/metal salts and/or different treatment techniques used in the aforementioned studies. Similar studies investigating the effect of metals and metal oxides on irreversible adsorption have not been completed for gas phase applications.

2.2.5 Impacts of Regeneration Conditions on Irreversible Adsorption

Regeneration of saturated adsorbents is expected to remove adsorbates from pores with minimal impact on the physical or chemical properties of the adsorbent, or the chemical composition of the adsorbate. Ideally, adsorption capacity of the regenerated adsorbent matches the starting material (Aktas and Cecen, 2007). During regeneration, factors such as environment, temperature, and heating rate affect irreversible adsorption as discussed below.

2.2.5.1 Regeneration Environment

Alvarez et al. (2004) studied thermal and ozone regeneration of activated carbon saturated with phenol from aqueous solution. Regeneration efficiency $> 90\%$ was achieved only when performed in an oxidizing atmosphere (CO_2), which decomposed the carbon (15% burn

off). When heated in nitrogen, spent carbons recovered < 50% of their initial adsorption capacities. Room temperature ozonation of spent AC removed physisorbed and chemisorbed phenol, eliminating about 80% of the adsorbate.

Activated carbon loaded with phenol, p-chlorophenol, and p-bromophenol was regenerated via catalytic oxidation in air at 240 – 300 °C (Matatov-Meytal, 1997). Samples were impregnated with transition metal oxide catalysts before adsorption, decreasing the BET surface area and adsorption capacity by 23-25% and 12-18%, respectively, due to pore blockage. While phenol adsorption capacity decreased, catalytic oxidation completely regenerated the sorbent – a notable improvement compared to thermal desorption methods (40% regeneration efficiency at similar temperature). Only partial regeneration, however, was achieved for p-chlorophenol and p-bromophenol adsorbates because halide (Cl^- and Br^-) desorption poisoned the catalyst, decreasing its oxidation activity (Matatov-Meytal, 1997). Similar studies investigating the effect of regeneration environment on irreversible adsorption have not been completed for gas phase applications.

2.2.5.2 Regeneration Temperature

Regeneration of activated carbon saturated with m- or o-chlorophenol occurred in three temperature ranges (Ferro-Garcia, 1995). At low temperatures (< 227 °C), physisorbed chlorophenol was reversibly desorbed or transformed into chemisorbed chlorophenol (Ferro-Garcia, 1995). At moderate temperatures ($327\text{ °C} < T < 627\text{ °C}$), chemisorbed chlorophenol decomposed and was released as light gases (e.g. H_2O and CO_2) (Ferro-Garcia, 1995). At > 627 °C, ring condensation and hydrogen desorption occurred (Ferro-Garcia, 1995). Similar studies investigating the effect of regeneration temperature on irreversible adsorption have not been completed for gas phase applications.

2.2.5.3 Regeneration Heating Rate

Faster heating rate can shorten regeneration duration, resulting in shorter downtime of the capture system between cycles. Ferro Garcia et al. (1995, 1996) were the first group studying the effect of heating rate on irreversible adsorption of organic compounds. They reported that using high heating rates (as high as 40 °C/min) during regeneration of adsorbents loaded with o- and m-chlorophenol, decreased the reversibility of adsorption on carbon and resulted in conversion of physisorbed adsorbate into chemisorbed adsorbate (Ferro-Garcia et al., 1995, 1996).

Fayaz et al. (2015b) investigated the effect of regeneration heating rate on irreversible adsorption of organic vapors typically emitted from automotive painting booths. Two BACs (88% and 46% microporous) were loaded with 1,2,4-trimethylbenzene and regenerated at 288 or 400 °C with different heating rates (25, 50, 100, and 150 °C/min). For the higher regeneration temperature (400 °C), increasing heating rate increased heel buildup by as much as 92% and 169% for the mainly microporous and partially microporous BACs, respectively. The elevated heel formation at higher heating rates was attributed to adsorbate coking due to exposing a high concentration desorbate stream to high temperature. Conversely, for the lower regeneration temperature (288 °C), increasing the heating rate did not significantly affect the amount of heel buildup (< 16% and < 10% increase for the mainly microporous and partially microporous BACs, respectively). This was attributed to the lower regeneration temperature, which provided insufficient conditions for coking.

2.2.6 Characterizing Irreversible Adsorption

Previous studies used heat of adsorption, thermal analysis, adsorption breakthrough curve, and nitrogen adsorption isotherm to characterize irreversible adsorption (Table 2-5).

Table 2-5. Techniques used to characterize irreversible adsorption.

Characterization Method	Summary	Reference(s)
Heat of adsorption	Physisorption and chemisorption are distinguished by their heats of adsorption, allowing for a prediction of irreversibility (i.e., most chemisorbed species are irreversibly adsorbed).	Lukomskaya et al., 1986; Popescu et al., 2003
Thermal analysis	Weight loss as a function of temperature identifies the mass of adsorbed species that cannot be removed by heating to a given temperature. Irreversibly adsorbed species are not desorbed, even at very high temperatures.	Suzuki et al., 1978; Magne and Walker, 1986; Ferro-Garcia et al., 1993, 1995; Salvador and Merchan, 1996; Humayun et al., 1998; Nevskaya et al., 1999
Adsorption breakthrough curve	Breakthrough is achieved more rapidly in successive adsorption cycles as irreversible adsorption decreases the capacity of carbon.	Goto et al., 1986; Chatzopoulos and Varma, 1995; Sheintuch and Matatov-Meytal, 1999; Li et al., 2001; Delmas et al., 2009
Nitrogen adsorption isotherm	Irreversible adsorption results in pore blockage, causing decreased surface area, lower pore volume, and downward shifts in the pore size distribution of an adsorbent.	Rivera-Utrilla et al., 2003

2.2.6.1 Heat of Adsorption

Heat of adsorption is the sum of an adsorbate's heat of vaporization and the energy it loses in bonding with the adsorbent (Ramirez et al., 2005). Thus, heat of vaporization makes a significant contribution to the heat of adsorption, especially when bonding energy is negligible

(i.e., physical adsorption) (Ramirez et al., 2005). Comparing the heat of adsorption to the tabulated heat of vaporization for a given adsorbate provides an indication of adsorption strength. When the difference is high, irreversible chemisorption may occur. While the technique has the potential to quantitatively provide information about subtle differences in adsorption strength, it can be difficult to use because a high-resolution temperature measurement system is required to determine small amounts of heat released during adsorption.

Popescu et al. (2003) observed that butanol's heat of adsorption was $> 100\%$ higher than its heat of vaporization, attributing the difference to adsorbate/adsorbent interactions. In this case, a strong endothermic reaction between butanol and activated carbon's SOGs occurred, contributing to the increased heat of adsorption. Conversely, there was no significant difference ($< 30\%$) between the heat of adsorption and heat of vaporization of toluene and *n*-butylacetate, suggesting that physisorption was the main adsorption mechanism (Popescu et al., 2003). Lukomskaya, et al. (1986) studied adsorption of *o*-xylene on carbon, concluding that chemisorption occurred because the heat of adsorption (75 kJ/mol) exceeded the heat of vaporization (46 kJ/mol). The relatively small difference between the values, however, suggested that chemisorption was weak and possibly reversible.

2.2.6.2 Thermal Analysis

Thermal analysis is used extensively to characterize irreversible adsorption. It is an easy, automated method that allows for determination of desorption temperatures based on mass loss during heating. Multiple peaks corresponding to desorption at different temperatures allows for quantification of adsorption strength. Accordingly, slow heating rates ($\leq 2\text{ }^{\circ}\text{C/min}$) should be used to ensure that all desorption peaks are distinguishable, especially when the adsorbate contains multiple components. Artifacts may occur at high temperatures due to pyrolysis of the

carbon adsorbent, so differential experiments are generally used for comparing the mass loss curves of virgin and saturated sorbents. Combining thermal analysis with mass spectroscopy (MS) is useful for identifying desorbed species and thermal degradation byproducts.

Different weight loss peaks may be observed during TGA, possibly representing different adsorption states (Salvador and Merchan, 1996; Maroto-Valer et al., 2006). For similar results, Magne and Walker (1986) attributed the first TGA peak (80 – 323 °C) to physical adsorption and subsequent peaks (350 – 950 °C) to chemical adsorption. Maroto-Valer *et al.* (2006) concluded that peaks at moderate temperatures (e.g. 400 °C) represent weak chemisorption. Salvador and Merchan (1996) used temperature-programmed desorption (TPD) to study aqueous phase adsorption and desorption of phenol, 2-dichlorophenol, 2,6-dichlorophenol, 4-nitrophenol, and 2,6-dichloro-4-nitrophenol. Adsorption strength was proportional to the adsorbate's electrophilicity and comparable to hydrogen bonding in terms of energy.

Qin et al. (2009) used TGA to study dibenzothiophene desorption from polystyrene-based AC with different microporosities, finding two peaks, in all cases, from physisorption and chemisorption. The peak temperature corresponding to chemisorption increased with the carbon's narrow micropore (pores with widths comparable to common organic molecules) volume (Qin et al., 2009). Similar associations between porosity and strength of adsorbent/adsorbate bonding have been reported (Ferro-Garcia et al., 1995). Thermal analysis on spent activated carbons used for gas-phase methyl iodide adsorption yielded two peaks, again attributed to different adsorbate/adsorbent interactions (Park and Lee, 1993). Liu et al. (2003) examined thermal desorption of alkanes, alkenes, and aromatic hydrocarbons from GAC using TGA. Regeneration profiles for low molecular weight alkanes and alkenes ($\leq C_8$) had a single, broad derivative weight loss and a correspondingly broad endothermic peak, associated with

physical desorption. Heavier straight-chain hydrocarbons ($> C_8$) produced additional peaks due to thermal decomposition.

2.2.6.3 Nitrogen Adsorption Isotherm

Comparing the surface area and pore size distribution, obtained from nitrogen adsorption isotherms, of virgin and regenerated adsorbents provides information about pore blockage associated with irreversible adsorption. Rivera-Utrilla et al. (2003) found that irreversible adsorption of o-chlorophenol causes partial pore blockage, the amount of which is proportional to changes in surface area and pore volume.

2.3 References

- Abuzaid, N.; Nakhla, G.F. Dissolved oxygen effects on equilibrium and kinetics of phenols adsorption by activated carbon. *Environ. Sci. Technol.* **1994**, *28*, 216–221.
- Abuzaid, N.; Nakhla, G.F.; Farooq, S.; Osei-Twum, E. Activated carbon adsorption in oxidizing environments. *Water Res.* **1995**, *29*, 653–660.
- Abuzaid, N.; Nakhla, G.F. Modeling of the temperature variation effects on the polymerization reactions of phenolics on granular activated carbon. *Separ. Sci. Technol.* **1997**, *32*, 1255–1272.
- Aktas, O.; Cecen, F. Effect of type of carbon activation on adsorption and its reversibility. *J. Chem. Technol. Biot.* **2006**, *81*, 94–101.
- Aktas, O.; Cecen, F. Bioregeneration of activated carbon: A review. *Int. Biodeter. Biodegr.* **2007**, *59*, 257–272.
- Alvarez, P.M.; Beltran, F.J.; Gomez-Serrano, V.; Jaramillo, J.; Rodriguez, E.M. Comparison between thermal and ozone regenerations of spent activated carbon exhausted with phenol. *Water Res.* **2004**, *38*, 2155–2165.
- Alvarez, P.M.; Garcia-Araya, J.F.; Beltran, F.J.; Masaa, F.J.; Medina, F. Ozonation of activated carbons: Effect on the adsorption of selected phenolic compounds from aqueous solutions. *J. Colloid Interf. Sci.* **2005**, *283*, 503–512.
- Ania, C.O.; Menendez, J.A.; Parra, J.B.; Pis, J.J. Microwave-induced regeneration of activated carbons polluted with phenol: A comparison with conventional thermal regeneration. *Carbon* **2004**, *42*, 1383–1387.
- Bruanuer, S.; Emmett, P.H.; Teller, E. Adsorption of gases in multimolecular layers. *J. Am. Chem. Soc.* **1938**, *60*, 309–319.
- Chakma, A.; Meisen, A. Activated carbon adsorption of diethanolamine, methyl diethanolamine and their degradation products. *Carbon* **1989**, *27*, 573–284.
- Chatzopoulos, D.; Varma, A.; Irvine, R.L. Activated carbon adsorption and desorption of toluene in the aqueous phase. *AIChE J.* **1993**, *39*, 2027–2041.
- Chatzopoulos, D.; Varma, A.; Irvine, R.L. Adsorption and desorption studies in the aqueous phase for the toluene/activated carbon system. *Environ. Prog.* **1994**, *13*, 21–25.

- Chatzopoulos, D.; Varma, A. Aqueous-phase adsorption and desorption of toluene in activated carbon fixed beds: Experiments and model. *Chem. Eng. Sci.* **1995**, *50*, 127–141.
- Chiang, Y.; Chiang, P.; Huang, C. Effects of pore structure and temperature on VOC adsorption on activated carbon. *Carbon* **2001**, *39*, 523–534.
- Cooney, D.; Xi, Z. Activated carbon catalyzes reactions of phenolics during liquid-phase adsorption. *AIChE J.* **1994**, *40*, 341–344.
- Costa, E.; Calleja, G.; Marijuan, L. Comparative adsorption of phenol, *p*-nitrophenol and *p*-hydroxybenzoic acid on activated carbon. *Adsorpt. Sci. Technol.* **1989**, *5*, 213–228.
- Coughlin, R.W.; Ezra, F.S. Role of surface acidity in the adsorption of organic pollutants on the surface of carbon. *Environ. Sci. Technol.*, **1968**, *2*, 291–297.
- Dabrowski, A.; Podkoscielny, P.; Hubicki, Z.; Barczak, M. Adsorption of phenolic compounds by activated carbon-A critical review. *Chemosphere* **2005**, *58*, 1049–1070.
- Das, D.; Gaur, V.; Verma, N. Removal of volatile organic compound by activated carbon fiber. *Carbon* **2004**, *42*, 2949–2962.
- de Jonge, R.J.; Breure, A.M.; van Andel, J.G. Bioregeneration of powdered activated carbon (PAC) loaded with aromatic compound. *Water Res.* **1996a**, *30*, 875–882.
- de Jonge, R.J.; Breure, A.M.; van Andel, J.G. Reversibility of adsorption of aromatic compounds onto powdered activated carbon. *Water Res.* **1996b**, *30*, 883–892.
- Delmas, H.; Creanga, C.; Julcour-Lebigue, C.; Wilhelm, A.M. AD-OX: a sequential oxidative process for water treatment—adsorption and batch CWAO regeneration of activated carbon. *Chem. Eng. J.* **2009**, *152*, 189–194.
- Dubinin, M.M.; Radushkevich, L.V. The equation of the characteristic curve of the activated charcoal. *Proc. Acad. Sci. USSR Phys. Chem. Sect.* **1947**, *55*, 331–337.
- El-Khaiary, M.I. Least-squares regression of adsorption equilibrium data: Comparing the options. *J. Hazard. Mater.* **2008**, *158*, 73–87.
- Fayaz, M.; Wang, H.; Jahandar Lashaki, M.; Hashisho, Z.; Phillips, J. H.; Anderson, J. E. Accumulation of adsorbed of organic vapors from automobile painting operations on bead activated carbon. In *proceedings of 104th Air and Waste Management Association's Annual Conference and Exhibition*, Orlando, FL, 2011.
- Fayaz, M.; Shariaty, P.; Atkinson, J.D.; Hashisho, Z.; Phillips, J. H.; Anderson, J. E.; Nichols, M. The effect of microwave heating on regeneration of beaded activated carbon and a

- polymeric adsorbent. *In proceedings of 107th Air and Waste Management Association's Annual Conference and Exhibition*, Long Beach, CA, 2014.
- Fayaz, M.; Shariaty, P.; Hashisho, Z.; Phillips, J. H.; Anderson, J. E.; Nichols, M. Using microwave heating to improve the desorption efficiency of high molecular weight VOC from beaded activated carbon. *Environ. Sci. Technol.* **2015a**, *49*, 4536–4542.
- Fayaz, M.; Niknaddaf, S.; Jahandar Lashaki, M.; Shariaty, P.; Hashisho, Z.; Phillips, J.H.; Anderson, J.E.; Nichols, M. The effect of regeneration temperature and heating rate on heel build-up during microwave regeneration. *In Proceedings of the American Institute of Chemical Engineers' Annual Meeting*, Salt Lake City, UT, 2015b.
- Ferro-Garcia, M.A.; Utrera-Hidalgo, E.; Rivera-Utrilla, J.; Moreno-Castilla, C.; Joly, J.P. Regeneration of activated carbons exhausted with chlorophenols. *Carbon* **1993**, *31*, 857–863.
- Ferro-Garcia, M.A.; Joly, J.P.; Rivera-Utrilla, J.; Moreno-Castilla, C. Thermal desorption of chlorophenols from activated carbons with different porosity. *Langmuir* **1995**, *11*, 2648–2651.
- Ferro-Garcia, M. A.; Rivera-Utrilla, J.; Bautista-Toledo, I.; Moreno-Castilla, C., Chemical and thermal regeneration of an activated carbon saturated with chlorophenols. *J. Chem. Technol. Biotechnol.* **1996**, *67*, 183–189.
- Foo, K.Y.; Hameed, B.H. Insights into the modeling of adsorption isotherm systems. *Chem. Eng. J.* **2010**, *156*, 2–10.
- Freundlich, H.M.F. Over the adsorption in solution. *J. Phys. Chem.* **1906**, *57*, 385–471.
- Garcia-Araya, J.F.; Beltran, F.J.; Alvarez, P.A.; Masa, F.J. Activated carbon adsorption of some phenolic compounds present in agroindustrial wastewater. *Adsorption* **2003**, *9*, 107–115.
- Garner, I.A.; Watson-Craik, I.A.; Kirkwood, R.; Senior, E. Dual solute adsorption of 2,4,6-trichlorophenol and N-(2-(2,4,6-trichlorophenoxy) propyl) amine on to activated carbon. *J. Chem. Technol. Biotechnol.* **2001**, *76*, 932–940.
- Goto, M.; Hayaeh, N.; Goto, S. Adsorption and desorption of phenol on anion-exchange resin and activated carbon. *Environ. Sci. Technol.* **1986**, *20*, 463–467.
- Grant, T.M.; King, C.J. Mechanism of irreversible adsorption of phenolic compounds by activated carbons. *Ind. Eng. Chem. Res.* **1990**, *29*, 264–271.

- Ha, S.R.; Vinitnantharat, S. Competitive removal of phenol and 2,4-dichlorophenol in biological activated carbon system. *Environ. Technol.* **2000**, *21*, 387–396.
- Haghseresht, F.; Lu, G. Adsorption characteristics of phenolic compounds onto coal-reject-derived adsorbents. *Energ. Fuel.* **1998**, *12*, 1100–1107.
- Hashisho, Z.; Rood, M.J.; Botich, L. Microwave-swing adsorption to capture and recover vapors from air streams with activated carbon fiber cloth. *Environ. Sci. Technol.* **2005**, *39*, 6851–6859.
- Hashisho, Z.; Emamipour, H.; Rood, M.J.; Hay, K.J.; Kim, B.J.; Thurston, D. Concomitant adsorption and desorption of organic vapor in dry and humid air streams using microwave and direct electrothermal swing adsorption. *Environ. Sci. Technol.* **2008**, *42*, 9317–9322.
- Humayun, R.; Karakas, G.; Dahlstrom, P.R.; Ozkan, U.S.; Tomasko, D.L. Supercritical fluid extraction and temperature-programmed desorption of phenol and its oxidative coupling products from activated carbon. *Ind. Eng. Chem. Res.* **1998**, *37*, 3089–3097.
- Kawasaki, N.; Kinoshita, H.; Oue, T.; Nakamura, T.; Tanada, S. Study on adsorption kinetic of aromatic hydrocarbons onto activated carbon in gaseous flow method. *J. Colloid Interface Sci.* **2004**, *275*, 40–43.
- Khan, F.I.; Ghoshal, A.K. Removal of volatile organic compounds from polluted air. *J. Loss Prev. Process Ind.* **2000**, *13*, 527–545.
- Kilduff, J.E.; King, C.J. Effect of carbon adsorbent surface properties on the uptake and solvent regeneration of phenol. *Ind. Eng. Chem. Res.* **1997**, *36*, 1603–1613.
- Koh, M.; Nakajima, T.; Adsorption of aromatic compounds on C_xN-coated activated Carbon. *Carbon* **2000**, *38*, 1947–1954.
- Langmuir, I. The constitution and fundamental properties of solids and liquids. *J. Am. Chem. Soc.* **1916**, *38*, 2221–2295.
- Langmuir, I. The adsorption of gases on plane surfaces of glass, mica, and platinum. *J. Am. Chem. Soc.* **1918**, *40*, 1361–1403.
- Leng, C.C.; Pinto, N.G. Effects of surface properties of activated carbons on adsorption behavior of selected aromatics. *Carbon* **1997**, *35*, 1375–1385.
- Li, P.; Xiu, G.H.; Jiang, L. Adsorption and desorption of phenol on activated carbon fibers in a fixed bed. *Sep. Sci. Technol.* **2001**, *36*, 2147–2163.

- Li, L.; Liu, S.; Liu, J.; Surface modification of coconut shell based activated carbon for the improvement of hydrophobic VOC removal. *J. Hazard. Mater.* **2011**, *192*, 683–690.
- Lillo-Rodenas, M.A.; Cazorla-Amoros, D.; Linares-Solano, A. Behaviour of activated carbons with different pore size distributions and oxygen groups for benzene and toluene adsorption at low concentrations. *Carbon* **2005**, *43*, 1758–1767.
- Liu, P.K.T.; Feltch, S.M.; Wagner, N.J. Thermal desorption behavior of aliphatic and aromatic hydrocarbons loaded on activated carbon. *Ind. Eng. Chem. Res.* **1987**, *26*, 1540–1545.
- Liu, W.; Vidic, R.D. Optimization of sulfur impregnation protocol for fixed-bed application of activated carbon-based sorbents for gas-phase mercury removal. *Environ. Sci. Technol.* **1998**, *32*, 531–538.
- Liu, P.K.T.; Feltch, S.M.; Merchan, M.D. Regeneration of ortho-chlorophenol-exhausted activated carbons with liquid water at high pressure and temperature. *Water Res.* **2003**, *37*, 1905–1911.
- Lowell, S.; Shields, J.E. *Powder Surface Area and Porosity*; Chapman & Hall: London, New York, USA, **1991**.
- Lu, Q.; Sorial, G.A. The role of adsorbent pore size distribution in multicomponent adsorption on activated carbon. *Carbon* **2004a**, *42*, 3133–3142.
- Lu, Q.; Sorial, G.A. Adsorption of phenolics on activated carbon- impact of pore size and molecular oxygen. *Chemosphere* **2004b**, *55*, 671–679.
- Lu, Q.; Sorial, G.A. Impact of pore size on competitive adsorption of phenolic compounds. *Water Sci. Technol.* **2004c**, *4*, 1–7.
- Lu, Q.; Sorial, G.A. The effect of functional groups on oligomerization of phenolics on activated carbon. *J. Hazard. Mater.* **2007**, *148*, 436–445.
- Lu, Q.; Sorial, G.A. A comparative study of multicomponent adsorption of phenolic compounds on GAC and ACFC. *J. Hazard. Mater.* **2009**, *167*, 89–96.
- Lukomskaya, A.Y.; Tarkovskaya, I.A.; Strelko, V.V. Chemisorption of o-xylene on activated carbons. *Theor. Exp. Chem.* **1986**, *22*, 357–360.
- Magne, P.; Walker Jr., P.L. Phenol adsorption on activated carbons: application to the regeneration of activated carbons polluted with phenol. *Carbon* **1986**, *24*, 101–107.

- Maroto-Valer, M.M.; Dranca, I.; Clifford, D.; Lupascu, T.; Nastas, R.; Leon y Leon, C.A. Thermal regeneration of activated carbons saturated with ortho- and meta-chlorophenols. *Thermochimica Acta* **2006**, *444*, 148–156.
- Matatov-Meytal, Y.I.; Sheintuch, M. Abatement of pollutants by adsorption and oxidative catalytic regeneration. *Ind. Eng. Chem. Res.* **1997**, *36*, 4374–4380.
- Mattson, J.S.; Mark, H.B.; Malbin, M.D.; Weber, W.J.; Crittenden, J.C. Surface chemistry of active carbon: Specific adsorption of phenols. *J. Colloid Interface Sci.* **1969**, *31*, 116–130.
- Nakhla, G.F.; Abuzaid, N.; Farooq, S.; Ala'ama, S. Oxygen-induced enhancement of the adsorptive capacity of activated charcoal. *Environ. Technol.* **1992**, *13*, 181–188.
- Nakhla, G.; Abuzaid, N.; Farooq, S. Activated carbon adsorption of phenolics in oxic systems: Effect of pH and temperature variations. *Water Environ. Res.* **1994**, *66*, 842–850.
- Nevskaia, D.M.; Santianes, A.; Muñoz, V.; Guerrero-Ruiz, A. Interaction of aqueous solutions of phenol with commercial activated carbons: an adsorption and kinetic study. *Carbon* **1999**, *37*, 1065–1074.
- Niknaddaf, S.; Jahandar Lashaki, M.; Shariaty, P.; Hashisho, Z.; Phillips, J.H.; Anderson, J.E.; Nichols, M. Effect of pore size distribution of activated carbon fiber cloth on irreversible adsorption of organic vapors. In *proceedings of 107th Air and Waste Management Association's Annual Conference and Exhibition*, Long Beach, CA, 2014.
- Niknaddaf, S.; Atkinson, J.D.; Shariaty, P.; Jahandar Lashaki, M.; Hashisho, Z.; Phillips, J.H.; Anderson, J.E.; Nichols, M. Heel formation during volatile organic compound desorption from activated carbon fiber cloth. *Carbon* **2016**, *96*, 131–138.
- Osei-Twum, E.Y.; Abuzaid, N.S.; Nahkla, G. Carbon-catalyzed oxidative coupling of phenolic compounds. *B. Environ. Contam. Tox* **1996**, *56*, 513–519.
- Park, S.W.; Lee, W.K. Adsorption and desorption of gaseous methyl iodide in a triethylenediamine impregnated activated carbon bed. *Sep. Technol.* **1993**, *3*, 133–142.
- Popescu, M.; Joly, J. P.; Carre, J.; Danatoiu, C. Dynamical adsorption and temperature-programmed desorption of VOCs (toluene, butyl acetate and butanol) on activated carbons. *Carbon* **2003**, *41*, 739–748.

- Qin, W.; Xiao-yi, L.; Rui, Z.; Chao-jun, L.; Xiao-jun, L.; Wen-ming, Q.; Liang, Z.; Li-cheng, L. Preparation of polystyrene-based activated carbon spheres and their adsorption of dibenzothiophene. *New Carbon Mater.* **2009**, *24*, 55–60.
- Ramirez, D.; Sullivan, P.D.; Rood, M.J.; Hay, K.J. Equilibrium adsorption of phenol-, tire-, and coal-derived activated carbons for organic vapors. *J. Environ. Eng.* **2004**, *130*, 231–241.
- Ramirez, D.; Qi, S.Y.; Rood, M.J. Equilibrium and heat of adsorption for organic vapors and activated carbons. *Environ. Sci. Technol.* **2005**, *39*, 5864–5871.
- Ravi, V.P.; Jasra, R.V.; Bhat, T.S.G. Adsorption of phenol, cresol isomers and benzyl alcohol from aqueous solution on activated carbon at 278, 298 and 323 K. *J. Chem. Technol. Biotechnol.* **1998**, *71*, 173–179.
- Rivera-Utrilla, J.; Ferro-Garcia, M.A.; Bautista-Toledo, I.; Sanchez-Jimenez, C.; Salvador, F.; Merchan, M.D. Regeneration of ortho-chlorophenol-exhausted activated carbons with liquid water at high pressure and temperature. *Water Res.* **2003**, *37*, 1905–1911.
- Ruthven, D.M. *Principles of Adsorption Processes*; John Wiley: New York, NY, USA, 1984.
- Salvador, F.; Merchan, M.D. Study of the desorption of phenol and phenolic compounds from activated carbon by liquid-phase temperature-programmed desorption. *Carbon* **1996**, *34*, 1543–1551.
- Schnelle, K.B.; Brown, C.A. *Air Pollution Control Technology Handbook*; CRC press: Florida, USA, 2002.
- Sheintuch, M.; Matatov-Meytal, Y.I. Comparison of catalytic processes with other regeneration methods of activated carbon. *Catal. Today* **1999**, *53*, 73–80.
- Sorial, G.A.; Suidan, M.T.; Vidic, R.D.; Brenner, R.C. Effect of GAC characteristics on adsorption of organic pollutants. *Water Environ. Res.* **1993**, *65*, 53–57.
- Soto, M.L.; Moure, A.; Dominguez, H.; Parajo, J.C. Recovery, concentration and purification of phenolic compounds by adsorption: A review. *J. Food Eng.* **2011**, *105*, 1–27.
- Suzuki, M.; Misic, D.M.; Koyama, O.; Kawazoe, K. Study of thermal regeneration of spent activated carbons: thermogravimetric measurement of various single component organics loaded on activated carbons. *Chem. Eng. Sci.* **1978**, *33*, 271–279.
- Tamon, H.; Saito, T.; Kishimura, M.; Okazaki, M.; Toei, R. Solvent regeneration of spent activated carbon in wastewater treatment. *J. Chem. Eng. Japan* **1990**, *23*, 426–432.

- Tamon, H.; Atsushi, M.; Okazaki, M. On irreversible adsorption of electron-donating compounds in aqueous solution. *J. Colloid Interface Sci.* **1996**, *177*, 384–390.
- Tamon, H.; Okazaki, M. Desorption characteristics of aromatic compounds in aqueous solution on solid adsorbents. *J. Colloid Interface Sci.* **1996**, *179*, 181–187.
- Tanthapanichakoon, W.; Ariyadejwanich, P.; Japthong, P.; Nakagawa, K.; Mukai, S. R.; Tamon, H. Adsorption-desorption characteristics of phenol and reactive dyes from aqueous solution on mesoporous activated carbon prepared from waste tires. *Water Res.* **2005**, *39*, 1347–1353.
- Tefera, D.T.; Jahandar Lashaki, M.; Fayaz, M.; Hashisho, Z.; Phillips, J.H.; Anderson, J.E.; Nichols, M. Two-dimensional modelling of temperature swing adsorption of volatile organic compounds using beaded activated carbon. *Environ. Sci. Technol.* **2013a**, *47*, 11700–11710.
- Terzyk, A.P. Further insights into the role of carbon surface functionalities in the mechanism of phenol adsorption. *J. Colloid Interface Sci.* **2003**, *268*, 301–329.
- Terzyk, A.P. The impact of carbon surface chemical composition on the adsorption of phenol determined at the real oxic and anoxic conditions. *Appl. Surf. Sci.* **2007**, *253*, 5752–5755.
- Tessmer, C.H.; Vidic, R.D.; Uranowski, L.J. Impact of oxygen-containing surface functional groups on activated carbon adsorption of phenols. *Environ. Sci. Technol.* **1997**, *31*, 1872–1878.
- Tobias, H.; Soffer, A. Chemisorption of halogen on carbons—I. Stepwise chlorination and exchange of C-Cl with C-H bonds. *Carbon* **1985**, *23*, 281–289.
- Uranowski, L.J.; Tessmer, C.H.; Vidic, R.D. The effect of surface metal oxides on activated carbon adsorption of phenolics. *Water Res.* **1998**, *32*, 1841–1851.
- Vidic, R.D.; Suidan, M.T.; Traegner, U.K.; Nakhla, G.F. Adsorption isotherms: Illusive capacity and role of oxygen. *Water Res.* **1990**, *24*, 1187–1195.
- Vidic, R.D.; Suidan, M.T. Role of dissolved oxygen on the adsorptive capacity of activated carbon for synthetic and natural organic matter. *Environ. Sci. Technol.* **1991**, *25*, 1612–1618.
- Vidic, R.D.; Sorial, G.A.; Papadimas, S.P.; Suidan, M.T.; Speth, T.F. Effect of molecular oxygen on the scale-up of GAC adsorbents. *J. Am. Water Works Assoc.* **1992**, *84*, 98–105.

- Vidic, R.D.; Suidan, M.T.; Brenner, R.C. Oxidative coupling of phenols on activated carbon: impact on adsorption equilibrium. *Environ. Sci. Technol.* **1993**, *27*, 2079–2085.
- Vidic, R.D.; Suidan, M.T.; Brenner, R.C. Impact of oxygen mediated oxidative coupling on adsorption kinetics. *Water Res.* **1994a**, *28*, 263–268.
- Vidic, R.D.; Suidan, M.T.; Sorial, G.A.; Brenner, R.C. Effect of molecular oxygen on adsorptive capacity and extraction efficiency of granulated activated carbon for three ortho-substituted phenols. *J. Hazard. Mater.* **1994b**, *38*, 373–388.
- Vidic, R.D.; Tessmer, C.H.; Uranowski, L.J. Impact of surface properties of activated carbons on oxidative coupling of phenolic compounds. *Carbon* **1997**, *35*, 1349–1359.
- Vinitnantharat, S.; Baral, A.; Ishibashi, Y.; Ha, S.R. Quantitative bioregeneration of granular activated carbon loaded with phenol and 2,4-dichlorophenol. *Environ. Technol.* **2001**, *22*, 339–344.
- Wang, H.; Jahandar Lashaki, M.; Fayaz, M.; Hashisho, Z.; Phillips, J.H.; Anderson, J.E.; Nichols, M. Adsorption and desorption of mixtures of organic vapors on beaded activated carbon. *Environ. Sci. Technol.* **2012**, *46*, 8341–8350.
- Wark, K.; Warner, C.F.; Davis, W.T. *Air Pollution: Its Origin and Control*; Addison-Wesley: 1998.
- Yan, L.; Sorial, G.A. Chemical activation of bituminous coal for hampering oligomerization of organic contaminants. *J. Hazard. Mater.* **2011**, *197*, 311–319.
- Yonge, D.R.; Keinath, T.M.; Poznanska, K.; Jiang, Z.P. Single-solute irreversible adsorption on granular activated carbon. *Environ. Sci. Technol.* **1985**, *19*, 690–694.

CHAPTER 3. EFFECT OF THE ADSORBATE KINETIC DIAMETER ON THE ACCURACY OF THE DUBININ-RADUSHKEVICH EQUATION FOR MODELING ADSORPTION OF ORGANIC VAPORS ON ACTIVATED CARBON¹

3.1 Introduction

Microporous adsorbents such as activated carbon can be effectively used for controlling organic vapors emission from a wide range of industrial gas streams (Sullivan et al., 2004; Ramirez et al., 2005; Kotdawala et al., 2008; Li et al., 2011). The adsorption capacity of activated carbon is an important parameter for the design of a reliable adsorption system. Experimentally determining the adsorption capacity of AC needs considerable effort, time, and cost especially at low concentrations or for the case of hazardous compounds (Wood, 1992; Duchowicz et al., 2006; Hung and Lin, 2007). Hence, there is interest in developing reliable models to predict the adsorption capacity of adsorbents (Wu et al., 2002; Duchowicz et al., 2006; Hung and Lin, 2007).

The D-R equation, based on Polanyi's potential theory of physical adsorption, could be used for estimating the adsorption capacity for VOCs on microporous adsorbents such as activated carbon (Wood 2001; Hung and Lin, 2007). The D-R equation can include the effect of temperature as well as the properties of both adsorbent and adsorbate (Wood 2002). According to the D-R equation, the volumetric adsorption capacity (W) is related to the adsorption potential

¹ A version of this chapter has been published as: Jahandar Lashaki, M.; Fayaz, M.; Niknaddaf, S.; Hashisho, Z. Effect of the adsorbate kinetic diameter on the accuracy of the Dubinin-Radushkevich equation for modeling adsorption of organic vapors on activated carbon. *J. Hazard. Mater.* **2012**, 241–242, 154–163. Reproduced with permission from Elsevier.

(ε) as given by (Golovoy and Braslaw, 1981; Urano et al., 1982; Ramirez et al., 2004; Jiun-Horng et al., 2008; Long et al., 2012):

$$W = W_o \exp\left(-k \frac{\varepsilon^2}{\beta^2}\right) \quad (1)$$

and

$$\varepsilon = RT \ln \frac{P_o}{P} \quad (2)$$

where W is the volume of adsorbed adsorbate per gram of adsorbent ($\frac{cm^3}{g}$), W_o is the limiting pore volume of the adsorbent ($\frac{cm^3}{g}$), k is a constant related to the adsorbate as well as adsorbent ($\frac{J}{mol}$)⁻² (Qi et al., 2000), β is the affinity coefficient which permits the comparison of the adsorption potential of the test adsorbate to that of a reference adsorbate, R is the ideal gas constant ($8.314 \frac{J}{mol.K}$), T is the absolute temperature (K), P_o is the saturated vapor pressure of the test adsorbate at test temperature, and P the equilibrium vapor pressure of the test adsorbate. The affinity coefficient depends on the properties of the adsorbate and is independent of the adsorbent properties; therefore, it could be a reliable basis for developing a model for predicting the adsorption capacity (Nirmalakhandan and Speece, 1983).

To predict the adsorption capacity of an adsorbent for an adsorbate with Eq. 1, the affinity coefficient has to be calculated based on the dominant force of adsorption. For nonpolar and weakly polar adsorbates, dispersion (London potential) force is the dominant force of adsorption. In this case, β could be estimated using the ratio of the molar volumes of the test (V) and reference (V_{ref}) adsorbates (Golovoy and Braslaw, 1981; Wood, 2001):

$$\beta = \frac{V}{V_{ref}} \quad (3)$$

For cases where forces and interactions other than dispersion forces are important, β could be calculated based on the ratio of electronic polarization of the test (P_e) and reference (P_{eref}) adsorbates (Golovoy and Braslaw, 1981; Wood, 2001):

$$\beta = \frac{P_e}{P_{eref}} \quad (4)$$

and

$$P_e = \frac{(n^2 - 1)M}{(n^2 + 2)\rho} \quad (5)$$

where n is the refractive index of the adsorbate in liquid phase, M is the molecular weight of the adsorbate ($\frac{g}{mol}$), and ρ is the density of the adsorbate in liquid phase ($\frac{g}{cm^3}$).

β could also be estimated based on the ratio of molecular parachors, Ω (Golovoy and Braslaw, 1981; Wood, 2001):

$$\beta = \frac{\Omega}{\Omega_{ref}} \quad (6)$$

and

$$\Omega = \frac{\gamma^{\frac{1}{4}} * M}{\rho} \quad (7)$$

where γ is the surface tension ($\frac{dynes}{cm}$) of the adsorbate in liquid phase.

Substituting Eqs. 3, 4, or 6 for β in the D-R equation (Eq. 1) yields the following equations to predict the adsorption capacity of the adsorbent:

$$W = W_o \exp \left(-k \frac{\varepsilon^2 (V_{ref})^2}{V^2} \right) \quad (8)$$

$$W = W_o \exp \left(-k \frac{\varepsilon^2 (P_{eref})^2}{(P_e)^2} \right) \quad (9)$$

$$W = W_o \exp \left(-k \frac{\varepsilon^2 (\Omega_{ref})^2}{\Omega^2} \right) \quad (10)$$

Previous research (Reucroft et al., 1971; Golovoy and Braslaw, 1981; Noll et al., 1989) mainly focused on the effect of the polarity of the adsorbates and reference compounds; however, contradictory results were obtained for the effect of this parameter. The experimental adsorption capacities for 15 organic adsorbates on microporous activated carbon were compared to those obtained with the D-R model based on polarizabilities and parachors of the adsorbates. The results showed that using a reference adsorbate with similar polarity to the test adsorbate could reduce the deviation from experimental values particularly when polarizability-based β values are used for polar adsorbates (Reucroft et al., 1971). Similarly, Noll et al. (1989) used molar volumes, molecular parachors, and polarization methods and revealed that using a reference adsorbate with similar polarity to the test adsorbate could decrease the error in calculating the affinity coefficients of the test adsorbates. Conversely, Golovoy and Braslaw (1981) used all of the aforementioned equations for calculating β and the adsorption capacity for 14 organic adsorbates on microporous activated carbon and compared the results to experimentally determined adsorption capacities (from breakthrough tests). They selected three reference adsorbates with different polarities and found that using a reference adsorbate with similar polarity to the test adsorbate doesn't necessarily improve the fit between measured and calculated affinity coefficients. Wu et al. (2002) calculated the affinity coefficients of eight organic compounds from different organic groups based on the adsorbates' physico-chemical properties such as molar volume, molecular weight, the interaction energy between the adsorbate and the adsorbent (E_{inter}) and compared the yielded coefficients to those based on molar

polarizability, molar volume, and parachor. Their model could predict the experimental results with relatively lower root-mean-square errors of predication (RMSEP=0.09 compared to 0.18, 0.18, and 0.14 in case of using affinity coefficients based on parachor, molar volume, and molar polarizability, respectively); however, inconsistencies in E_{inter} prediction were reported. These contradictory results and inconsistencies show the lack of understanding of the parameter(s) influencing the accuracy of the D-R model.

Based on molecular size exclusion characteristics of the adsorbent, narrow pores are not available for adsorbates with kinetic diameters larger than the width of the pore while the specified pore might be accessible for a smaller adsorbate. As a result, the limiting pore volume (W_0) of the adsorbent may vary based on the kinetic diameter of the adsorbate. The purpose of this paper is to investigate the effect of the choice of the reference adsorbate on the accuracy of the D-R equation in predicting the adsorption capacity of organic compounds. We hypothesize that the accuracy of the D-R equation would increase if the reference and test adsorbates have similar kinetic diameter. To the best of our knowledge, no report has investigated this hypothesis. Four reference adsorbates with distinct kinetic diameters were used to calculate the affinity coefficients using molar volumes, electronic polarization, and molecular parachors. Then the affinity coefficients were used with the D-R equation to calculate the adsorption capacity for 13 organic adsorbates on microporous activated carbon. Compounds are considered to have similar kinetic diameter if the absolute difference in their kinetic diameters is $\leq 0.6 \text{ \AA}$. This criterion was developed to have at least one reference adsorbate with similar kinetic diameter for all test adsorbates. The kinetic diameters for two of the reference adsorbates were similar to explore the effect of dipole moment on the deviation of the model. Finally, the results were compared to experimentally determined adsorption capacities over a wide range of relative

pressure (0.01 to 0.9) to verify the above hypothesis. The outcomes of this study can be useful in designing an effective abatement system for the purpose of organic vapors capturing from polluted gaseous streams with minimal effort, time, and cost.

3.2 Materials and Methods

3.2.1 Adsorbent

The adsorbent used in this study was microporous BAC from Kureha Corporation. The BAC has an average particle diameter of 0.70 mm while 99% by mass was between 0.60 and 0.84 mm. The BAC has a BET surface area, micropore and mesopore volumes of 1339 m²/g, 0.44 cm³/g and 0.12 cm³/g, respectively (Jahandar Lashaki et al., 2012a; Wang et al., 2012). Pore size distribution of the BAC indicates that the majority of the pores lies in the micropore (< 20 Å) as indicated in Figure 3-1. Prior to use, the BAC was dried in a laboratory oven at 150 °C for 24 hours and then kept in a desiccator.

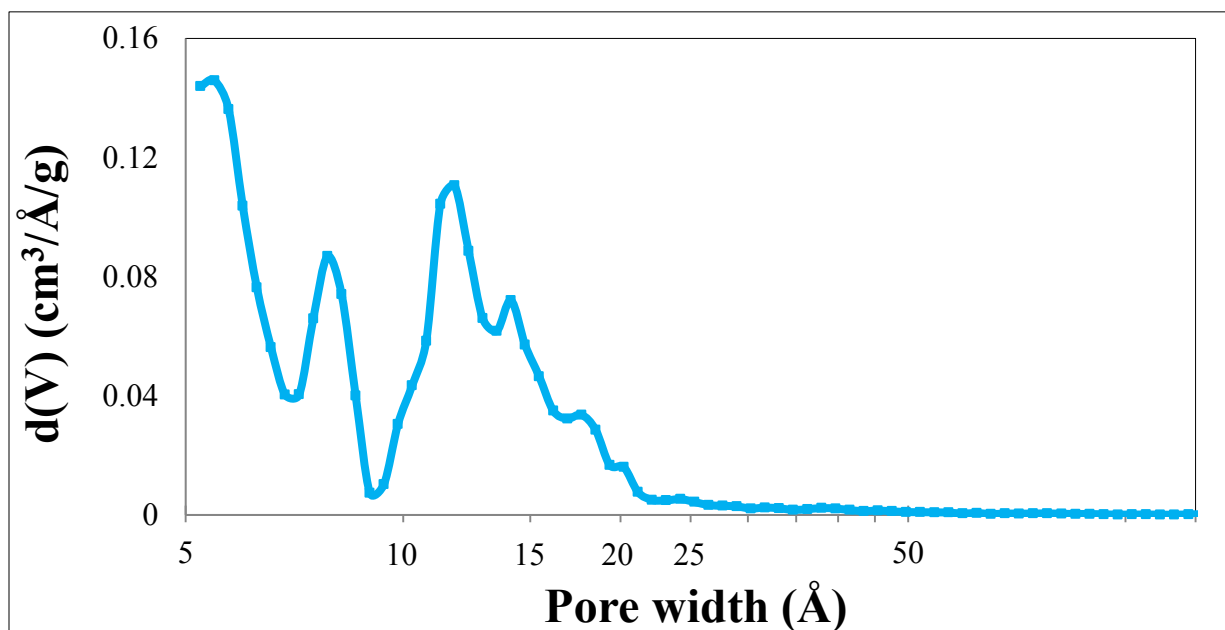

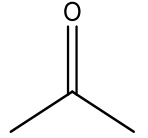
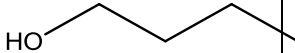
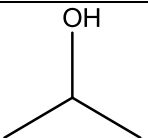
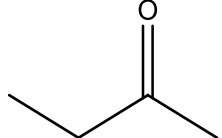
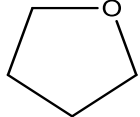


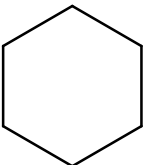
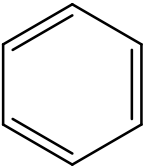
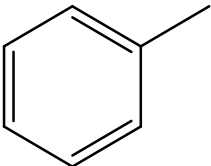
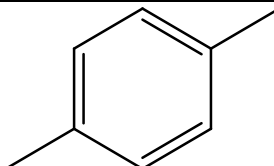
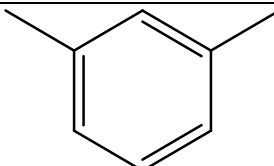
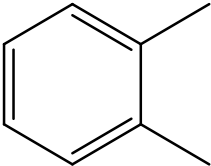
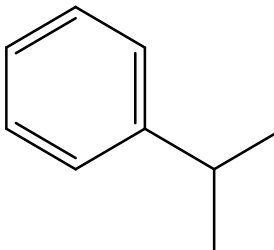
Figure 3-1. Pore size distribution of the beaded activated carbon.

3.2.2 Adsorbates

Thirteen adsorbates representing various organic groups were tested. Table 3-1 shows the list of the adsorbates with their kinetic diameters and other relevant physical properties. These compounds are commonly found in many environmental systems. Different kinetic diameters were reported in the literature for some of the test adsorbates such as *n*-hexane, toluene, and cumene. In this case, the value reported by multiple independent references was used.

Table 3-1. List of the adsorbates with their kinetic diameters (references provided in the table) and physical properties (Knovel Critical Tables, 2008).

Compound	Chemical structure	Kinetic diameter (Å)	γ (dynes/cm ²)	n	ρ (g/cm ³)	M (g/mol)	P_o (mmHg)
<i>n</i> -hexane		4.3 (Breck, 1974; Canham and Groszek, 1992)	17.98	1.375	0.656	86.16	151.38
acetone		4.4 (Jones, 2010)	23.06	1.357	0.786	58.08	229.52
1-butanol		4.3 (Tuan et al., 2002)	25.67	1.397	0.806	74.12	6.64
2-propanol		4.7 (Tuan et al., 2002)	22.4	1.375	0.783	60.10	42.74
2-butanone		5.25 (Monneyron et al., 2003)	23.96	1.376	0.799	72.11	90.00
THF		6.3 (Lee et al., 2007)	24.98	1.405	0.880	72.11	162.18

Compound	Chemical structure	Kinetic diameter (Å)	γ (dynes/cm ²)	n	ρ (g/cm ³)	M (g/mol)	P _o (mmHg)
cyclohexane		6.0 (Magalhaes et al., 1998)	24.65	1.424	0.773	84.16	100.18
benzene		5.85 (Tung et al., 2000)	28.22	1.497	0.873	78.11	95.08
toluene		5.85 (Tung et al., 2000; Dehdashti et al., 2011)	27.93	1.497	0.865	92.14	28.56
<i>p</i> -xylene		5.85 (Karsli et al., 2003)	27.92	1.493	0.858	106.17	8.86
<i>m</i> -xylene		6.8 (Karsli et al., 2003)	28.26	1.497	0.861	106.17	8.35
<i>o</i> -xylene		6.8 (Karsli et al., 2003)	29.6	1.503	0.876	106.17	6.60
cumene		6.8 (Al-Khattaf and de Lasa, 2002)	27.69	1.493	0.860	120.19	4.56

3.2.3 Reference Adsorbates

n-hexane, acetone, benzene, and *m*-xylene were selected as reference compounds. These compounds have distinct kinetic diameters ranging from 4.3 to 6.8 Å which allows investigating the effect of this parameter on the accuracy of the model. The kinetic diameters of *n*-hexane and acetone are similar (4.3 and 4.4 Å, respectively) to survey the effect of dipole moment of the reference compound on the goodness of fit.

3.2.4 Adsorption Experiments

The adsorption isotherms were obtained gravimetrically using a sorption analyzer (TA Instruments, model VTI-SA) at 25 °C using nitrogen as carrier gas. The system logged the equilibrium weight of the BAC sample (3 to 5 mg) in response to a step change in the concentration of the adsorbate (relative pressure range of 0.01 to 0.9) in the carrier gas. The equilibrium was assumed to be reached when the weight changed less than 0.001 wt% in 5 min. Adsorption isotherms for all reference adsorbates and some of the test adsorbates were duplicated and average values are reported herein.

3.2.5 Relative Error Calculation

The measured adsorption capacities were then compared to values predicted by the D-R model at the same relative pressure. The mean relative error between the measured and predicted results was used to quantitatively evaluate the goodness of fit for the experimental and modeled results. The mean relative error between the measured and predicted adsorption isotherms was calculated as follows:

$$\text{Mean relative error} = \frac{1}{N_i} \sum_{i=1}^{N_i} \left[\frac{|W_{pred} - W_{exp}|}{W_{exp}} * 100 \right] \quad (11)$$

where W_{pred} is the amount of material adsorbed on the adsorbent predicted with the model; W_{exp} is the amount of material adsorbed on the adsorbent based on the experiment; and N_i is the number of data points for a specified isotherm. Figure 3-2 demonstrates the flow chart of the modeling procedure.

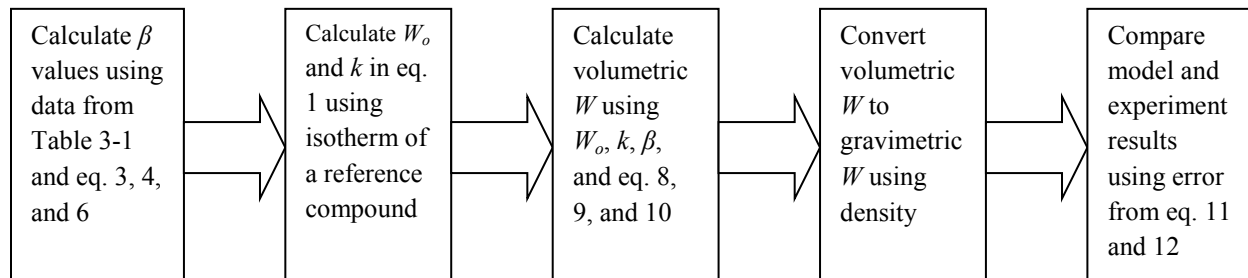


Figure 3-2. Flow chart for prediction of the adsorption capacity.

The total mean relative error between the measured and predicted adsorption isotherms for all adsorbates was calculated as follows:

$$Total\ mean\ relative\ error = \frac{1}{N_j} \sum_{j=1}^{N_j} \left(\frac{1}{N_i} \sum_{i=1}^{N_i} \left[\frac{|W_{pred} - W_{exp}|}{W_{exp}} * 100 \right] \right) \quad (12)$$

where N_j is the number of adsorption isotherms.

3.3 Results and Discussion

3.3.1 Reference Compounds

Experimental adsorption isotherms were fitted with the D-R model (Eq. 1) to calculate W_o and k of the reference compounds. Least squares analysis of the experimental data yielded the following D-R correlations:

$$n - hexane: W = 0.522 * \exp \left(-10^{-9} * \frac{\varepsilon^2}{\beta^2} \right); \quad r^2 = 0.9887; \quad W_o = 0.522 \text{ cm}^3/\text{g} \quad (13)$$

$$acetone: W = 0.521 * \exp \left(-2 * 10^{-9} * \frac{\varepsilon^2}{\beta^2} \right); \quad r^2 = 0.9847; \quad W_o = 0.521 \text{ cm}^3/\text{g} \quad (14)$$

$$\text{benzene: } W = 0.487 * \exp\left(-10^{-9} * \frac{\varepsilon^2}{\beta^2}\right); \quad r^2 = 0.9818; \quad W_o = 0.487 \text{ cm}^3/\text{g} \quad (15)$$

$$m - \text{xylene: } W = 0.444 * \exp\left(-8 * 10^{-10} * \frac{\varepsilon^2}{\beta^2}\right); \quad r^2 = 0.9961; \quad W_o = 0.444 \text{ cm}^3/\text{g} \quad (16)$$

The limiting pore volume for *n*-hexane and acetone are quite similar reflecting the fact that both adsorbates have similar kinetic diameter. However, *m*-xylene has smaller limiting pore volume than benzene or *n*-hexane possibly due to its larger kinetic diameter. In this case, a portion of the narrow micropores are not accessible to the adsorbate. Based on the results, the limiting pore volume of the adsorbent might be predicted using the pore size distribution of the adsorbent and the kinetic diameter of the adsorbate (Hung and Lin, 2007).

3.3.2 Affinity Coefficients

Table 3-2 shows the calculated affinity coefficients (using Eqs. 3 to 7) for each adsorbate and corresponding relative errors between measured and predicted adsorption capacity (using Eqs. 8, 9, and 10).

Table 3-2. Affinity coefficients and corresponding relative errors considering different relative pressure ranges (compounds with similar kinetic diameter to that of the reference adsorbate are marked in bold).

Reference adsorbate	Test adsorbate	Affinity coefficients (β)			Mean relative error (%) in W for $0.01 \leq P/P_o \leq 0.9$			Mean relative error (%) in W for $0.01 \leq P/P_o \leq 0.1$		
		Eq. 3	Eq. 4	Eq. 6	Eq. 8	Eq. 9	Eq. 10	Eq. 8	Eq. 9	Eq. 10
	<i>n</i>-hexane	1	1	1	0.7	0.7	0.7	1.2	1.2	1.2
	acetone	0.562	0.538	0.599	3.2	4.0	2.2	6.8	8.9	4.6
	1-butanol	0.700	0.737	0.765	0.8	0.4	0.6	1.6	0.5	0.5
	2-propanol	0.584	0.585	0.617	5.1	5.2	6.3	6.9	7.0	9.5
	2-butanone	0.687	0.689	0.738	7.4	7.4	8.4	6.9	7.0	9.2

Reference adsorbate	Test adsorbate	Affinity coefficients (β)			Mean relative error (%) in W for $0.01 \leq P/P_o \leq 0.9$			Mean relative error (%) in W for $0.01 \leq P/P_o \leq 0.1$		
		Eq. 3	Eq. 4	Eq. 6	Eq. 8	Eq. 9	Eq. 10	Eq. 8	Eq. 9	Eq. 10
<i>n</i> -hexane	THF	0.624	0.668	0.677	7.8	9.0	9.2	5.3	7.9	8.4
	cyclohexane	0.829	0.923	0.897	11.5	12.6	12.3	12.8	15.3	14.7
	benzene	0.681	0.871	0.762	4.8	7.9	6.4	2.0	8.6	5.4
	toluene	0.811	1.036	0.905	6.1	8.2	7.2	3.9	8.6	6.2
	<i>p</i> -xylene	0.942	1.196	1.051	7.1	8.7	7.9	7.1	10.7	9.0
	<i>m</i> -xylene	0.939	1.200	1.051	18.7	20.6	19.7	20.4	22.5	24.5
	<i>o</i> -xylene	0.923	1.191	1.045	17.9	19.9	19.0	20.7	25.3	23.2
	cumene	1.064	1.351	1.185	25.0	26.8	26.0	38.3	42.3	40.4
acetone	<i>n</i>-hexane	1.778	1.858	1.671	1.9	2.1	1.6	3.9	4.3	3.2
	acetone	1	1	1	1.5	1.5	1.5	2.8	2.8	2.8
	1-butanol	1.245	1.369	1.278	2.0	2.8	2.2	4.0	5.8	4.5
	2-propanol	1.039	1.086	1.031	9.2	9.9	9.1	16.3	14.5	15.8
	2-butanone	1.221	1.279	1.233	10.2	10.7	10.3	13.2	14.3	13.4
	THF	1.109	1.241	1.131	11.2	12.5	11.4	12.9	15.8	13.4
	cyclohexane	0.792	0.797	0.795	13.4	14.4	13.5	17.3	19.4	17.6
	benzene	1.211	1.618	1.274	7.5	9.8	8.0	8.1	13.1	9.1
	toluene	1.442	1.926	1.512	7.9	9.6	8.3	8.1	11.6	8.8
	<i>p</i> -xylene	1.675	2.223	1.757	8.4	9.7	8.7	10.4	13.0	10.9
	<i>m</i> -xylene	1.669	2.230	1.756	20.3	21.7	20.6	24.1	27.2	24.8
	<i>o</i> -xylene	1.640	2.213	1.746	19.6	21.1	20.0	24.7	28.1	25.6
	cumene	1.891	2.509	1.980	26.6	27.9	26.8	41.9	44.9	42.5
	<i>n</i> -hexane	1.468	1.149	1.312	4.9	5.4	5.1	3.0	3.9	3.3
	acetone	0.826	0.618	0.785	5.8	7.9	6.0	5.2	9.5	5.6
	1-butanol	1.028	0.846	1.004	4.8	5.2	4.8	2.8	3.7	2.8
	2-propanol	0.858	0.810	0.671	6.9	4.5	6.3	12.7	6.5	11.3
	2-butanone	1.009	0.968	0.791	4.4	2.1	4.1	8.7	3.7	8.0

Reference adsorbate	Test adsorbate	Affinity coefficients (β)			Mean relative error (%) in W for $0.01 \leq P/P_o \leq 0.9$			Mean relative error (%) in W for $0.01 \leq P/P_o \leq 0.1$		
		Eq. 3	Eq. 4	Eq. 6	Eq. 8	Eq. 9	Eq. 10	Eq. 8	Eq. 9	Eq. 10
benzene	THF	0.916	0.767	0.888	5.5	3.7	5.2	9.0	4.8	8.3
	cyclohexane	1.217	1.060	1.176	6.9	6.0	6.7	11.6	9.8	11.2
	benzene	1	1	1	1.7	1.7	1.7	3.8	3.8	3.8
	toluene	1.190	1.190	1.187	1.7	1.7	1.7	3.0	3.0	3.0
	<i>p</i>-xylene	1.383	1.374	1.379	2.1	2.1	2.1	4.6	4.6	4.6
	<i>m</i>-xylene	1.378	1.379	1.379	11.2	11.2	11.2	14.2	14.2	14.2
	<i>o</i>-xylene	1.355	1.371	1.368	12.5	12.6	12.6	18.3	18.4	18.4
	cumene	1.562	1.551	1.555	11.5	11.5	11.5	17.5	17.4	17.4
<i>m</i> -xylene	<i>n</i> -hexane	1.065	0.833	0.952	13.6	14.9	14.1	12.1	15.0	13.3
	acetone	0.599	0.448	0.570	14.9	19.8	15.6	15.0	25.5	16.6
	1-butanol	0.746	0.614	0.728	13.8	15.8	14.0	12.5	16.9	12.9
	2-propanol	0.622	0.487	0.587	10.0	12.1	10.2	8.0	12.2	8.4
	2-butanone	0.732	0.574	0.702	7.0	9.7	7.2	5.4	11.3	5.8
	THF	0.665	0.56	0.644	6.0	8.5	6.4	5.3	10.6	6.1
	cyclohexane	0.883	0.769	0.853	4.1	5.0	4.2	1.6	3.4	1.8
	benzene	0.726	0.725	0.725	9.0	9.0	9.0	9.1	9.1	9.1
	toluene	0.864	0.863	0.861	8.5	8.5	8.5	8.7	8.7	8.8
	<i>p</i> -xylene	1.004	0.996	1.000	8.6	8.6	8.6	8.1	8.1	8.1
	<i>m</i>-xylene	1	1	1	2.2	2.2	2.2	5.0	5.0	5.0
	<i>o</i>-xylene	0.983	0.992	0.994	4.5	4.4	4.4	8.4	8.3	8.3
	cumene	1.133	1.125	1.128	5.8	5.8	5.8	10.7	10.7	10.7

Based on the results in Table 3-2, the affinity coefficients are independent of the method of calculation when the reference and test adsorbates are from the same organic group. For example, considering benzene as the reference adsorbate for aromatic adsorbates such as toluene, *m*-xylene, *o*-xylene, *p*-xylene, and cumene will result in similar ($\leq 1.2\%$ difference) calculated

affinity coefficients using equations 3, 4, and 6. In this case, the corresponding mean relative errors in the prediction of the adsorption isotherms are also similar ($\leq 1.2\%$ difference). Same conclusion is obtained when using acetone and *m*-xylene as reference adsorbate for 2-butanone and aromatic compounds, respectively.

Table 3-2 also depicts the mean relative errors between measured and predicted adsorption capacity based on different methods for β calculation. In most of the cases, the errors are minimal when using equation 8 followed by values obtained from equations 9 and 10. The total mean relative errors for all adsorbates using equations 8, 9, and 10 are 8.9, 9.7, and 10.1%, respectively for *n*-hexane, 10.7, 10.9, and 11.8, respectively for acetone, 6.1, 6.1, and 5.8, respectively for benzene, and 8.3, 8.5, and 9.6, respectively for *m*-xylene. The errors at low relative pressure range ($P/P_0=0.01$ to 0.1) are larger than that at higher relative pressure range ($0.1 \leq P/P_0 \leq 0.9$) possibly due to deviation of D-R equation from Henry's law at low loading, as reported by other researchers (Hutson and Yang, 1997; Sullivan et al., 2007). In order to have a thermodynamically consistent isotherm, the isotherm should reach a finite Henry's law slope at low concentrations, while D-R equation reaches a Henry's law slope of zero which results in large deviation (Hutson and Yang, 1997; Sullivan et al., 2007). This phenomenon is more significant in case of large molecules such as *m*-xylene, *o*-xylene, and cumene. Large errors in predicting the isotherms of these compounds might be attributed to their large molecular size which causes a slow diffusion at low relative pressure within the pores of the adsorbent. Due to the aforementioned equilibrium criteria of 0.001% weight change in 5 minutes, the gravimetric sorption analyzer might assume reaching equilibrium while adsorption is slowly progressing. Similar observations are reported elsewhere (Yang et al., 2011).

Based on the relative errors between measured and predicted adsorption capacities, a difference in adsorption behavior of *m*-xylene, *o*-xylene, and *p*-xylene, could be observed. The cross sectional areas of these compounds are 37.9, 37.5, and 38.0 Å², respectively, which are quite similar (Guo et al., 2000). Despite this fact, the adsorption behavior of *p*-xylene could be predicted with higher accuracy using benzene as the reference compound while that of *o*-xylene is consistent with *m*-xylene prediction. This behavior could be because the kinetic diameter of *p*-xylene (KD=5.85 Å) is smaller than that of *o*-xylene (KD=6.8 Å) or *m*-xylene (KD=6.8 Å). Due to the para position of the methyl groups on *p*-xylene, the adsorbate would enter the pores by its smallest plane while *m*-xylene and *o*-xylene have to enter it by their largest plane; consequently a number of pores are accessible to *p*-xylene only (but not to *o*-xylene or *m*-xylene) and the limiting pore volume for *p*-xylene is consistent with that of benzene (Yang et al., 2011).

3.3.3 Adsorption Isotherms

Figure 3-3 depicts the experimental and predicted, gravimetric isotherms (calculated with eqs. 8, 9, and 10) for 1-butanol, toluene, THF, and *o*-xylene using *n*-hexane and acetone as reference adsorbates. All measured and predicted adsorption isotherms (gravimetric and volumetric) are provided in Appendix A. All experimental isotherms reached a plateau approximately at $P/P_0 \geq 0.2$. Figure 3-3 qualitatively proves that using a reference adsorbate with similar kinetic diameter to that of the test adsorbate yields a better fit between measured and predicted adsorption capacity. Figure 3-3a-d show that the predicted isotherms are increasingly deviating from the experimental isotherms as the kinetic diameter of the test adsorbate deviates from that of *n*-hexane, the reference adsorbate.

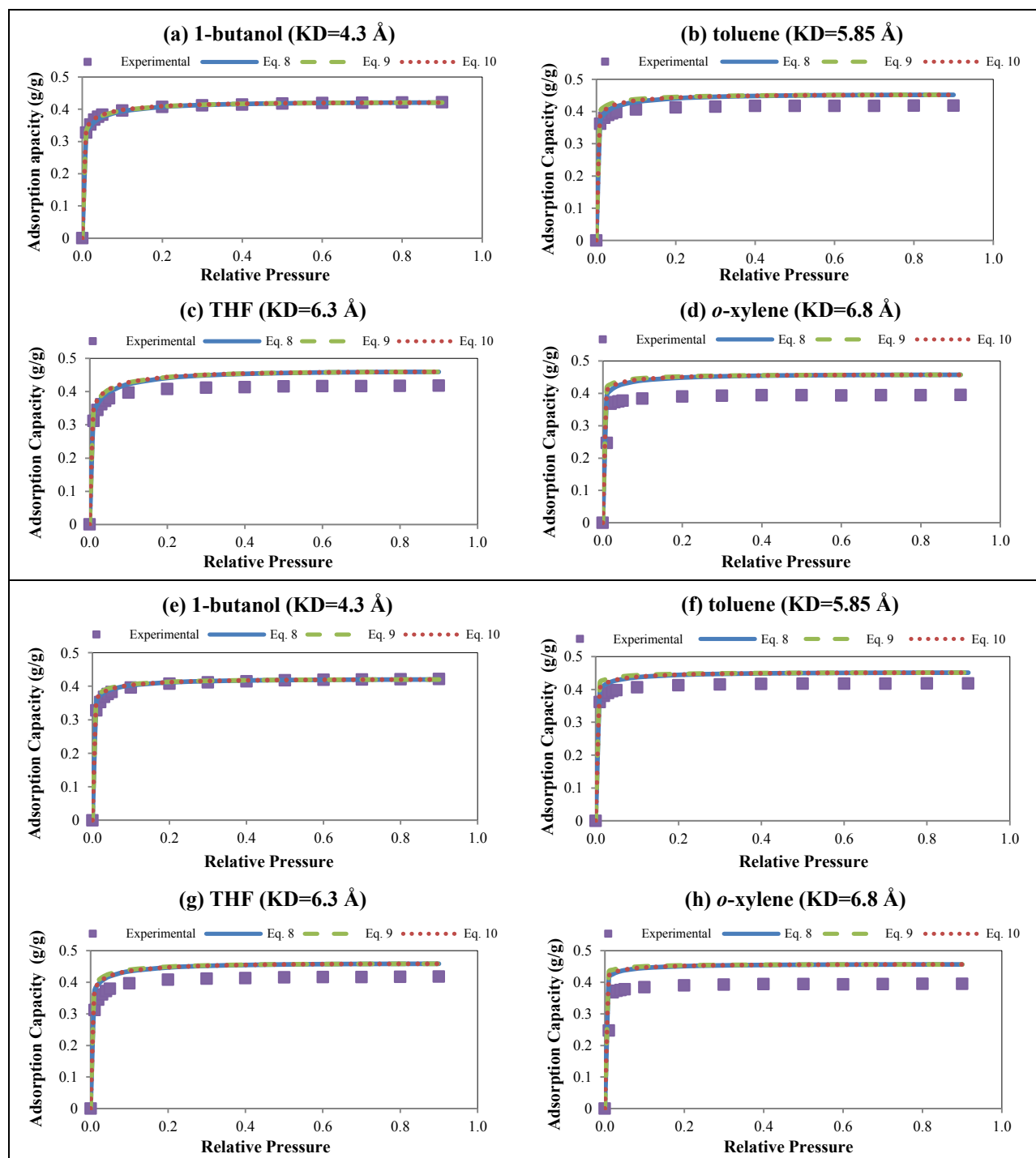


Figure 3-3. Measured and predicted, gravimetric adsorption isotherms for (a) 1-butanol, (b) toluene, (c) THF, and (d) *o*-xylene using *n*-hexane (KD=4.3 Å) as reference adsorbate and for (e) 1-butanol, (f) toluene, (g) THF, and (h) *o*-xylene using acetone (KD=4.4 Å) as the reference adsorbate.

Same trend is observed when using acetone as reference adsorbate (Figure 3-3e-h). These two reference adsorbates have kinetic diameters of 4.3 and 4.4 Å and can penetrate into narrow micropores, which are not accessible to larger molecules. If *n*-hexane and acetone were used for predicting the adsorption isotherm of a compound with similar kinetic diameter such as 1-butanol (KD=4.3 Å), then the errors would be negligible (Figure 3-3a and e). Conversely, using these compounds as reference adsorbate for larger adsorbates such as toluene (KD=5.85 Å), THF (KD=6.3 Å), and *o*-xylene (KD=6.8 Å) will overestimate their adsorption isotherms.

Figure 3-4 shows the experimental and predicted, gravimetric isotherms for 1-butanol, toluene, THF, and *o*-xylene using benzene and *m*-xylene as the reference compound. Choosing benzene (KD=5.85 Å) as the reference adsorbate results in the best fit for toluene (KD=5.85 Å) because of the similarity of their kinetic diameters (Figure 3-4b), while, it underestimates the adsorption isotherm for 1-butanol (KD=4.3 Å) and overestimates the adsorption isotherm for *o*-xylene (KD=6.8 Å) because the former has a smaller kinetic diameter while the latter has a larger kinetic diameter than benzene. Similarly, *m*-xylene (KD=6.8 Å) has the best fit for *o*-xylene (with same kinetic diameter) but it underestimates the isotherms for all other adsorbates possibly due to its large kinetic diameter.

THF isotherms could be the best example for demonstrating the hypothesis. THF kinetic diameter is between those of benzene and *m*-xylene. Based on the hypothesis, it is expected to obtain an isotherm which could be estimated by both of these reference compounds. Figure 3-4c and g depicts the predicted isotherms versus the experimental ones for THF. It is obvious that THF's experimental isotherm lied between the isotherms predicted with benzene and *m*-xylene as reference adsorbates, as it is slightly overestimated (mean relative error of 4.7%) and underestimated (mean relative error of 6.9%) by benzene and *m*-xylene, respectively.

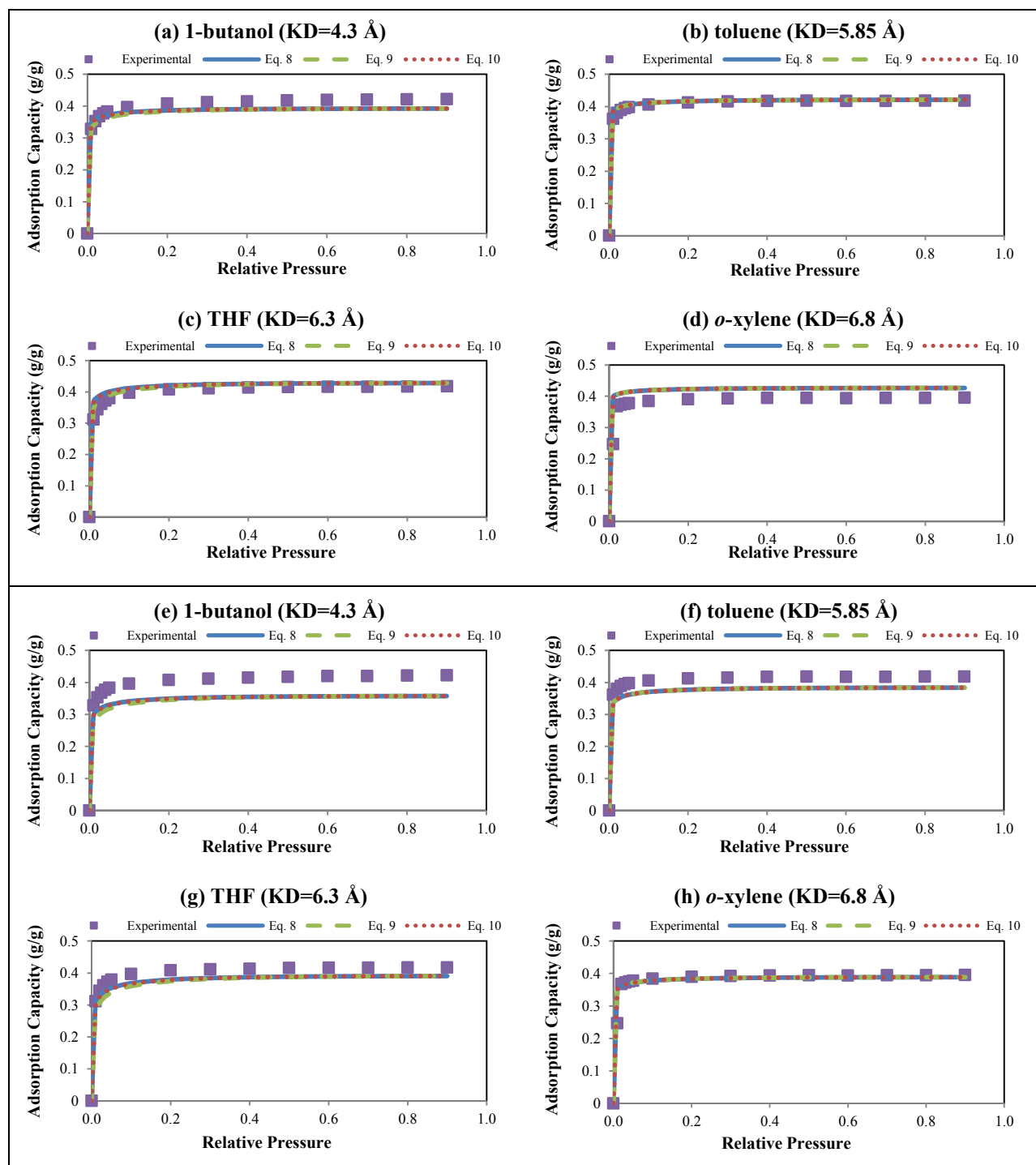


Figure 3-4. Measured and predicted, gravimetric adsorption isotherms for (a) 1-butanol, (b) toluene, (c) THF, and (d) *o*-xylene using benzene (KD=5.85 Å) as reference adsorbate and for (e) 1-butanol, (f) toluene, (g) THF, and (h) *o*-xylene using *m*-xylene (KD=6.8 Å) as the reference adsorbate.

3.3.4 Effect of Adsorbate Kinetic Diameter

Figure 3-5 depicts the total mean relative errors between measured and predicted adsorption isotherms for all 13 tested adsorbates as well as for adsorbates with kinetic diameters similar ($|KD_{\text{reference}} - KD_{\text{test}}| \leq 0.6 \text{ \AA}$) and non-similar ($|KD_{\text{reference}} - KD_{\text{test}}| > 0.6 \text{ \AA}$) to that of the reference adsorbates for two pressure ranges. For $0.01 \leq P/P_o \leq 0.9$, the total mean relative error ranged from 2.5 to 4.6% for test adsorbates with similar kinetic diameters to the reference adsorbates while it ranged from 8.1 to 14.4% for test adsorbates with non-similar kinetic diameters to the reference adsorbates.

As previously mentioned, the D-R equation might have large deviation at low relative pressures; consequently, the goodness of the fit in this region is instructive in verifying the hypothesis. Figure 3-5 illustrates that even for low relative pressure range the total mean relative errors are smaller when using a reference adsorbate with similar kinetic diameter to the test adsorbate. For $0.01 \leq P/P_o \leq 0.1$, the total mean relative error ranged from 4.2 to 7.8% for test adsorbates with similar kinetic diameters to the reference adsorbates while it ranged from 10.1 to 19.0% for test adsorbates with non-similar kinetic diameters to the reference adsorbates. As a result, it could be concluded that irrespective of the pressure range, using a reference adsorbate with similar kinetic diameter to that of the test adsorbate will result in a better prediction of the adsorption isotherm.

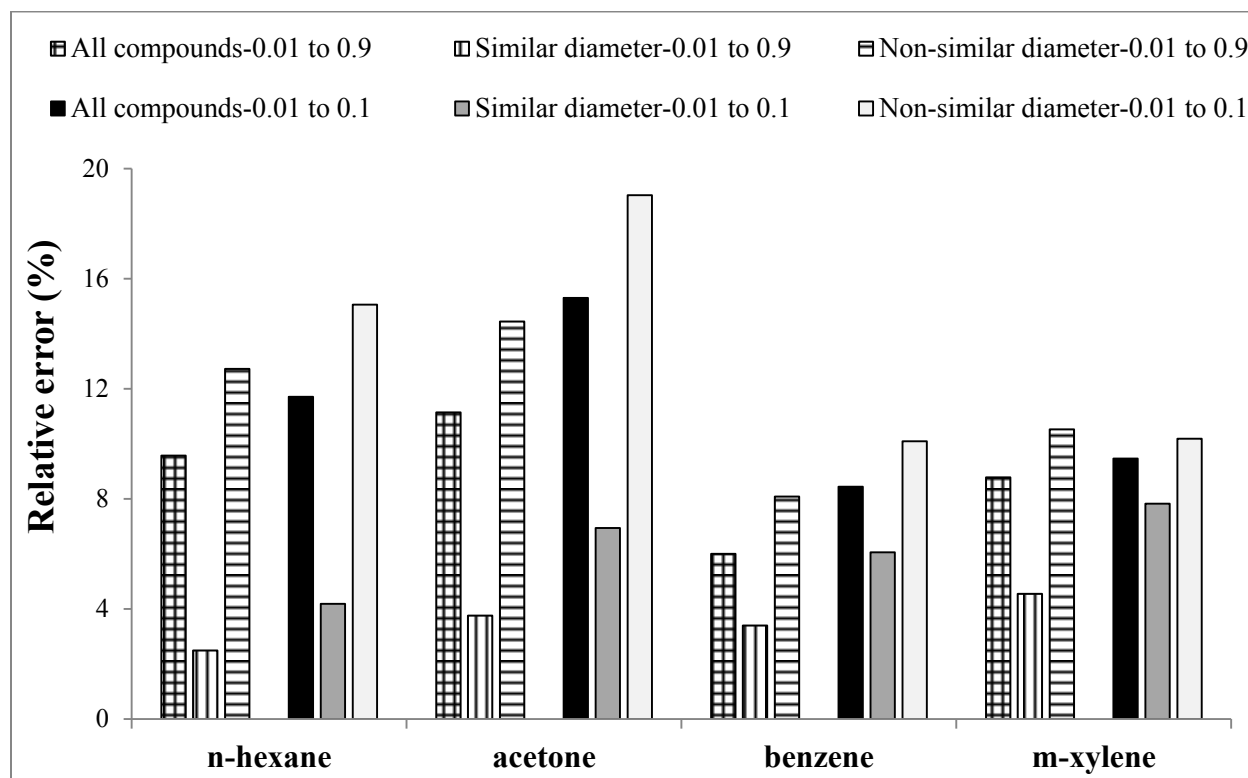


Figure 3-5. Total mean relative errors when predicting the adsorption isotherms of all 13 adsorbates, adsorbates with similar ($|KD_{\text{reference}} - KD_{\text{test}}| \leq 0.6 \text{ \AA}$) and non-similar ($|KD_{\text{reference}} - KD_{\text{test}}| > 0.6 \text{ \AA}$) kinetic diameters for $0.01 \leq P/P_o \leq 0.9$ and $0.01 \leq P/P_o \leq 0.1$.

Another important point that should be considered is the total mean relative error for each reference adsorbate considering all test adsorbates. Acetone has the highest relative error at both relative pressure ranges (Figure 3-5) possibly due to its large dipole moment (2.88 D). Previous studies showed large deviation when the D-R equation is used for predicting the adsorption isotherms of compounds with a dipole moment greater than 2 Debye (Yao et al., 2009; Carter et al., 2011). In addition to its large dipole moment, acetone has small kinetic diameter ($KD=4.4 \text{ \AA}$). For all relative pressure ranges, benzene has the best fit amongst the reference adsorbates. This also might be attributed to the closeness of its kinetic diameter (5.85 \AA) to the average kinetic diameter of all compounds (5.63 \AA).

Figure 3-6 depicts the mean relative error between measured and predicted adsorption isotherms versus the absolute difference in the kinetic diameters of the reference and test adsorbates. Generally, the mean relative error increases as the absolute difference in the kinetic diameter increases. This supports the above hypothesis that using a reference compound with similar kinetic diameter to that of the test adsorbate would result in better prediction of the adsorption isotherm. Moreover, the degree of over-estimation and/or under-estimation seems to be proportional to the differences between the kinetic diameters of the reference and test adsorbates.

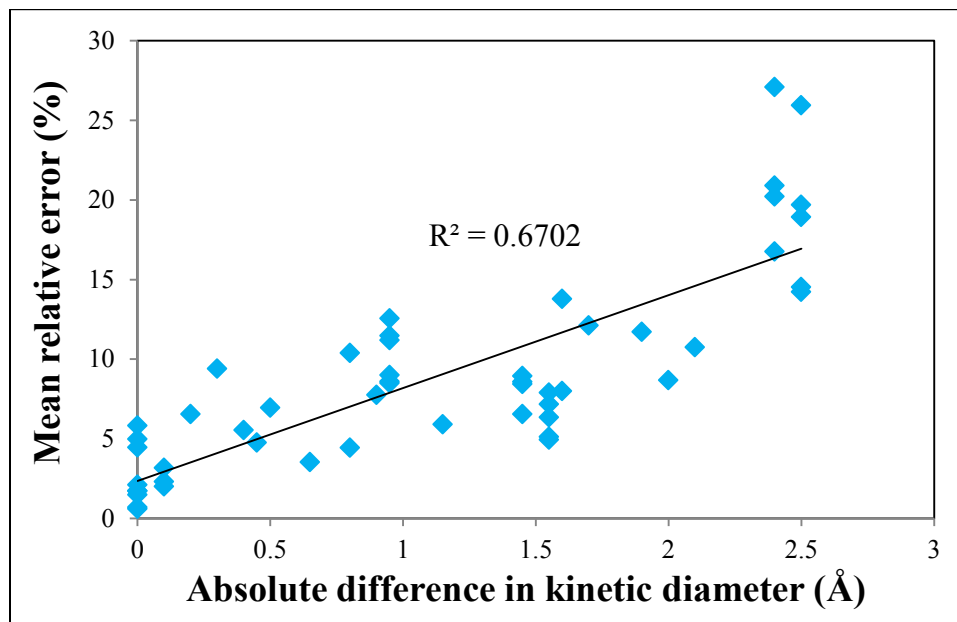


Figure 3-6. Mean relative error versus absolute difference in the kinetic diameter between the reference and test adsorbates ($|KD_{\text{reference}} - KD_{\text{test}}|$).

Figure 3-6 also shows that even when the test and reference adsorbates have similar kinetic diameters, there is some difference between measured and predicted adsorption capacities which might be attributed to factors such as the large dissimilarities in dipole moments of the compounds; although, the difference in the kinetic diameters seems to be the dominant factor.

The last few points in Figure 3-6 have the largest errors possibly due to the slow diffusion of the large adsorbates such as *m*-xylene, *o*-xylene, and cumene inside the narrow micropores of the BAC.

Figure 3-7 compares the predicted and measured adsorption capacities for all adsorbates at all concentrations. For adsorbates with KD similar to that of the reference adsorbate, predicted and measured adsorption capacities are distributed closer to the diagonal line, indicating a good agreement. This is confirmed by calculating the RMSEP. RMSEP of the adsorbates with similar KD to that of the reference adsorbate based on 18 isotherms is 0.02, while those based on all adsorbates (52 isotherms) and compounds with non-similar KD to the reference adsorbate (34 isotherms) are 0.04 and 0.05, respectively.

An independent-samples t-test with unequal variance was conducted to compare experimental and modeling adsorption capacities in case of similar and non-similar KD. The test resulted in a t value of 11.4 for 731 degree of freedom. There was a significant difference at the 99% confidence level in the relative error values for cases of similar (mean=3.5%, standard deviation=5.5%) and non-similar (mean=11.9%, standard deviation=14.2%) KD. These results indicate that the difference in the KD of the reference and test adsorbate does have a significant effect on the accuracy of the D-R equation for modeling adsorption of organic vapors on activated carbon. Specifically, our results indicate that the D-R equation can better predict the adsorption isotherm if a reference compound with similar KD to that of the test adsorbate was used.

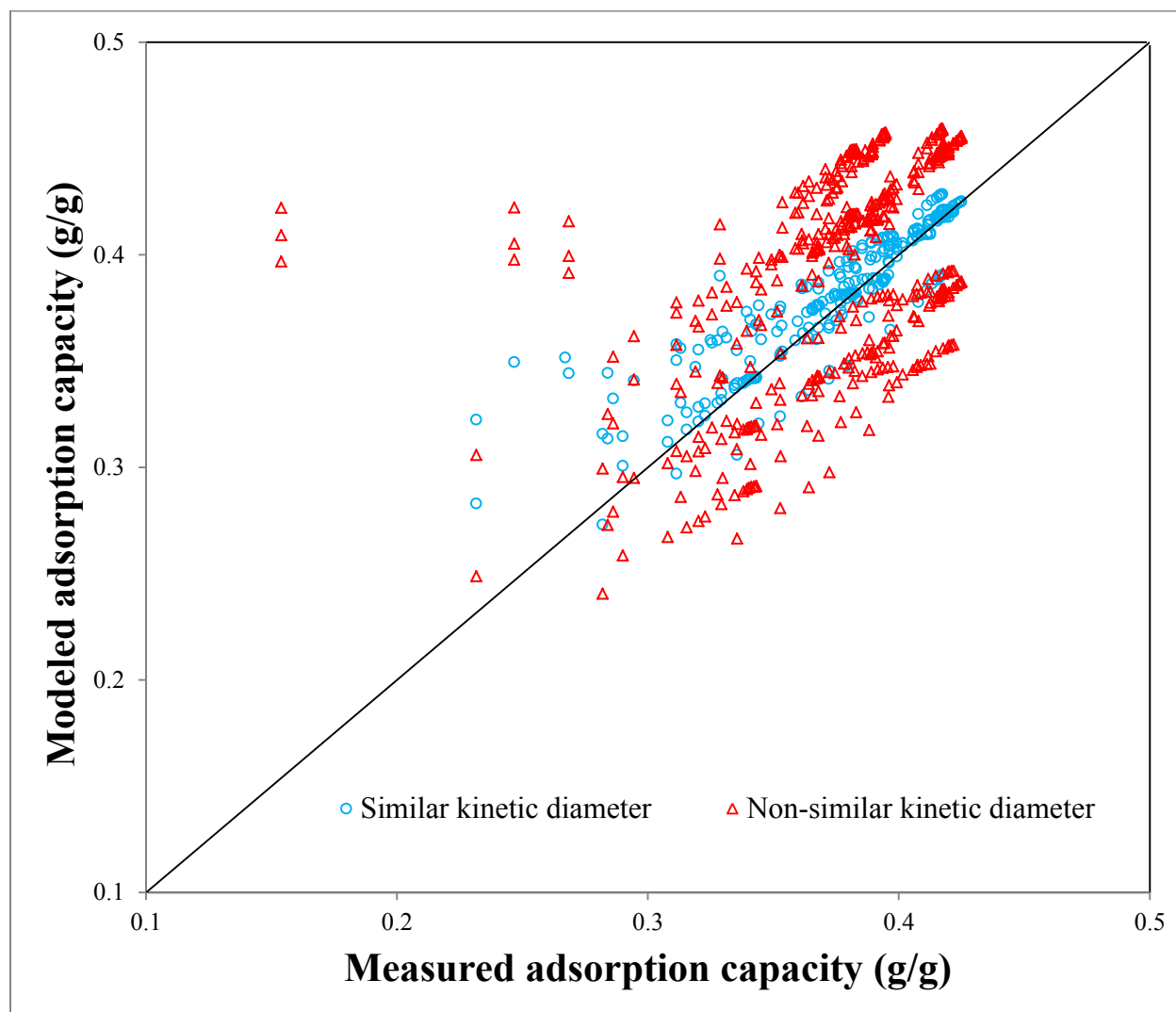


Figure 3-7. Comparison between modeled and measured adsorption capacities for adsorbates with similar ($|KD_{\text{reference}} - KD_{\text{test}}| \leq 0.6 \text{ \AA}$) and non-similar ($|KD_{\text{reference}} - KD_{\text{test}}| > 0.6 \text{ \AA}$) kinetic diameters.

3.3.5 Explanation of Previously Published Contradictory Results

The effect of the kinetic diameter can be used to explain contradictory results from previous studies. For instance, Golovoy and Braslaw (1981) reported that the similarity in the polarity of the reference and test adsorbate doesn't necessarily improve the fit between measured and calculated affinity coefficients, while Reucroft et al. (1971) and Noll et al. (1989) found that

it does. Based on results by Golovoy and Braslaw (1981), using *n*-heptane ($KD=4.3\text{\AA}$) (Breck, 1974) as a reference adsorbate resulted in mean relative errors of 2.5, 5.1, and 27.9% when calculating the experimental affinity coefficients of 1-butanol ($KD=4.3\text{\AA}$), acetone ($KD=4.4\text{\AA}$), and *m*-xylene ($KD=6.8\text{\AA}$), respectively. Similarly, applying 1-butanol as the reference adsorbate for *n*-heptane, acetone, and *m*-xylene resulted in mean relative errors of 6.4, 10.5, and 21.2, respectively. Reucroft et al. (1971) used acetone ($KD=4.4\text{\AA}$) as a reference adsorbate for *n*-hexane ($KD=4.3\text{\AA}$) and benzene ($KD=5.85\text{\AA}$) and reported deviations of 11.7 and 21.2%, respectively. These examples show that choosing a reference adsorbate with a kinetic diameter similar to the test adsorbate results in better prediction of the adsorption isotherm while a reference adsorbate with smaller kinetic diameter compared to the test adsorbate would overestimate the adsorption capacity.

3.4 Conclusions

The choice of a reference adsorbate has an important effect on the accuracy of the D-R equation for predicting the adsorption capacity of organic compounds on microporous activated carbon. While the polarity of the reference adsorbate has often been investigated, conflicting results about the impact of this parameter were reported in the literature. This paper demonstrates that the kinetic diameter of the adsorbate is the main factor affecting the accuracy of the D-R equation. The choice of the reference adsorbate in the D-R equation should take into consideration the kinetic diameter of the adsorbate. Choosing a reference adsorbate with a kinetic diameter similar to that of the test adsorbate results in better prediction of the adsorption isotherm with the D-R equation while a reference adsorbate with smaller or larger kinetic diameter compared to that of the test adsorbate would overestimate or underestimate the adsorption capacity, respectively. The proposed model was successful in explaining previously

published contradictory results that tried to relate the accuracy of the D-R model to the polarity of the adsorbate. These results are important because they are useful for accurately predicting the adsorption isotherms of pollutants and hazardous compounds and finally designing a reliable system for their abatement.

3.5 References

- Al-Khattaf, S.; de Lasa, H. The role of diffusion in alkyl-benzenes catalytic cracking, *Appl. Catal. A* **2002**, 226, 139–153.
- Breck, D.E. *Zeolites Molecular Sieves: Structure, Chemistry and Use*; Wiley: New York, 1974.
- Canham, L.T.; Groszek, A.J. Characterization of microporous Si by flow calorimetry: Comparison with a hydrophobic SiO₂ molecular sieve. *J. Appl. Phys.* **1992**, 72, 1558–1565.
- Carter, E.M.; Katz, L.E.; Speitel, G.E.; Ramirez, D. Gas-phase formaldehyde adsorption isotherm studies on activated carbon: Correlations of adsorption capacity to surface functional group density. *Environ. Sci. Technol.* **2011**, 45, 6498–6503.
- Dehdashti, A.; Khavanin, A.; Rezaee, A.; Assilian, H.; Motalebi, M. Application of microwave irradiation for the treatment of adsorbed volatile organic compounds on granular activated carbon. *Iran. J. Environ. Health. Sci. Eng.* **2011**, 8, 85–94.
- Duchowicz, P.R.; Castaneta, H.; Castro, E.A.; Fernandez, F.M.; Vicente, J.L. QSPR prediction of the Dubinin-Radushkevich's k parameter for the adsorption of organic vapors on BPL carbon. *Atmos. Environ.* **2006**, 40, 2929–2934.
- Golovoy, A.; Braslaw, J. Adsorption of automotive paint solvents on activated carbon: Equilibrium adsorption of single vapors. *Air Pollution Control Assoc.* **1981**, 31, 861–865.
- Guo, G.Q.; Chen, H.; Long, Y.C. Separation of p-xylene from C-8 aromatics on binder-free hydrophobic adsorbent of MFI zeolite. I. Studies on static equilibrium. *Micropor. Mesopor. Mater.* **2000**, 39, 149–161.
- Hung, H.; Lin, T. Prediction of the adsorption capacity for volatile organic compounds onto activated carbons by the Dubinin–Radushkevich–Langmuir model. *J. Air Waste Manage. Assoc.* **2007**, 57, 497–506.
- Hutson, N.D.; Yang, R.T. Theoretical basis for the Dubinin-Radushkevich (D-R) adsorption isotherm equation. *Adsorption* **1997**, 3, 189–195.
- Jahandar Lashaki, M.; Fayaz, M.; Wang, h.; Hashisho, Z.; Phillips, J.H.; Anderson, J.E.; Nichols, M. Effect of adsorption and regeneration temperature on irreversible adsorption of organic vapors on beaded activated carbon. *Environ. Sci. Technol.* **2012a**, 46, 4083–4090.

- Jiun-Horng, T.; Hsiu-Mei, C.; Guan-Yinag, H.; Hung-Lung, C. Adsorption characteristics of acetone, chloroform and acetonitrile on sludge-derived adsorbent, commercial granular activated carbon and activated carbon fibers. *J. Hazard. Mater.* **2008**, *154*, 1183–1191.
- Jones, D.P. *Biomedical sensors*; Momentum Press: New York, 2010.
- Karsli, H.; Culfaz, A.; Yucel, H. Sorption properties of synthetic ferrierite. *Chem. Eng. Comm.* **2003**, *190*, 693–704.
- Knovel Critical Tables (2nd Edition). (2008);
http://www.knovel.com/web/portal/browse/display?_EXT_KNOVEL_DISPLAY_bookid=761&VerticalID=0
- Kotdawala, R.R.; Kazantzis, N.; Thompson, R.W. Molecular simulation studies of adsorption of hydrogen cyanide and methyl ethyl ketone on zeolite NaX and activated carbon. *J. Hazard. Mater.* **2008**, *159*, 169–176.
- Lee, J.Y.; Yun, T.S.; Santamarina, J.C.; Ruppel, C. Observations related to tetrahydrofuran and methane hydrates for laboratory studies of hydrate-bearing sediments. *Geochem. Geophys. Geosyst.* **2007**, *8*, Q06003, doi:10.1029/2006GC001531.
- Li, L.; Liu, S.; Liu, J. Surface modification of coconut shell based activated carbon for the improvement of hydrophobic VOC removal. *J. Hazard. Mater.* **2011**, *192*, 683–690.
- Long, C.; Li, Y.; Yu, W.; Li, A. Removal of benzene and methyl ethyl ketone vapor: Comparison of hypercrosslinked polymeric adsorbent with activated carbon. *J. Hazard. Mater.* **2012**, *203–204*, 251–256.
- Magalhaes, F.D.; Laurence, R.L.; Conner, W.C. Diffusion of cyclohexane and alkylcyclohexanes in silicalite. *J. Phys. Chem. B* **1998**, *102*, 2317–2324.
- Monneyron, P.; Manero, M.H.; Foussard, J.N. Measurement and modeling of single- and multi-component adsorption equilibria of VOC on high-silica zeolites. *Environ. Sci. Technol.* **2003**, *37*, 2410–2414.
- Nirmalakhandan, N.N.; Speece, R.E. Prediction of activated carbon adsorption capacities for organic vapors using quantitative structure-activity relationship methods. *Environ. Sci. Technol.* **1983**, *27*, 1512–1516.
- Noll, K.E.; Wang, D.; Shen, T. Comparison of three methods to predict adsorption isotherms for organic vapors from similar polarity and nonsimilar polarity reference vapors. *Carbon* **1989**, *27*, 239–245.

- Qi, S.; Hay, K.J.; Rood, M.J.; Cal, M.P. Carbon fiber adsorption using quantitative structure-activity relationship. *J. Environ. Eng.* **2000**, *126*, 865–868.
- Ramirez, D.; Sullivan, P.D.; Rood, M.J.; Hay, K.J. Equilibrium adsorption of phenol-, tire-, and coal-derived activated carbons for organic vapors. *J. Environ. Eng.* **2004**, *130*, 231–241.
- Ramirez, D.; Qi, S.; Rood, M.J.; Hay, K.J. Equilibrium and heat of adsorption for organic vapors and activated carbons. *Environ. Sci. Technol.* **2005**, *39*, 5864–5871.
- Reucroft, P.J.; Simpson, W.H.; Jonas, L.A. Sorption properties of activated carbon. *J. Phys. Chem.* **1971**, *75*, 3526–3531.
- Sullivan, P.D.; Rood, M.J.; Grevillot, G.; Wander, J.D.; Hay, K.J. Activated carbon fiber cloth electrothermal swing adsorption system. *Environ. Sci. Technol.* **2004**, *38*, 4865–4877.
- Sullivan, P.D.; Stone, B.R.; Hashisho, Z.; Rood, M.J. Water adsorption with hysteresis effect onto microporous activated carbon fabrics. *Adsorption* **2007**, *13*, 173–189.
- Tuan, V.A.; Li, S.; Falconer, J.L.; Noble, R.D. In situ crystallization of beta zeolite membranes and their permeation and separation properties. *Chem. Mater.* **2002**, *14*, 489–492.
- Tung, C.; Wu, L.; Zhang, L.; Li, H.; Yi, X.; Song, K.; Xu, M.; Yuan, Z.; Guan, J.; Wang, H.; Ying, Y.; Xu, X. Microreactor-controlled selectivity in organic photochemical reactions. *Pure Appl. Chem.* **2000**, *72*, 2289–2298.
- Urano, K.; Omori, S.; Yamamoto, E. Prediction method for adsorption capacities of commercial activated carbons in removal of organic vapors. *Environ. Sci. Technol.* **1982**, *16*, 10–14.
- Wang, H.; Jahandar Lashaki, M.; Fayaz, M.; Hashisho, Z.; Phillips, J.H.; Anderson, J.E.; Nichols, M. Adsorption and desorption of mixtures of organic vapors on beaded activated carbon. *Environ. Sci. Technol.* **2012**, *46*, 8341–8350.
- Wood, G.O. Activated carbon adsorption capacities for vapors. *Carbon* **1992**, *30*, 593–599.
- Wood, G.O. Affinity coefficients of the Polanyi /Dubinin adsorption isotherm equations: A review with compilations and correlations. *Carbon* **2001**, *39*, 343–356.
- Wood, G.O. Review and comparisons of D/R models of equilibrium adsorption of binary mixtures of organic vapors on activated carbons. *Carbon* **2002**, *40*, 231–239.
- Wu, J.; Stromqvist, E.; Claesson, O.; Fangmark, I.E.; Hammarstrom, L.G. A systematic approach for modeling the affinity coefficient in the Dubinin–Radushkevich equation. *Carbon* **2002**, *40*, 2587–2596.

- Yang, K.; Sun, Q.; Xue, F.; Liu, D. Adsorption of volatile organic compounds by metal–organic frameworks MIL-101: Influence of molecular size and shape. *J. Hazard. Mater.* **2011**, *195*, 124–131.
- Yao, M.; Zhang, Q.; Hand, D.W.; Perram, D.L. Investigation of the treatability of the primary indoor volatile organic compounds on activated carbon fiber clothes at typical indoor concentrations. *J. Air Waste Manage.* **2009**, *59*, 882–890.

CHAPTER 4. EFFECT OF ADSORPTION AND REGENERATION TEMPERATURE ON IRREVERSIBLE ADSORPTION OF ORGANIC VAPORS ON BEADED ACTIVATED CARBON¹

4.1 Introduction

Vehicle painting operations are the primary source of VOCs emissions from the automobile manufacturing sector (Golovoy and Braslaw, 1981; Kim, 2011). These emissions consist of a mixture of high and low molecular weight compounds including aromatic hydrocarbons, esters, ketones, alcohols, and glycol ethers (Golovoy and Braslaw, 1981; Kim, 2011). On average, 6.58 kg of VOCs is used as paint solvents per vehicle in typical automotive plants in North America (Kim, 2011). VOC emissions are of concern because of their health effects and/or ozone formation potential (Fuertes et al., 2003; Das et al., 2004; Johnsen et al., 2011; Kim, 2011), so, the gaseous stream needs to be treated before discharging to the atmosphere (Emamipour et al., 2007). Methods to control emission of organic vapors include adsorption, absorption, oxidation, biofiltration, condensation, and membrane separation (Leethochawalit et al., 2001; Hunter and Oyama, 2002; Fuertes et al., 2003; Li and Moe, 2005; Kim et al., 2006; Hashisho et al., 2007; Ramos et al., 2010; Mallouk et al., 2010; Johnsen et al., 2011;). Amongst these methods, adsorption is widely used because of its cost effectiveness, high efficiency at low concentrations (i.e., ppm_v) for recovering the VOCs from gaseous streams, and ability to recover the adsorbate for reuse (Golovoy and Braslaw, 1981; Shonnard and Hiew, 2000; Gupta and Verma, 2002; Lapkin et al., 2004; Dabrowski et al., 2005; Ramos et al., 2010).

¹ A version of this chapter has been published as: Jahandar Lashaki, M.; Fayaz, M.; Wang, H.; Hashisho, Z.; Phillips, J.H.; Anderson, J.E.; Nichols, M. Effect of adsorption and regeneration temperature on irreversible adsorption of organic vapors on beaded activated carbon. *Environ. Sci. Technol.* **2012**, *46*, 4083–4090. Reproduced with permission from ACS Publications.

Adsorption can be categorized into physical adsorption and chemical adsorption. In chemical adsorption or chemisorption, the adsorbate reacts on the surface of the adsorbent and adheres through chemical bonds; consequently, the heat of adsorption is high and approaches the energy of chemical bonds (Khan and Ghoshal, 2000). Chemisorbed species are generally difficult to desorb and as a result they accumulate on the surface of the adsorbent and reduce its adsorption capacity. Higher temperatures during adsorption can favor chemisorption as it provides the activation energy needed for the formation of adsorbate-adsorbent complex (Schnelle and Brown, 2002). Other factors promoting chemisorption include the presence of adsorbates with electron-donating functional groups such as amine (-NH_2) and hydroxyl (-OH) (Tamon and Okazaki, 1996; Tamon et al., 1996; Tanthapanichakoon et al., 2005; Fayaz et al., 2011), the difference between the boiling point of the adsorbate and the regeneration temperature (Fayaz et al., 2011), and π - π electron donor-acceptor interaction between the aromatic ring and unsaturated bond on the carbon (Zhu and Pignatello, 2005).

Due to its low cost and high surface area, activated carbon is one of the most commonly used adsorbents in air and water treatment (Popescu et al., 2003; Kawasaki et al., 2004; Alvarez et al., 2005; Aktas and Cecen, 2006; Kim et al., 2006; Aktas and Cecen, 2007). One of the challenges of capturing organic vapors from painting operations is the irreversible adsorption (aka buildup of heel) of these compounds onto activated carbon which reduces the lifetime of the adsorbent and increases the operation and maintenance cost of the system due to the cost of the adsorbent, disposal of the spent adsorbent, and labor cost to replace the adsorbent. Irreversible adsorption on an adsorbent surface can be described as the combined result of formation of permanent bonds between the adsorbate and the surface (chemisorption) and the irreversible transformation of the adsorbed species through chemical reactions catalyzed by the adsorbent

surface (Chatzopoulos et al., 1993). Previous studies have investigated the irreversible adsorption of organic compounds (particularly phenolic and aromatic compounds) from water onto activated carbon, particularly the conventional granular activated carbon (Grant and King, 1990; Chatzopoulos et al., 1993; Ferro-Garcia et al., 1995; Lu and Sorial, 2007; Lu and Sorial, 2009). However, there is little or no information about the irreversible adsorption of organic compounds from the gas phase onto activated carbon, particularly novel forms of activated carbon such as BAC.

The objective of this study is to explore the effect of adsorption and regeneration temperature on the irreversible adsorption of a mixture of vapor-phase organic compounds commonly emitted from automotive painting operations. Understanding the factors promoting irreversible adsorption is the first step for solving the problem of heel buildup and increasing the lifetime of the adsorbent. For this purpose, a bench-scale adsorption-regeneration system was built and adsorption and regeneration cycles of a mixture of organic compounds onto BAC were completed at different temperatures. The BAC was also analyzed for irreversible adsorption in terms of the amount of accumulated adsorbates and changes in adsorption capacity, specific area and pore size distribution.

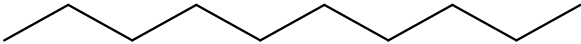
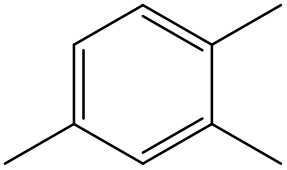
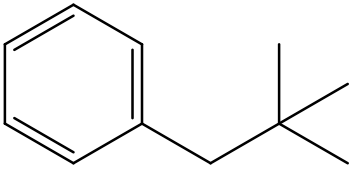
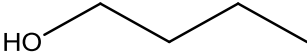
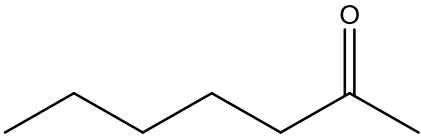
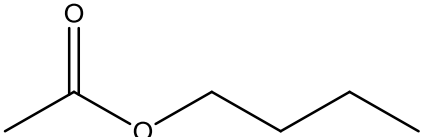
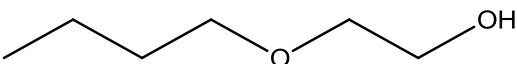
4.2 Materials and Methods

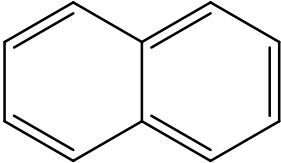
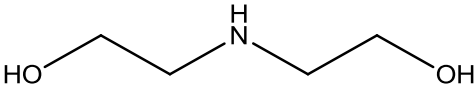
4.2.1 Adsorbent and Adsorbate

The adsorbent used in this study was Kureha beaded activated carbon (Anderson et al., 2006). The BAC is characterized by its high microporosity, attrition-resistance, and narrow particle size distribution (average particle diameter of 0.70 mm, 99% by mass between 0.60 and 0.84mm). Prior to use, the BAC was dried in air in a laboratory oven at 150 °C for 24 hours and then kept in a desiccator. The BAC was tested with a mixture of compounds typically emitted

from automotive painting operations and representative of various functional groups including alkane, aromatic, ester, alcohol, ketone, polyaromatic hydrocarbon, and amine. To prepare the mixture, equal volumes of each of the compounds were mixed as liquids. The density of the mixture was 0.86 g/cm^3 , determined based on the weight of a known mixture volume. The composition of the mixture is presented in Table 4-1.

Table 4-1. Composition of the test mixture.

Name	Chemical structure	Weight percentage (%)	Concentration	
			(ppm _v)	($\mu\text{mol/L}$)
<i>n</i> -decane		9.01	36	1.43
1,2,4-trimethylbenzene		10.86	52	2.05
2,2-dimethyl propylbenzene		10.55	41	1.61
1-butanol		9.99	77	3.05
2-heptanone		10.12	51	2.01
<i>n</i> -butylacetate		10.86	54	2.12
2-butoxyethanol		11.10	54	2.13

Name	Chemical structure	Weight percentage (%)	Concentration	
			(ppm _v)	(μmol/L)
naphthalene		14.06	63	2.49
diethanolamine		13.45	73	2.90

4.2.2 Experimental Setup and Methods

The experimental setup used in this study is depicted in Figure 4-1. The setup consisted of an adsorption-regeneration reactor, an adsorbate generation system, a gas detection system, a power application module, and a data acquisition and control (DAC) system. The adsorption-regeneration reactor consisted of a stainless steel tube (1.44 cm inner diameter, 15.24 cm long) containing 7 to 8 g of dry virgin BAC. The BAC bed length was 8 cm. Glass wool was used at the bottom and top of the reactor as a support for the BAC bed.

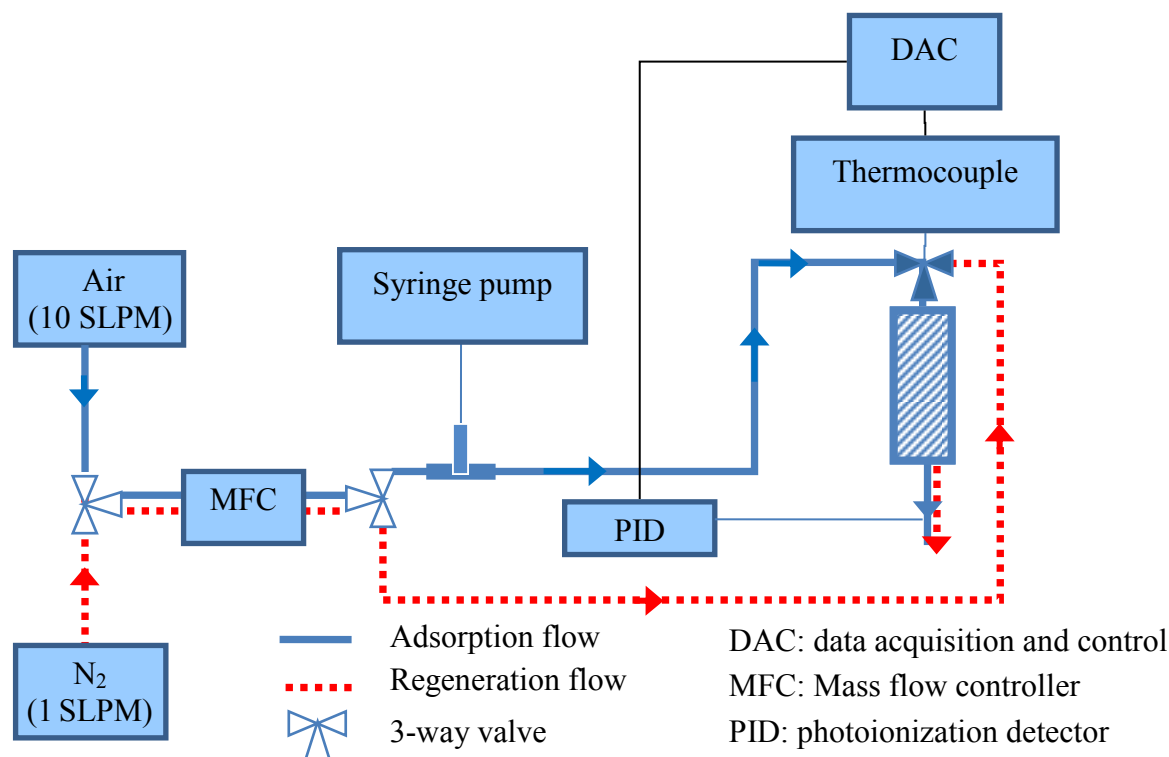


Figure 4-1. Schematic diagram of the adsorption/regeneration setup.

The adsorbate generation system consisted of a syringe pump (kd Scientific, KDS-220) used to inject the mixture into a 10 SLPM dry air stream. The air stream was purified using a compressed air filter (Norman Filter Co.) to remove hydrocarbons and water. The injection rate was calculated based on the ideal gas law using the average molecular weight and density of the mixture. The flow rate of air was controlled with a 0-20 SLPM mass flow controller (Alicat Scientific). The adsorbate detection system consisted of a photoionization detector (Minirae 2000, Rae Systems). The concentration at the outlet of the reactor during adsorption was intermittently measured with the photoionization detector (PID) to avoid contaminating the PID lamp with overexposure to high boiling point adsorbates. The PID was calibrated before each adsorption test using the generated gas stream.

The heat application module consisted of heating tape (Omega) wrapped around the adsorption-regeneration reactor. Insulation tape (Omega) was wrapped outside the heating tape to minimize heat loss. A 0.9 mm OD type K thermocouple (Omega) inserted at the center of the reactor was used to measure the temperature of the BAC bed during adsorption and regeneration. A solid-state relay was used to control the power application to the heating tape.

The DAC system consisted of Labview Software (National Instruments) and a data logger (National Instruments, Compact DAQ) equipped with analog input and output modules. The data logger was interfaced to the PID, thermocouple, and the solid state relay. During adsorption and regeneration, temperature was measured using the thermocouple and a proportional-integral-derivative algorithm was used to control the power applied to achieve the set-point temperature. The DAC system controlled the power application to maintain a bed temperature of 25, 35 or 45 °C during adsorption and 288 or 400 °C during regeneration. A mass flow controller (Alicat Scientific) was used to provide 1 SLPM of high purity (99.998%) grade nitrogen (Praxair) to purge both oxygen and desorbed compounds during regeneration.

Two-point calibration of the PID was completed with fresh air for zero and the steady state concentration adsorbate stream from the adsorbate generation system for span. The calibration was performed at the same gas flow rate as during adsorption to avoid any bias in the PID readings. After calibration, the adsorbate gas stream was directed into the reactor to start adsorption. The adsorption process continued until the BAC was fully saturated as indicated by the PID. The reactor was weighed before and after adsorption to determine the adsorption capacity, as follows:

Adsorption capacity (%)

$$= \frac{\text{Reactor weight after adsorption} - \text{Reactor weight before adsorption}}{\text{Weight of virgin BAC}} \times 100$$

Regeneration was accomplished by heating the BAC with simultaneous purge with nitrogen for 3 hours and then cooling for 50 minutes while continuing to purge with nitrogen. The reactor was then weighed again. The difference in the reactor weight before the adsorption cycle and after the regeneration cycle represented the amount of irreversible adsorption or heel built up during that cycle. The mass balance cumulative heel after five complete adsorption/regeneration cycles represents the total amount of heel building up throughout all five cycles and is defined as follows:

Mass balance cumulative heel (%)

$$= \frac{\text{Reactor weight after last regeneration cycle} - \text{Reactor weight before 1}^{\text{st}} \text{ adsorption cycle}}{\text{Weight of virgin BAC}} \times 100$$

4.2.3 BAC Characterization

4.2.3.1 Thermo-Gravimetric Analysis

After completing five consecutive adsorption/regeneration cycles, the loaded BAC was analyzed by TGA (TGA/ DSC 1, Mettler Toledo). The analysis was started with the temperature at 30 °C and immediately increased to 120 °C and then maintained there for 15 minutes to remove adsorbed moisture from the BAC. Then the temperature was increased to 288 or 400 °C (depending on the temperature used for regenerating the BAC) and kept for 30 min to simulate the basic regeneration process. Finally, it was raised to 1000 °C and maintained for 30 min to desorb strongly adsorbed species from the BAC. Throughout the TGA test, the sample was heated at 20 °C/min in 50 standard cubic centimeter per minute (SCCM) of N₂.

4.2.3.2 Micropore Surface Analysis

BAC samples were analyzed using a micropore surface analysis system (IQ2MP, Quantachrome) with nitrogen as the testing gas with relative pressure range from 10⁻⁷ to 1 at

77K. BAC samples of 30 to 50 mg were degassed at 120 °C for 5 hours to remove any moisture within the pores of the material. BET surface area and micropore volume were obtained using the relative pressure ranges of 0.01 to 0.07 and 0.2 to 0.4, respectively. The micropore volume was determined by the V-t model. The mesopore volume and surface area were calculated by subtracting the relevant micropore values from the total pore values. Pore size distributions were also obtained from nitrogen adsorption/desorption isotherms using the density functional theory (DFT) model for slit pores (Olivier, 1998).

4.3 Results and Discussion

4.3.1 Breakthrough Curves

Figure 4-2a and b depict the breakthrough curves for five consecutive adsorption cycles of BAC regenerated at 288 and 400 °C, respectively. During the first cycle of all experiments, the organic vapors were detected after about 2 hours by the calibrated PID at the reactor outlet indicating occurrence of breakthrough. All tests were continued until full saturation of the BAC as indicated by a stable concentration at the reactor outlet. For BAC regenerated at 288 °C, the breakthrough time ($t_{5\%}$, 5% of influent concentration) decreased progressively with each cycle indicating that regeneration at 288 °C was unsuccessful in desorbing the adsorbed chemicals from some of the adsorption sites which led to accumulation of heel on the BAC. The largest change in breakthrough time occurred after the 1st cycle and corresponded to the largest heel buildup as measured by mass balance. Conversely, for BAC regenerated at 400 °C, the breakthrough time remained almost unchanged after the 1st cycle indicating negligible heel buildup.

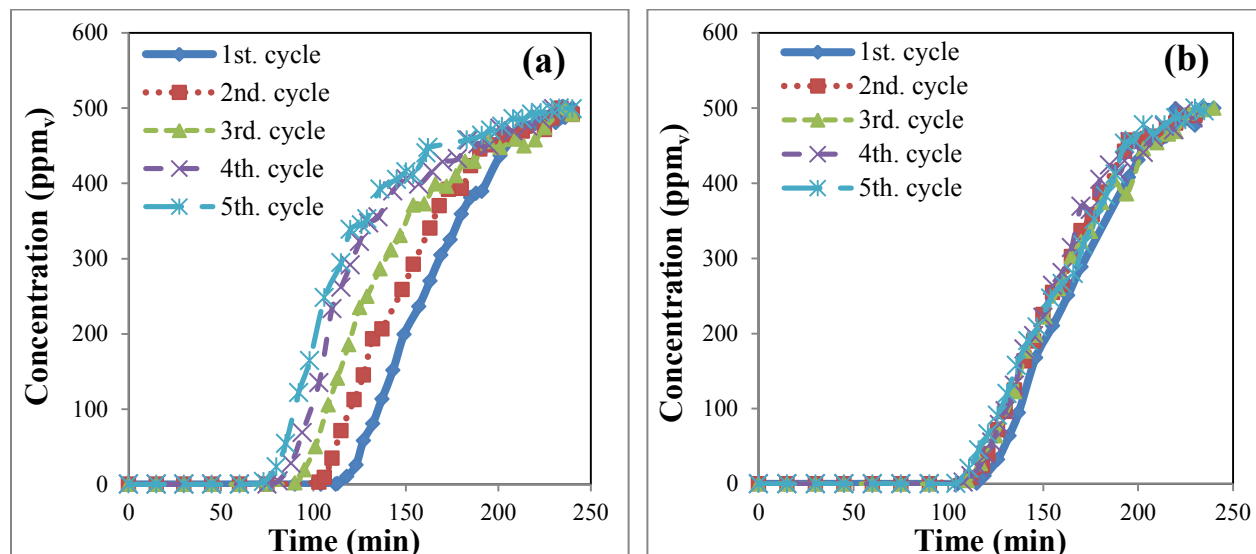


Figure 4-2. Breakthrough curves for adsorption on BAC at 35 °C and regeneration at (a) 288 °C and (b) 400 °C.

Figure 4-3 depicts the difference in breakthrough time ($t_{5\%}$) between the first and all of the following adsorption cycles as a function of mass balance cumulative heel expressed in % by weight of virgin BAC. The reduction in the breakthrough time linearly increased with the mass balance cumulative heel. For the configuration used in this study, a one percent increase in heel resulted in 3.1 minutes reduction in the breakthrough time of the next adsorption cycle. Completing additional cycles resulted in further reduction of the breakthrough time. Continuing this pattern, the BAC will become completely spent and would need to be replaced with virgin BAC. Considering a breakthrough time of 120 min, the adsorbent becomes completely spent after reaching a cumulative heel of 38%. This heel is lower than the adsorption capacity due to possible pore blockage as discussed later in the paper and the fact that the rear (outlet) portion of the carbon is not completely spent when the 5% breakthrough occurs.

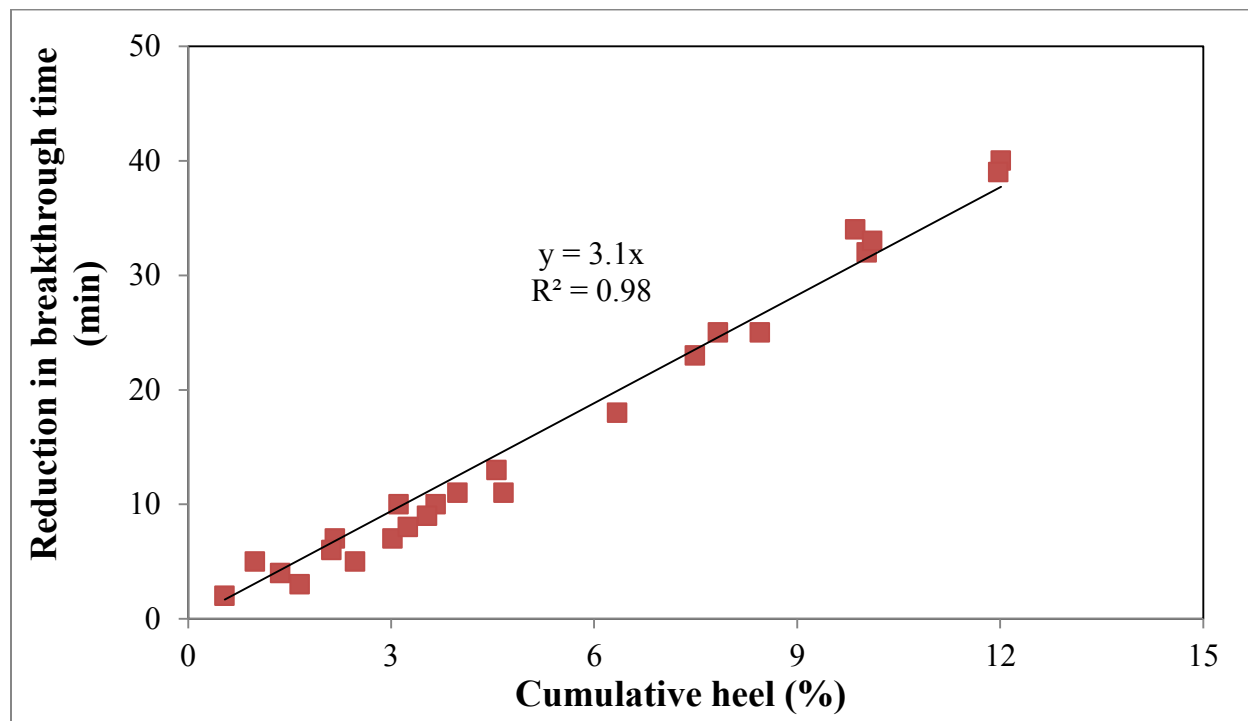


Figure 4-3. Reduction in breakthrough time ($t_{5\%}$) with mass balance cumulative heel for all adsorption and desorption temperatures.

4.3.2 Adsorption and Regeneration Temperature

The adsorption capacities on virgin BAC (i.e., for the first adsorption cycle) at different adsorption temperatures are illustrated in Figure 4-4. For comparison, the adsorption capacities of 1-butanol and *n*-decane at different adsorption temperatures were also obtained. These compounds were selected because previous research (Fayaz et al., 2011) indicated that *n*-decane formed heel on BAC while 1-butanol didn't, suggesting that 1-butanol physisorbed while *n*-decane may have been chemisorbed onto the BAC. The results of the present study showed that the adsorption capacity (for the first cycle) of the mixture and *n*-decane remained almost unchanged as the adsorption temperature increased while the adsorption capacity of 1-butanol showed a 30% reduction as the temperature increased from 25 to 45 °C (Figure 4-4). The behavior of the mixture and *n*-decane is consistent with the characteristics of chemisorption since

a higher temperature provides the energy needed to overcome the activation energy for the reactions between the adsorbate and adsorbent. Since chemisorption involves the formation of chemical bonds between the adsorbate and the adsorbent, the adsorbates will typically occupy certain adsorption sites on the surface of the activated carbon in a monolayer arrangement. Henning et al. (1989) investigated the effect of temperature on adsorption mechanism and adsorption capacity of vapor-phase cyclohexanone onto activated carbon. The adsorption capacity for cyclohexanone remained unchanged as the adsorption temperature increased from 25 to 50 °C. This behavior was attributed to chemisorption of cyclohexanone and presence of some unsaturated carbon bonds on the edge of carbonaceous layers, forming high energy “active-centers” suitable for oxygen and hydrogen to bind (Henning et al., 1989). Another possibility is that higher adsorption temperature might have enhanced the diffusion of the large chain molecules (Chiang et al., 2001).

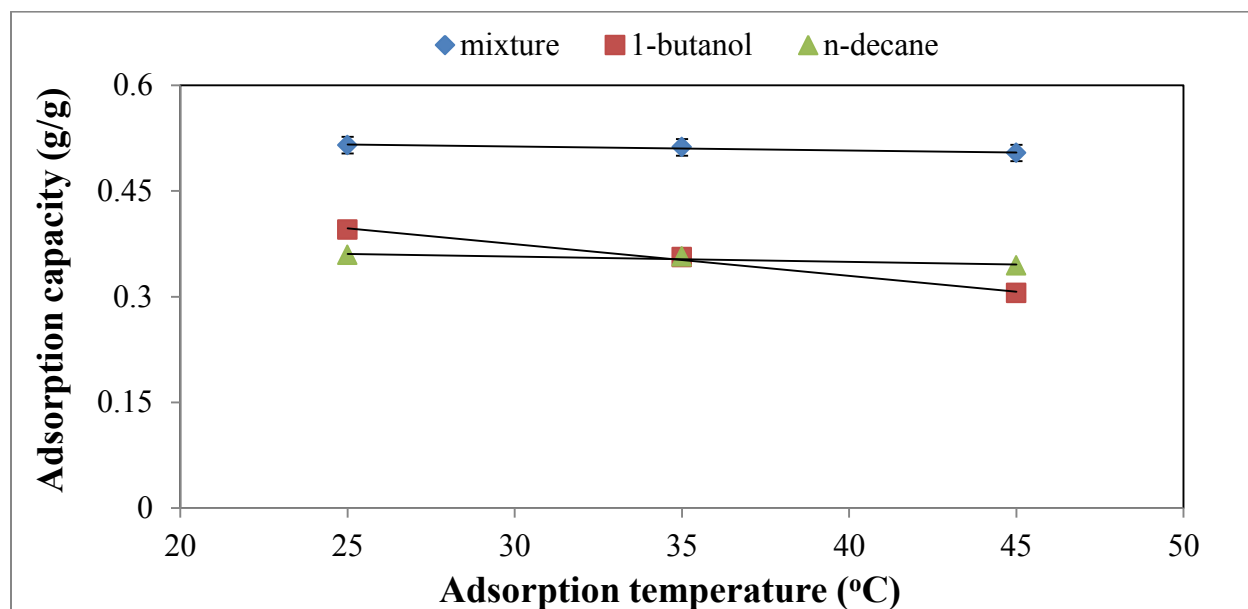


Figure 4-4. Effect of adsorption temperature on adsorption capacity on virgin BAC.

Measurements of heel percentage from the mass balance and the TGA are compared in Figure 4-5 for BAC adsorbed with the tested mixture. For the same regeneration temperature, increasing the adsorption temperature from 25 to 35 °C resulted in greater accumulation of adsorbates on the BAC while further increase in temperature to 45 °C had no effect possibly due to a similar adsorption mechanism at 35 and 45 °C. Previous researchers reported that high temperature is favorable for chemisorption (Chatzopoulos et al., 1993; Schnelle and Brown, 2002) thus the greater heel remaining may be attributable to occurrence of chemisorption. At higher temperature, the adsorption mechanism likely shifts from physisorption (reversible state) to chemisorption (irreversible state) and the adsorption becomes irreversible (Tamon et al., 1996).

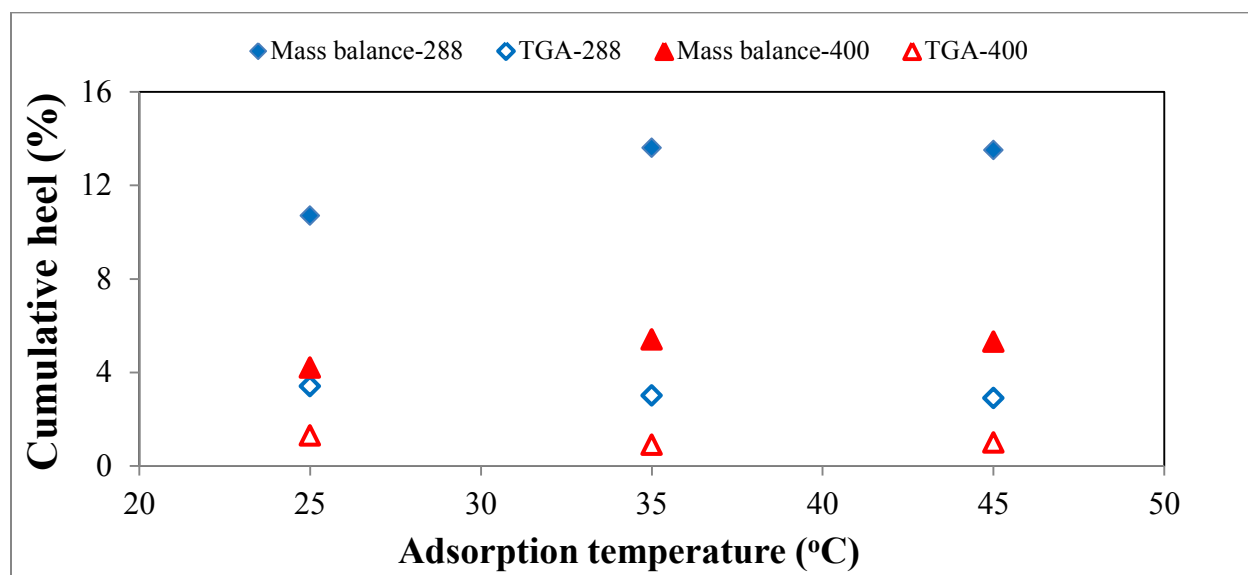


Figure 4-5. Heel percentages as determined by mass balance and TGA for BAC adsorbed with tested mixture and regenerated at 288 or 400 °C. Legends are labeled as Mass balance- or TGA-x where x corresponds to the regeneration temperature in °C.

The effect of regeneration temperature on irreversible adsorption was also evaluated (Figure 4-5). Comparing the heel remaining after regeneration at 288 and 400 °C it can be seen

that using a higher regeneration temperature resulted in 60-61% reduction in mass balance cumulative heel since more adsorbates are desorbed from the pores. In this case, the difference between the regeneration temperature and the boiling point of the tested adsorbates, which ranged from 118 to 271 °C, is larger which provides a greater driving force for desorption. Qin et al. (2009) investigated the irreversible adsorption of dibenzothiophene from *n*-heptane solution and concluded that because of the tendency for adsorbate to remain inside the micropores, applying higher temperatures during the regeneration process may increase the regeneration efficiency.

The difference between heel as determined from mass balance and TGA may be attributed to irreversible chemisorption. Heel determination with TGA is based on the change in the sample weight between the regeneration temperature (288 or 400 °C) and a higher temperature (1000 °C). It is assumed that all of the adsorbate is desorbed at 1000 °C. However, if irreversible adsorption occurs (as is the case in chemisorption), some of the adsorbate will remain adsorbed to the BAC even after exposure to high temperature; hence the TGA heel will be less than the mass balance heel. The difference between the mass balance heel and the TGA heel is larger for 35 and 45 °C than for 25 °C which may be due to increased chemisorption at 35 and 45 °C. The chemisorbed material is harder to desorb even after heating to high temperature (1000 °C); consequently, the difference would be greater in this case.

4.3.3 BET Surface Area and Pore Size Distribution

The BET surface area and pore size distribution of all virgin and regenerated BAC samples were determined to find the effect of irreversible adsorption on these parameters. The BET surface area of the BAC linearly decreased with the mass balance cumulative heel (Figure 4-6). This indicates that as heel accumulates, some adsorption sites remain occupied by

adsorbates since regeneration is unsuccessful in removing them from the active sites, and as a result, the number of vacant available sites will decrease. The effect of irreversible adsorption on the total and micropore volumes is similar to its effect on BET surface area (Figure 4-6). On average, for every 1% of mass balance cumulative heel, BET area, micropore, mesopore, and pore volume decreased by 2.7, 2.8, 2.0, and 3.0%, respectively.

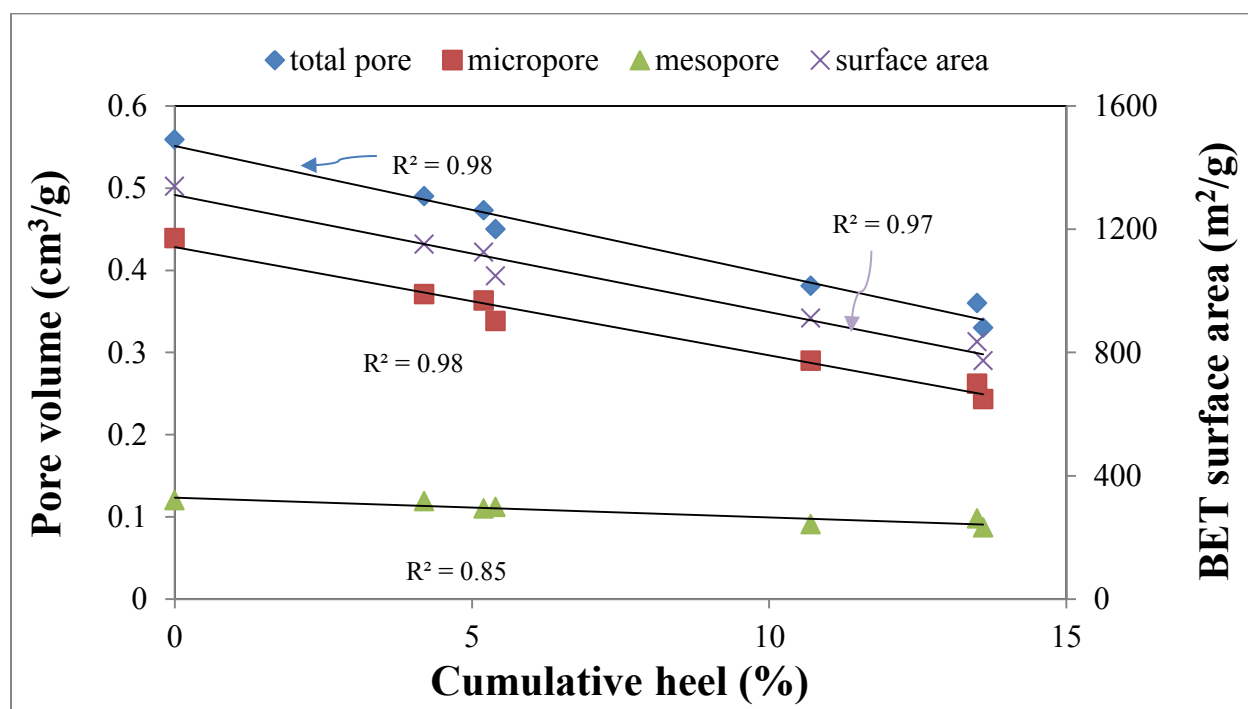
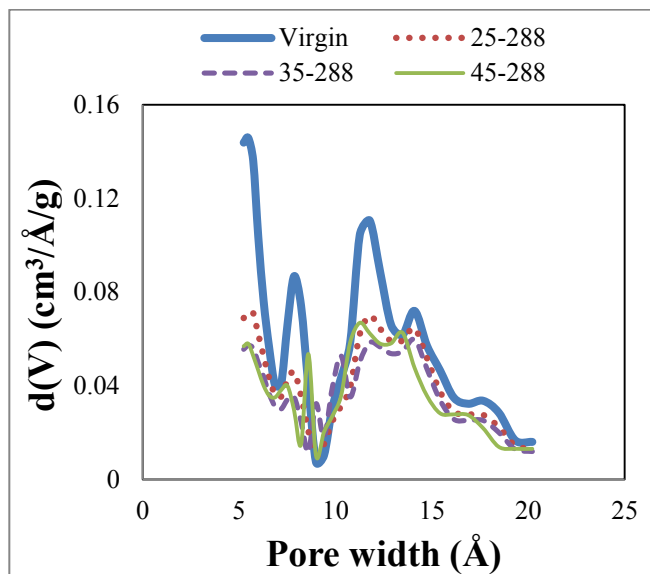


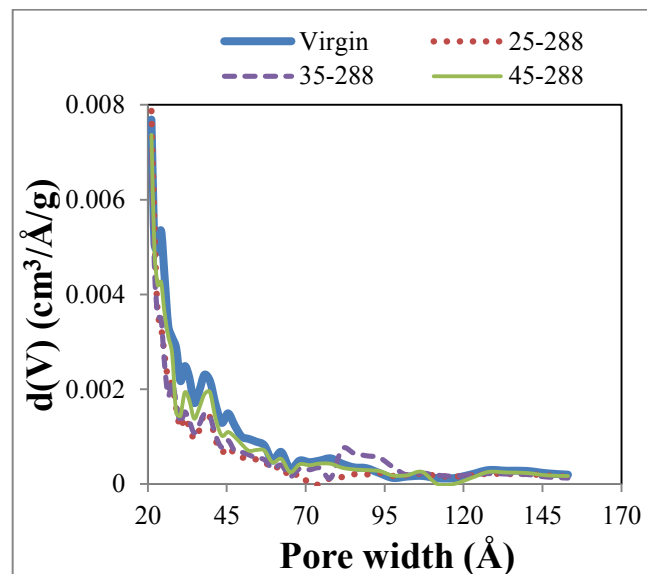
Figure 4-6. Relationship between mass balance cumulative heel on BET surface area and pore volume of regenerated BAC. Values for virgin BAC are presented for comparison.

Determining pore size distribution for the regenerated carbon helps identify the location of the heel. Figure 4-7a indicates that irreversible adsorption resulted in blockage of the micropores, particularly the narrow micropores (5-7 Å). As the adsorption temperature increased, more chemisorption occurred, and more heel accumulated resulting in blockage of more micropores. Figure 4-7a indicates that irreversible adsorption greatly decreased the number of

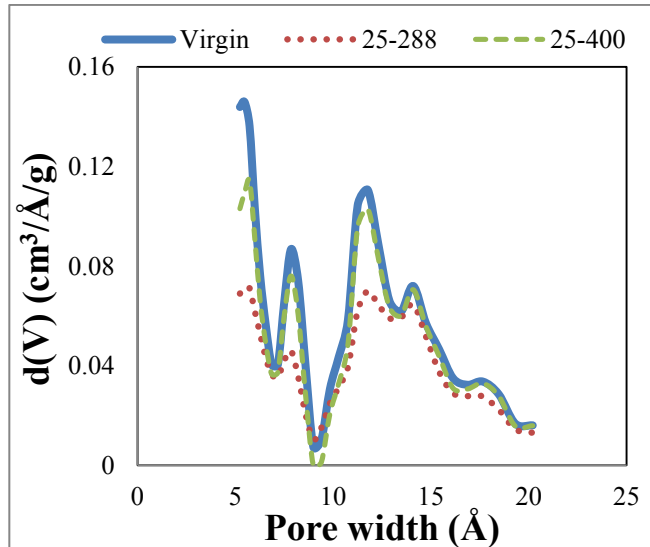
micropores. Irreversible adsorption reduced the number of available mesopores below 100 Å at all adsorption temperatures (Figure 4-7b).



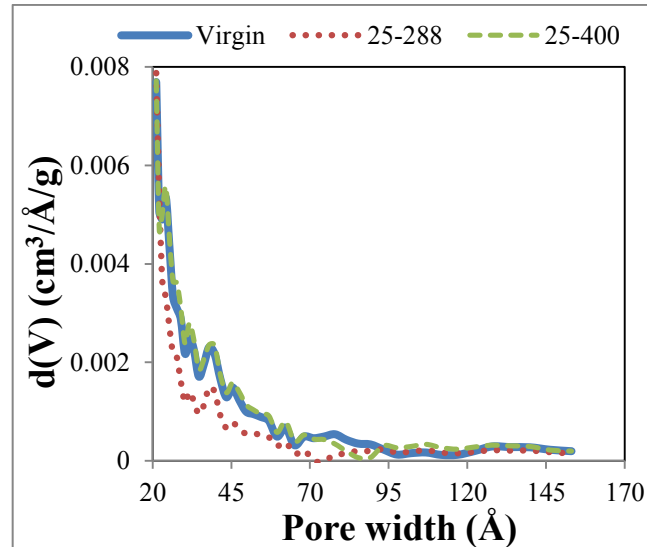
a) Effect of adsorption temperature on micropore size distribution



b) Effect of adsorption temperature on mesopore size distribution



c) Effect of regeneration temperature on micropore size distribution



d) Effect of regeneration temperature on mesopore size distribution

Figure 4-7. Effect of adsorption and regeneration temperature on pore size distribution of BAC.

Legends are labeled as x-y where x and y correspond to the adsorption and regeneration temperatures in °C, respectively.

Increasing the regeneration temperature from 288 to 400°C enhanced the desorption of some of the adsorbates from the micropores including narrow (5-7 Å) micropores (Figure 4-7c) and mesopores (Figure 4-7d). Qin et al. (2009) revealed similar conclusions about the effect of regeneration temperature on the elimination of adsorbates from narrow micropores. BAC containing adsorbed dibenzothiophene regenerated at 400°C had a similar pore size distribution to virgin BAC except that the narrow micropores in the regenerated BAC were not fully desorbed.

The volume of the accumulated adsorbates (i.e., heel) inside the pores of the BAC could be calculated based on weight and bulk density of the adsorbed mixture or directly measured based on the reduction in pore volume from N₂ adsorption isotherms. The measured decrease in pore volume was consistently higher than the calculated value (Figure 4-8). This may be attributed to pore blockage by compounds with large kinetic diameter. For instance, the kinetic diameter of naphthalene, one of the main contributors to irreversible adsorption and a primary constituent of the test gas stream, is 6.2 Å (Long et al., 2008) while 19% of the total pore volume (based on integration of the PSD of the adsorbent) of the BAC corresponds to pores smaller than 6.2 Å in diameter. In this case, naphthalene molecules could block the entrance of these narrow micropores making them unavailable for adsorption, consequently, these sites are vacant but are not able to adsorb anymore. Another mechanism which might have contributed to heel formation could be the oligomerization of adsorbates producing materials that are more difficult to desorb due to their higher boiling points. The difference between calculated and measured pore volume reduction increased as the mass balance cumulative heel increased, consistent with the above hypothesis but increasing in extent.

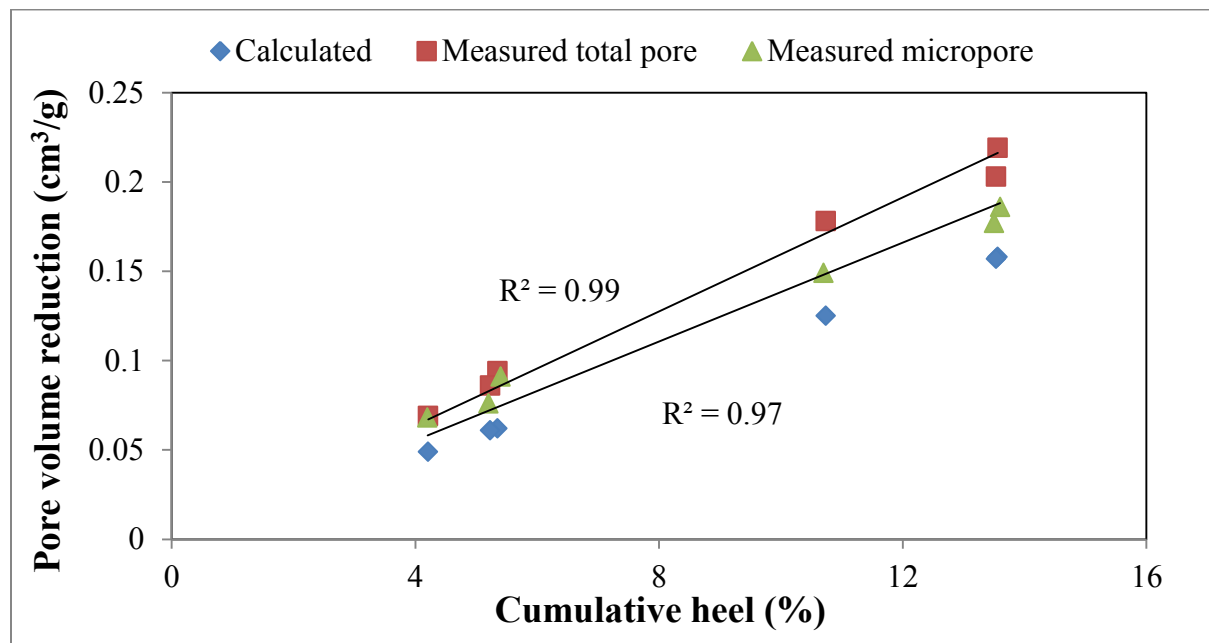


Figure 4-8. Relationship between mass balance cumulative heel and pore volume reduction.

4.4 Conclusions

The effect of adsorption and regeneration temperature on the irreversible adsorption of a mixture of organic compounds typically emitted from automobile painting operations was investigated. Increasing the adsorption temperature from 25 °C to 45 °C will increase heel buildup on BAC by about 30% independent of the regeneration temperature. In this case, the BAC progressively loses its adsorption capacity with more cycles; consequently, it is better to complete the adsorption process at the lowest possible temperature to preserve the adsorption capacity of the BAC. Applying more energy by increasing the regeneration temperature enhances the regeneration efficiency independent of the adsorption temperature and will eliminate more adsorbates from the narrow micropores and increase the lifetime of the BAC. BET area and pore volumes of the BAC decreased significantly because of higher cumulative heel. Pore size distribution confirmed that narrow micropores have a significant role in the accumulation of adsorbates inside the pores of the BAC. The measured reduction in pore volume

due to heel formation was larger than calculated one possibly due to blockage of narrow micropores.

4.5 References

- Aktas, O.; Cecen, F. Effect of type of carbon activation on adsorption and its reversibility. *J. Chem. Technol. Biot.* **2006**, *81*, 94–101.
- Aktas, O.; Cecen, F. Competitive adsorption and desorption of a bi-solute mixture: Effect of activated carbon type. *Adsorption* **2007**, *13*, 159–169.
- Alvarez, P. M.; Garcia-Araya, J. F.; Beltran, F. J.; Masaa, F. J.; Medina, F. Ozonation of activated carbons: Effect on the adsorption of selected phenolic compounds from aqueous solutions. *J. Colloid Interf. Sci.* **2005**, *283*, 503–512.
- Anderson, J.E.; Gilland, R.D.; Adams, J.A.; Saloka, G.S.; Dearth, M.A.; Novak, R.F.; Kim, B.R.; Wherrett, M.R.; Davies, K.L.; Hula, A.C.; Edgeworth, R.K.; Ryan, P.A.; Cowles, H. Recovering VOCs from paint spray booth air using an activated-carbon fluidized-bed adsorber for subsequent power generation. In *Proceedings of 99th Air and Waste Management Association's Annual Conference and Exhibition*, New Orleans, LA, 2006.
- Chatzopoulos, D.; Varma, A.; Irvine, R.L. Activated carbon adsorption and desorption of toluene in the aqueous phase. *AIChE J.* **1993**, *39*, 2027–2041.
- Chiang, Y.; Chiang, P.; Huang, C. Effects of pore structure and temperature on VOC adsorption on activated carbon. *Carbon* **2001**, *39*, 523–534.
- Dabrowski, A.; Podkoscielny, P.; Hubicki, Z.; Barczak, M. Adsorption of phenolic compounds by activated carbon-A critical review. *Chemosphere* **2005**, *58*, 1049–1070.
- Das, D.; Gaur, V.; Verma, N. Removal of volatile organic compound by activated carbon fiber. *Carbon* **2004**, *42*, 2949–2962.
- Emamipour, H.; Hashisho, Z.; Cevallos, D.; Rood, M.J.; Thurston, D.L.; Hay, K.J.; Kim, B.J.; Sullivan, P.D. Steady-state and dynamic desorption of organic vapor from activated carbon with electrothermal swing adsorption. *Environ. Sci. Technol.* **2007**, *41*, 5063–5069.
- Fayaz, M.; Wang, H.; Jahandar Lashaki, M.; Hashisho, Z.; Phillips, J.H.; Anderson, J.E. Accumulation of adsorbed organic vapors from automobile painting operations on bead activated carbon. In *proceedings of 104th Air and Waste Management Association's Annual Conference and Exhibition*, Orlando, FL, 2011.

- Ferro-Garcia, M.A.; Joly, J. P.; Rivera-Utrilla, J.; Moreno-Castilla, C. Thermal desorption of chlorophenols from activated carbons with different porosity. *Langmuir* **1995**, *11*, 2648–2651.
- Fuertes, A.B.; Marban, G.; Nevskaya, D.M. Adsorption of volatile organic compounds by means of activated carbon fiber-based monoliths. *Carbon* **2003**, *41*, 87–96.
- Golovoy, A.; Braslaw, J. Adsorption of automotive paint solvents on activated carbon: Equilibrium adsorption of single vapors. *J. Air Pollution Control Assoc.* **1981**, *31*, 861–865.
- Grant, T.M.; King, C.J. Mechanism of irreversible adsorption of phenolic compounds by activated carbons. *Ind. Eng. Chem. Res.* **1990**, *29*, 264–271.
- Gupta, V.K.; Verma, N. Removal of volatile organic compounds by cryogenic condensation followed by adsorption. *Chem. Eng. Sci.* **2002**, *57*, 2679–96.
- Hashisho, Z.; Emamipour, H.; Cevallos, D.; Rood, M.J.; Hay, K.J.; Kim, B.J. Rapid response concentration-controlled desorption of activated carbon to dampen concentration fluctuations. *Environ. Sci. Technol.* **2007**, *41*, 1753–1758.
- Henning, K. D.; Bongartz, W.; Degel, J. Adsorptive Recovery of Problematic Solvents, *In proceedings of Biennial Conference on Carbon*, Pennsylvania State University, USA, 1989.
- Hunter, P.; and Oyama, S.T. *Control of Volatile Organic Compound Emissions: Conventional and Emerging Technologies*; John Wiley: New York, USA, 2002.
- Johnsen, D.L.; Mallouk, K.E.; Rood, M.J. Control of electrothermal heating during regeneration of activated carbon fiber cloth. *Environ. Sci. Technol.* **2011**, *45*, 738–743.
- Kawasaki, N.; Kinoshita, H.; Oue, T.; Nakamura, T.; Tanada, S. Study on adsorption kinetic of aromatic hydrocarbons onto activated carbon in gaseous flow method. *J. Colloid Interface Sci.* **2004**, *275*, 40–43.
- Khan, F.I.; Ghoshal, A.K. Removal of volatile organic compounds from polluted air. *J. Loss Prev. Process Ind.* **2000**, *13*, 527–545.
- Kim, K.J.; Kang, C.S.; You, Y.J.; Chung, M.C.; Jeong, S.W.; Jeong, W.J.; Woo, M.W.; Ahn, H.G. Adsorption-desorption characteristics of modified activated carbons for volatile organic compounds. *Stud. Surf. Sci. Catal.* **2006**, *159*, 457–460.

- Kim, B.R. VOC emissions from automotive painting and their control: A review. *Environ. Eng. Res.* **2011**, *16*, 1–9.
- Lapkin, A.; Joyce, L.; and Crittenden, B. Framework for evaluating the “Greenness” of chemical processes: Case studies for a novel VOC recovery technology. *Environ. Sci. Technol.* **2004**, *38*, 5815–5823.
- Leethochawalit, M.; Bustard, M.T.; and Wright, P.C.; Meeyoo, V. Novel vapor-phase biofiltration and catalytic combustion of volatile organic compounds. *Ind. Eng. Chem. Res.*, **2001**, *40*, 5334–5341.
- Li, C.; and Moe, W.M. Activated carbon load equalization of discontinuously generated acetone and toluene mixtures treated by biofiltration. *Environ. Sci. Technol.* **2005**, *39*, 2349–2356.
- Long, C.; Lu, J.D.; Li, A.; Hu, D.; Liu, F.; Zhang, Q. Adsorption of naphthalene onto the carbon adsorbent from waste ion exchange resin: Equilibrium and kinetic characteristics. *J. Hazard. Mater.* **2008**, *150*, 656–661.
- Lu, Q.; Sorial, G.A. The effect of functional groups on oligomerization of phenolics on activated carbon. *J. Hazard. Mater.* **2007**, *148*, 436–445.
- Lu, Q.; Sorial, G.A. A comparative study of multicomponent adsorption of phenolic compounds on GAC and ACFs. *J. Hazard. Mater.* **2009**, *167*, 89–96.
- Mallouk, K.E.; Johnsen, D.L.; Rood, M.J. Capture and recovery of isobutane by electrothermal swing adsorption with post-desorption liquefaction. *Environ. Sci. Technol.* **2010**, *44*, 7070–7075.
- Olivier, J.P. Improving the models used for calculating the size distribution of micropore volume of activated carbons from adsorption data. *Carbon* **1998**, *36*, 1469–1472.
- Popescu, M.; Joly, J.P.; Carre, J.; Danatoiu, C. Dynamical adsorption and temperature-programmed desorption of VOCs (toluene, butyl acetate and butanol) on activated carbons. *Carbon* **2003**, *41*, 739–748.
- Qin, W.; Xiao-yi, L.; Rui, Z.; Chao-jun, L.; Xiao-jun, L.; Wen-ming, Q.; Liang, Z.; Li-cheng, L. Preparation of polystyrene-based activated carbon spheres and their adsorption of dibenzothiophene. *New Carbon Mater.* **2009**, *24*, 55–60.

- Ramos, M.E.; Bonelli, P.R.; Cukierman, A.L.; Ribeiro Carrott, M.M.L.; Carrott, P.J.M. Adsorption of volatile organic compounds onto activated carbon cloths derived from a novel regenerated cellulosic precursor. *J. Hazard. Mater.* **2010**, *177*, 175–182.
- Schnelle, K.B.; Brown, C.A. *Air Pollution Control Technology Handbook*; CRC press: Florida, USA, 2002.
- Shonnard, D.R.; and Hiew, D.S. Comparative environmental assessments of VOC recovery and recycle design alternatives for a gaseous waste stream. *Environ. Sci. Technol.* **2000**, *34*, 5222–5228.
- Tamon, H.; Okazaki, M. Desorption characteristics of aromatic compounds in aqueous solution on solid adsorbents. *J. Colloid Interf. Sci.* **1996**, *179*, 181–187.
- Tamon, H.; Atsushi, M.; Okazaki, M. On irreversible adsorption of electron-donating compounds in aqueous solution. *J. Colloid Interf. Sci.* **1996**, *177*, 384–390.
- Tanthapanichakoon, W.; Ariyadejwanich, P.; Japthong, P.; Nakagawa, K.; Mukai, S.R.; Tamon, H. Adsorption-desorption characteristics of phenol and reactive dyes from aqueous solution on mesoporous activated carbon prepared from waste tires. *Water Res.* **2005**, *39*, 1347–1353.
- Zhu, D.; Pignatello, J.J. A Concentration-dependent multi-term linear free energy relationship for sorption of organic compounds to soils based on the hexadecane dilute-solution reference state. *Environ. Sci. Technol.* **2005**, *39*, 2033–2041.

CHAPTER 5. THE ROLE OF BEADED ACTIVATED CARBON'S SURFACE OXYGEN GROUPS ON IRREVERSIBLE ADSORPTION OF ORGANIC VAPORS¹

5.1 Introduction

Paint booths are a major source of VOCs in the auto manufacturing sector (Kim, 2011). These emissions are typically controlled through adsorption and/or oxidation (Kim, 2011). Adsorption on AC is widely used in air (Hashisho et al., 2005, 2007, 2008; Ramos et al., 2010) and water treatment (Dabrowski et al., 2005; Lu and Sorial, 2007, 2009; Busca et al., 2008), for controlling organic contaminants. One challenge in removing VOCs from gas streams is irreversible adsorption, or heel formation (Kim, 2011). Accumulation of adsorbed species on the adsorbent shorten the lifetime of the adsorbent, and increases the operation and maintenance costs for the system increase (Jahandar Lashaki et al., 2012a). Heel formation is attributed to stronger interactions, as might occur with chemisorption, adsorbate decomposition, or oligomerization. While physisorption is generally considered reversible (Popescu et al., 2003), scenarios exist where physical adsorption is difficult to reverse under practical regeneration conditions. These scenarios may be associated with adsorbates with high boiling point and/or molecular weight (Wang et al., 2012), or adsorbates with dimensions close to that of the adsorbent's pore width (Jahandar Lashaki et al., 2012a). In this case, strong dispersive forces acting on adsorbate molecules make regeneration difficult due to overlapping attractive forces from neighboring pore walls (Li et al., 2011). Chemisorption occurs when the adsorbate and

¹ A version of this chapter was presented at a conference as: Jahandar Lashaki, M.; Atkinson, J.D; Hashisho, Z.; Phillips, J.H.; Anderson, J.E.; Nichols, M. Effect of surface oxygen groups on the irreversible adsorption of organic vapors. *In proceedings of 107th Air & Waste Management Association Annual Conference and Exhibition*, Long Beach, CA, 2014.

adsorbent are united by chemical bonds, especially covalent bonds (Yonge et al., 1985; de Jonge et al., 1996b). Adsorbates may decompose during regeneration, resulting in coke deposition inside the pores of adsorbent (Ania et al., 2004; Niknaddaf et al., 2016). In aqueous systems, oxidative polymerization (oligomerization) of phenolic compounds also contributes to irreversible adsorption (Dabrowski et al., 2005; Soto et al., 2011).

Surface functional groups impact the AC's adsorption properties by changing its polarity and/or acidity (Li et al., 2011). Functional groups are formed on or removed from the AC surface during activation, or during post-activation heat and/or chemical treatments (Qiao et al., 2002; Stavropoulos et al., 2008). For example, SOGs form on AC due to chemisorption of oxygen, which can result from AC treatment with HNO_3 , O_2 , O_3 , NO_2 , or KMnO_4 (Boehm, 2002; Stavropoulos et al., 2008). SOGs can be removed from AC by high temperature treatments in N_2 or H_2 (Hashisho et al., 2009).

The impact of activated carbon's SOGs on its adsorption behavior has been well documented (Rivera-Utrilla et al., 2011 and references therein) but lesser studies are available on the effect of SOGs on adsorption reversibility of organic compounds during regeneration. The effect of SOGs on irreversible adsorption of organics, especially phenolics, has been described for the aqueous phase. Phenolic compounds interact with SOGs on the AC (de Jonge et al., 1996a). Terzyk (2007) reported that oxidative coupling was inversely proportional to the concentration of carboxylic groups. Acidic SOGs decrease irreversible adsorption of phenolics by inhibiting oxidative coupling (Radovic et al., 2001; Terzyk et al., 2008) due to hydration of the SOGs, which is prevalent in aqueous environments (Coughlin and Ezra, 1968; Mahajan et al., 1980). Alvarez et al. (2004) showed that acidic SOGs prevent irreversible adsorption under oxic conditions by hampering oxidative coupling, while phenol chemisorption on carbonyl and

carboxyl groups may be promoted through donor-acceptor mechanisms and ester formation, respectively. Leng and Pinto (1997) found that phenol polymerization occurred under oxic conditions, but was suppressed by increasing acidic SOGs on AC.

The aforementioned studies investigated the effect of AC's SOGs on adsorption reversibility of phenols in *water*. Oxidative coupling is the main contributor to *aqueous phase* irreversible adsorption of phenols (Dabrowski et al., 2005; Soto et al., 2011). Since this phenomenon has not been reported in the *gas phase*, results cannot be expected to directly transfer to the *gas phase*. The effect of SOGs on irreversible adsorption of *non-phenolic* organic compounds is also important and warrants scientific investigation. To the best of our knowledge, however, there is little or no information about the impact of SOGs on irreversible adsorption of *non-phenolic* organic compounds from *air* onto AC, particularly heel formation during cyclic adsorption/regeneration. The objective of this study, therefore, is to determine the contribution of SOGs to irreversible adsorption during cyclic adsorption/regeneration of a mixture of organic vapors commonly found in industrial systems, including vehicle-painting operations. A better understanding of the factors contributing to heel buildup can be helpful for finding ways to reduce heel formation and increase the adsorbent's useful lifetime.

5.2 Materials and Methods

5.2.1 Adsorbent Preparation

Three treated BACs were used. Virgin petroleum pitch-based BAC (G-70R; Kureha Corporation) was used in all treatments. The BAC has very low ash content ($< 0.05\%$) (Kureha Corporation Website), ruling out the possible complexities associated with catalytic reactions (Matatov-Meytal and Sheintuch, 1998). Virgin BAC was treated with nitric acid to add oxygen. Carbon was stirred for 16 h in 5.3 M HNO_3 , washed with deionized water until neutral pH, and

then heated at 150 °C overnight to eliminate water (labeled as BAC-O-N). The carbon was then heated to 400 °C under 1.0 standard liter per minute (SLPM) N₂ for 3 h to remove adsorbed nitrate groups (Stavropoulos et al., 2008) (identified as BAC-O). Virgin BAC was heat treated at 400 °C under 1.0 SLPM N₂ for 3 h before characterization and use (identified as BAC-V). Hydrogen was added to virgin BAC, displacing residual SOGs. Carbon was treated in hydrogen (0.5 SLPM) for 3 h at 850 °C to remove surface oxygen functionalities (Sullivan et al., 2007; Hashisho et al., 2009). For consistency, this sample was then heat-treated at 400 °C under 1.0 SLPM N₂ for 3 h before characterization and use (identified as BAC-H).

5.2.2 Adsorbates

The adsorbates were tested individually as well as a mixture. The mixture was primarily prepared by mixing equal parts (by volume) of nine organic compounds, representing different organic groups commonly present in automotive paint solvents. The mixture was subsequently tested in gas phase (total concentration of 500 ppm_v). The concentration of the mixture components in the gas phase were as follows (all in ppm_v): *n*-decane, 36; 1,2,4-trimethylbenzene, 52; 2,2-dimethylpropylbenzene, 41; *n*-butylacetate, 54; 2-butoxyethanol, 54; 1-butanol, 77; 2-heptanone, 51; naphthalene, 63; and diethanolamine, 72 (Jahandar Lashaki et al., 2012a). The components of the mixture have a wide range of boiling points (118 to 271 °C) and kinetic diameters (4.3 to 6.8 Å) (Jahandar Lashaki et al., 2012b), and previously showed a high tendency to form heel (Jahandar Lashaki et al., 2012a; Wang et al., 2012). Using a mixture of organic compounds (with different functionalities) as test adsorbate provides an adsorbate stream that is more representative of VOCs generated from vehicle painting operations (Kim, 2011; Jahandar Lashaki et al., 2012a; Wang et al., 2012). All components of the test mixture were also individually tested to verify the hypothesis proposed in this article.

5.2.3 Setup and Methods

The experimental setup consisted of a stainless steel adsorption/regeneration tube, VOC vapor generation system, gas-phase VOC detection system, power application module, and DAC system (Jahandar Lashaki et al., 2012a; Wang et al., 2012; Tefera et al., 2013a). Adsorption experiments were completed at 25 °C using 7 ± 0.1 g of dry treated BACs. Adsorption cycles lasted 120 min, providing partial loading (approximately 70% by weight of maximum adsorption capacity) of treated BACs. Partial loading avoids preferential adsorption of high molecular weight adsorbates due to competitive adsorption, hence allows for adsorption of all species of the test mixture. This is also representative of the industry practice where adsorption is stopped before reaching breakthrough for more efficient VOC capture.

Regeneration was completed at 288 °C to simulate industrial operational conditions (Anderson et al., 2006; Kim, 2011), and allow for desorption of adsorbed species while minimizing potential damages to the structure of adsorbent as a result of exposure to high temperature (Salvador et al., 2015). The adsorption/regeneration tube was heated to 288 °C for 3 h while purged with 1 SLPM N₂ then cooled to 50 °C for 50 min while continuing the N₂ purge.

The term “mass balance cumulative heel” is used to characterize the total accumulated adsorbate after 5 adsorption/regeneration cycles and is calculated as follows:

$$\text{Mass balance cumulative heel (\%)} = \frac{W_{AR} - W_{BA}}{W_{BAC}} \times 100$$

where W_{AR} is the BAC weight after the last (5th) regeneration cycle, W_{BA} the BAC weight before adsorption, and W_{BAC} the initial dry BAC weight. Regenerated BACs were labeled as x-5C where x corresponds to the treated BAC used during cycling. All regenerated BAC samples were characterized after the 5th adsorption/regeneration cycle, and adsorption/regeneration

experiments were completed in duplicates to assess reproducibility. A blank (no adsorbate) 5-cycle adsorption/regeneration experiment was also completed on BAC-O (identified as BAC-O-Blank-5C) using the aforementioned experimental conditions to support the hypothesis proposed in this work.

Screening experiments individually tested each component of the mixture on small samples (15–20 mg) of the treated BACs. The BACs were spiked with 20–40 mg of the adsorbates and were then left in ambient air for 2 to 4 days (depending on their vapor pressure) to vaporize excess adsorbate. The loaded samples were subsequently regenerated in a TGA as described below.

5.2.4 BAC Characterization

Virgin, treated, and regenerated BAC samples were characterized before and after cycling using a micropore surface analyzer (iQ2MP, Quantachrome). N₂ adsorption was performed at -196 °C after degassing the samples for 5 h at 120 °C. Specific surface area was calculated by the BET method (Brunauer et al., 1938) from relative pressures ranging from 0.01 to 0.07, which allowed for high coefficient of determination (R^2) values and positive BET constants (C). Total pore volume was recorded at $P/P_0 = 0.975$ (Quantachrome Autosorb 1 Operating Manual, 2006). The quenched solid density functional theory (QSDFT) method provided pore width distributions, and the V-t method provided micropore volume (Quantachrome Autosorb 1 Operating Manual, 2006).

The pH_{PZC} for virgin and treated BACs was measured with a pH meter (Oakton, model pH-700) as described elsewhere (Atkinson et al., 2013). Aqueous dispersions containing 2 wt% carbon (approximately 540 mg in 27 mL deionized H₂O) were stirred for 20 h. After the

suspensions settled, the pH of the solution was measured in duplicates and the average was taken as the pH_{PZC} for that material.

Surface elemental composition (C, O, and N) of virgin, treated, and regenerated BACs was determined with XPS using an AXIS 165 spectrometer (Kratos Analytical). High resolution scans (with signal to noise ratio of >10) were collected for binding energy spanning from 1100 eV to 0 eV with analyzer pass energy of 20 eV and a step of 0.1 eV. CasaXPS Software was used to process the scans and the results were reported in terms of atomic concentration.

The thermal stability of treated and regenerated samples and the relative concentration of SOGs were assessed using derivative thermo-gravimetric (TGA/DSC 1, Mettler Toledo). Samples were heated from 25 to 900 °C at 1 °C/min in 50 SCCM of N_2 .

Treated BACs loaded with the single adsorbates were regenerated using the above mentioned TGA instrument. The temperature was increased from 25 °C to 288 °C at 10 °C/min and was then maintained at 288 °C for 180 min to simulate the regeneration process. The temperature was then raised to 900 °C at 1 °C/min. Throughout the test, the BAC samples were heated in 50 SCCM of N_2 . The results are presented for temperature ≥ 288 °C for clearer depiction of high temperature peaks associated with materials not desorbed under the standard 288 °C condition.

Select virgin, treated, and regenerated BAC samples were analyzed using Boehm titration to determine the concentration of different SOGs (Boehm, 1994). Triplicate 50 mg of BAC samples were shaken in 5 mL of 0.05 M NaHCO_3 , Na_2CO_3 , and NaOH for 24 h using a wrist shaker (Burrell Scientific). The solution was separated from the carbon sample. Excess 0.05 M HCl (2:1 volume ratio for NaHCO_3 and NaOH, and 3:1 volume ratio for Na_2CO_3) was then added to ensure acidity, followed by one or two drops of phenolphthalein indicator. Finally, the

solutions were back-titrated with 0.05 M NaOH solution until reaching a faint but permanent pink color. NaOH solution was standardized daily using 0.05 M potassium hydrogen phthalate. The concentrations of various SOGs were calculated assuming NaHCO_3 neutralizes carboxylic groups (including carboxylic anhydrides), Na_2CO_3 neutralizes carboxylic and lactonic groups, and NaOH neutralizes carboxylic, lactonic, and phenolic groups (Boehm, 1994).

TGA-MS of select virgin, treated, and regenerated samples was completed to evaluate the gases evolved during thermal analysis. Thermal analysis was performed using TGA (TA Instruments, Q500) from 25 to 900 °C at 10 °C/min in 150 SCCM of Ar. The mass spectrometer (Pfeiffer, Omnistar QMA 200) was connected to the TGA with a stainless steel adapter and a 0.64 cm (inner diameter) T-fitting. The capillary was positioned at the center of the tee, close to the furnace exhaust, to sample evolved gases. Experiments were run in multiple ion detection mode with fragments at mass to charge ratios (m/z) of 18 and 44 tracked at 200 ms intervals.

5.3 Results and Discussion

5.3.1 BAC Characterization

Treated BACs were characterized prior to cyclic adsorption/regeneration experiments (Table 5-1). Treatments to add or remove SOGs did not cause significant changes (< 3%) in BET surface area, micropore volume, and total pore volume as compared to virgin BAC. The treatments, however, changed the amount of oxygen on the BAC surface, with BAC-O containing more than twice as much surface oxygen as BAC-H (Table 5-1). Additionally, pH_{PZC} measurements indicate that BAC-O is notably more acidic than BAC-H (Table 5-1), potentially due to added acidic SOGs (Atkinson et al., 2013).

Table 5-1. Physical and chemical properties of virgin, treated, and regenerated BACs before and after adsorption/regeneration cycling.

Carbon Description	Carbon Sample	Physical Properties			Surface Composition			
		BET Surface Area (m ² /g)	Micropore Volume (cm ³ /g)	Pore Volume (cm ³ /g)	pH _{PZC}	C (%) ^a	O (%) ^a	N (%) ^a
Virgin BAC	Virgin BAC	1371±21	0.50±0.01	0.57±0.01	6.67	94.0	6.0	0.0
BAC Before Ads/Des Cycles	BAC-O	1355	0.49	0.57	6.09	91.7	8.3	0.0
	BAC-H	1359	0.50	0.57	7.25	96.2	3.8	0.0
	BAC-V	1334	0.49	0.56	6.79	94.6	5.4	0.0
BAC After Ads/Des Cycles	BAC-O-5C	1053	0.38	0.45	NA	87.7	10.6	1.7
	BAC-H-5C	1131	0.42	0.49	NA	93.2	5.8	1.0
	BAC-V-5C	1136	0.42	0.48	NA	92.6	6.5	0.9

^a Relative atomic percentages (%C + %O + %N = 100); Other elements were not considered in surface composition

PSDs for all treated BACs were measured (Figure 5-1a). No significant difference among the unused treated BACs was observed. All samples were microporous with pore sizes comparable to the molecular size of common VOCs, which provides high affinity towards the VOCs studied (Jahandar Lashaki et al., 2012b). Overall, these characterization results satisfy our primary purpose of investigating carbons with similar physical properties (i.e., porosity) but different chemical properties (i.e., SOGs).

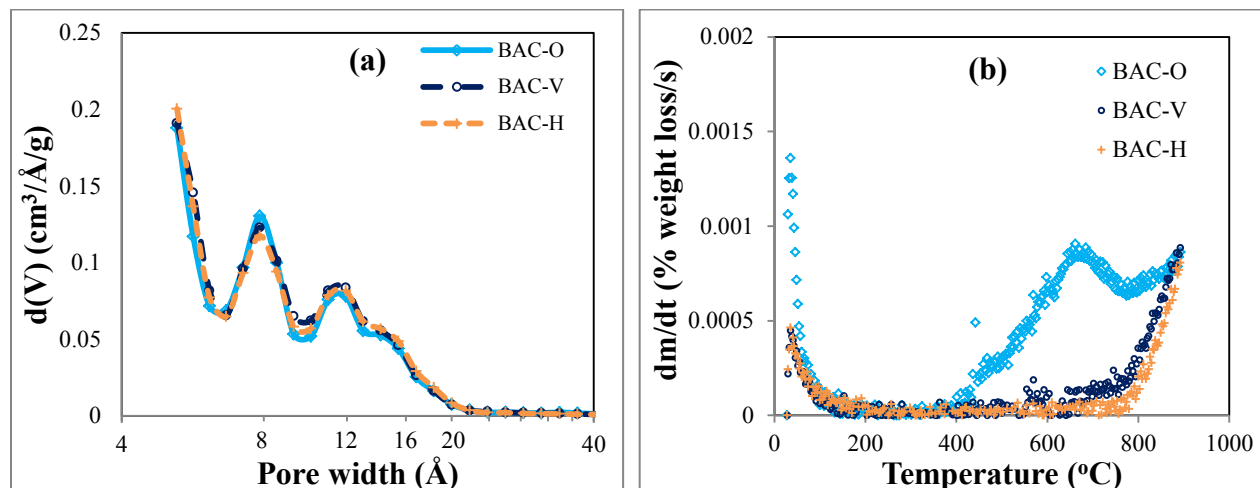


Figure 5-1. Pore size distributions (a) and DTG analysis (b) of unused treated BACs.

DTG analysis was performed to evaluate the thermal stability of the treated BACs and to provide a qualitative description of SOGs on the treated BACs (Figure 5-1b). For all samples, the first DTG peak (at 50 °C) is attributed to desorption of water vapor adsorbed during exposure to ambient air prior to analysis (Popescu et al., 2003). This peak was highest for BAC-O due to hydrophilicity associated with SOGs (Sullivan et al., 2007). Additional mass loss did not occur until 400 °C because all samples were preheated at this temperature. Beginning from 400 °C, a wide peak was observed for BAC-O. This peak is attributed to removal of SOGs deposited onto the surface of the carbon that can be liberated at high temperatures (Nevskaia et al., 1999). All other samples showed negligible weight loss until temperatures > 700 °C, which is most likely due to carbon decomposition.

Boehm titration was completed on select samples to determine the concentration of various acidic SOGs. Phenol functional groups were detected on all samples. Phenol groups decompose at > 550 °C (de la Puente et al., 1997), so no difference was observed between virgin BAC and BAC-V (heat-treated at 400 °C) while a 43% reduction in phenol groups' concentration was observed for BAC-H due to hydrogen treatment at 850 °C. Acid-treated BAC before heat

treatment (BAC-O-N) showed the highest level of acidity due to presence of carboxylic, lactonic, and phenolic groups. Following heat treatment at 400 °C (BAC-O), part of the carboxylic groups (33%) was removed. The remaining carboxylic groups are most likely due to carboxylic anhydrides, which are more stable (Perrard et al., 2012).

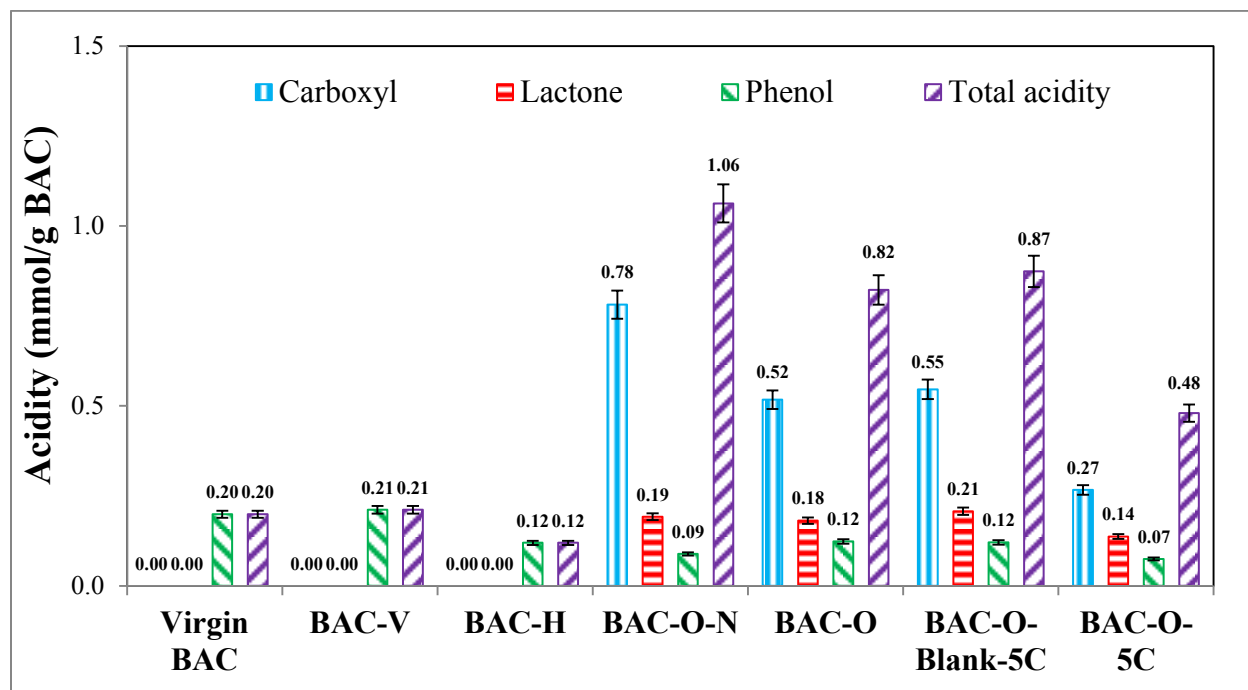


Figure 5-2. Contribution of various SOGs based on Boehm titration.

To further assess the type of SOGs, TGA-MS analysis of select samples was completed (Figure 5-3). For virgin BAC, CO₂ was evolved at > 600 °C, most likely due to carbon decomposition and/or SOGs removal, as discussed before. CO also evolved at T > 800 °C, possibly because of SOGs decomposition (de la Puente et al., 1997). Following HNO₃ treatment (BAC-O-N), H₂O and NO were released with CO₂. CO₂ evolves due to decomposition of carboxylic and lactone groups, added via nitric acid treatments, which are expected to be removed at < 350 °C and 350–550 °C, respectively (de la Puente et al., 1997). Furthermore, some carboxylic groups may transform to anhydride groups (carboxylic anhydrides) (Boehm, 1994;

Perrard et al., 2012), which can then evolve at > 450 °C (de la Puente et al., 1997; Perrard et al., 2012).

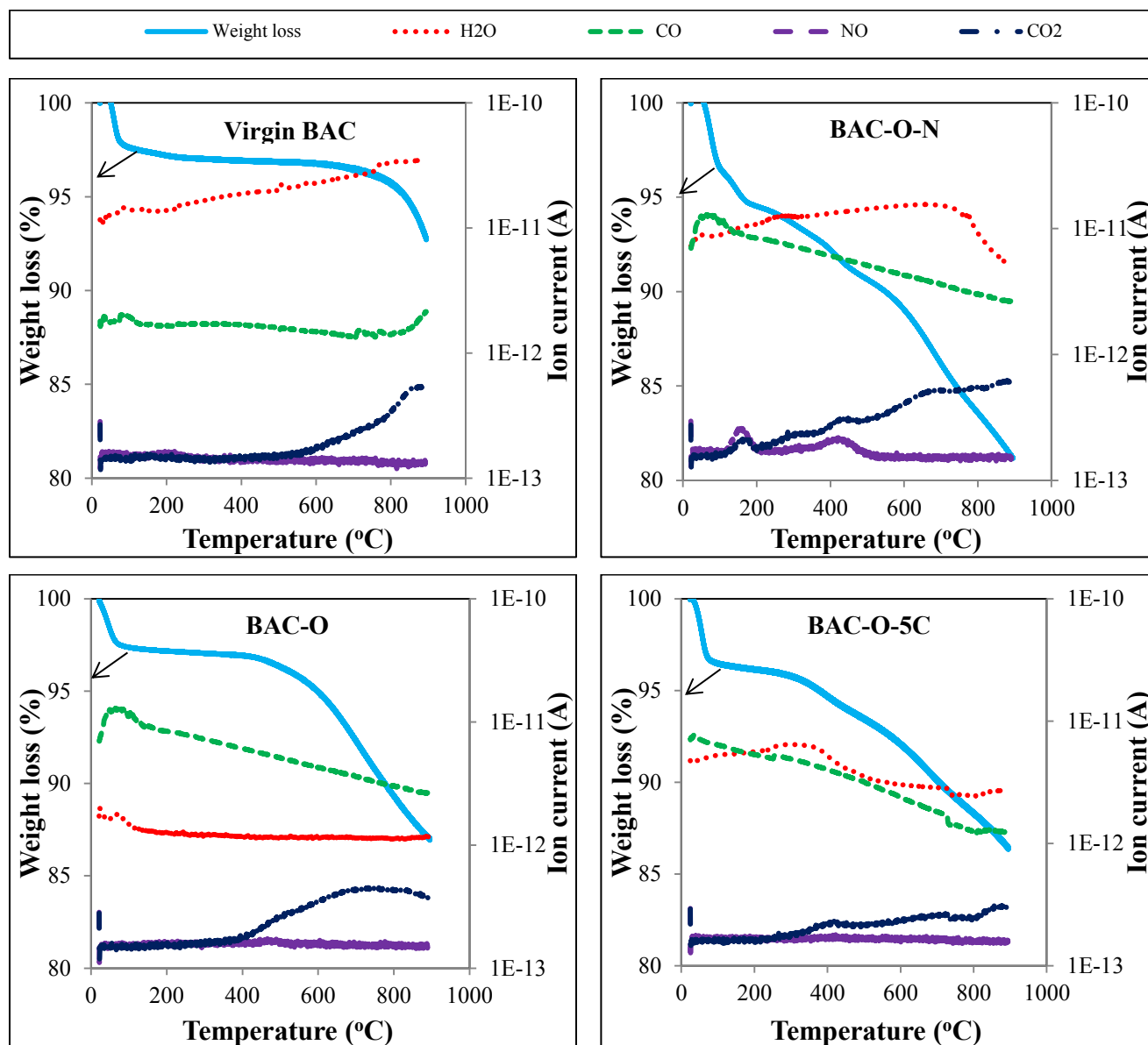


Figure 5-3. TGA-MS results of BAC samples.

Before acid treatment (virgin BAC), no CO_2 evolved at temperatures < 600 °C, but, after acid treatment (BAC-O-N), CO_2 evolution occurs as early as 125 °C due to presence of carboxylic groups (de la Puente et al., 1997) as previously confirmed by titration results (Figure 5-2). NO generation is attributed to the removal of residual nitrate groups (Stavropoulos

et al., 2008). Water desorption at temperatures as high as 600–700 °C might be due to dehydration of the SOGs (Otake and Jenkins, 1993; Moreno-Castilla et al., 1997; Perrard et al., 2012). Following heat treatment at 400 °C (BAC-O), carboxylic (excluding carboxylic anhydride) and nitrate groups are completely removed; consequently, CO₂ evolution starts at > 400 °C because of carboxylic anhydride and lactone groups' decomposition (de la Puente et al., 1997; Perrard et al., 2012), and NO is no longer generated.

5.3.2 Cyclic Adsorption/Regeneration

After characterizing the treated BACs, they were used in 5 adsorption/regeneration cycles. Duplicates 5-cycle cumulative heels for the BACs are presented in Figure 5-4. The cumulative heel after 5 adsorption/regeneration cycles was 14 and 20% higher for BAC-O-5C and BAC-H-5C, respectively, relative to BAC-V-5C. Since the physical properties of the treated samples were similar (Table 5-1), differences in their chemical properties may justify the trends. These results suggest that pre-treatments to tailor the chemical properties of BACs (i.e., oxidation or reduction) may worsen performance for the considered application.

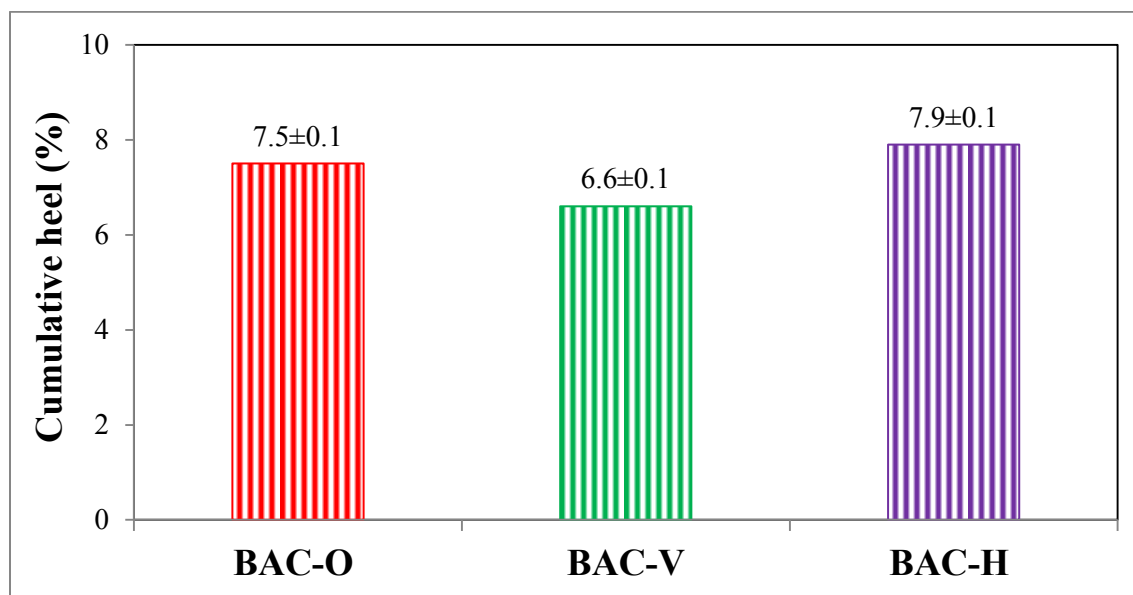


Figure 5-4. Mass balance cumulative heel after 5 adsorption/regeneration cycles.

5.3.3 Regenerated BAC Characterization

5.3.3.1 DTG Analysis of 5-Cycle Samples

DTG curves for the regenerated BACs after 5 adsorption/regeneration cycles were obtained at a low heating rate (1 °C/min) to allow high peak resolution (Figure 5-5a). Multiple peaks corresponding to desorption at different temperatures allow for quantification of adsorption strength and contribution of physisorption and chemisorption (Ferro-Garcia et al., 1993). All samples exhibited a peak at approximately 400 °C, which was higher than the regeneration temperature (288 °C) and the boiling points of the mixture components (ranging from 118 to 271 °C). This peak could be attributed to accumulation of physisorbed and/or chemisorbed species as will be discussed in subsequent sections. The physisorbed species may accumulate on adsorbent due to superposition of wall effects in pores comparable in size ($< 7 \text{ \AA}$) to adsorbed species (4.3 to 6.8 Å) (Jahandar Lashaki et al., 2012b) and/or diffusion limitations associated with the narrow micropores of the adsorbent, especially in the case of bulky adsorbates (e.g. naphthalene and diethanolamine) (Jahandar Lashaki et al., 2012a). The earliest peak was observed for BAC-O-5C and is most likely a result of weakened interactions between the adsorbates and the adsorbent due to acidic SOGs, which has been suggested previously for aqueous-phase naphthalene adsorption on AC (Ania et al., 2007). This hypothesis will also be discussed in upcoming sections.

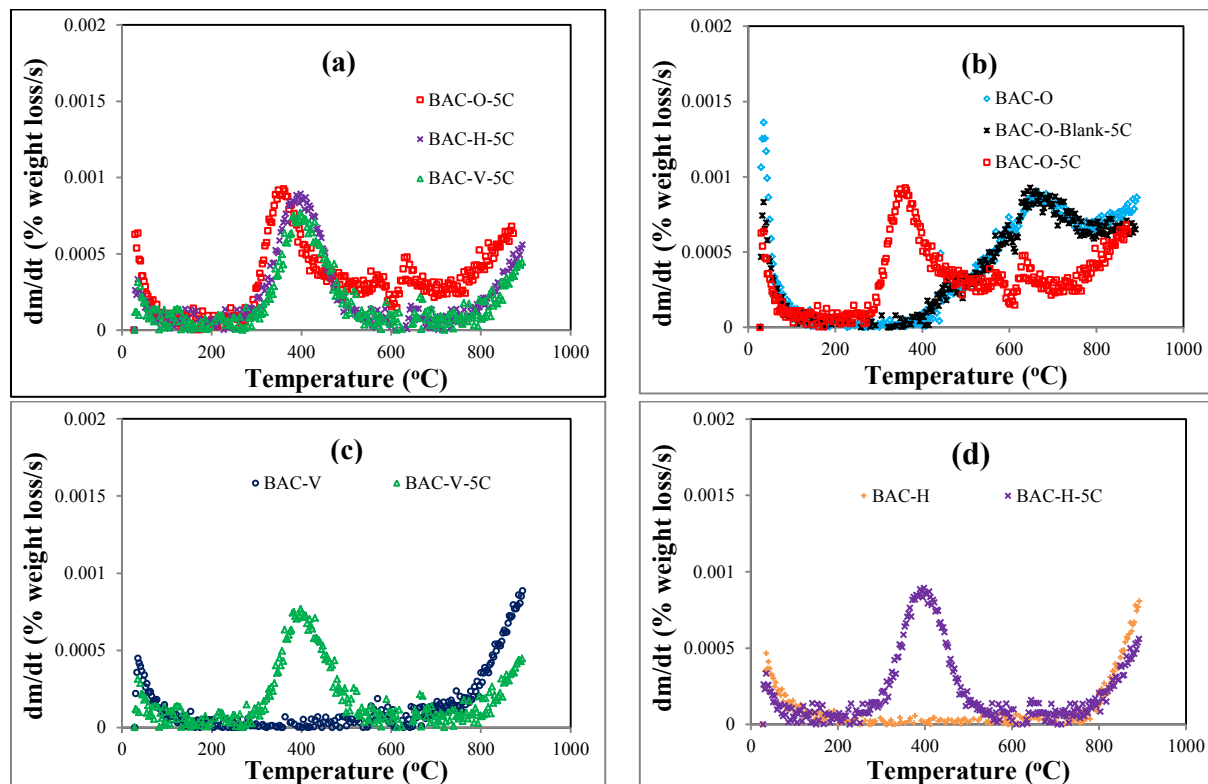


Figure 5-5. DTG analysis of: (a) BAC-O-5C, BAC-V-5C, and BAC-H-5C, (b) BAC-O, BAC-O-5C, and BAC-O-Blank-5C, (c) BAC-V and BAC-V-5C, and (d) BAC-H and BAC-H-5C.

The only regenerated sample showing weight loss at high temperature (500 to 800 °C) is BAC-O-5C (Figure 5-5a). However, the unused BAC-O sample lost more weight in this temperature range (Figure 5-5b), possibly due to removal or consumption of SOGs during cycling. A 5-cycle blank (no adsorbate) experiment performed on BAC-O (BAC-O-Blank-5C) resulted in no mass loss, indicating that SOGs are not removed during cycling in absence of adsorbate. Furthermore, the DTG profile for this blank sample matches the unused sample (BAC-O), suggesting that SOGs in BAC-O-5C were not removed (Figure 5-5b) as a result of exposure to regeneration temperature. Titration results also demonstrated no significant change (< 15%) in the concentrations of SOGs on the blank sample compared to unused BAC-O (Figure 5-2) compared to unused BAC-O. Consequently, SOGs could have been consumed due

to reactions with adsorbed species on BAC-O (Ania and Bandosz, 2005), possibly forming new volatile byproducts and/or chemisorbed species. During regeneration at 288 °C, these species may either come off the adsorbent (volatile ones) or accumulate on it (chemisorbed ones). The chemisorbed species could develop due to formation of large (i.e., high boiling point) oxidation byproducts or bonding between the adsorbates and SOGs. This hypothesis is consistent with titration results that showed a 48, 22, and 42% reduction in the concentrations of carboxylic, lactonic, and phenolic groups, respectively, on BAC-O-5C compared to unused BAC-O (Figure 5-2).

5.3.3.2 DTG Analysis of 1-Cycle Samples

Since the mixture tested here consists of compounds with different functionalities and a wide range of boiling points, the byproducts of the reactions between the SOGs of the BAC-O and the adsorbates may widely vary in terms of thermal stability, warranting further investigation. For this purpose, 1-cycle adsorption/regeneration experiments were completed on BAC-O, BAC-V, and BAC-H adsorbing each component of the mixture individually. In all cases, BAC-O loaded with a single adsorbate exhibited larger weight loss at moderate temperature (300 to 500 °C) and lower mass loss at higher temperature (500 to 800 °C), compared to unused BAC-O (Figure 5-6). This may confirm the SOGs consumption hypothesis made earlier where SOGs may be consumed through reacting with adsorbed species on BAC-O, likely resulting in formation of volatile and/or chemisorbed byproducts, which may subsequently be desorbed at low (< 300 °C) and moderate (300 to 500 °C) temperatures, respectively.

In most cases, lower weight loss at moderate temperature was observed for BAC-V and BAC-H loaded with single adsorbates relative to their BAC-O counterparts (Figure 5-6). This can be due to a different adsorption mechanism on these samples compared to BAC-O. In

general, physisorbed species with relatively low boiling point such as 1-butanol (118 °C), *n*-butylacetate (126 °C), and 2-heptanone (151 °C) can be completely desorbed during regeneration at 288 °C, which is well beyond their boiling points, and therefore will not appear in DTG curves (starting at 288 °C). The lack of a DTG peak for BAC-V and BAC-H samples loaded with these adsorbates confirm that their adsorption mainly occurred via physisorption. For adsorption on BAC-O, however, these compounds may have undergone chemical reactions with the SOGs (supported by lower mass loss at high temperature), resulting in accumulation of high boiling point species, which subsequently appears as a DTG peak at 300 to 400 °C (Figure 5-6). A possible example for this could be oxidation of 1-butanol by SOGs to form volatile (formaldehyde) and large (oxalic acid) byproducts (Popescu et al., 2003).

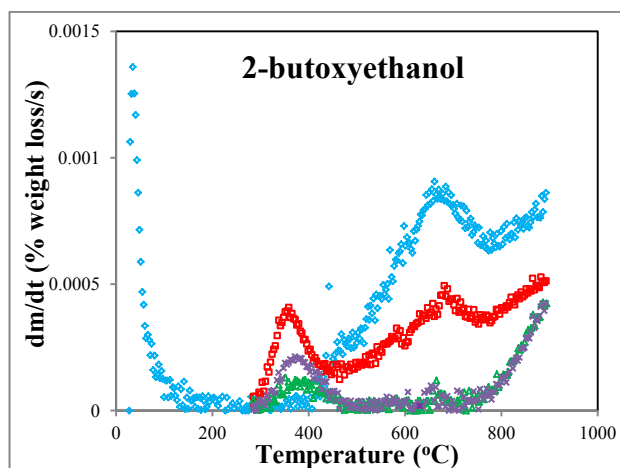
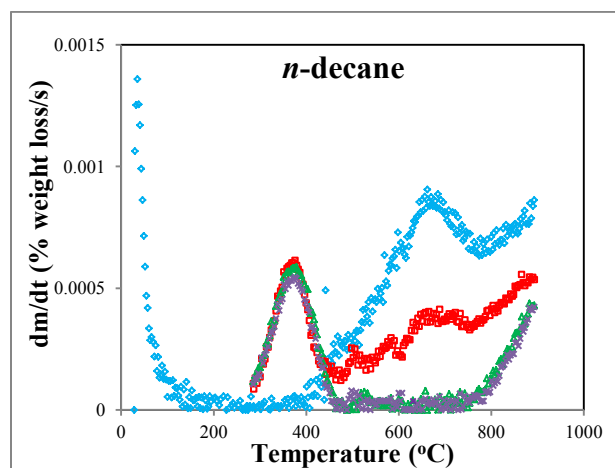
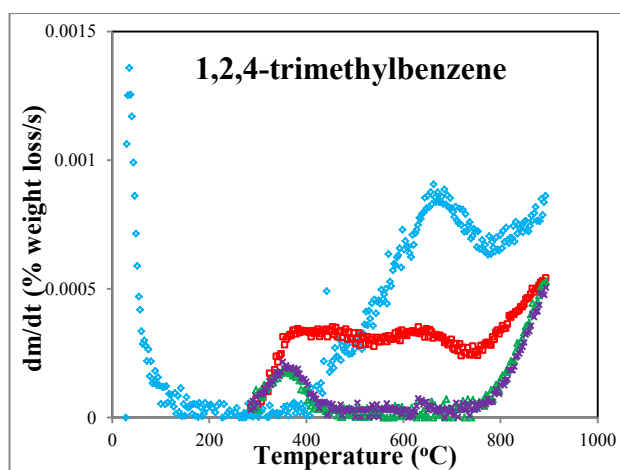
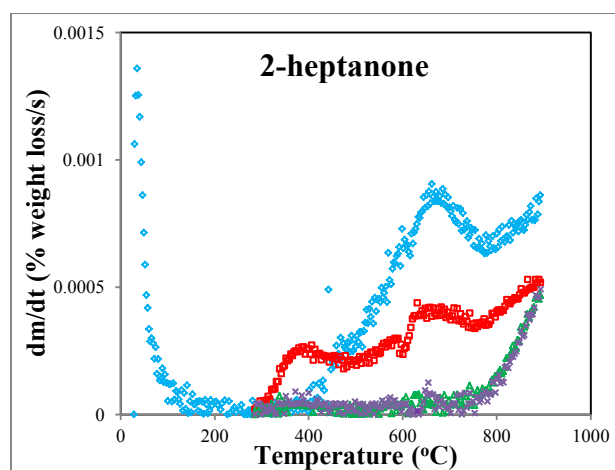
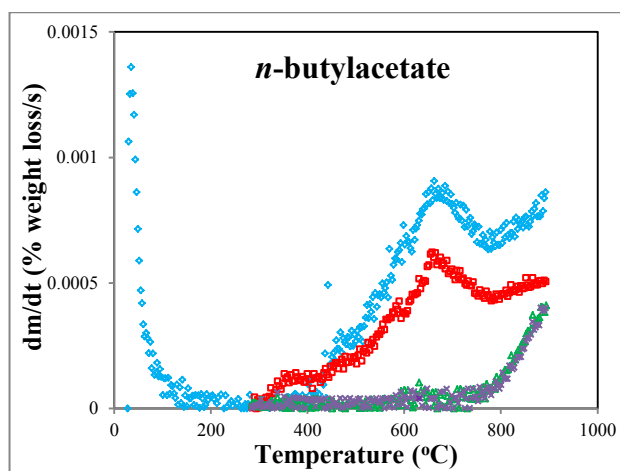
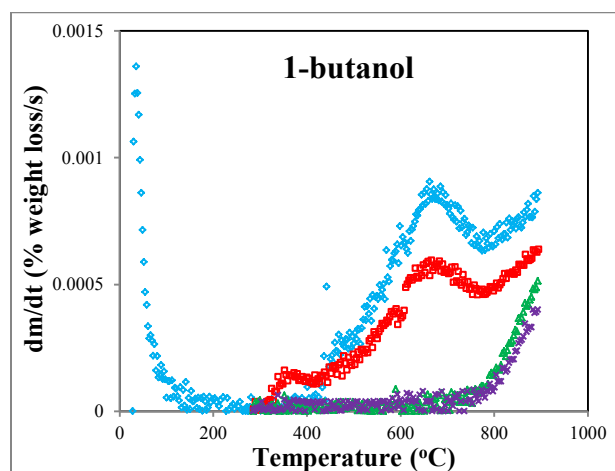
Similarly, physisorbed 1,2,4-trimethylbenzene and 2-butoxyethanol can mostly be removed during regeneration at 288 °C. Both compounds are bulky with relatively high boiling points (170 and 171 °C, respectively), therefore, diffusion limitations may cause minor heel formation on BAC-V and BAC-H, which subsequently appears as a small DTG peak (Figure 5-6). This peak is higher for BAC-H loaded with 2-butoxyethanol than its BAC-V counterpart, which is unexpected because they have similar physical properties and both have low surface oxygen content (Table 5-1). This could be justified by the effect of high temperature thermal treatment on activated carbon's surface, which may leave a surface with high affinity towards oxygen adsorption. Thermal treatment at 950 °C with simultaneous hydrogen purge has been recommended to stabilize the surface (Menendez et al., 1996). Since a lower temperature of 850 °C was used in our study, this may cause 2-butoxyethanol (an oxygen-containing adsorbate) to interact with BAC-H, resulting in a higher adsorbate accumulation compared to BAC-V. For BAC-O, however, 1,2,4-trimethylbenzene and 2-butoxyethanol may consume the SOGs to form

chemisorbed species, resulting in higher mass loss at moderate temperature, compared to BAC-V and BAC-H. A possible example of this could be H-bonding between SOGs and methyl group ($-\text{CH}_3$) of 1,2,4-trimethylbenzene (Franz et al., 2000; Arafat et al., 2004).

For *n*-decane and 2,2-dimethylpropylbenzene, the DTG peaks coincided for all the treated samples (Figure 5-6), possibly due to accumulation of physisorbed species. It is possible that some volatile oxidation byproducts were formed during their adsorption on BAC-O (lower mass loss at high temperature) but were eliminated during regeneration at 288 °C, resulting in a similar DTG peak to BAC-V and BAC-H.

Diethanolamine and naphthalene may also accumulate on all samples due to the regeneration temperature of 288 °C, which was likely insufficiently high relative to the boiling points of these compounds (271 and 218 °C, respectively) (Figure 5-6). For diethanolamine, BAC-O depicted the highest DTG peak. This higher DTG peak may be explained by a condensation reaction between its amino group ($-\text{NH}_2$) and SOGs (Tamon et al., 1996; Tamon and Okazaki, 1996), resulting in formation of chemisorbed species. The DTG peak for BAC-H loaded with diethanolamine was also slightly higher than that of BAC-V, possibly due to high affinity of BAC-H to this oxygen-containing compound, as discussed earlier. Finally, for naphthalene, the lowest and earliest peak was observed for BAC-O, most likely due to weakened dispersive interactions between the carbon surface and naphthalene as a result of π -electrons removal from the carbon surface by SOGs, as previously suggested in the literature for aqueous phase naphthalene adsorption (Ania et al., 2007).

◇ Unused BAC-O □ Loaded BAC-O △ Loaded BAC-V × Loaded BAC-H



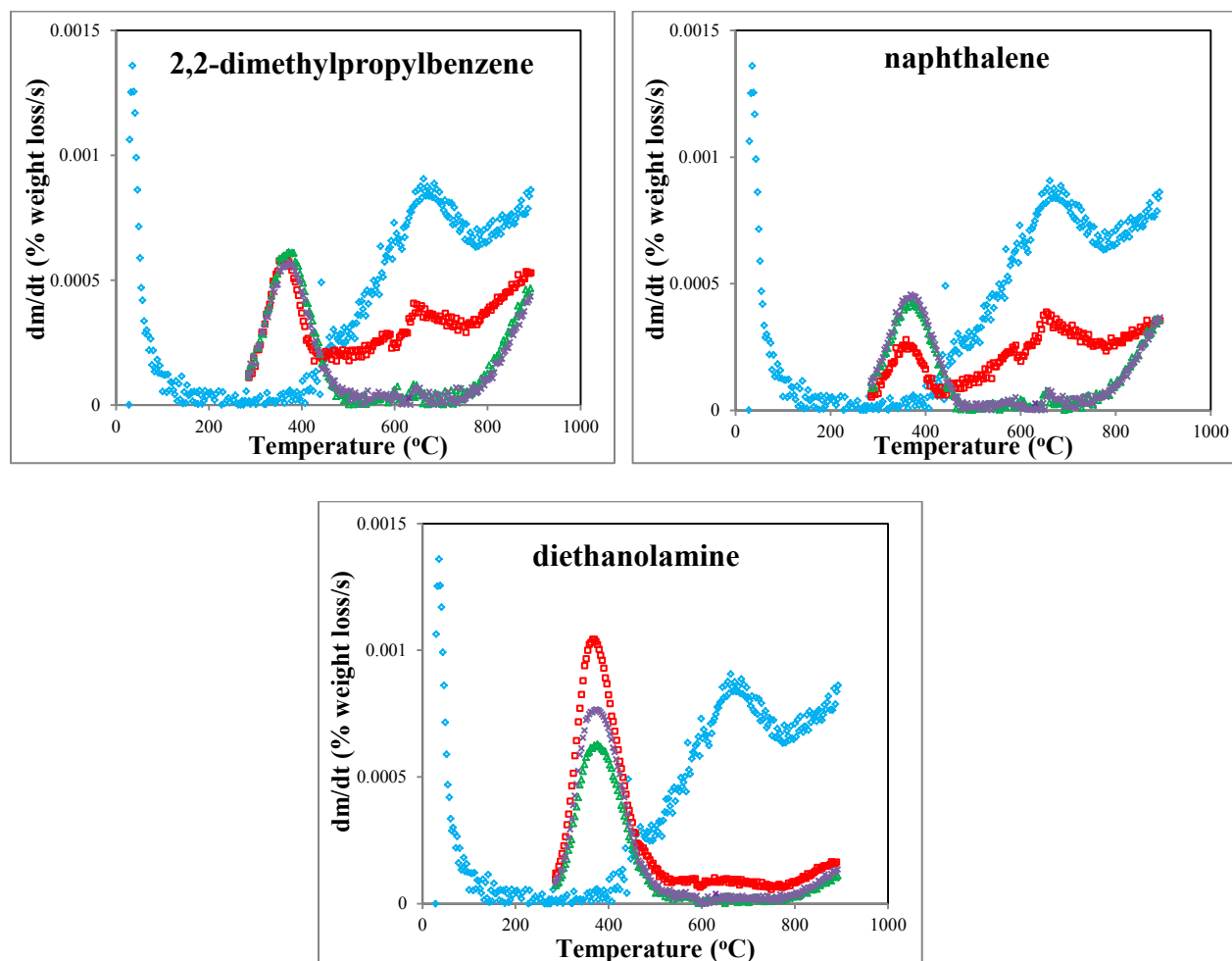


Figure 5-6. DTG analysis of treated BACs loaded with single adsorbates.

5.3.3.3 Heel Formation Mechanism for 5-Cycle Samples

The results from the single cycle tests help explain the heel formation mechanism for the 5-cycle samples loaded with the adsorbate mixture. The DTG peak of physisorbed species (e.g. *n*-decane and 2,2-dimethylpropylbenzene) may overlap with the DTG peak of species with heel contributions from both physisorption and chemisorption (e.g. 2-butoxyethanol and 1,2,4-trimethylbenzene). Combining the findings of the DTG analyses from Figure 5-5 and Figure 5-6, it can be concluded that for BAC-V-5C and BAC-H-5C heel formation was due to physisorption. In contrast, a combination of physisorption and chemisorption contributed to heel formation on

BAC-O-5C. DTG results support the cumulative heel percentages for the tested BACs (Figure 5-4) where BAC-O-5C exhibited larger mass balance cumulative heel compared to BAC-V-5C, possibly because two mechanisms (i.e., physisorption and chemisorption) were contributing heel. Higher heel formation on BAC-H-5C relative to BAC-V-5C could be explained by higher affinity of hydrogen-treated BAC to oxygen-containing compounds (i.e., 2-butoxyethanol and diethanolamine). The results from single cycle naphthalene adsorption (weakened physisorption on BAC-O; Figure 5-6) may also justify the earlier DTG peak for BAC-O-5C as compared to BAC-V-5C and BAC-H-5C samples (Figure 5-5).

5.3.3.4 TGA-MS of 5-Cycle Samples

BAC-O-5C was also analyzed using TGA-MS (Figure 5-3). CO₂ evolution started at > 300 °C, slightly higher than the regeneration temperature during cycling (288 °C) showing that decomposed heel compounds as well as the previously described decomposed carboxylic anhydride and lactone groups are contributing mass losses. Comparing BAC-O and BAC-O-5C, especially at high temperatures, less CO₂ is generated after cycling than before cycling, supporting the SOGs consumption argument made earlier.

5.3.3.5 XPS of 5-Cycle Samples

XPS analysis was completed on the regenerated samples to assess changes in surface elemental composition following adsorption/regeneration cycling (Table 5-1). Notable increases in oxygen and nitrogen content were observed when comparing treated BACs before and after cycling. Nitrogen increases, in all cases, were attributed to accumulation of diethanolamine, since this is the only nitrogen-containing compound among the species in the test mixture. Diethanolamine has a high boiling point (271 °C) and has previously been shown to be a major heel contributor (Jahandar Lashaki et al., 2012a). The largest increase in nitrogen content was

observed for BAC-O-5C compared to BAC-V-5C and BAC-H-5C (Table 5-1) possibly due to reactions between diethanolamine and BAC-O, as discussed earlier. Since diethanolamine has two hydroxyl groups, this can also partially explain the increase in oxygen content of all samples after cycling.

5.3.3.6 Micropore Surface Analysis of 5-Cycle Samples

Regenerated BACs were characterized to quantify the effect of irreversible adsorption on their physical properties (Table 5-1). Some adsorption sites remained occupied by adsorbates after regeneration, and, as a result, the number of vacant sites quantified with N₂ adsorption decreased. Reduction in total pore volume after cycling was 21%, 14%, and 14% for BAC-O-5C, BAC-V-5C, and BAC-H-5C, respectively. The reduction in BET surface area after cycling was 22%, 17%, and 18% for BAC-O-5C, BAC-V-5C, and BAC-H-5C, respectively. The largest reduction in the aforementioned physical properties was observed for BAC-O-5C, which may result from additional pore blockage caused by large, chemisorbed species. No significant differences were observed between BAC-V-5C and BAC-H-5C.

PSDs for the regenerated BACs help to identify the location of the formed heel in terms of pore size. Irreversibly adsorbed compounds occupied a portion of the micropores, but in different pore size ranges (Figure 5-7). Blockage occurred mainly in narrow micropores ($< 7 \text{ \AA}$) for BAC-V-5C and BAC-H-5C (Figure 5-7c and d). These pores were comparable in size to the tested adsorbates (4.3 to 6.8 \AA) (Jahandar Lashaki et al., 2012b), which may cause pore blockage due to strong dispersive forces caused by superposition of wall effects (Li et al., 2011). This supports DTG results (Figure 5-5) that showed physisorption as the primary mechanism for heel formation on BAC-V-5C and BAC-H-5C. Conversely, no significant blockage of narrow micropores ($< 7 \text{ \AA}$) was observed for BAC-O-5C. Instead, blockage shifted to micropores

between 7 and 12 Å (Figure 5-7b). It is possible that large, chemisorbed byproducts and physisorbed species accumulated in these pores. Since the pores (7–12 Å) were larger, the superposition of wall effects and diffusion limitations were decreased compared to the narrow micropores, so physical adsorption was weaker, resulting in an earlier DTG peak for BAC-O-5C (Figure 5-5a). Moreover, acidic SOGs can remove π -electrons from the carbon surface, causing weakened dispersive interactions between the carbon surface and adsorbates such as naphthalene (Ania et al., 2007), as discussed earlier.

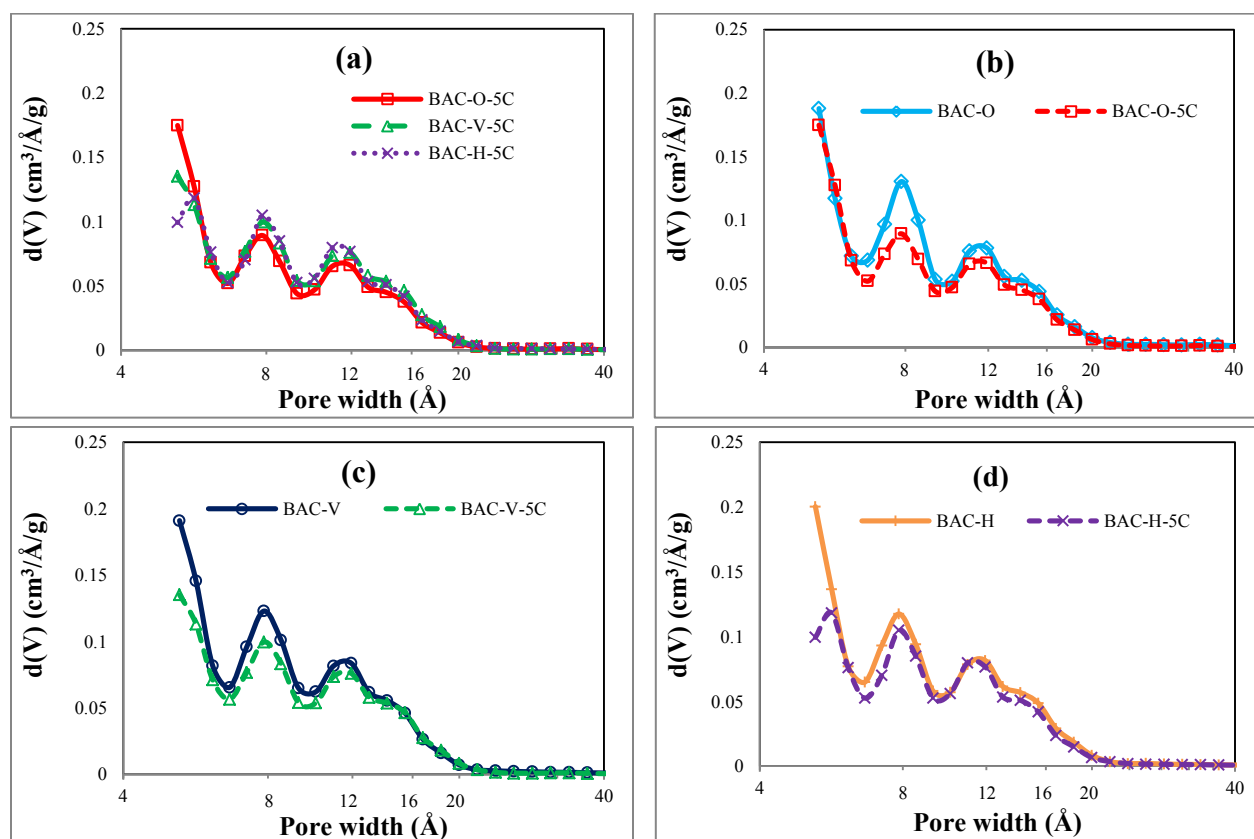


Figure 5-7. PSD of: (a) BAC-O-5C, BAC-V-5C, and BAC-H-5C, (b) BAC-O and BAC-O-5C, (c) BAC-V and BAC-V-5C, and (d) BAC-H and BAC-H-5C.

5.4 Conclusions

The effect of adsorbent surface oxygen groups on the irreversible adsorption of a mixture of organic compounds was investigated using three BACs tailored to have similar pore size

distributions but different amounts of surface oxygen groups. For these samples, higher mass balance cumulative heel was observed for oxygen functionalized and hydrogen-treated BACs compared to heat-treated BAC. Based on derivative thermo-gravimetric analysis, heel formation due to accumulation of physisorbed species was observed for heat-treated and hydrogen-treated carbons. In contrast, a combination of chemisorption and physisorption was responsible for heel formation on oxygen functionalized BAC; surface oxygen groups were consumed by adsorbed species to form chemisorbed species. Pore size distributions indicate that narrow micropores (< 7 Å) have a significant role in the accumulation of adsorbates in heat-treated and hydrogen-treated BACs. Larger micropores (7–12 Å), however, were responsible for heel formation in nitric acid-treated BAC, resulting in weakened physisorption. Fundamentally, these results help to explain the irreversible adsorption mechanism by showing how surface oxygen groups impact adsorbate-adsorbent interactions.

5.5 References

- Alvarez, P.M.; Beltran, F. J.; Gomez-Serrano, V.; Jaramillo, J.; Rodriguez, E. M. Comparison between thermal and ozone regenerations of spent activated carbon exhausted with phenol. *Water Res.* **2004**, *38*, 2155–2165.
- Anderson, J.E.; Gilland, R.D.; Adams, J.A.; Saloka, G.S.; Dearth, M.A.; Novak, R.F.; Kim, B.R.; Wherrett, M.R.; Davies, K.L.; Hula, A.C.; Edgeworth, R.K.; Ryan, P.A.; Cowles, H. Recovering VOCs from paint spray booth air using an activated-carbon fluidized-bed adsorber for subsequent power generation. *In Proceedings of 99th Air and Waste Management Association's Annual Conference and Exhibition*, New Orleans, LA, 2006.
- Ania, C.O.; Menendez, J.A.; Parra, J.B.; Pis, J.J. Microwave-induced regeneration of activated carbons polluted with phenol: A comparison with conventional thermal regeneration. *Carbon* **2004**, *42*, 1383–1387.
- Ania, C.O.; Bandosz, T.J. Importance of structural and chemical heterogeneity of activated carbon surfaces for adsorption of dibenzothiophene. *Langmuir* **2005**, *21*, 7752–7759.
- Ania, C.O.; Cabal, B.; Pevida, C.; Arenillas, A.; Parra, J.B.; Rubiera, F.; Pis, J.J. Effects of activated carbon properties on the adsorption of naphthalene from aqueous solutions. *Appl. Surf. Sci.* **2007**, *253*, 5741–5746.
- Arafat, H.A.; Ahnert, F.; Pinto, N.G.; On the adsorption of aromatics on oxygenated activated carbon in nonaqueous adsorption media. *Sep. Sci. Tech.* **2004**, *39*, 43–62.
- Atkinson, J.D.; Zhang, Z.; Yan, Z.; Rood, M.J. Evolution and impact of acidic oxygen functional groups on activated carbon fiber cloth during NO oxidation. *Carbon* **2013**, *54*, 444–453.
- Boehm H.P. Some Aspects of the Surface Chemistry of Carbon Black and Other Carbons. *Carbon* **1994**, *32*, 759 – 769.
- Boehm, H.P. Surface oxides on carbon and their analysis: A critical Assessment. *Carbon* **2002**, *40*, 145–149.
- Brunauer, S.; Emmett, P.H.; Teller, E. Adsorption of gases in multimolecular layers. *J. Am. Chem. Soc.* **1938**, *60*, 309–319.
- Busca, G.; Berardinelli, S.; Resini, C.; Arrighi, L. Technologies for the removal of phenol from fluid streams: A short review of recent developments. *J. Hazard. Mater.* **2008**, *160*, 265–288.

- Coughlin, R.W.; Ezra, F.S. Role of surface acidity in the adsorption of organic pollutants on the surface of carbon. *Environ. Sci. Technol.*, **1968**, *2*, 291–297.
- Dabrowski, A.; Podkoscielny, P.; Hubicki, Z.; Barczak, M. Adsorption of phenolic compounds by activated carbon-A critical review. *Chemosphere* **2005**, *58*, 1049–1070.
- de Jonge, R.J.; Breure, A.M.; van Andel, J.G. Bioregeneration of powdered activated carbon (PAC) loaded with aromatic compound. *Water Res.* **1996a**, *30*, 875–882.
- de Jonge, R.J.; Breure, A.M.; van Andel, J.G. Reversibility of adsorption of aromatic compounds onto powdered activated carbon. *Water Res.* **1996b**, *30*, 883–892.
- de la Puente, G.; Pis, J. J.; Menendez, J. A.; Grange, P. Thermal stability of oxygenated functions in activated carbons. *J. Anal. Appl. Pyrol.* **1997**, *43*, 125–138.
- Ferro-Garcia, M.A.; Utrera-Hidalgo, E.; Rivera-Utrilla, J.; Moreno-Castilla, C.; Joly, J.P. Regeneration of activated carbons exhausted with chlorophenols. *Carbon* **1993**, *31*, 857–863.
- Franz, M.; Arafat, H.A.; Pinto, N.G. Effect of chemical surface heterogeneity on the adsorption mechanism of dissolved aromatics on activated carbon. *Carbon* **2000**, *38*, 1807–1819.
- Hashisho, Z.; Rood, M.J.; Botich, L. Microwave-swing adsorption to capture and recover vapors from air streams with activated carbon fiber cloth. *Environ. Sci. Technol.* **2005**, *39*, 6851–6859.
- Hashisho, Z.; Emamipour, H.; Cevallos, D.; Rood, M.J.; Hay, K.J.; Kim, B.J. Rapid response concentration-controlled desorption of activated carbon to dampen concentration fluctuations. *Environ. Sci. Technol.* **2007**, *41*, 1753–1758.
- Hashisho, Z.; Emamipour, H.; Rood, M.J.; Hay, K.J.; Kim, B.J.; Thurston, D. Concomitant adsorption and desorption of organic vapor in dry and humid air streams using microwave and direct electrothermal swing adsorption. *Environ. Sci. Technol.* **2008**, *42*, 9317–9322.
- Hashisho, Z.; Rood, M.J.; Barot, S.; Bernhard, J. Role of functional groups on the microwave attenuation and electric resistivity of activated carbon fiber cloth. *Carbon* **2009**, *47*, 1814–1823.
- Jahandar Lashaki, M.; Fayaz, M.; Wang, H.; Hashisho, Z.; Phillips, J.H.; Anderson, J.E.; Nichols, M. Effect of adsorption and regeneration temperature on irreversible adsorption

- of organic vapors on beaded activated carbon. *Environ. Sci. Technol.* **2012a**, *46*, 4083–4090.
- Jahandar Lashaki, M.; Fayaz, M.; Niknaddaf, S.; Hashisho, Z. Effect of the adsorbate kinetic diameter on the accuracy of the Dubinin-Radushkevich equation for modeling adsorption of organic vapors on activated carbon. *J. Hazard. Mater.* **2012b**, *241–242*, 154–163.
- Kim, B.R. VOC emissions from automotive painting and their control: A review. *Environ. Eng. Res.* **2011**, *16*, 1–9.
- Kureha Corporation Website; <http://www.kureha.com/pdfs/Kureha-BAC-Bead-Activated-Carbon.pdf>
- Leng, C.C.; Pinto, N.G. Effects of surface properties of activated carbons on adsorption behavior of selected aromatics. *Carbon* **1997**, *35*, 1375–1385.
- Li, L.; Liu, S.; Liu, J. Surface modification of coconut shell based activated carbon for the improvement of hydrophobic VOC removal. *J. Hazard. Mater.* **2011**, *192*, 683–690.
- Lu, Q.; Sorial, G.A. The effect of functional groups on oligomerization of phenolics on activated carbon. *J. Hazard. Mater.* **2007**, *148*, 436–445.
- Lu, Q.; Sorial, G.A. A comparative study of multicomponent adsorption of phenolic compounds on GAC and ACFC. *J. Hazard. Mater.* **2009**, *167*, 89–96.
- Mahajan, O.P.; Moreno-Castilla, C.; Walker Jr., P.L. Surface-treated activated carbon for removal of phenol from water. *Sep. Sci. Technol.* **1980**, *15*, 1733–1752.
- Matatov-Meytal, Y.I.; Sheintuch, M. Catalytic abatement of water pollutants. *Ind. Eng. Chem. Res.* **1998**, *37*, 309–326.
- Menendez, J.A.; Phillips, J.; Xia, B.; Radovic, L.R. On the modification and characterization of chemical surface properties of activated carbon: In the search of carbons with stable basic properties. *Langmuir* **1996**, *12*, 4404–4410.
- Moreno-Castilla C.; Carrasco-Marin F.; Mueden A. The creation of acid carbon surfaces by treatment with $(\text{NH}_4)_2\text{S}_2\text{O}_8$. *Carbon* **1997**, *35*, 1619–1626.
- Nevskaia, D.M.; Santianes, A.; Munoz, V.; Guerrero-Ruiz, A. Interaction of aqueous solutions of phenol with commercial activated carbons: An adsorption and kinetic study. *Carbon* **1999**, *37*, 1065–1074.

- Niknaddaf, S.; Atkinson, J.D.; Shariaty, P.; Jahandar Lashaki, M.; Hashisho, Z.; Phillips, J.H.; Anderson, J.E.; Nichols, M. Heel formation during volatile organic compound desorption from activated carbon fiber cloth. *Carbon* **2016**, *96*, 131–138.
- Otake, Y.; Jenkins, R.G. Characterization of oxygen-containing surface complexes created on a microporous carbon by air and nitric acid treatment. *Carbon* **1993**, *31*, 109–121.
- Perrard, A.; Retailleau, L.; Berjoan, R.; Joly, J.P. Liquid phase oxidation kinetics of an ex-cellulose activated carbon cloth by NaOCl. *Carbon* **2012**, *50*, 2226–2234.
- Popescu, M.; Joly, J.P.; Carre, J.; Danatoiu, C. Dynamical adsorption and temperature-programmed desorption of VOCs (toluene, butyl acetate and butanol) on activated carbons. *Carbon* **2003**, *41*, 739–748.
- Qiao, W.M.; Korai, Y.; Mochida, I.; Hori, Y.; Maeda, T. Preparation of an activated carbon artifact: oxidative modification of coconut shell-based carbon to improve the strength. *Carbon* **2002**, *40*, 351–358.
- Quantachrome Autosorb 1 Operating Manual; **2006**.
- Radovic, L.R.; Moreno-Castilla, C.; Rivera-Utrilla, J. Carbon materials as adsorbents in aqueous solutions. *Chem. Phys. Carbon* **2001**, *27*, 227–405.
- Ramos, M.E.; Bonelli, P.R.; Cukiermana, A.L.; Ribeiro Carrott, M.M.L.; Carrott, P.J.M. Adsorption of volatile organic compounds onto activated carbon cloths derived from a novel regenerated cellulosic precursor. *J. Hazard. Mater.* **2010**, *177*, 175–182.
- Rivera-Utrilla, J.; Sánchez-Polo, M.; Gomez-Serrano, V.; Alvarez, P.M. Alvim-Ferraz, M.C.M.; Dias, J.M. Activated carbon modifications to enhance its water treatment applications: An overview. *J. Hazard. Mater.* **2011**, *187*, 1–23.
- Salvador, F.; Martin-Sanchez, N.; Sanchez-Hernandez, R.; Sanchez-Montero, M.J.; Izquierdo, C. Regeneration of carbonaceous adsorbents. Part I: Thermal regeneration. *Micropor. Mesopor. Mat.* **2015**, *202*, 259 – 276.
- Soto, M.L.; Moure, A.; Dominguez, H.; Parajo, J.C. Recovery, concentration and purification of phenolic compounds by adsorption: A review. *J. Food Eng.* **2011**, *105*, 1–27.
- Stavropoulos, G.G.; Samaras, P.; Sakellariopoulos, G.P. Effect of activated carbons modification on porosity, surface structure and phenol adsorption. *J. Hazard. Mater.* **2008**, *151*, 414–421.

- Sullivan, P.D.; Stone, B.R.; Hashisho, Z.; Rood, M.J. Water adsorption with hysteresis effect onto microporous activated carbons. *Adsorption* **2007**, *13*, 173–89.
- Tamon, H.; Atsushi, M.; Okazaki, M. On irreversible adsorption of electron-donating compounds in aqueous solution. *J. Colloid Interface Sci.* **1996**, *177*, 384–390.
- Tamon, H.; Okazaki, M. Desorption characteristics of aromatic compounds in aqueous solution on solid adsorbents. *J. Colloid Interface Sci.* **1996**, *179*, 181–187.
- Tefera, D.T.; Jahandar Lashaki, M.; Fayaz, M.; Hashisho, Z.; Phillips, J.H.; Anderson, J.E.; Nichols, M. Two-dimensional modelling of temperature swing adsorption of volatile organic compounds using beaded activated carbon. *Environ. Sci. Technol.* **2013a**, *47*, 11700–11710.
- Terzyk, A.P.; Wisniewski, M.; Gauden, P.A.; Rychlicki, G.; Furmaniak, S. Carbon surface chemical composition in para-nitrophenol adsorption determined under real oxic and anoxic conditions. *J. Colloid Interface Sci.* **2008**, *320*, 40–51.
- Terzyk, A.P. The impact of carbon surface chemical composition on the adsorption of phenol determined at the real oxic and anoxic conditions. *Appl. Surf. Sci.* **2007**, *253*, 5752–5755.
- Wang, H.; Jahandar Lashaki, M.; Fayaz, M.; Hashisho, Z.; Phillips, J.H.; Anderson, J.E.; Nichols, M. Adsorption and desorption of mixtures of organic vapors on beaded activated carbon. *Environ. Sci. Technol.* **2012**, *46*, 8341–8350.
- Yonge, D.R.; Keinath, T.M.; Poznanska, K.; Jiang, Z.P. Single-solute irreversible adsorption on granular activated carbon. *Environ. Sci. Technol.* **1985**, *19*, 690–694.

CHAPTER 6. EFFECT OF DESORPTION PURGE GAS OXYGEN IMPURITY ON IRREVERSIBLE ADSORPTION OF ORGANIC VAPORS¹

6.1 Introduction

Adsorption onto activated carbon is widely used for capturing organic pollutants from gaseous and aqueous streams (Hashisho et al., 2007, 2009; Das et al., 2004) because it is cost effective, and allows adsorbent reuse and the possibility of adsorbate recovery (Hashisho et al., 2005, 2008; Dabrowski et al., 2005). A challenge for the use of adsorption onto activated carbon is the irreversible adsorption or heel formation due to strongly, or even permanently, adsorbed species (Jahandar Lashaki et al., 2012a; Niknaddaf et al., 2016). This prevents complete adsorbent regeneration, decreasing its capacity and lifetime, which correspondingly increases operation and maintenance costs due to the need for more frequent adsorbent replacement (Jahandar Lashaki et al., 2012a; Niknaddaf et al., 2016).

Adsorbent physical and chemical properties (Chang and Savage, 1981; Vidic et al., 1993; Lu and Sorial 2004a, 2004b), adsorbate size and chemical structure (Tamon and Okazaki, 1996; Tanthapanichakoon, et al., 2005), dissolved oxygen in the adsorption solution (Vidic and Suidan, 1991; Abuzaid and Nakhla, 1994; Uranowski et al., 1998), and, to a lesser extent, metals and metal oxides in/on the adsorbent (Grant and King, 1990; Kilduff and King, 1997; Leng and Pinto, 1997), affect the extent of aqueous-phase irreversible adsorption of organic compounds. This has been thoroughly described in the literature, but similar studies are not available for the gas phase.

¹ A version of this chapter has been published as: Jahandar Lashaki, M.; Atkinson, J.D.; Hashisho, Z.; Phillips, J.H.; Anderson, J.E.; Nichols, M.; Misovski, T. Effect of desorption purge gas oxygen impurity on irreversible adsorption of organic vapors. *Carbon* **2015**, doi:10.1016/j.carbon.2015.12.037. Reproduced with permission from Elsevier.

Ideally, regeneration of saturated adsorbents should remove the adsorbates from the adsorbent pores with minimal impact on the physical or chemical properties of the adsorbent, or the chemical composition of the adsorbate. Most irreversible adsorption studies in the *aqueous phase* use thermal decomposition at temperatures as high as 900 °C or solvent extraction for regenerating activated carbon adsorbents saturated with organic pollutants (Salvador et al., 2015). On the other hand, thermal desorption at < 300 °C is industrially used for regenerating adsorbents loaded with *gas phase* pollutants, such as VOCs (Salvador et al., 2015).

During high-temperature thermal desorption, the adsorbent bed must be purged with an inert gas to remove desorbed species and avoid bed fires caused by exposing the concentrated organic compounds to temperatures higher than their ignition temperature (Zerbonia et al., 2001). High purity N₂ is widely used in industrial regeneration applications and many facilities use on-site N₂ generators for its production (Compressed Air Best Practices Website). Impurities such as O₂, CO₂, and H₂O exist in the generated gas, but CO₂ and H₂O concentrations are typically small compared to the O₂ concentration (Compressed Air Best Practices Website). During long-term use, operational experience by the authors (data not shown) suggests that trace levels of oxygen may increase heel formation by initiating chemical reactions with adsorbents (United States Naval Research Laboratory, 1984) and/or adsorbates at the regeneration temperatures used in gas-phase thermal desorption.

Membrane separation and pressure swing adsorption (PSA) are widely used for nitrogen separation from air. However, membrane separation is not recommended for large plants that require high N₂ flow rates (Compressed Air Best Practices Website). Nitrogen purity impacts operational costs associated with N₂ generation, specifically, electricity consumption. In a typical PSA process, compressor power consumption increases from 37 to 56, 93, and 149 kW as N₂

purity increases from 95% to 99.5%, 99.99%, and 99.999%, respectively (Compressed Air Best Practices Website). While using lower purity N₂ can reduce the cost of adsorbent regeneration, it has potential to increase heel buildup and reduce adsorbent lifetime. Hence, the objective of this work is to elucidate the impact of purge gas oxygen impurity on irreversible adsorption of organic vapors. To the best of our knowledge, no previous research investigated the effect of purge gas purity on gas-phase irreversible adsorption of organic vapors. Furthermore, a better understanding of the factors contributing to irreversible adsorption can be constructive in finding ways to reduce heel buildup and increase the adsorbent's useful lifetime.

6.2 Materials and Methods

6.2.1 Adsorbent

Petroleum pitch-based beaded activated carbon (G-70R; Kureha Corporation) was used for all tests. The BAC has very low ash content (< 0.05%) (Kureha Corporation Website), ruling out the possible complexities associated with catalytic reactions (Matatov-Meytal and Sheintuch, 1998). Prior to use, the BAC was dried in air at 150 °C for > 24 h and then stored in a desiccator.

6.2.2 Adsorbates

Two adsorbate mixtures were used in this study (Table 6-1). Using a mixture of organic compounds as test adsorbate provides a more realistic surrogate for VOCs emitted from automotive painting operations. Mixture 1 consisted of compounds representing different organic groups commonly present in automotive painting solvents (Jahandar Lashaki et al., 2012a). The components of the mixture have a wide range of boiling points (118 to 271 °C) and kinetic diameters (4.3 to 6.8 Å) (Jahandar Lashaki et al., 2012b), and previously showed a high tendency to form heel (Wang et al., 2012; Tefera et al., 2014). As such, Mixture 1 was used as worst case scenario for heel formation. To prepare Mixture 1, equal volumes of each component were

mixed. The density of the mixture was 0.86 g/cm^3 . A second mixture, Mixture 2, was used to generate a VOC laden stream that is more representative of automotive painting booth air streams. Mixture 2 was used in two 50-cycle adsorption/regeneration experiments to assess the impact of long-term exposure to high O_2 concentrations on heel buildup. Overall, Mixture 2 consists of compounds with lower boiling point relative to Mixture 1.

Table 6-1. Composition of test mixtures.

Mixture 1			
Compound	CAS number	Boiling point (°C)	Volume fraction (%)
1-butanol	71-36-3	118	11.1
<i>n</i> -butylacetate	123-86-4	126	11.1
2-heptanone	110-43-0	151	11.1
1,2,4-trimethylbenzene	95-63-6	170	11.1
2-butoxyethanol	111-76-2	171	11.1
<i>n</i> -decane	124-18-5	174	11.1
2,2-dimethylpropylbenzene	1007-26-7	186	11.1
naphthalene*	91-20-3	218	11.1
diethanolamine*	111-42-2	271	11.1
Mixture 2			
isopropanol	67-63-0	83	5.1
<i>n</i> -heptane	142-82-5	98	5.7
1-butanol	71-36-3	118	19.9
propylpropionate	106-36-5	123	8.1
<i>n</i> -butylacetate	123-86-4	126	13.7
butylpropionate	590-01-2	146	7.5
<i>n</i> -amylacetate	628-63-7	147	5.6
1,2,4-trimethylbenzene	95-63-6	170	11.7
light aromatic naphtha	64742-95-6	135-210	17.0
medium aliphatic solvent naphtha	64742-88-7	179-210	5.7

* Naphthalene and diethanolamine were measured by weight using the corresponding densities.

6.2.3 Setup and Methods

The experimental setup and methods used here are consistent with our previous irreversible adsorption studies (Jahandar Lashaki et al., 2012a; Wang et al., 2012; Tefera et al., 2013a). A stainless steel adsorption/regeneration tube was filled with 4.0 ± 0.1 g of dry BAC. The VOC vapor stream was generated using a syringe pump to inject the adsorbate mixture into a 10 SLPM air stream, generating a constant VOC concentration (500 ppm_v). A PID (Minirae 2000, Rae Systems) intermittently measured total VOC concentration during adsorption to generate breakthrough curves for Mixture 1. The PID was calibrated before each adsorption test using the generated gas stream. Adsorption cycles lasted 240 min, allowing saturation of the BAC.

During regeneration (thermal desorption), heating and insulation tapes (Omega) were wrapped around the adsorption/regeneration tube. A DAC system with a LabVIEW program (National Instruments) and a data logger (National Instruments, Compact DAQ) equipped with analog input and output modules controlled and logged the adsorption bed temperature. A 0.9 mm diameter type K thermocouple (Omega) inserted at the center of the adsorption/regeneration tube was used to measure the temperature of the BAC bed during adsorption and regeneration. Temperatures of 25 °C and 288 °C were used during adsorption and regeneration, respectively. The regeneration temperature of 288 °C was chosen to allow for elimination of adsorbed species (with boiling points ranged from 118 to 271 °C) while minimizing potential damages to the structure of adsorbent as a result of exposure to high temperatures (Salvador et al., 2015). For regeneration, the adsorption/regeneration tube was heated for 3 h with 1 SLPM of purge gas, and then cooled for 50 min while continuing to purge at the same flow rate. Different concentrations of oxygen (≤ 5 , 625, 1,250, 2,500, 5,000, and 10,000 ppm_v) in N₂ were used as the purge gas,

corresponding to N₂ purities between 99 and 99.9984%. The purge gases were generated by mixing compressed air (99.999% pure, Praxair) and compressed N₂ (99.9984% pure, Praxair). Mixing was performed using a 100 SCCM mass flow controller (Alicat Scientific) for air (accuracy of ± 0.3 SCCM) and a 1 SLPM mass flow controller (Alicat Scientific) for N₂ (accuracy of ± 3 SCCM). Since the compressed N₂ cylinder contained a maximum of 5 ppm_v O₂, it was solely (i.e., with no mixing) used as purge gas for the ≤ 5 ppm_v O₂ case.

Gravimetric measurements were used to quantify irreversible adsorption. The difference between initial BAC mass and pre-regeneration (i.e., post-adsorption) BAC mass is the amount of VOC adsorbed during an adsorption cycle. The difference between the initial BAC mass and the BAC mass after first regeneration cycle describes the amount of heel during first cycle. The difference between the initial BAC mass and the BAC mass after fifth regeneration cycle describes the amount of cumulative or five-cycle heel. Adsorbed mass, first cycle heel, and cumulative heel are reported as percentages relative to the initial BAC mass. 5-cycle adsorption/regeneration experiments were completed in duplicate and average values are reported.

Other samples were used for comparison purposes. Blank (no VOC) adsorption/regeneration tests were performed using the carrier gas (i.e., air) during adsorption and the purge gases during regeneration to assess changes that can be attributed exclusively to the purge gas. Only the highest (10,000 ppm_v) and lowest (≤ 5 ppm_v) concentrations of O₂ in N₂ were tested as purge gas for blank regeneration tests. Two regenerated Kureha BAC samples previously used in 50 successive adsorption/regeneration cycles were also studied to evaluate the effect of long-term exposure to high O₂ concentrations during regeneration. For these experiments, 1 g of the virgin BAC was loaded with 0.2 mL of Mixture 2. Adsorption was

completed at 35 °C for 35 min using 3.5 SLPM air as carrier gas. Regeneration of these samples was completed for 2 h at 343 °C using 50 and 5,000 ppm_v O₂ in N₂ as the purge gas (total purge gas flow of 50 SCCM). The regeneration temperature used for 50-cycle experiments (343 °C) was higher than the corresponding temperature for 5-cycle experiments (288 °C) to ensure effective regeneration and be more representative of the current process conditions.

6.2.4 BAC Characterization

All BAC samples were characterized before and after cycling using a micropore surface analysis system (iQ2MP, Quantachrome). N₂ adsorption was performed at -196 °C. Samples were first degassed for 5 h at 120 °C. Specific surface area was calculated by the BET method (Brunauer et al., 1938) from relative pressures ranging from 0.01 to 0.07, which allowed for high coefficient of determination (R^2) values and positive BET constant (C). Total pore volume was recorded at $P/P_0 = 0.975$ (Quantachrome Autosorb 1 Operation Manual, 2006). PSDs were obtained using the quenched solid density functional theory method and micropore volume was obtained using the V-t method (Quantachrome Autosorb 1 Operation Manual, 2006).

Surface elemental composition (C, O, and N) of all BACs was determined with XPS using an AXIS 165 spectrometer (Kratos Analytical). The base pressure in the analytical chamber was lower than 3×10^{-8} Pa. Monochromatic Al K α source ($h\nu = 1486.6$ eV) was used at a power of 168 W. The resolution of the instrument is 0.55 eV for Ag 3d and 0.70 eV for Au 4f peaks. High resolution scans (with signal to noise ratio of > 10) were collected for binding energy spanning from 1100 eV to 0 with analyzer pass energy of 20 eV and a step of 0.1 eV. CasaXPS Software was used to process the XPS scans and the results were reported in terms of atomic concentration.

Temperature stability of the heel was assessed using DTG analysis (TGA/DSC 1, Mettler Toledo). BAC samples were heated from 25 °C to 800 °C at 2 °C/min in 50 SCCM of N₂. Percentages of accumulated heel eliminated during DTG analysis were calculated. Cumulative weight loss at 800 °C was corrected based on weight loss of the corresponding virgin BAC. This was then divided by mass balance cumulative heel and multiplied by 100 to determine percent heel removal.

6.3 Results and Discussion

6.3.1 Adsorption Breakthrough Curves of 5-cycle BAC samples

Adsorption breakthrough curves for all 5-cycle experiments using Mixture 1 as adsorbate are described in Figure 6-1. During the first cycle of all experiments, 5% breakthrough was achieved after 58 ± 2 min for duplicate experiments of the six regeneration O₂ conditions (average \pm standard deviation, n=12). With subsequent cycles, breakthrough time progressively decreased, indicating that regeneration at 288 °C was not sufficient for eliminating all adsorbed species from the BAC, resulting in heel buildup (Jahandar Lashaki et al., 2012a).

Breakthrough time reduction during subsequent adsorption cycles was more prominent when high concentrations of O₂ were present in the regeneration purge gas. For regeneration with ≤ 5 ppm_v O₂, the breakthrough time for the fifth cycle was 20 min, indicating that the adsorbent maintained much of its VOC adsorption capacity after 5 cycles. For 625 ppm_v O₂ in the regeneration purge gas, breakthrough occurred shortly after starting the fifth cycle. Immediate breakthrough occurred during the fourth cycle for 1,250 ppm_v O₂ and during the third cycle for 2,500, 5,000, and 10,000 ppm_v O₂. Two 5-cycle blank experiments (no adsorbate) using the lowest and highest considered purge gas O₂ concentrations in N₂ (≤ 5 ppm_v and 10,000 ppm_v) resulted in no heel (Figure 6-2a), showing that the presence of O₂ in the purge gas alone cannot

explain the aforementioned trends. As a result of exposure to higher O₂ concentrations during regeneration, non-desorbed species are either permanently occupying or blocking a higher share of the BAC's active sites or causing diffusion limitations that hinder adsorption, decreasing breakthrough times.

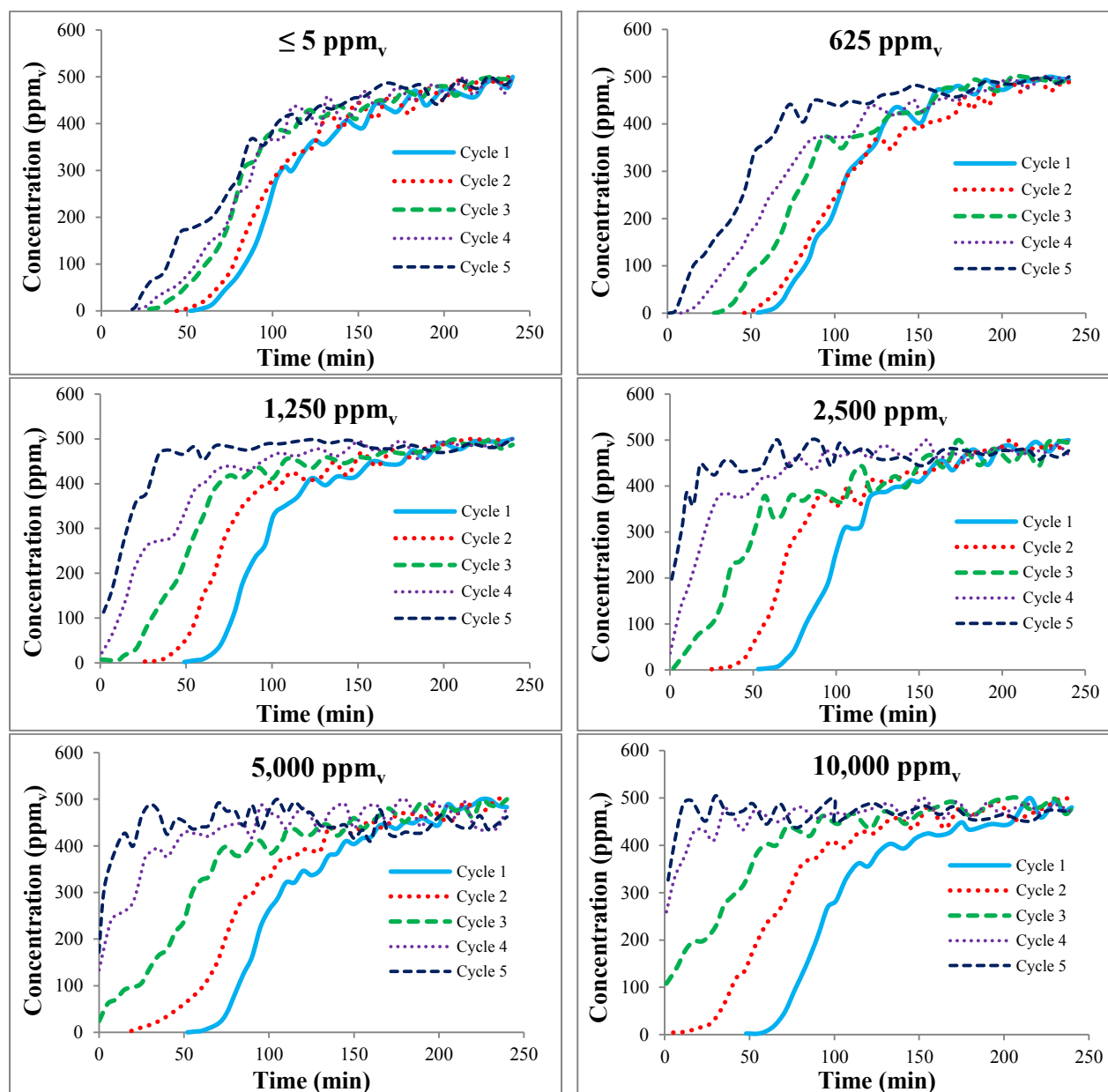


Figure 6-1. Adsorption breakthrough curves for 5-cycle BAC samples exposed to different concentrations of O₂ in the desorption purge gas.

6.3.2 Mass Balance Heel of 5-Cycle BAC Samples

Measurements of mass balance heel (cumulative and first cycle) for 5-cycle BAC samples as a function of O₂ concentration in the desorption purge gas are compared in Figure 6-2a. Heel accumulated during five adsorption/regeneration cycles increased with increasing O₂ concentration in the purge gas. The cumulative heel for the BAC sample regenerated in ≥ 625 ppm_v O₂ was up to 34% greater than that for the sample regenerated with ≤ 5 ppm_v O₂. Also, first cycle heel formation was as much as 47% higher for samples regenerated in ≥ 625 ppm_v O₂ relative to baseline scenario (≤ 5 ppm_v O₂). These observations might be attributed to higher chemisorption in the presence of oxygen, which is discussed in the following sections. Greater heel accumulation causes a loss of adsorption capacity in subsequent cycles (Jahandar Lashaki et al., 2012a), indicating that an increase in purge gas oxygen content decreases the performance of the adsorption/regeneration system. In an industrial emissions control system, increased oxygen in the purge gas leading to these impacts would necessitate more frequent replacement of the adsorbent, increasing materials, reactivation and/or disposal, and labor costs and possibly process downtime.

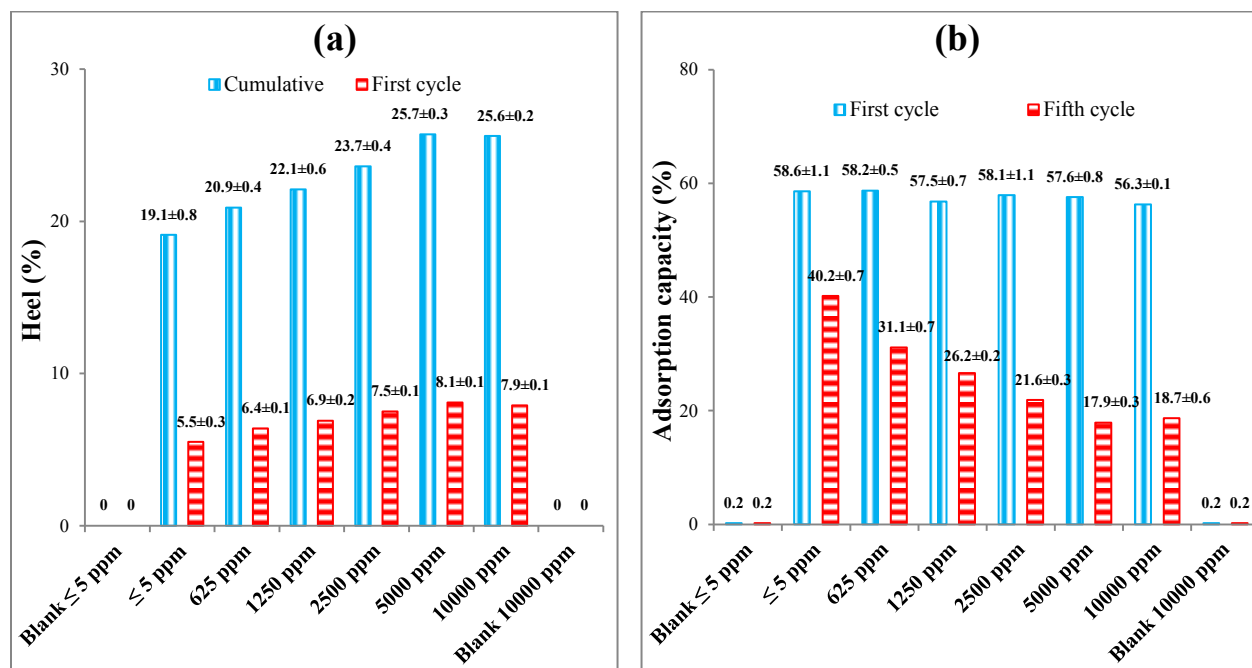


Figure 6-2. (a) Cumulative (5 cycles) and first cycle mass balance heel of 5-cycle BAC samples
 (b) Adsorption capacity of 5-cycle BAC samples for first and fifth cycles. Data labels are presented as $x \pm y$ where x and y correspond to mean and standard deviation ($n=2$), respectively.

6.3.3 Adsorption Capacity of 5-Cycle BAC Samples

Adsorption capacities during the first and fifth cycles are compared in Figure 6-2b, for 5-cycle BAC samples. Similar adsorption capacity (range of $57.7 \pm 1.4\%$) was observed in the first cycle for all conditions because all conditions used virgin BAC that had not been exposed to the purge gas. For the fifth cycle, adsorption capacity decreased by 31 to 69% (compared to the first cycle), corresponding to 1.6% to 2.7% average capacity loss (calculated over 5-cycle experiments) per percent heel formed during cycling. For the 10,000 ppm_v O₂ sample, cumulative heel was 34% higher but the fifth cycle adsorption capacity was 53% lower compared to ≤ 5 ppm_v O₂ sample, indicating exposure to more O₂ resulted in greater loss of adsorption capacity for the heel accumulated.

6.3.4 Characterization of 5-Cycle BACs

DTG results for virgin and 5-cycle adsorbents are shown in Figure 6-3. DTG analysis was performed to evaluate the temperature stability of the heel generated during cyclic use. This allows for quantification of even strongly adsorbed adsorbates, as temperatures as high as 800 °C can break many chemical bonds to quantify chemisorption (Ferro-Garcia et al., 1993). Multiple peaks corresponding to desorption at different temperatures give an indication of the range of adsorption strength (Moreno-Castilla et al., 1995). A slow heating rate (2 °C/min) ensures distinguishable desorption peaks.

For all samples, the first DTG peak occurred at about 50 °C and is attributed to removal of water vapor that was adsorbed during ambient air exposure after adsorption, prior to analysis (Popescu et al., 2003). This peak was higher for samples regenerated with additional O₂ (e.g. 2,500 and 5,000 in the purge gas, suggesting more hydrophilic surface functional groups on the adsorbent (Sullivan et al., 2007).

All but the virgin BAC sample exhibited a peak at approximately 400 °C (Figure 6-3), which was higher than the regeneration temperature (288 °C) and the boiling points of the species in Mixture 1 (ranging from 118 to 271 °C). This peak is attributed to physisorption resulting from superposition of wall effects in pores comparable in size to the adsorbed species and/or diffusion limitations associated with the narrow micropores of the adsorbent, especially in the case of bulky adsorbates (e.g. naphthalene, diethanolamine) (Jahandar Lashaki et al., 2012a). Only one physisorption peak was observed despite the fact that Mixture 1 consists of nine compounds, which could result in multiple peaks. This is most likely due to competitive adsorption among the species in Mixture 1 that leaves only few high boiling compounds (e.g. naphthalene, diethanolamine) on the adsorbent following adsorption (Jahandar Lashaki et al.,

2012a; Wang et al., 2012). Also, the peak is broad, which could be attributed to the removal of multiple compounds. This peak was highest for the sample regenerated with the least amount of O_2 (≤ 5 ppm_v), implying the highest occurrence of physisorption, and it decreased with increasing O_2 concentration.

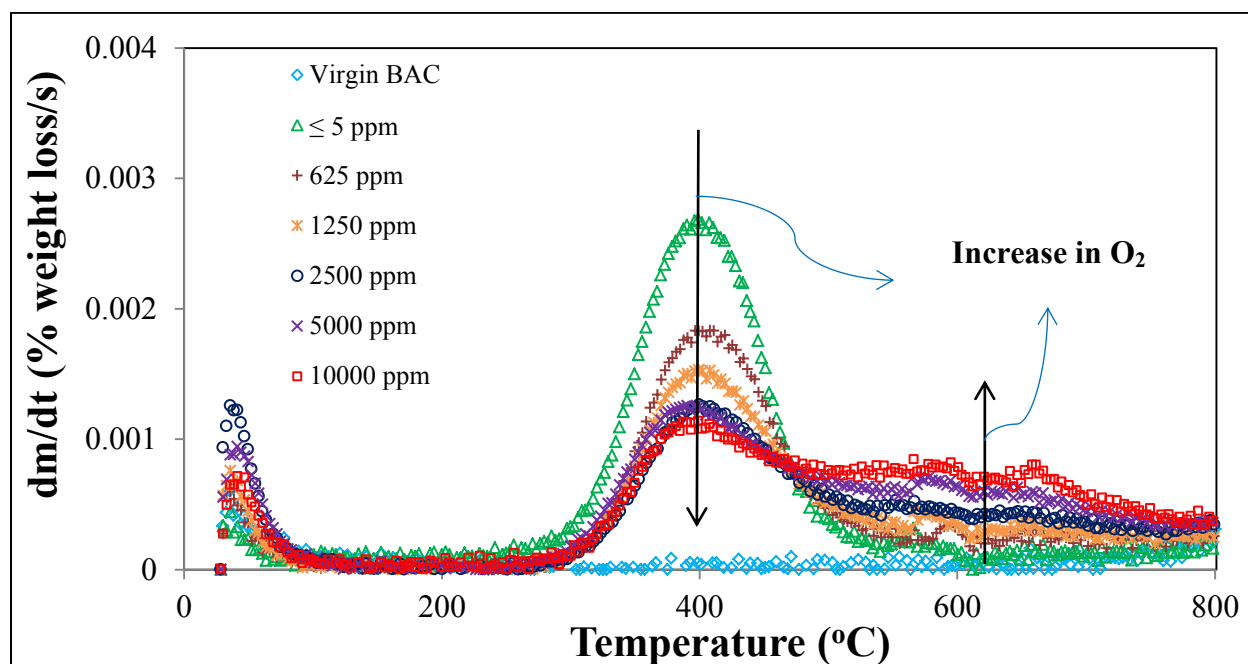


Figure 6-3. DTG analysis of 5-cycle BAC samples regenerated by different levels of O_2 in N_2 (after 5 cycles).

Samples regenerated with 625, 1,250, 2,500, 5,000, and 10,000 ppm_v O_2 in N_2 showed a second wide peak between 500 and 800 °C (Figure 6-3). These peaks are attributed to stronger adsorption interactions, such as chemisorption – consistent with previous literature (Magne and Walker, 1986; Ferro-Garcia et al., 1993). The amplitude of this broad peak increased with increasing O_2 concentration in the purge gas, contrary to the trend for the physisorption peak. This may indicate that with increasing oxygen concentration, some compounds that would be physically adsorbed in pure N_2 may undergo chemical reactions, forming chemisorbed species. In summary, physisorption was the main contributor to heel formation with ≤ 5 ppm_v O_2 , while a

combination of physisorption and chemisorption contributed to heel formation at higher O_2 levels. On a heel mass basis, these chemisorbed species appear to reduce the adsorption capacity and shorten breakthrough time more than physisorbed species, as shown in Figure 6-1 and Figure 6-2b, requiring more frequent replacement of the adsorbent.

The percentages of accumulated heel eliminated during thermal analysis of 5-cycle BAC samples were calculated (Figure 6-4). The higher the heel removal percentage, the weaker the energy of interaction associated with the formed heel. The highest removal percentage was observed for ≤ 5 ppm_v O_2 while the rest of the cases were lower and similar. This is consistent with the aforementioned heel formation mechanisms; physical adsorption for low O_2 concentration (≤ 5 ppm_v O_2) in desorption purge gas and a combination of physisorption and chemisorption for higher O_2 concentrations (625-10,000 ppm_v O_2).

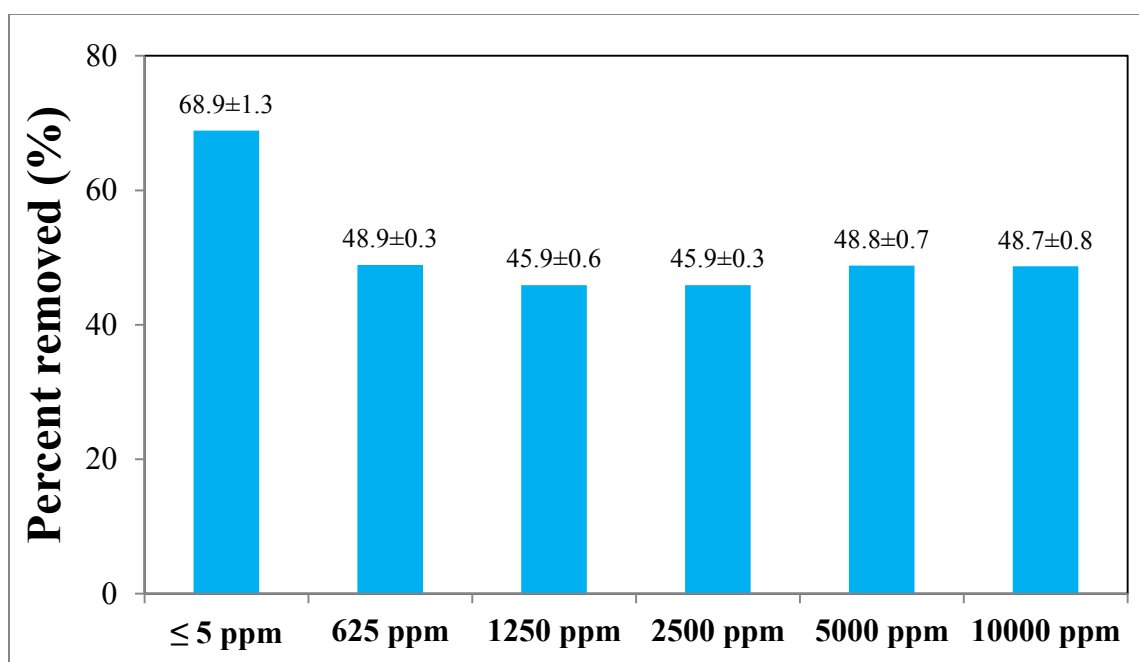


Figure 6-4. Percent of cumulative heel removed during DTG analysis (up to 800 °C) of different 5-cycle BACs. Data labels are presented as $x \pm y$ where x and y correspond to mean and standard deviation ($n=2$), respectively.

XPS analysis was carried out on all BAC samples to determine surface elemental composition (Table 6-2). Increases in oxygen and nitrogen content were observed when comparing the regenerated 5-cycle BACs with virgin BAC. Nitrogen increases could be due to accumulation of diethanolamine (the only nitrogen-containing compound in the test mixture) or chemisorption of nitrogen from the purge gas. Similarly, oxygen increases could be due to reactions between O_2 and adsorbates or chemisorption of oxygen from the purge gas to the surface of the BACs. XPS analysis on a 5-cycle blank experiment (no adsorbate) performed on virgin BAC showed only small increases in BAC nitrogen and oxygen content (Table 6-2), indicating that the purge gas, independent of oxygen content, does not alter the chemical properties of the BAC, and chemisorption of O_2 and N_2 is unlikely. Consequently, diethanolamine is believed to be the main contributor to increases in BAC nitrogen content. Diethanolamine has a high boiling point (271 °C) and has previously been shown to form heel (Chakma and Meisen, 1989). Similarly, reactions between O_2 and organic adsorbates can form oxygen-rich chemisorbed species, explaining the increase in surface oxygen content. Increases in oxygen and nitrogen content were highest for 2,500, 5,000, and 10,000 ppm_v O_2 and lowest for ≤ 5 ppm_v O_2 , which is consistent with and can be supported by mass balance cumulative heel results (Figure 6-2).

BET surface area, micropore volume, and total pore volume of virgin, blank, and regenerated BACs were measured to quantify the effect of heel on the adsorbent's physical properties (Table 6-2). Some adsorption sites remain occupied after regeneration, and, as a result, the number of vacant sites quantified with N_2 adsorption decreased. Lower BET surface area, total pore volume, and micropore volume were obtained for regenerated 5-cycle BACs compared to virgin BAC. Reductions in BET surface area, micropore volume, and total pore volume for

every 1% of mass balance cumulative heel were calculated (Table 6-2). Changes in micropore volume and total pore volume were similar, confirming that heel was formed in micropores, which comprise > 85% of the virgin BACs pore volume (Jahandar Lashaki et al., 2012a). Previous research (with regeneration completed in ≤ 5 ppm_v O₂) shows that BET surface area, micropore volume, and pore volume decreases are linearly proportional to mass balance cumulative heel (Jahandar Lashaki et al., 2012a), but this is not observed here. Cumulative heel was 9, 16, 24, 35, and 34% higher for 625 ppm_v, 1,250 ppm_v, 2,500 ppm_v, 5,000 ppm_v, and 10,000 ppm_v O₂, respectively, compared to the ≤ 5 ppm_v O₂ sample, but BET surface area was 6 – 15% *higher*, micropore volume was 23 – 31% *higher*, and total pore volume was 8 – 16% *higher* for samples exposed to ≥ 625 ppm_v O₂ during desorption. This is uncommon and unexpected – as noted above, increased heel is expected to decrease surface area and pore volumes (Jahandar Lashaki et al., 2012a). This behavior is not believed to be due to direct reactions between O₂ and activated carbon sites that change the adsorbent's physical properties without depositing heel (i.e., pore widening or new pore formation to increase BET surface area, total pore volume, and micropore volume). The 5-cycle blank experiment with 10,000 ppm_v O₂ (no adsorbate) had minimal impact on the physical properties and composition of BAC (Table 6-2) and no significant mass loss/gain was observed (Figure 6-2a), indicating that even the highest O₂ concentration used in this study does not alter the adsorbent's structure. Consequently, direct O₂-C reactions are not likely.

Table 6-2. Physical and chemical properties of virgin, blank, and regenerated (5-cycle and 50-cycle) Kureha BACs.

Carbon Description	Carbon Sample	Physical Properties				Change in Physical Properties per 1% Heel			Chemical Properties		
		BET Surface Area (m ² /g)	BET C constant	Micropore Volume (cm ³ /g)	Total Pore Volume (cm ³ /g)	BET Surface Area (m ² /g)	Micropore Volume (cm ³ /g)	Total Pore Volume (cm ³ /g)	C (%) ^a	O (%) ^a	N (%) ^a
Virgin	Kureha	1371±21	415	0.50±0.01	0.57±0.01	NA	NA	NA	93.0	7.0	0.0
Blank Tests	≤ 5 ppm _v	1345±20	428	0.48±0.01	0.56±0.00	NA	NA	NA	91.6	7.9	0.3
	10,000 ppm _v	1323±17	419	0.48±0.00	0.57±0.01	NA	NA	NA	91.9	7.6	0.3
BAC After 5 Ads/Regen Cycles	≤ 5 ppm _v	484±19	243	0.13±0.01	0.25±0.02	-46	-0.019	-0.017	92.5	5.4	2.1
	625 ppm _v	513±23	274	0.16±0.01	0.27±0.02	-41	-0.016	-0.014	81.4	11.4	7.2
	1,250 ppm _v	523±5	298	0.16±0.00	0.28±0.00	-38	-0.015	-0.013	79.2	12.1	8.7
	2,500 ppm _v	533±12	329	0.16±0.01	0.28±0.01	-35	-0.014	-0.012	75.2	13.7	11.1
	5,000 ppm _v	558±9	348	0.17±0.01	0.28±0.01	-32	-0.013	-0.011	76	13.3	10.7
	10,000 ppm _v	552±7	334	0.17±0.01	0.27±0.01	-32	-0.013	-0.012	75.3	13.8	10.9
BAC After 50 Ads/Regen Cycles	50 ppm _v	1133±2	356	0.40±0.00	0.50±0.00	NA	NA	NA	92.7	7.2	0.1
	5,000 ppm _v	NA	NA	NA	NA	NA	NA	NA	79.7	19.7	0.6

^a Relative atomic percentages (%C + %O + %N = 100); Other elements not considered in surface composition

The observed trends could be due to interactions between the quadrupole moment of N₂ (adsorption probe molecule in this study) and oxygen-rich chemisorbed species (XPS results in Table 6-2), which act as strong adsorption sites (Thommes et al., 2015), localizing the adsorption (Gregg and Sing, 1982). As a result of localized adsorption, adsorbate molecules spend longer times near these sites, which could make the adsorption kinetics slower, causing diffusional limitations (Gregg and Sing, 1982). The aforementioned interaction could subsequently force the nitrogen molecules to tilt away from parallel position on the adsorbent surface, resulting in a smaller cross sectional area (as low as 13.5 Å²) than the default one assumed in our calculations (16.2 Å²) (Jelinek and Kovats, 1994). In this case, nitrogen molecules are highly packed, resulting in a potential overestimation of physical properties (i.e., BET surface area, pore volume, etc.) by about 20% (Gregg and Sing, 1982; Jelinek and Kovats, 1994). The presence of localized adsorption can be confirmed by a higher BET C constant (Gregg and Sing, 1982) for samples regenerated in ≥ 625 ppm_v O₂, relative to ≤ 5 ppm_v O₂, indicating higher adsorbent-adsorbate interactions (Table 6-2). The BET C constant of regenerated samples ($\leq 5 - 10,000$ ppm_v O₂) was lower than the virgin, 5-cycle blank, and 50-cycle (50 ppm_v O₂) samples, because regenerated samples have lower BET surface area and/or different history.

The presence of diffusional limitations is also supported by the time needed to achieve the equilibrium criterion in obtaining N₂ adsorption isotherms on regenerated BACs. The analysis duration was 111, 151, 160, 207, and 222 min per milligram of analyzed sample for 625 ppm_v, 1,250 ppm_v, 2,500 ppm_v, 5,000 ppm_v, and 10,000 ppm_v O₂, respectively, compared to corresponding durations of 36 and 62 min per milligram of sample for virgin BAC and 5 ppm_v O₂, respectively. Specific surface areas of only these samples varied by ~15%, but the time required for adsorption varied by 80-260%. Internal surface area is clearly accessible and not

completely blocked or occupied, but the longer times required for adsorption indicate that greater diffusion resistance has slowed the process, leading to earlier breakthrough (Figure 6-1) and lower adsorption capacity (Figure 6-2b). Pore size distributions for regenerated 5-cycle BACs were obtained to identify the location of the formed heel (Figure 6-5). In all cases, retained adsorbates occupied micropores (pore width < 20 Å). The BAC regenerated in ≤ 5 ppm_v O₂ showed the greatest volume reduction for pores in the 5 – 8 Å range. PSDs for all samples were similar for pore width > 8 Å. The lesser decrease in 5 – 8 Å pores (peak at 6 Å) at high oxygen content (625 to 10,000 ppm_v) despite greater heel accumulation is uncommon and unexpected. This trend may again be explained by the specified interactions between oxygen-rich chemisorbed species and quadrupole moment of nitrogen molecule, which may result in overestimation of physical properties (PSD in this case).

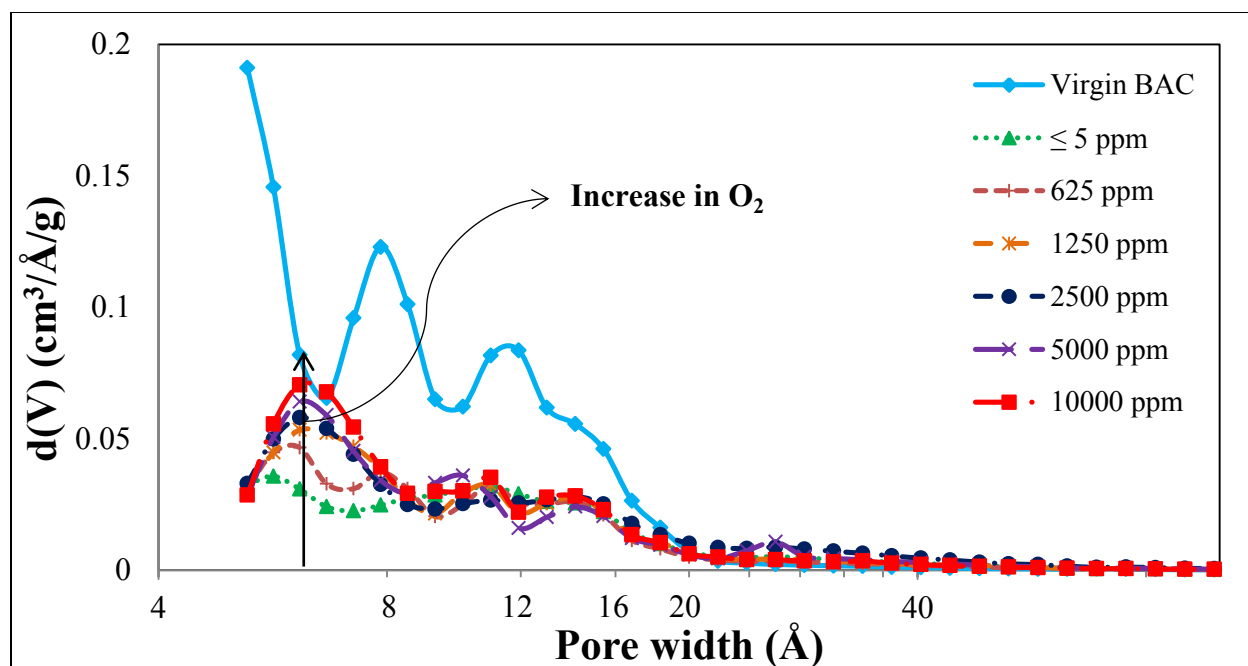


Figure 6-5. Pore size distributions of 5-cycle BACs.

6.3.5 Effect of Long-Term Exposure to Oxygen

Longer-duration adsorption/desorption testing was conducted using Mixture 2 as adsorbate to confirm the shorter-duration (i.e., 5-cycle), more fundamental test results described above. DTG analysis was carried out on two BAC samples that underwent 50 adsorption/regeneration cycles with regeneration occurring at 343 °C using a purge gas composed of 50 ppm_v and 5,000 ppm_v O₂ in N₂ (Figure 6-6). Similar to samples from the earlier experiments (Figure 6-3), a peak (higher for higher O₂ regeneration) was observed at 50 °C in both 50-cycle samples due to desorption of water vapor. Unlike Figure 6-3, no physisorption peak was observed near 400 °C. Two factors may have contributed to this difference. First, regeneration for 50-cycle samples was completed at 343 °C, higher than the regeneration temperature used for 5-cycle samples (288 °C). Second, the adsorbates of the nine-component mixture (Mixture 1) have higher boiling points than the adsorbates of the industrial plant mixture (Mixture 2). Overall, the greater volatility of Mixture 2 and the higher desorption temperature resulted in more complete removal of physisorbed species during regeneration and no physisorption peak in the DTG curve.

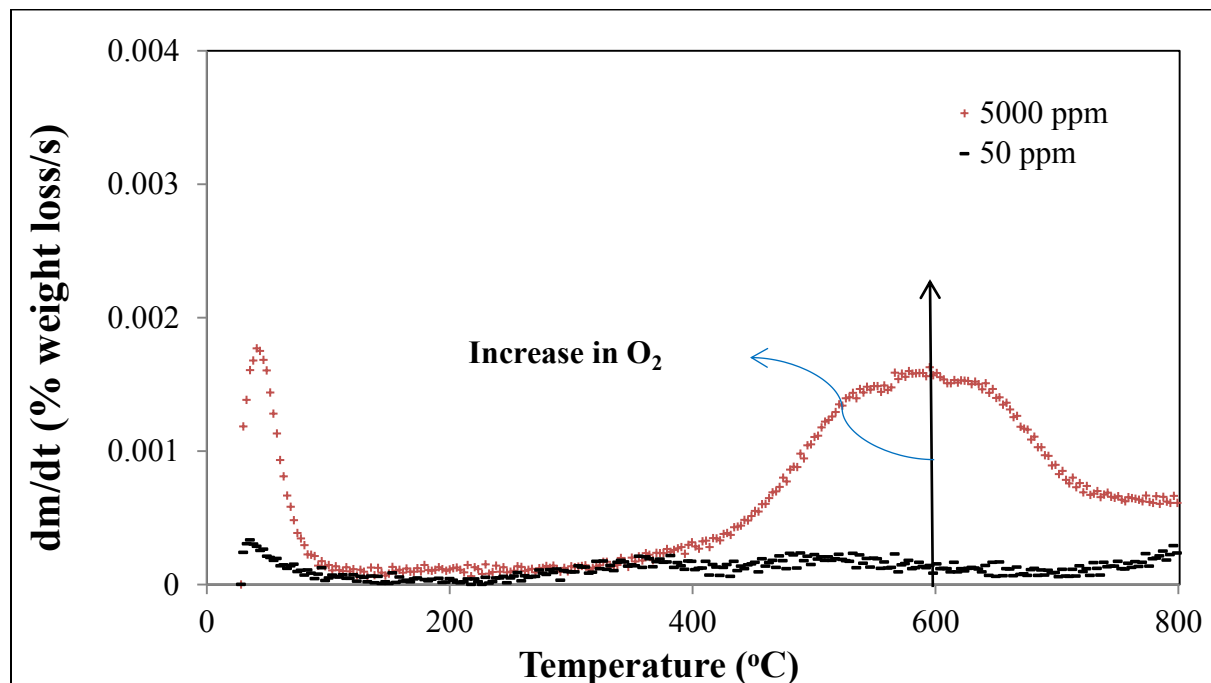


Figure 6-6. DTG analysis of 50-cycle BACs regenerated with N₂ purge gas with two O₂ concentrations.

The sample regenerated with 5,000 ppm_v O₂ exhibited a broad chemisorption peak centered at 600 °C, similar to that observed for the 5-cycle samples exposed to high O₂ in the desorption purge gas (Figure 6-3). The sample regenerated with 50 ppm_v O₂ showed no chemisorption peak. Trends observed in the 5-cycle experiments, therefore, are consistent with these 50-cycle experiments. Both experiments suggest purge gas purity (in terms of O₂ content) should be as high as possible (operationally and economically) to minimize heel formation on BAC and maximize its lifespan.

Oxygen content for the 5,000 ppm_v 50-cycle sample was 181% greater than virgin BAC (Table 6-2), an increase about double that of the 5,000 ppm_v 5-cycle sample (90% increase). While the chemisorption peaks from both the 5- and 50-cycle samples occurred around 600 °C, the intensity (peak height) of the chemisorption peak for the 50-cycle sample is likewise more

than twice (Figure 6-6) that of the 5-cycle sample (Figure 6-3). These differences are attributed to increased heel buildup and chemisorption with the greater number of adsorption cycles. In contrast to the 5,000 ppm_v sample, only a minor increase (4%) in oxygen content was observed for the 50 ppm_v O₂ BAC at 50 cycles, which is consistent with the lack of a chemisorption peak in the DTG curve, showing small heel formation. Together, these results suggest regeneration with high O₂ concentration leads to the chemisorption peak shown with DTG. Nitrogen content of the 50-cycle samples was negligible (comparable to 5-cycle blank experiments) due to lack of nitrogen-containing VOCs in the industrial adsorbate mixture.

Micropore surface analysis could not be completed for the 5,000 ppm_v O₂ sample due to an excessively slow N₂ adsorption rate (> 250 min per mg of sample), most likely resulting from large diffusion resistance. The analysis exceeded 250 min per milligram of sample, which for a sample with a typical weight of 50 mg will take more than 8 days and was aborted by the instrument. This behavior is consistent with the previously presented data that showed longer analyses for samples with chemisorbed species because of diffusion resistance caused by interactions between oxygen-rich chemisorbed species and quadrupole moment of N₂.

This study is the first evidence for the detrimental effect of oxygen impurity in the desorption purge gas on activated carbon lifetime. This effect can be controlled by using high purity nitrogen to purge the adsorbent bed during regeneration to decrease irreversible adsorption. Using lower purity nitrogen (e.g. 625 to 10,000 ppm_v O₂ in N₂) as regeneration purge gas, results in higher heel formation and shorter adsorbent lifetime. In this case, more frequent reactivation /replacement of the adsorbent would be necessary. Both scenarios increase the operational costs of the VOC abatement process. Further research on optimum N₂ purity and detailed cost analysis would be helpful to find the most cost effective regeneration conditions.

6.4 Conclusions

The effect of desorption purge gas oxygen content on the irreversible adsorption of volatile organic compounds commonly emitted from industrial painting operations was investigated. Regeneration with high oxygen concentration (625 to 10,000 ppm_v) in the desorption purge gas resulted in shorter breakthrough time, greater loss of adsorption capacity, and greater cumulative heel accumulation compared to a low level of oxygen (≤ 5 ppm_v), indicating that an increase in purge gas oxygen content decreases the performance of the adsorption/regeneration system. Based on derivative thermo-gravimetric analysis, chemisorption plays a relatively more significant role than physisorption as a result of adsorbent exposure to oxygen during regeneration. Micropore surface analysis confirmed increased diffusion resistance likely associated with accumulation of chemisorbed species. Long-term exposure (50 cycles) during regeneration with oxygen-containing purge gas resulted in trends similar to that of short-term exposure (5 cycles). Fundamentally, these results help to explain mechanisms of irreversible adsorption by evaluating how the degree of oxygen exposure during regeneration impacts heel formation.

6.5 References

- Abuzaid, N.; Nakhla, G.F. Dissolved oxygen effects on equilibrium and kinetics of phenols adsorption by activated carbon. *Environ. Sci. Technol.* **1994**, *28*, 216–221.
- Brunauer, S.; Emmett, P.H.; Teller, E. Adsorption of gases in multimolecular layers. *J. Am. Chem. Soc.* **1938**, *60*, 309–319.
- Chakma, A.; Meisen, A. Activated carbon adsorption of diethanolamine, methyl diethanolamine and their degradation products. *Carbon* **1989**, *27*, 573–284.
- Chang, C.H.; Savage, D.W. Investigations of solvent-regenerable carbon-sulfur surface compounds for phenol removal in packed column. *Environ. Sci. Technol.* **1981**, *15*, 201–206.
- Compressed Air Best Practices, The Energy Costs Associated with Nitrogen Specifications. <http://www.airbestpractices.com/system-assessments/air-treatment/n2/energy-costs-associated-nitrogen-specifications>.
- Dabrowski, A.; Podkoscielny, P.; Hubicki, Z.; Barczak, M. Adsorption of phenolic compounds by activated carbon-A critical review. *Chemosphere* **2005**, *58*, 1049–1070.
- Das, D.; Gaur, V.; Verma, N. Removal of volatile organic compound by activated carbon fiber. *Carbon* **2004**, *42*, 2949–2962.
- Ferro-Garcia, M.A.; Utrera-Hidalgo, E.; Rivera-Utrilla, J.; Moreno-Castilla, C.; Joly, J.P. Regeneration of activated carbons exhausted with chlorophenols. *Carbon* **1993**, *31*, 857–863.
- Grant, T.M.; King, C.J. Mechanism of irreversible adsorption of phenolic compounds by activated carbons. *Ind. Eng. Chem. Res.* **1990**, *29*, 264–271.
- Gregg, S.J.; Sing, K.S.W. *Adsorption, Surface Area, and Porosity*; Academic Press: London, U.K., 1982.
- Hashisho, Z.; Rood, M.J.; Botich, L. Microwave-swing adsorption to capture and recover vapors from air streams with activated carbon fiber cloth. *Environ. Sci. Technol.* **2005**, *39*, 6851–6859.
- Hashisho, Z.; Emamipour, H.; Cevallos D.; Rood, M.J.; Hay, K.J.; Kim, B.J. Rapid response concentration-controlled desorption of activated carbon to dampen concentration fluctuations. *Environ. Sci. Technol.* **2007**, *41*, 1753–1758.

- Hashisho, Z.; Emamipour, H.; Rood, M.J.; Hay, K.J.; Kim, B.J.; Thurston, D. Concomitant adsorption and desorption of organic vapor in dry and humid air streams using microwave and direct electrothermal swing adsorption. *Environ. Sci. Technol.* **2008**, *42*, 9317–9322.
- Hashisho, Z.; Rood, M.J.; Barot, S.; Bernhard, J. Role of functional groups on the microwave attenuation and electric resistivity of activated carbon fiber cloth. *Carbon* **2009**, *47*, 1814–1823.
- Jahandar Lashaki, M.; Fayaz, M.; Wang, H.; Hashisho, Z.; Phillips, J.H.; Anderson, J.E.; Nichols, M. Effect of adsorption and regeneration temperature on irreversible adsorption of organic vapors on beaded activated carbon. *Environ. Sci. Technol.* **2012a**, *46*, 4083–4090.
- Jahandar Lashaki, M.; Fayaz, M.; Niknaddaf, S.; Hashisho, Z. Effect of the adsorbate kinetic diameter on the accuracy of the Dubinin-Radushkevich equation for modeling adsorption of organic vapors on activated carbon. *J. Hazard. Mater.* **2012b**, *241–242*, 154–163.
- Jelinek, L.; Kovats, E.S. True surface areas from nitrogen adsorption experiments. *Langmuir* **1994**, *10*, 4225–4231.
- Kilduff, J.E.; King, C.J. Effect of carbon adsorbent surface properties on the uptake and solvent regeneration of phenol. *Ind. Eng. Chem. Res.* **1997**, *36*, 1603–1613.
- Kureha Corporation Website; <http://www.kureha.com/pdfs/Kureha-BAC-Bead-Activated-Carbon.pdf>.
- Leng, C.C.; Pinto, N.G. Effects of surface properties of activated carbons on adsorption behavior of selected aromatics. *Carbon* **1997**, *35*, 1375–1385.
- Lu, Q.; Sorial, G.A. The role of adsorbent pore size distribution in multicomponent adsorption on activated carbon. *Carbon* **2004a**, *42*, 3133–3142.
- Lu, Q.; Sorial, G.A. Adsorption of phenolics on activated carbon- impact of pore size and molecular oxygen. *Chemosphere* **2004b**, *55*, 671–679.
- Magne, P.; Walker Jr., P.L. Phenol adsorption on activated carbons: application to the regeneration of activated carbons polluted with phenol. *Carbon* **1986**, *24*, 101–107.
- Matatov-Meytal, Y.I.; Sheintuch, M. Catalytic abatement of water pollutants. *Ind. Eng. Chem. Res.* **1998**, *37*, 309–326.

- Moreno-Castilla, C.; Rivera-Utrilla, J.; Joly, J.P.; Lopez-Ramon, M.V.; Ferro-Garcia, M.A.; Carrasco-Marin, F. Thermal regeneration of an activated carbon exhausted with different substituted phenols. *Carbon* **1995**, *33*, 1417–1423.
- Niknaddaf, S.; Atkinson, J.D.; Shariaty, P.; Jahandar Lashaki, M.; Hashisho, Z.; Phillips, J.H.; et al., Heel formation during volatile organic compound desorption from activated carbon fiber cloth. *Carbon* **2016**, *96*, 131–138.
- Popescu, M.; Joly, J.P.; Carre, J.; Danatoiu, C. Dynamical adsorption and temperature-programmed desorption of VOCs (toluene, butyl acetate and butanol) on activated carbons. *Carbon* **2003**, *41*, 739–748.
- Quantachrome Autosorb 1 Operating Manual; **2006**.
- Salvador, F.; Martin-Sanchez, N.; Sanchez-Hernandez, R.; Sanchez-Montero, M.J.; Izquierdo, C. Regeneration of carbonaceous adsorbents. Part I: Thermal regeneration. *Micropor. Mesopor. Mat.* **2015**, *202*, 259–276.
- Sullivan, P.D.; Stone, B.R.; Hashisho, Z.; Rood, M.J. Water adsorption with hysteresis effect onto microporous activated carbons. *Adsorption* **2007**, *13*, 173–89.
- Tamon, H.; Okazaki, M. Desorption characteristics of aromatic compounds in aqueous solution on solid adsorbents. *J. Colloid Interface Sci.* **1996**, *179*, 181–187.
- Tanthapanichakoon, W.; Ariyadejwanich, P.; Japthong, P.; Nakagawa, K.; Mukai, S.R.; Tamon, H. Adsorption-desorption characteristics of phenol and reactive dyes from aqueous solution on mesoporous activated carbon prepared from waste tires. *Water Res.* **2005**, *39*, 1347–1353.
- Tefera, D.T.; Jahandar Lashaki, M.; Fayaz, M.; Hashisho, Z.; Phillips, J.H.; Anderson, J.E.; Nichols, M. Two-dimensional modelling of temperature swing adsorption of volatile organic compounds using beaded activated carbon. *Environ. Sci. Technol.* **2013a**, *47*, 11700–11710.
- Tefera, D.T.; Hashisho, Z.; Phillips, J.H.; Anderson, J.E.; Nichols, M. Modeling competitive adsorption of mixtures of volatile organic compounds in a fixed-bed of beaded activated carbon. *Environ. Sci. Technol.* **2014**, *48*, 5108–5117.
- Thommes, M.; Guillet-Nicolas, R.; Cychosz, K.A. Physical adsorption characterization of mesoporous zeolites. In *Mesoporous Zeolites: Preparation, Characterization and*

- Applications; Garica-Martinez, J., Li, K., Eds.; Wiley-VCH Verlag GmbH & Co. KGaA: Weinheim, Germany, 2015; pp 349–383.
- United States Naval Research Laboratory (1984); The reaction of oxygen-nitrogen mixtures with granular activated carbons below the spontaneous ignition temperature; <http://www.dtic.mil/dtic/tr/fulltext/u2/a149041.pdf>.
- Uranowski, L.J.; Tessmer, C.H.; Vidic, R.D. The effect of surface metal oxides on activated carbon adsorption of phenolics. *Water Res.* **1998**, 32, 1841–1851.
- Vidic, R.D.; Suidan, M.T. Role of dissolved oxygen on the adsorptive capacity of activated carbon for synthetic and natural organic matter. *Environ. Sci. Technol.* **1991**, 25, 1612–1618.
- Vidic, R.D.; Suidan, M.T.; Brenner, R.C. Oxidative coupling of phenols on activated carbon: impact on adsorption equilibrium. *Environ. Sci. Technol.* **1993**, 27, 2079–2085.
- Wang, H.; Jahandar Lashaki, M.; Fayaz, M.; Hashisho, Z.; Phillips, J.H.; Anderson, J.E.; Nichols, M. Adsorption and desorption of mixtures of organic vapors on beaded activated carbon. *Environ. Sci. Technol.* **2012**, 46, 8341–8350.
- Zerbonia, R.A.; Brockmann, C.M.; Peterson, P.R. Carbon bed fires and the use of carbon canisters for air emissions control on fixed-roof tanks. *J. Air & Waste Manage. Assoc.* **2001**, 51, 1617–1627.

CHAPTER 7. THE ROLE OF BEADED ACTIVATED CARBON'S PORE SIZE DISTRIBUTION ON HEEL FORMATION DURING CYCLIC ADSORPTION/DESORPTION OF ORGANIC VAPORS¹

7.1 Introduction

Automotive painting booths are a major source of VOCs emissions in car manufacturing sector (Papavasava et al., 2001; Kim, 2011). The emissions consist of aromatic hydrocarbons, aliphatic hydrocarbons, esters, ketones, alcohols, ethers, etc. (Kim, 2011). Adsorption is an established technology for removing VOCs from air (Hashisho et al., 2005, 2007, 2008; Ramos et al., 2010) because it is relatively low cost, allows for adsorbate recovery, and is efficient, even for low concentration contaminants (Dabrowski et al., 2005). However, a challenge with adsorbing VOCs onto activated carbon is irreversible adsorption, or heel formation, which prevents complete adsorbent regeneration and decreases its capacity and lifetime (Jahandar Lashaki et al., 2012a). This increases operation and maintenance costs because more frequent adsorbent replacement is necessary to maintain compliance with local regulations (Jahandar Lashaki et al., 2012a).

Heel formation can be due to chemisorption (Yonge et al., 1985; de Jonge et al., 1996b), adsorbate coupling (Dabrowski et al., 2005), or adsorbate decomposition (Ania et al., 2004; Niknaddaf et al., 2014, 2016; Fayaz et al., 2015b). While physisorption is generally reversible (Popescu et al., 2003), conditions exist where physical adsorption is difficult to reverse. These scenarios may be associated with adsorbates with high boiling point and/or molecular weight

¹ A version of this chapter was presented at a conference: Jahandar Lashaki, M.; Atkinson, J.D; Hashisho, Z.; Phillips, J.H.; Anderson, J.E.; Nichols, M. The impact of activated carbon's pore size distribution on heel formation during adsorption of organic vapors. *In proceedings of American Institute of Chemical Engineers Annual Meeting*, Salt Lake City, UT, 2015.

(Wang et al., 2012), or adsorbates with dimensions close to that of the adsorbent's pores (Jahandar Lashaki et al., 2012a). In the latter case, which is the focus of this work, strong dispersive forces acting on adsorbates make regeneration difficult due to overlapping attractive forces from neighboring pore walls (Jahandar Lashaki et al., 2012a).

The effect of various operational parameters on irreversible vapor-phase adsorption of VOCs has been described in previous studies. An increase in the adsorption temperature from 25 to 45 °C increased irreversible adsorption of a mixture of nine organic compounds by about 30% (Jahandar Lashaki et al., 2012a). An increase in the regeneration temperature from 288 to 400 °C, however, improved regeneration efficiency by 61% (Jahandar Lashaki et al., 2012a). The effect of activated carbon's SOGs on irreversible adsorption of organic vapors was investigated (Jahandar Lashaki et al., 2014). Thermal analysis identified physisorption as the main heel formation mechanism for adsorbents with low levels of SOGs (Jahandar Lashaki et al., 2014). For adsorbent with high levels of SOGs, however, irreversible adsorption was attributed to weakened physisorption combined with chemisorption due to consumption of SOGs by adsorbed species (Jahandar Lashaki et al., 2014). The effect of desorption purge gas oxygen content (≤ 5 to 10,000 ppm_v) on irreversible adsorption of two mixtures of organic vapors has also been investigated (Jahandar Lashaki et al., 2015a). With increasing O₂ concentration from ≤ 5 to 10,000 ppm_v, accumulated heel increased by up to 35% and the fifth cycle adsorption capacity decreased by up to 55% (Jahandar Lashaki et al., 2015a). Thermal analysis showed heel formation due to physisorption for ≤ 5 ppm_v O₂ and a combination of physisorption and chemisorption for samples regenerated at high O₂ concentrations (625 to 10,000 ppm_v) (Jahandar Lashaki et al., 2015a).

The PSD of activated carbon, which is influenced by the organic precursor and the activation method, affects adsorption performance (Chiang et al., 2002; Qiao et al., 2002; Lillo-Rodenas et al., 2005; Li et al., 2011). With activated carbon being used in many environmental engineering applications, carbon adsorbents with different PSDs can, generally, be readily obtained from suppliers. The choice of the optimal PSD for a given application, however, can prove difficult – especially when treating challenging adsorbates that promote heel formation. Previous studies showed that narrow pores hamper oxidative coupling of phenols, decreasing aqueous-phase irreversible adsorption (Lu and Sorial 2004a, 2004b, 2004c, 2007, 2009; Yan and Sorial, 2011). Other studies show that narrow pores promote physical adsorption, increasing irreversible adsorption (Qin et al., 2009; Jahandar Lashaki et al., 2012a). From an adsorption perspective, micropores enhance adsorption capacity due to their higher adsorption energy (Hashisho et al., 2007). Their presence in the structure of the adsorbent, therefore, is necessary to ensure the effectiveness of the mitigation process. Larger pores, however, are often associated with lower organic adsorption capacities because of decreased adsorption energy, resulting in higher adsorbate elimination during regeneration (i.e., lower heel formation). A balance between reversibility and capacity, therefore, must be sought when selecting the most effective activated carbon adsorbent for systems using on-site regeneration.

Previous studies of the effect of adsorbent porosity on irreversible adsorption of organic compounds focused on phenols (e.g. phenol, 2-methylphenol, 2-ethylphenol) in water, for which oxidative coupling is the main contributor to irreversible adsorption (Dabrowski et al., 2005; Soto et al., 2011). Such coupling has not been reported in the gas phase, thus it is also essential to expand these studies to include non-phenolic compounds of industrial significance. Therefore, it is important to assess the contribution of adsorbent porosity to heel formation during gas-phase

capture of a mixture of industrially-relevant organic compounds. A better understanding of the factors contributing to heel formation can aid in the reduction of heel buildup and maximization of carbon lifetime. Specifically, considering the one-time cost of adsorbent preparation versus repeated energy consumption during regeneration cycles over the lifetime of the adsorbent, it may be more efficient and cost effective to develop physically-tailored materials that *resist heel buildup* than it is to intensify regeneration techniques to *remove formed heel*. This work, therefore, provides data to help identify preferred PSDs for gas-phase, industrial adsorbents used in adsorption/regeneration systems for control of VOCs.

7.2 Materials and Methods

7.2.1 Adsorbents

Five BACs (B100777, B101412, B102546, and B102076 supplied by Blucher GmbH, and G-70R supplied by Kureha Corporation) were used. The BACs were selected because they have similar surface chemical compositions but varying physical properties, allowing for isolating the PSD contributions to heel formation. Prior to use, BACs were dried in air at 150 °C for 24 h and stored in a desiccator.

7.2.2 Adsorbate

The adsorbates were tested as a mixture primarily prepared in liquid phase by mixing equal parts (by volume) of nine organic compounds, representing different organic groups commonly present in automotive paint solvents including aliphatic hydrocarbons, aromatic hydrocarbons, esters, ethers, alcohols, ketones, polyaromatic hydrocarbons, and amines. The mixture was subsequently tested in gas phase (total concentration of 500 ppm_v). The concentration of the mixture components in the gas phase were as follows (all in ppm_v): *n*-decane, 36; 1,2,4-trimethylbenzene, 52; 2,2-dimethylpropylbenzene, 41; *n*-butylacetate, 54; 2-

butoxyethanol, 54; 1-butanol, 77; 2-heptanone, 51; naphthalene, 63; and diethanolamine, 72 (Jahandar Lashaki et al., 2012a, 2014, 2015a). The components of the mixture have a wide range of boiling points (118 to 271°C) and kinetic diameters (4.3 to 6.8 Å) (Jahandar Lashaki et al., 2012b), and previously showed a high tendency to form heel (Jahandar Lashaki et al., 2012a; Wang et al., 2012). Using a mixture of organic compounds as test adsorbate provides an adsorbate stream that is more representative of VOCs generated from vehicle painting operations (Kim, 2011; Jahandar Lashaki et al., 2012a; Wang et al., 2012).

7.2.3 Setup and Methods

The experimental setup and methods are described in previous studies (Jahandar Lashaki et al., 2012a, 2014, 2015a; Wang et al., 2012; Tefera et al., 2013a). The setup included a stainless steel adsorption/regeneration tube, organic vapor generation system, organic vapor detection system, power application module, and DAC system. For all experiments, 4.0 ± 0.1 g of dry BAC was added to the adsorption/regeneration tube between quartz wool plugs. Organic vapors were generated by using a syringe pump (kd Scientific, KDS-220) to inject the adsorbate mixture into a 10 SLPM air stream, generating a constant concentration (500 ppm_v) adsorbate stream. The flow rate of the gas stream was controlled with a mass flow controller (Alicat Scientific). The organic vapor detection system consisted of a photoionization detector (Minirae 2000, Rae Systems) to monitor the concentration during adsorption. Adsorption cycles lasted 240 min, providing full saturation of the BAC, as determined by equal inlet and outlet VOC concentrations (500 ppm_v).

The power application module used for regeneration consisted of heating (Omega) and insulation tapes (Omega) wrapped around the adsorption/regeneration tube. A DAC system consisting of a LabVIEW program (National Instruments) and a data logger (National

Instruments, Compact DAQ) equipped with analog input and output modules controlled and logged the bed temperature. Temperatures of 25 and 288 °C (measured in the center of the BAC bed using type K thermocouple) were used during adsorption and regeneration, respectively. Regeneration was completed by heating the adsorption/regeneration tube for 3 h with 1 SLPM N₂ and then cooling for 50 min while continuing the N₂ purge.

Mass balance was used to quantify adsorption capacity and cumulative heel formation, as follows:

$$\text{Adsorption capacity (\%)} = \frac{W_{AA} - W_{BA}}{W_{BAC}} \times 100$$

where W_{AA} is the BAC weight after adsorption, W_{BA} is the BAC weight before adsorption, and W_{BAC} is the initial dry BAC weight.

The term “mass balance cumulative heel” is used to characterize the total accumulated adsorbate after 5 successive adsorption/regeneration cycles and is calculated as follows:

$$\text{Mass balance cumulative heel (\%)} = \frac{W_{AR} - W_{BA}}{W_{BAC}} \times 100$$

where W_{AR} is the BAC weight after the last (5th) regeneration cycle.

Regenerated BAC samples were characterized after the 5th adsorption/regeneration cycle. Adsorption/regeneration experiments were duplicated, and average values are reported herein.

7.2.4 BAC Characterization

BAC samples were characterized before and after cycling using a micropore surface analyzer (iQ2MP, Quantachrome). N₂ adsorption was performed at -196 °C. Samples were degassed for 5 h at 120 °C prior to analysis. Specific surface area was calculated by the BET method (Brunauer et al., 1938) from relative pressures ranging from 0.01 to 0.07, which allowed for high coefficient of determination (R^2) values and positive BET constants (C). Total pore

volume was recorded at $P/P_0 = 0.975$ (Quantachrome Autosorb 1 Operating Manual, 2006). The QSDFT method provided pore size distributions, and the V-t method provided micropore volume (Quantachrome Autosorb 1 Operating Manual, 2006). Microporosity (%) was calculated by dividing micropore volume into total pore volume.

Surface elemental composition (C, O, and N) of all BACs was determined with XPS using an AXIS 165 spectrometer (Kratos Analytical). Survey scans were collected for binding energy spanning from 1100 eV to 0 with analyzer pass energy of 160 eV and a step of 0.4 eV. CasaXPS Software was used to process the scans and the results were reported in terms of atomic concentration.

Virgin BAC samples were analyzed using Boehm titration to determine the concentration of different SOGs (Boehm, 1994). Triplicate 50 mg of BAC samples were shaken in 5 mL of 0.05 M NaHCO_3 , Na_2CO_3 , and NaOH for 24 h using a wrist shaker (Burrell Scientific). The solution was separated from the carbon sample. Excess 0.05 M HCl (2:1 volume ratio for NaHCO_3 and NaOH, and 3:1 volume ratio for Na_2CO_3) was then added to ensure acidity, followed by one or two drops of phenolphthalein indicator. Finally, the solutions were back-titrated with 0.05 M NaOH solution until reaching a faint but permanent pink color. The concentrations of various SOGs were calculated assuming NaHCO_3 neutralizes carboxylic groups (including carboxylic anhydrides), Na_2CO_3 neutralizes carboxylic and lactonic groups, and NaOH neutralizes carboxylic, lactonic, and phenolic groups (Boehm, 1994).

The thermal stability of formed heel was assessed using DTG analysis (TGA/DSC 1, Mettler Toledo). The weight of the sample was measured as it was heated from 25 to 800 °C at 2 °C/min in 50 SCCM of N_2 . The slow heating rate provides high peak resolution. Percentages of accumulated heel eliminated during DTG analysis were calculated. Cumulative weight loss at

800 °C was corrected based on weight loss of the corresponding virgin BAC. This was then divided by mass balance cumulative heel to determine percent heel removal.

7.3 Results and Discussion

7.3.1 Characterization of Virgin BACs

Virgin BACs were characterized before 5-cycle adsorption/regeneration experiments (Table 7-1). All samples have micropore volume between 0.40 and 0.52 cm³/g, indicating a strong capability to adsorb organic vapors, even at low concentrations. Samples B100777, B101412, B102546, and G-70R have similar micropore volume (0.49 to 0.52 cm³/g), while the micropore volume of B102076 is about 20% lower (0.40 cm³/g). BET surface area (1097 to 1835 m²/g) and total pore volume (0.51 to 1.71 cm³/g) of the BACs explain the differences in microporosity (30 to 88%).

PSDs for all BACs were also measured (Figure 7-1). All samples have a substantial micropore contribution ($\geq 30\%$, for all samples, Table 7-1) with a pore volume of 0.25 to 0.28 cm³/g for pores $< 8 \text{ \AA}$. This pore size is similar to the size of common VOCs ($6 \pm 2 \text{ \AA}$) (Jahandar Lashaki et al., 2012b), providing high adsorption affinity (Figure 7-1a). PSD differences are observed in the mesopore region where B100777 shows the highest mesopore volume followed by B101412, B102546, B102076, and G-70R (Figure 7-1b).

Table 7-1. Physical and chemical properties of BACs before and after cycling.

Carbon Description	Carbon Sample	Physical Properties				Surface Composition		
		BET Surface Area (m ² /g)	Micropore Volume (cm ³ /g)	Total Pore Volume (cm ³ /g)	Microporosity (%)	C (%) ^a	O (%) ^a	N (%) ^a
BAC Before Ads/Regen Cycles	B100777	1835	0.52	1.71	30	93.7	6.3	No Peak
	B101412	1658	0.51	1.18	43	93.9	6.1	
	B102546	1400	0.49	0.63	78	93.3	6.7	
	G-70R	1359	0.50	0.57	88	93	7	
	B102076	1097	0.40	0.51	78	92.6	7.4	
BAC After Ads/Regen Cycles	B100777	1032	0.15	1.29	12	92.7	4.9	2.4
	B101412	850	0.17	0.78	22	93.1	4.4	2.5
	B102546	611	0.17	0.30	47	93.1	4.7	2.2
	G-70R	465	0.13	0.21	52	92.5	5.4	2.2
	B102076	387	0.08	0.16	50	93.0	5.2	1.8

^a Relative atomic percentages (%C + %O + %N = 100); Other elements not considered in surface composition

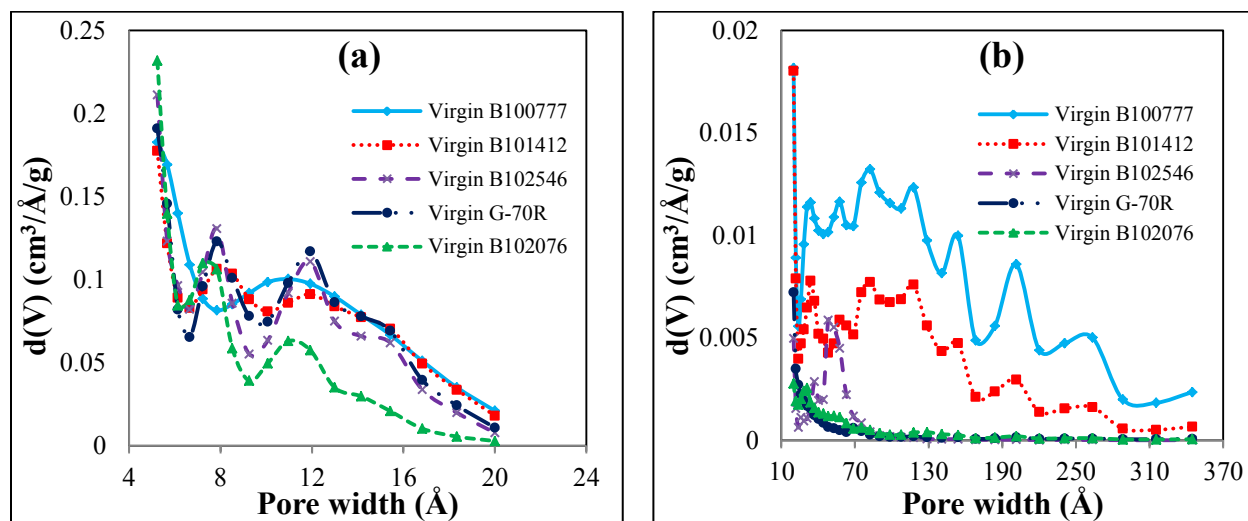


Figure 7-1. PSD analysis of BACs: (a) micropore (≤ 20 Å) and (b) mesopore (20-500 Å) regions.

DTG analysis evaluated the temperature stability of the virgin BACs (Figure 7-2). For all samples, a DTG peak at 50 °C is attributed to desorption of water vapor accumulated during exposure to ambient air prior to analysis (Popescu et al., 2003). No additional mass loss occurred until about 550-600 °C and > 700 °C, attributed to removal of surface phenol groups and char decomposition, respectively (Jahandar Lashaki et al., 2014).

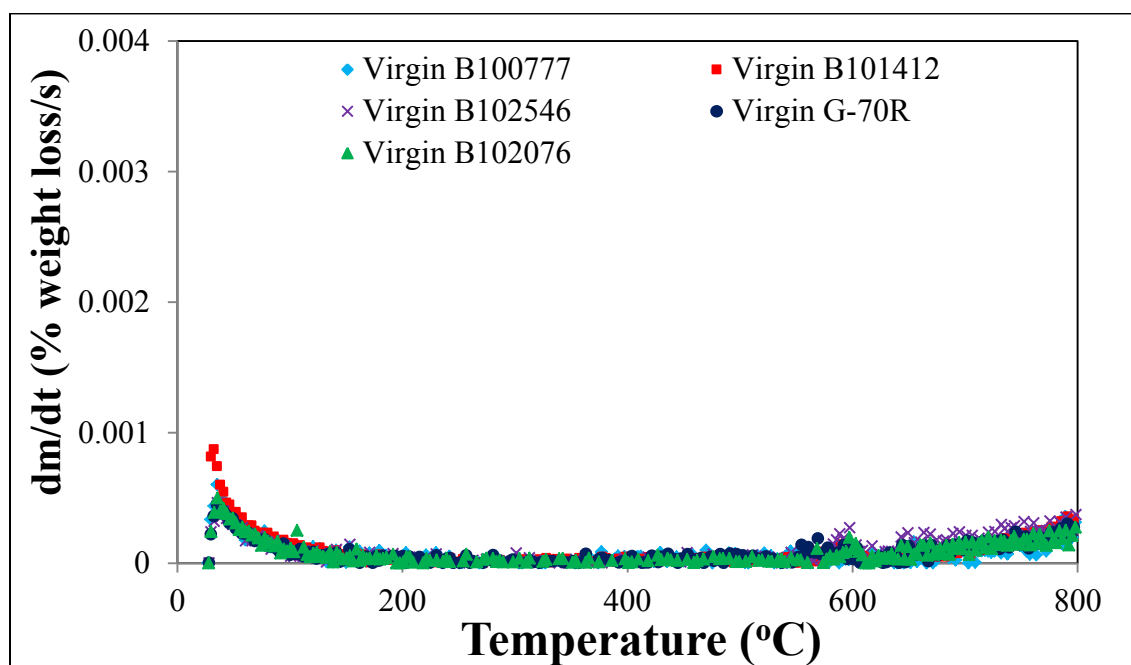


Figure 7-2. DTG analysis of different virgin BACs.

According to XPS results, all BACs have similar surface chemistry, including negligible nitrogen content and similar oxygen content (6.1 to 7.4%, Table 7-1). Boehm titration was also completed on all virgin samples to determine the concentration of different SOGs (Figure 7-3). Similar levels of phenol functional group were found on all virgin samples while no carboxyl and lactone groups were detected. Overall, pre-adsorption characterization results confirms that the carbons have similar chemical properties (i.e., nitrogen and oxygen content, and SOGs) but different physical properties (i.e., porosity), as intended.

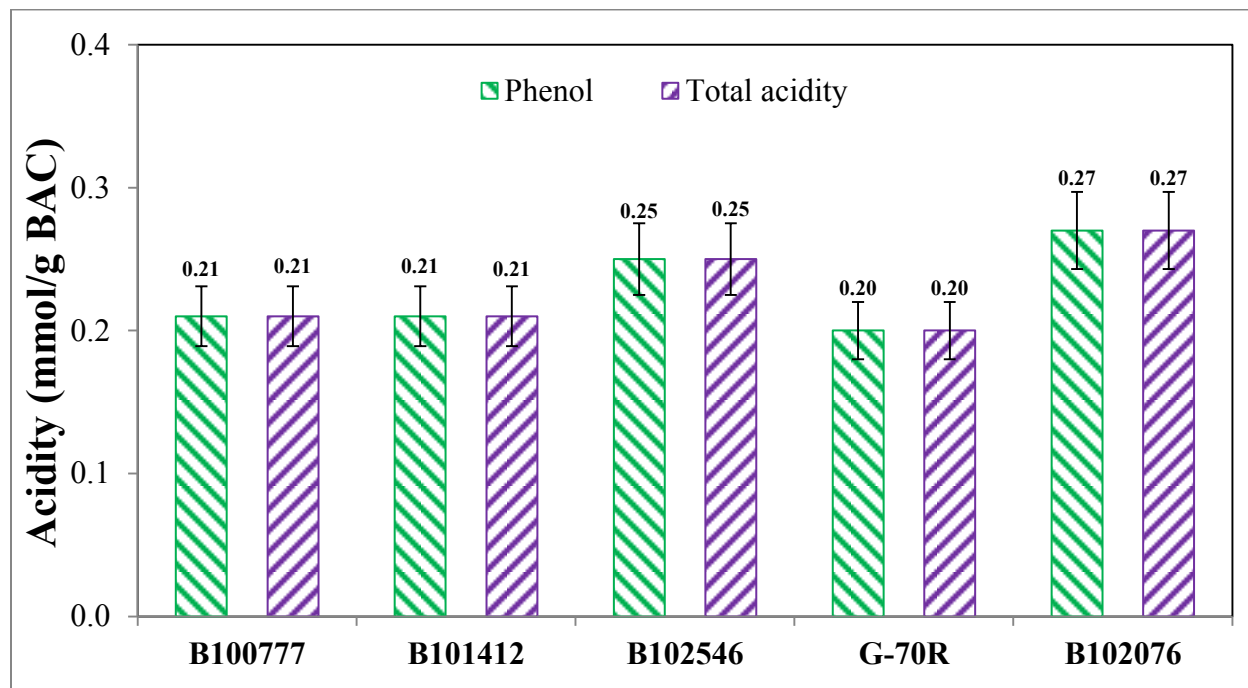


Figure 7-3. Boehm titration of different virgin BACs.

7.3.2 Adsorption/Regeneration Cycles

Five cycles of breakthrough curves for the VOC test mixture were obtained for all BACs to assess adsorption performance (Figure 7-4). The longest breakthrough time for first adsorption cycle was observed for B10777 followed by B101412, B102546, G-70R, and B102076, consistent with the surface area and porosity data in Table 7-1. For all samples, breakthrough time decreased with cyclic use, indicating that regeneration at 288 °C did not completely remove the adsorbed organic vapors, resulting in heel formation. If additional cycles (i.e., > 5) were run, breakthrough time would continue to decrease until the BAC becomes spent, requiring replacement. Breakthrough times during the fifth adsorption cycle followed the same rank order as the first adsorption cycle.

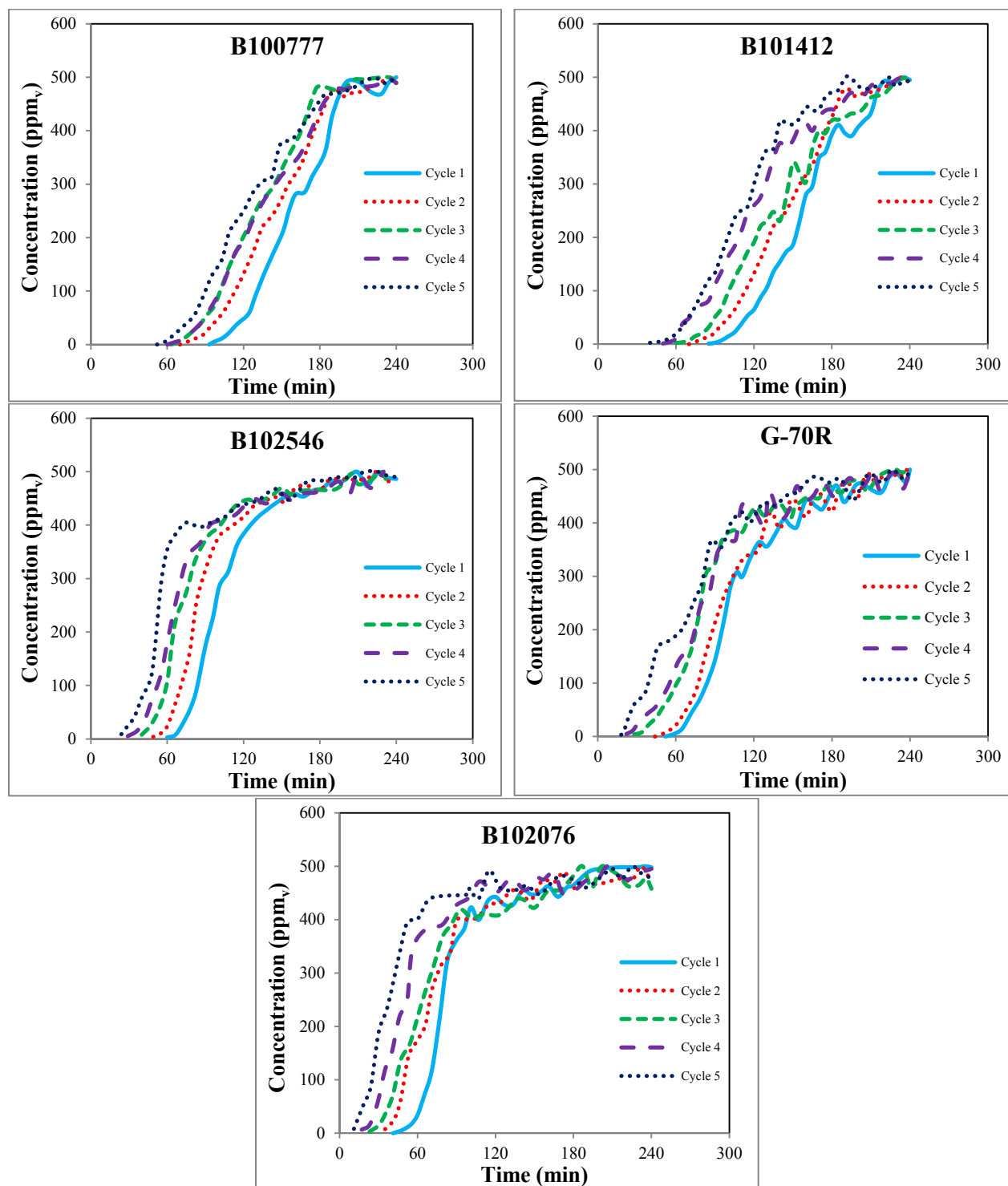


Figure 7-4. Breakthrough curves of different BACs.

Mass balance cumulative heel values are compared in Figure 7-5a. Accumulated heel after 5 cycles was similar for B100777, B101412, B102546, and G-70R but 20% lower for B102076. This difference is attributed to differences in the micropore volumes of the BAC samples (Table 7-1). A strong correlation ($R^2 = 0.91$) was found between cumulative heel percentage and micropore volume (Figure 7-5b), while the correlation with total pore volume was much weaker. Larger micropore volume can increase heel formation because of overlapping attractive forces from opposing pore walls (Jahandar Lashaki et al., 2012a). This phenomenon increases adsorption energy, necessitating higher energy input during regeneration (Qin et al., 2009). Regeneration at 288 °C does not suffice for achieving complete removal of adsorbates, causing substantial heel formation (Jahandar Lashaki et al., 2012a).

Adsorption capacities and breakthrough times for the BACs (i.e., for the first adsorption cycle) are described in Figure 7-6a. First cycle adsorption capacities were between 49.8 ± 0.6 and $77.9 \pm 0.7\%$ and breakthrough times were between 47 ± 1 and 100 ± 3 min. Adsorption capacities and breakthrough times correlate more closely with total pore volume of the BACs (R^2 of 0.87 and 0.93, respectively) than with micropore volume (R^2 of 0.70 and 0.58, respectively), indicating that BAC mesopores contribute to organic vapor adsorption (Figure 7-6b).

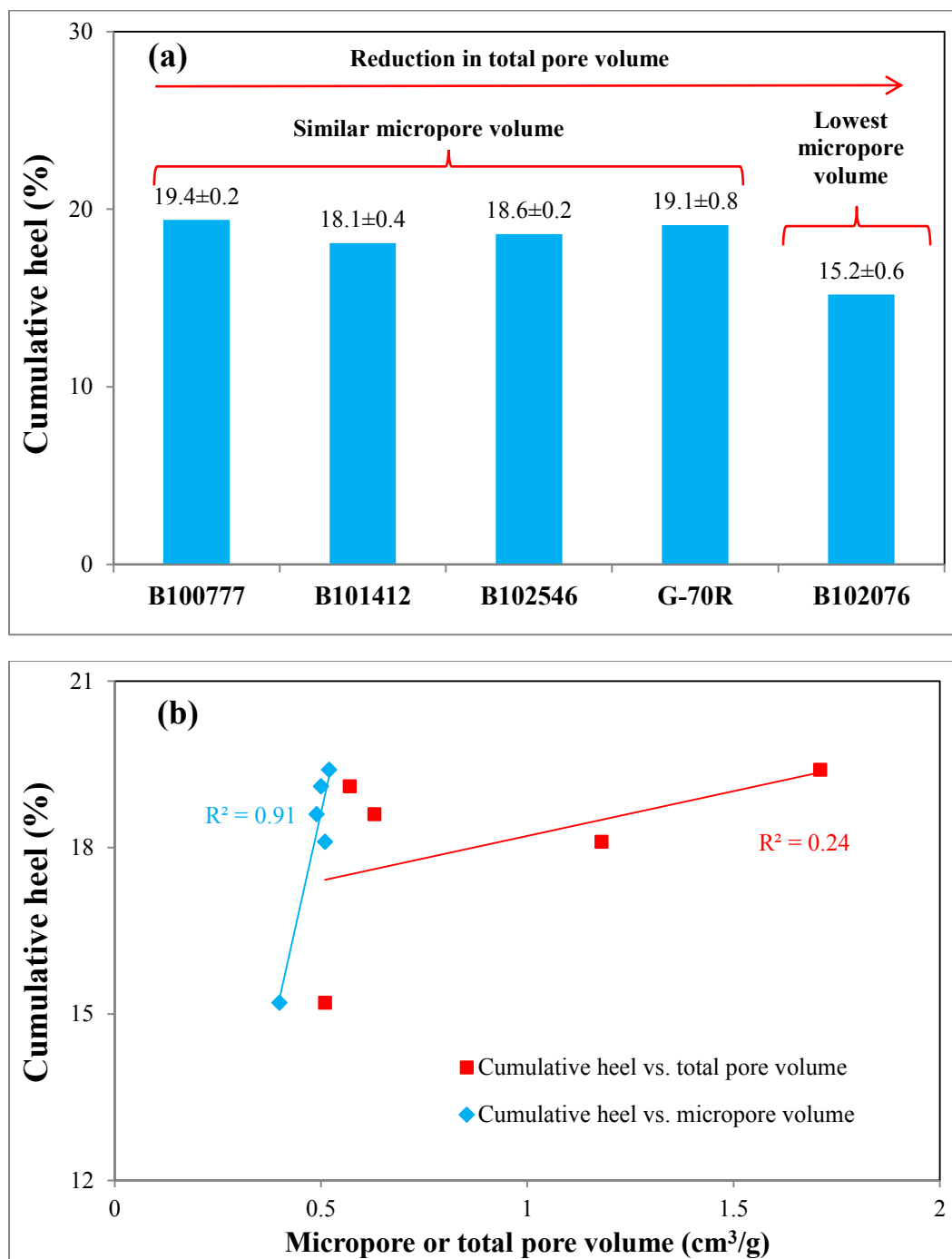


Figure 7-5. Mass balance cumulative heel after 5 successive adsorption/regeneration cycles: (a) Comparison of different BACs, (b) Correlations to micropore and total pore volumes of the virgin BAC. Data labels are presented as $x \pm y$ where x and y correspond to mean and standard deviation ($n=2$), respectively.

After 5-cycle adsorption/regeneration experiments, for every 1% of adsorption capacity, 0.25, 0.26, 0.30, 0.33, and 0.31% of cumulative heel was formed for B100777, B101412, B102546, G-70R, and B102076, respectively, which correspond to overall desorption efficiency of 75, 74, 70, 67, and 69%. This indicates that B100777 and B101412 exhibited the best performance among the BACs, likely due to mesopore contributions to adsorption but not to heel formation. This is also consistent with their low microporosity (30 and 43% for B100777 and B101412, respectively). G-70R, with the highest microporosity (88%), retained the highest portion of adsorbed VOCs as heel. To avoid confusion, this does not mean that solely mesoporous carbons are the ideal adsorbents for this application because zero micropore volume would significantly decrease the adsorption capacity, especially at low VOC concentrations where mesopores have low adsorption affinity.

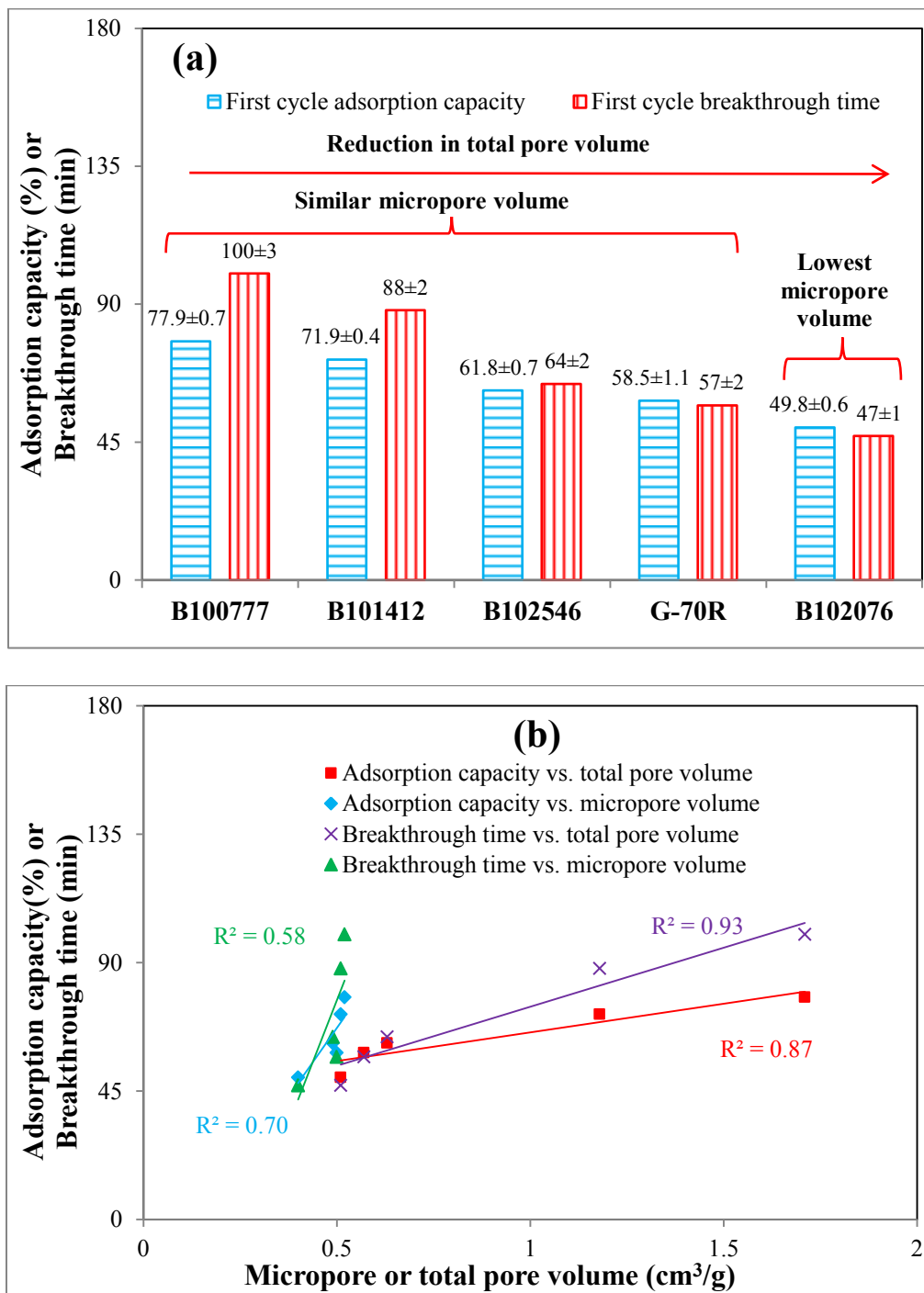


Figure 7-6. First cycle adsorption capacity and breakthrough time: (a) Comparison of different BACs, (b) Correlations with micropore and total pore volumes of the virgin BAC. Data labels are presented as $x \pm y$ where x and y correspond to mean and standard deviation ($n=2$), respectively.

7.3.3 Characterization of Regenerated BACs

DTG curves for regenerated adsorbents are shown in Figure 7-7 to compare the thermal stability of the heel formed on different BACs. All samples began losing mass around 300 °C, which is slightly higher than the BAC regeneration temperature used (288 °C). The largest peak is located at approximately 400 °C for all samples, which is higher than the boiling points of the species in the mixture (ranging from 118 to 271 °C). The peak was similar for B100777, B101412, B102546, and G-70R while it was lowest for B102076. These results are consistent with the mass balance cumulative heel results shown in Figure 7-5a, where B102076 showed the lowest heel. This peak could be attributed to non-desorbed physisorbed species resulting from superposition of wall effects in pores comparable in size to adsorbed species and/or diffusional limitations associated with the narrow micropores of the adsorbent, especially in the case of bulky adsorbates (e.g. naphthalene, diethanolamine) (Jahandar Lashaki et al., 2012a, 2014, 2015a).

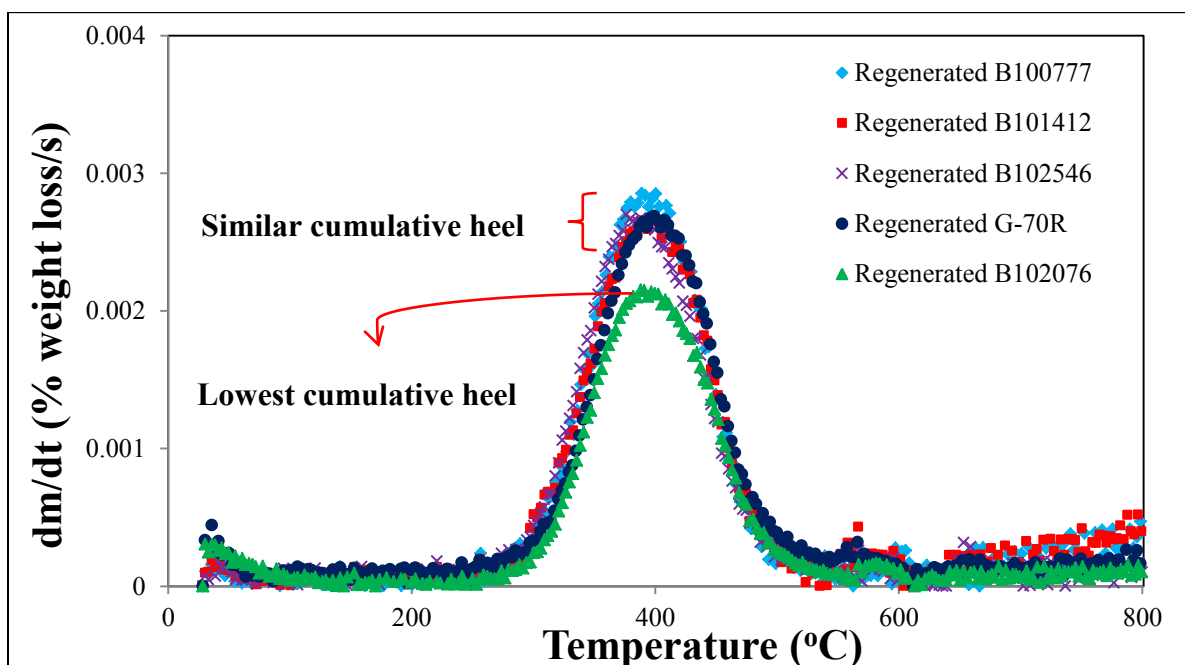


Figure 7-7. DTG analysis of different regenerated BACs. Note same scale as Figure 7-2.

The area under the DTG peak corresponds to the amount of heel removed during the DTG analysis (Figure 7-7). Due to differences in mass balance cumulative heel between BAC types, a direct comparison between the samples in terms of heel removal during thermal analysis is difficult. Percentages of heel eliminated during thermal analysis were calculated to better assess heel strength (Figure 7-8). Similar percentages (65.4 to 67.1 %) of heel were removed from all samples, so no differences in heel strength are notable. This again suggests a similar heel formation mechanism for all samples (i.e., non-desorbed physisorption), possibly because all of the BAC materials have similar narrow micropore volumes (between 0.25 and 0.28 cm³/g for pores < 8 Å). These pores are comparable in size to the organic compounds tested (6±2 Å) (Jahandar Lashaki et al., 2012b), and they therefore, should be the highest energy sites for physical adsorption (Qiao et al., 2002; Jahandar Lashaki et al., 2012a).

Physical properties of regenerated BACs were also characterized (Table 7-1) to identify the changes in the physical properties of the regenerated adsorbents as a result of heel formation. As expected, all of the measured physical parameters (i.e., BET surface area, micropore volume, and total pore volume) decreased as heel accumulated (Jahandar Lashaki et al., 2012a). Desorption at 288 °C does not yield complete regeneration for this mixture (Jahandar Lashaki et al., 2012a), so certain adsorption sites remain occupied after regeneration, and, as a result, vacant sites (as quantified with N₂ adsorption) decreased. Micropore volume reductions between 65 and 80% were observed for all samples following cyclic adsorption/regeneration experiments, compared to their virgin counterparts (Table 7-1), because of the predominant contribution of these pores to heel formation. This is consistent with the lower reductions in mesopore volume (ranged between 0 and 27%) for the samples.

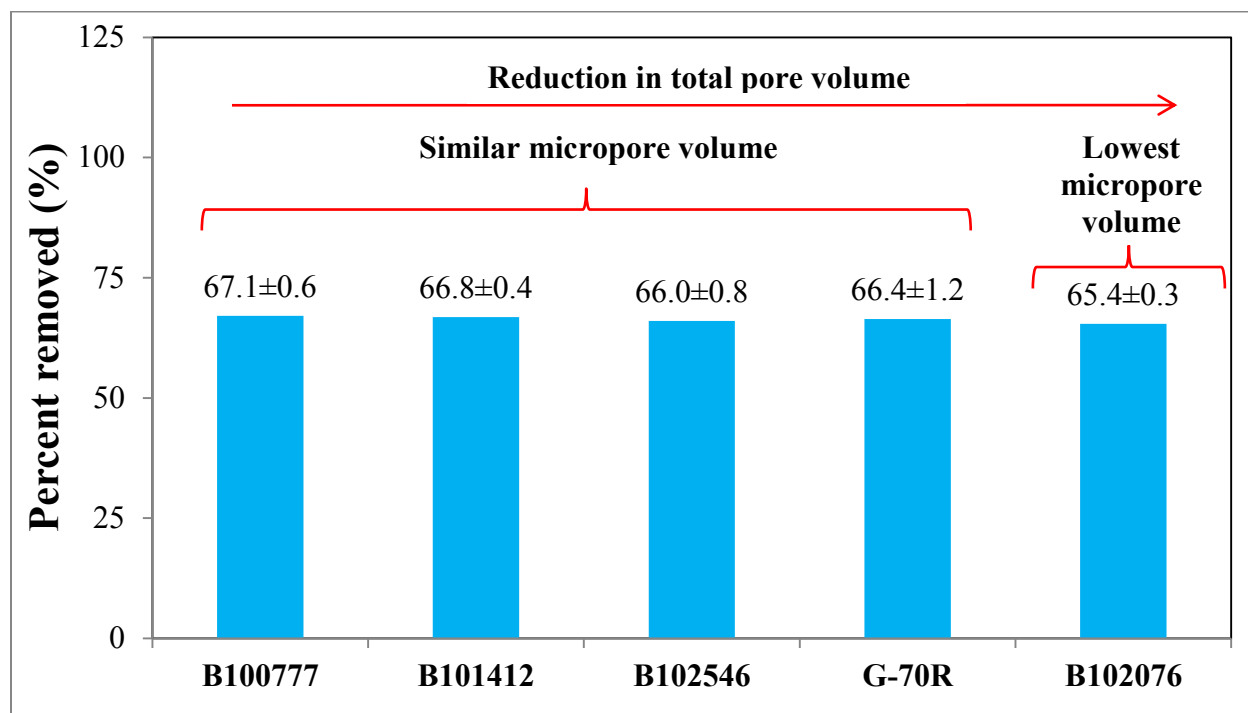


Figure 7-8. Percent heel removal during DTG analysis of regenerated BACs. Data labels are presented as $x \pm y$ where x and y correspond to mean and standard deviation ($n=2$), respectively.

For every 1% of mass balance cumulative heel, BET surface area decreased between 42 and 45 m^2/g , micropore volume decreased between 0.017 and 0.020 cm^3/g , and total pore volume decreased between 0.018 and 0.022 cm^3/g . Independent of the mass of heel formed, a given amount of heel caused a similar change in BAC physical properties for each BAC type. To be clear, this does not mean that *relative* impacts after 5 cycles are equal – virgin BACs with less surface area and pore volume (e.g. B102076) are impacted the most by a given amount of accumulated heel, as evidenced by a short breakthrough time during the 5th adsorption cycle (Figure 7-4). Note also that because changes in micropore and total pore volumes are similar, heel is preferentially being deposited in the higher energy, more narrow pores (Jahandar Lashaki et al., 2012a), as discussed before.

XPS analyses of regenerated samples are included in Table 7-1. Universal increases in nitrogen content were observed when comparing the BACs before and after cycling. Nitrogen increases are attributed to irreversibly adsorbed diethanolamine, since this is the only nitrogen-containing compound in the test mixture and the nitrogen purge gas does not react with the adsorbent (Jahandar Lashaki et al., 2015a). Diethanolamine has a high boiling point (271 °C) and has previously been shown to form heel (Chakma and Meisen, 1989; Jahandar Lashaki et al., 2014, 2015a). The lowest increase in surface nitrogen content was observed for B102076, consistent with this BAC showing the lowest mass balance cumulative heel Figure 7-5a.

Determining PSDs for regenerated BACs helps identify the location of the formed heel. Similar PSDs were obtained for regenerated B100777, B101412, B102546, and G-70R BACs while B102076 showed notably less nitrogen adsorption (Figure 7-9a). This is consistent with porosity data in Table 7-1, where regenerated B102076 showed less micropore and total pore volume than other BACs. Similar PSDs for the other BACs, specifically in the micropore region (Figure 7-9a) supports similarities in mass balance cumulative heel results (Figure 7-5a).

For all samples, changes within the micropore region (pore width < 20 Å) are observed after regeneration. Retained adsorbates were most notable in the narrow micropore region (< 8 Å) (Figure 7-9b to f). Similar results were revealed by Rivera-Utrilla et al. (2003). Smaller amounts of retained heel were observed in the mesopore region, relative to micropores.

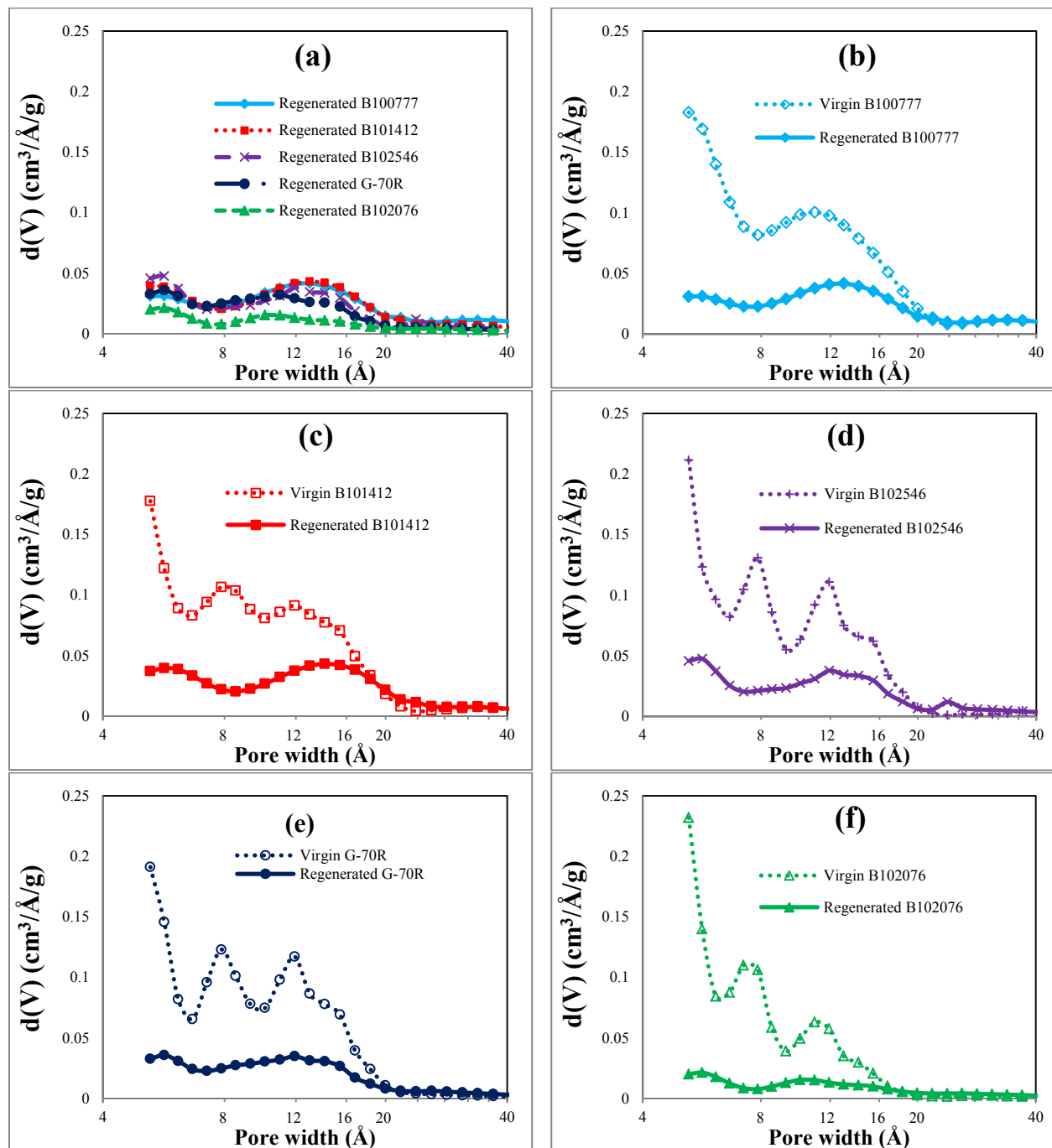


Figure 7-9. Pore size distribution of virgin and regenerated BACs.

In summary, four BAC samples having different porosity characteristics accumulated a similar mass of heel (Figure 7-5a) with similar DTG characteristics (Figure 7-7), which caused similar breakthrough changes (Figure 7-4) and resulted in similar pore volume decreases

(Table 7-1) over a similar pore size range (Figure 7-9). A fifth BAC, with the lowest micropore volume, accumulated the least heel, but also had the lowest initial adsorption capacity. The PSDs help describe how the carbons lost much of their adsorption capability after 5 cycles. In an emissions control system, such carbons would need to be periodically replaced by virgin carbon with increased costs associated with the new adsorbent, disposal of the spent adsorbent, and the associated labor.

7.4 Conclusions

The effect of adsorbent porosity on heel formation during capture of a mixture of organic compounds commonly emitted from automobile painting operations was investigated using five BACs with similar chemical properties but different pore size distributions. Similar mass balance cumulative heel was observed for BACs with similar micropore volume while it was 20% lower for the BAC with lowest micropore volume, showing a strong correlation ($R^2 = 0.91$) with micropore volume. First cycle adsorption capacities and breakthrough times, however, correlated linearly (R^2 equal to 0.87 and 0.93, respectively) with BAC total pore volume, not its micropore volume (R^2 of 0.70 and 0.58, respectively). This indicates that BAC mesopores contribute to organic vapor adsorption but not to heel formation. Based on DTG analysis, non-desorbed physisorption was observed for all BACs. Similar percentage of heel was eliminated during DTG analysis of all BACs, suggesting same heel strength due to presence of similar volumes of high energy adsorption sites (pore width $< 8 \text{ \AA}$) in them. Fundamentally, these results show that adsorbents consisted of notable volumes of micropores and mesopores perform better in terms of adsorption capacity and depict longer lifetime when used in cyclic adsorption/regeneration.

7.5 References

- Ania, C.O.; Menendez, J.A.; Parra, J.B.; Pis, J.J., Microwave-induced regeneration of activated carbons polluted with phenol. A comparison with conventional thermal regeneration. *Carbon* **2004**, *42*, 1383–1387.
- Brunauer, S; Emmett, P.H.; Teller, E. Adsorption of gases in multimolecular layers. *J. Am. Chem. Soc.* **1938**, *60*, 309–319.
- Chakma, A.; Meisen, A. Activated carbon adsorption of diethanolamine, methyl diethanolamine and their degradation products. *Carbon* **1989**, *27*, 573–284.
- Chiang, H.L.; Huang, C.P.; Chiang, P.C. The surface characteristics of activated carbon as affected by ozone and alkaline treatment. *Chemosphere* **2002**, *47*, 257–265.
- Dabrowski, A.; Podkoscielny, P.; Hubicki, Z.; Barczak, M. Adsorption of phenolic compounds by activated carbon-A critical review. *Chemosphere* **2005**, *58*, 1049–1070.
- de Jonge, R.J.; Breure, A.M.; van Andel, J.G. Reversibility of adsorption of aromatic compounds onto powdered activated carbon. *Water Res.* **1996b**, *30*, 883–892.
- Fayaz, M.; Niknaddaf, S.; Jahandar Lashaki, M.; Shariaty, P.; Hashisho, Z.; Phillips, J.H.; Anderson, J.E.; Nichols, M. The effect of regeneration temperature and heating rate on heel build-up during microwave regeneration. *In Proceedings of the American Institute of Chemical Engineers' Annual Meeting*, Salt Lake City, UT, 2015b.
- Hashisho, Z.; Rood, M.J.; Botich, L. Microwave-swing adsorption to capture and recover vapors from air streams with activated carbon fiber cloth. *Environ. Sci. Technol.* **2005**, *39*, 6851–6859.
- Hashisho, Z.; Emamipour, H.; Cevallos D.; Rood, M.J.; Hay, K.J.; Kim, B.J. Rapid response concentration-controlled desorption of activated carbon to dampen concentration fluctuations. *Environ. Sci. Technol.* **2007**, *41*, 1753–1758.
- Hashisho, Z.; Emamipour, H.; Rood, M.J.; Hay, K.J.; Kim, B.J.; Thurston, D. Concomitant adsorption and desorption of organic vapor in dry and humid air streams using microwave and direct electrothermal swing adsorption. *Environ. Sci. Technol.* **2008**, *42*, 9317–9322.
- Jahandar Lashaki, M.; Fayaz, M.; Wang, H.; Hashisho, Z.; Phillips, J.H.; Anderson, J.E.; Nichols, M. Effect of adsorption and regeneration temperature on irreversible adsorption

- of organic vapors on beaded activated carbon. *Environ. Sci. Technol.* **2012a**, *46*, 4083-4090.
- Jahandar Lashaki, M.; Fayaz, M.; Niknaddaf, S.; Hashisho, Z. Effect of the adsorbate kinetic diameter on the accuracy of the Dubinin-Radushkevich equation for modeling adsorption of organic vapors on activated carbon. *J. Hazard. Mater.* **2012b**, *241–242*, 154–163.
- Jahandar Lashaki, M.; Atkinson, J.D.; Hashisho, Z.; Phillips, J.H.; Anderson, J.E.; Nichols, M. The role of beaded activated carbon's surface oxygen groups on irreversible adsorption of organic vapors. In *Proceedings of 107th Air and Waste Management Association's Annual Conference and Exhibition*, Long Beach, CA, 2014.
- Jahandar Lashaki, M.; Atkinson, J.D.; Hashisho, Z.; Phillips, J.H.; Anderson, J.E.; Nichols, M. Misovski, T. Effect of desorption purge gas impurities on irreversible adsorption of organic vapors. In *Proceedings of the American Institute of Chemical Engineers' Annual Meeting*, Salt Lake City, UT, 2015a.
- Kim, B. R. VOC emissions from automotive painting and their control: A review. *Environ. Eng. Res.* **2011**, *16*, 1–9.
- Li, L.; Liu, S.; Liu, J.; Surface modification of coconut shell based activated carbon for the improvement of hydrophobic VOC removal. *J. Hazard. Mater.* **2011**, *192*, 683-690.
- Lillo-Rodenas, M.A.; Cazorla-Amoros, D.; Linares-Solano, A. Behaviour of activated carbons with different pore size distributions and oxygen groups for benzene and toluene adsorption at low concentrations. *Carbon* **2005**, *43*, 1758–1767.
- Lu, Q.; Sorial, G.A. The role of adsorbent pore size distribution in multicomponent adsorption on activated carbon. *Carbon* **2004a**, *42*, 3133-3142.
- Lu, Q.; Sorial, G.A. Adsorption of phenolics on activated carbon- impact of pore size and molecular oxygen. *Chemosphere* **2004b**, *55*, 671–679.
- Lu, Q.; Sorial, G.A. Impact of pore size on competitive adsorption of phenolic compounds. *Water Sci. Technol.* **2004c**, *4*, 1-7.
- Lu, Q.; Sorial, G.A. The Effect of Functional Groups on Oligomerization of Phenolics on Activated Carbon. *J. Hazard. Mater.* **2007**, *148*, 436-445.
- Lu, Q.; Sorial, G.A. A comparative study of multicomponent adsorption of phenolic compounds on GAC and ACFC. *J. Hazard. Mater.* **2009**, *167*, 89-96.

- Niknaddaf, S.; Atkinson, J.D.; Shariaty, P.; Jahandar Lashaki, M.; Hashisho, Z.; Phillips, J.H.; Anderson, J.E.; Nichols, M. Heel formation during volatile organic compound desorption from activated carbon fiber cloth using resistive heating. *In Proceedings of 107th Air and Waste Management Association's Annual Conference and Exhibition*, Long Beach, CA, 2014.
- Niknaddaf, S.; Atkinson, J.D.; Shariaty, P.; Jahandar Lashaki, M.; Hashisho, Z.; Phillips, J.H.; Anderson, J.E.; Nichols, M. Heel formation during volatile organic compound desorption from activated carbon fiber cloth. *Carbon* **2016**, *96*, 131–138.
- Papasavva, S.; Kia, S.; Claya, J.; Gunther, R. Characterization of automotive paints: An environmental impact analysis. *Prog. Org. Coat.* **2001**, *43*, 193–206.
- Popescu, M.; Joly, J.P.; Carre, J.; Danatoiu, C. Dynamical adsorption and temperature-programmed desorption of VOCs (toluene, butyl acetate and butanol) on activated carbons. *Carbon* **2003**, *41*, 739–748.
- Qiao, W.M.; Korai, Y.; Mochida, I.; Hori, Y.; Maeda, T. Preparation of an activated carbon artifact: oxidative modification of coconut shell-based carbon to improve the strength. *Carbon* **2002**, *40*, 351–358.
- Qin, W.; Xiao-yi, L.; Rui, Z.; Chao-jun, L.; Xiao-jun, L.; Wen-ming, Q.; Liang, Z.; Li-cheng, L. Preparation of polystyrene-based activated carbon spheres and their adsorption of dibenzothiophene. *New Carbon Mater.* **2009**, *24*, 55–60.
- Quantachrome Autosorb 1 Operating Manual; **2006**.
- Ramos, M.E.; Bonelli, P.R.; Cukierman, A.L.; Ribeiro Carrott, M.M.L.; Carrott, P.J.M. Adsorption of volatile organic compounds onto activated carbon cloths derived from a novel regenerated cellulosic precursor. *J. Hazard. Mater.* **2010**, *177*, 175–182.
- Rivera-Utrilla, J.; Ferro-Garcia, M.A.; Bautista-Toledo, I.; Sanchez-Jimenez, C.; Salvador, F.; Merchan, M.D. Regeneration of ortho-chlorophenol-exhausted activated carbons with liquid water at high pressure and temperature. *Water Res.* **2003**, *37*, 1905–1911.
- Soto, M.L.; Moure, A.; Dominguez, H.; Parajo, J.C. Recovery, concentration and purification of phenolic compounds by adsorption: A review. *J. Food Eng.* **2011**, *105*, 1–27.
- Tefera, D.T.; Jahandar Lashaki, M.; Fayaz, M.; Hashisho, Z.; Phillips, J.H.; Anderson, J.E.; Nichols, M. Two-dimensional modelling of temperature swing adsorption of volatile

- organic compounds using beaded activated carbon. *Environ. Sci. Technol.* **2013a**, *47*, 11700–11710.
- Wang, H.; Jahandar Lashaki, M.; Fayaz, M.; Hashisho, Z.; Phillips, J.H.; Anderson, J.E.; Nichols, M. Adsorption and desorption of mixtures of organic vapors on beaded activated carbon. *Environ. Sci. Technol.* **2012**, *46*, 8341–8350.
- Yan, L.; Sorial, G.A. Chemical activation of bituminous coal for hampering oligomerization of organic contaminants. *J. Hazard. Mater.* **2011**, *197*, 311–319
- Yonge, D.R.; Keinath, T.M.; Poznanska, K.; Jiang, Z.P. Single-solute irreversible adsorption on granular activated carbon. *Environ. Sci. Technol.* **1985**, *19*, 690–694.
- Yun, J.H.; Choi, D.K.; Moon, H. Benzene adsorption and hot purge regeneration in activated carbon beds. *Chem. Eng. Sci.* **2000**, *55*, 5857–5872.

CHAPTER 8. CONCLUSIONS AND RECOMMENDATIONS

8.1 Dissertation Overview

Automotive painting operations are the main source of VOC emissions from car manufacturing sector. Increasingly stringent regulations on VOC emissions warrant continuous research to develop more effective technologies to mitigate emissions of these pollutants. This research aimed at understanding and improving gas phase capture of VOCs from car painting operations by carbon-based adsorbents.

8.2 Summary of Findings

Chapter 3 investigated the effect of the KD of the reference adsorbate on the accuracy of the D-R equation for predicting the adsorption isotherms of organic vapors on microporous AC. It was found that the kinetic diameter of the adsorbate is the main factor affecting the accuracy of the D-R equation; the choice of the reference adsorbate in the D-R equation should take into consideration the kinetic diameter of the adsorbate. Choosing a reference adsorbate with a kinetic diameter similar to that of the test adsorbate resulted in better prediction of the adsorption isotherm with the D-R equation while a reference adsorbate with smaller or larger kinetic diameter compared to that of the test adsorbate would overestimate or underestimate the adsorption capacity, respectively.

The effect of adsorption and regeneration temperature on the irreversible adsorption of a mixture of organic compounds was investigated in Chapter 4. Based on results, increasing the adsorption temperature from 25 to 45 °C increased heel buildup on BAC by about 30%, independent of the regeneration temperature. In this case, the BAC progressively loses its adsorption capacity with more cycles; consequently, it is better to complete the adsorption process at the lowest possible temperature to preserve the adsorption capacity of the BAC.

Applying more energy by increasing the regeneration temperature enhanced the regeneration efficiency independent of the adsorption temperature and eliminated more adsorbates from the narrow micropores and increased the lifetime of the BAC. BET surface area and pore volumes of the BAC decreased significantly because of higher cumulative heel. Pore size distribution confirmed that narrow micropores have a significant role in the accumulation of adsorbates inside the pores of the BAC. The measured reduction in pore volume due to heel formation was larger than the calculated one, possibly due to blockage of narrow micropores.

In Chapter 5, the effect of AC's SOGs on irreversible adsorption of organic vapors was investigated. For the different BAC samples, mass balance cumulative heel was 14 and 20% higher for oxygen functionalized and hydrogen-treated BACs, respectively, relative to heat-treated BAC. DTG results, showed heel formation due to physisorption for heat-treated and hydrogen-treated BACs, and weakened physisorption combined with chemisorption for nitric acid-treated BAC. Chemisorption was attributed to consumption of SOGs by adsorbed species, resulting in formation of high boiling point oxidation byproducts or bonding between the adsorbates and the SOGs.

The effect of desorption purge gas oxygen impurities on irreversible adsorption of organic vapors was studied in Chapter 6. With increasing O₂ concentration ($\leq 5 - 10,000$ ppm_v), mass balance cumulative heel increased by up to 35% and the fifth cycle adsorption capacity decreased by up to 55% relative to baseline scenario (≤ 5 ppm_v O₂ in N₂). DTG analysis showed heel formation due to physisorption for ≤ 5 ppm_v O₂ and a combination of physisorption and chemisorption samples regenerated in 625 – 10,000 ppm_v O₂. BAC samples exposed to 50 successive adsorption/regeneration cycles showed trends consistent with short-term exposure (5 cycles).

Chapter 7 explored the effect of AC's PSD on heel formation during adsorption of organic vapors. Heel formation was linearly correlated ($R^2 = 0.91$) with BAC micropore volume; heel for the BAC with the lowest micropore volume was 20% lower than the BAC with the highest micropore volume. First cycle adsorption capacities and breakthrough times correlated linearly (R^2 equal to 0.87 and 0.93, respectively) with BAC total pore volume. A greater portion of adsorbed species are converted into heel on highly microporous adsorbents due to higher share of high energy adsorption sites in their structure.

8.3 Significance of the Research

A better understanding of the factors enhancing the irreversible adsorption is constructive in finding ways to decrease heel buildup and eventually increasing the lifetime of the adsorbent. By using the outcomes of this research, measures can be determined to diminish the magnitude of irreversible adsorption. Some of the outcomes of this research have been implemented in full scale adsorbers controlling VOC emissions from automobile painting operations, resulting in savings associated with the cost of the adsorbent, disposal of the spent adsorbent, and labor cost to replace the adsorbent. In addition, this work contributed to bridging the knowledge gap regarding the irreversible adsorption of VOCs from gas phase onto AC. The outcomes of this investigation can also be useful in designing an effective abatement system for capturing of organic vapors from polluted gaseous streams.

8.4 Recommendations for Future Work

This research investigated the effect of various operational parameters such as adsorption and regeneration temperature, adsorbent surface oxygen groups, desorption purge gas oxygen content, and adsorbent porosity on irreversible adsorption of organic vapors. Based on the

obtained results and conclusions, the following recommendations can be made for future research:

1. Many VOC laden gas streams contain water vapor, which can compete with organic adsorbates on available adsorption sites. Water vapor adsorption on activated carbon is negligible at relative humidities below 50%, therefore, polluted gas streams are usually heated prior to adsorption to reduce the relative humidity and minimize competitive adsorption between water vapor and organic compounds. As shown in Chapter 4 of the present work, increasing adsorption temperature can result in higher irreversible adsorption. Consequently, future work on irreversible adsorption of organic vapors should take into consideration the impact of relative humidity of the gas stream on this phenomenon. An optimum adsorption temperature may be determined for concurrent minimization of the competitive adsorption and heel formation.
2. This study used high purity nitrogen and mixtures of nitrogen and oxygen as regeneration purge gas. Producing high purity nitrogen is costly and oxygen impurities increase irreversible adsorption (Chapter 6). Alternative purge gases could be used to reduce the operational cost and irreversible adsorption at the same time. Future work should investigate the impact of other regeneration purge gases such as CO_2 , $\text{CO}_2 + \text{H}_2\text{O}$, $\text{N}_2 + \text{H}_2\text{O}$, flue gas ($\text{N}_2 + \text{CO}_2 + \text{H}_2\text{O}$), and O_3 on irreversible adsorption of organic vapors.
3. The effect of adsorbent porosity on irreversible adsorption of organic vapors was investigated in Chapter 7. Additional testing is required to shed some light on the effect of adsorbent porosity on adsorption and regeneration performance. Future work should explore the impact of this parameter on adsorption and regeneration kinetics, and competitive adsorption. GC-MS analysis of effluent gas during adsorption and regeneration can be used for this purpose.

4. All the successive adsorption/regeneration experiments on our bench-scale setup were completed for 5 cycles, however, in real world conditions, heel formation and/or transformation happens over a long period of time. Consequently, it is useful to monitor heel nature/characteristics over many adsorption/regeneration cycles to get a more realistic understanding of heel formation. For this purpose, an automated adsorption/regeneration setup could be built to test the effect of various parameters including adsorbate type (i.e., different functionalities), regeneration temperature and duration, and desorption purge gas type and flow rate. BAC samples may be collected every few cycles and characterized in terms of BET surface area, pore volume, PSD, XPS, and TGA to elucidate the long-term changes in physical and chemical properties of the adsorbent as well as in heel nature.

BIBLIOGRAPHY

- Abuzaid, N.; Nakhla, G.F. Dissolved oxygen effects on equilibrium and kinetics of phenols adsorption by activated carbon. *Environ. Sci. Technol.* **1994**, *28*, 216–221.
- Abuzaid, N.; Nakhla, G.F.; Farooq, S.; Osei-Twum, E. Activated carbon adsorption in oxidizing environments. *Water Res.* **1995**, *29*, 653–660.
- Abuzaid, N.; Nakhla, G.F. Modeling of the temperature variation effects on the polymerization reactions of phenolics on granular activated carbon. *Separ. Sci. Technol.* **1997**, *32*, 1255–1272.
- Aktas, O.; Cecen, F. Effect of type of carbon activation on adsorption and its reversibility. *J. Chem. Technol. Biot.* **2006**, *81*, 94–101.
- Aktas, O.; Cecen, F. Competitive adsorption and desorption of a bi-solute mixture: Effect of activated carbon type. *Adsorption* **2007**, *13*, 159–169.
- Al-Khattaf, S.; de Lasa, H. The role of diffusion in alkyl-benzenes catalytic cracking, *Appl. Catal. A* **2002**, *226*, 139–153.
- Alvarez, P.M.; Beltran, F.J.; Gomez-Serrano, V.; Jaramillo, J.; Rodriguez, E.M. Comparison between thermal and ozone regenerations of spent activated carbon exhausted with phenol. *Water Res.* **2004**, *38*, 2155–2165.
- Alvarez, P. M.; Garcia-Araya, J. F.; Beltran, F. J.; Masaa, F. J.; Medina, F. Ozonation of activated carbons: Effect on the adsorption of selected phenolic compounds from aqueous solutions. *J. Colloid Interf. Sci.* **2005**, *283*, 503–512.
- Anderson, J.E.; Gilland, R.D.; Adams, J.A.; Saloka, G.S.; Dearth, M.A.; Novak, R.F.; Kim, B.R.; Wherrett, M.R.; Davies, K.L.; Hula, A.C.; Edgeworth, R.K.; Ryan, P.A.; Cowles, H. Recovering VOCs from paint spray booth air using an activated-carbon fluidized-bed adsorber for subsequent power generation. *In Proceedings of 99th Air and Waste Management Association's Annual Conference and Exhibition*, New Orleans, LA, 2006.
- Ania, C.O.; Menendez, J.A.; Parra, J.B.; Pis, J.J. Microwave-induced regeneration of activated carbons polluted with phenol: A comparison with conventional thermal regeneration. *Carbon* **2004**, *42*, 1383–1387.
- Ania, C.O.; Bandosz, T.J. Importance of structural and chemical heterogeneity of activated carbon surfaces for adsorption of dibenzothiophene. *Langmuir* **2005**, *21*, 7752–7759.

- Ania, C.O.; Cabal, B.; Pevida, C.; Arenillas, A.; Parra, J.B.; Rubiera, F.; Pis, J.J. Effects of activated carbon properties on the adsorption of naphthalene from aqueous solutions. *Appl. Surf. Sci.* **2007**, *253*, 5741–5746.
- Arafat, H.A.; Ahnert, F.; Pinto, N.G. On the adsorption of aromatics on oxygenated activated carbon in nonaqueous adsorption media. *Sep. Sci. Tech.* **2004**, *39*, 43–62.
- Atkinson, J.D.; Zhang, Z.; Yan, Z.; Rood, M.J. Evolution and impact of acidic oxygen functional groups on activated carbon fiber cloth during NO oxidation. *Carbon* **2013**, *54*, 444–453.
- Atkinson, J.D.; Jahandar Lashaki, M.; Hashisho, Z.; Phillips, J.H.; Anderson, J.E.; Nichols, M. Reactivation of spent beaded activated carbon for decreasing irreversible adsorption. In *proceedings of 107th Air and Waste Management Association's Annual Conference and Exhibition*, Long Beach, CA, 2014.
- Boehm H.P. Some aspects of the surface chemistry of carbon black and other carbons. *Carbon* **1994**, *32*, 759 – 769.
- Boehm, H.P. Surface oxides on carbon and their analysis: a critical Assessment. *Carbon* **2002**, *40*, 145–149.
- Breck, D.E. *Zeolites Molecular Sieves: Structure, Chemistry and Use*; Wiley: New York, 1974.
- Bruanuer, S.; Emmett, P.H.; Teller, E. Adsorption of gases in multimolecular layers. *J. Am. Chem. Soc.* **1938**, *60*, 309–319.
- Busca, G.; Berardinelli, S.; Resini, C.; Arrighi, L. Technologies for the removal of phenol from fluid streams: A short review of recent developments. *J. Hazard. Mater.* **2008**, *160*, 265–288.
- Canham, L.T.; Groszek, A.J. Characterization of microporous Si by flow calorimetry: Comparison with a hydrophobic SiO₂ molecular sieve. *J. Appl. Phys.* **1992**, *72*, 1558–1565.
- Carter, E.M.; Katz, L.E.; Speitel, G.E.; Ramirez, D. Gas-phase formaldehyde adsorption isotherm studies on activated carbon: Correlations of adsorption capacity to surface functional group density. *Environ. Sci. Technol.* **2011**, *45*, 6498–6503.
- Chakma, A.; Meisen, A. Activated carbon adsorption of diethanolamine, methyl diethanolamine and their degradation products. *Carbon* **1989**, *27*, 573–284.

- Chang, C.H.; Savage, D.W. Investigations of solvent-regenerable carbon-sulfur surface compounds for phenol removal in packed column. *Environ. Sci. Technol.* **1981**, *15*, 201–206.
- Chatzopoulos, D.; Varma, A.; Irvine, R.L. Activated carbon adsorption and desorption of toluene in the aqueous phase. *AIChE J.* **1993**, *39*, 2027–2041.
- Chatzopoulos, D.; Varma, A.; Irvine, R.L. Adsorption and desorption studies in the aqueous phase for the toluene/activated carbon system. *Environ. Prog.* **1994**, *13*, 21–25.
- Chatzopoulos, D.; Varma, A. Aqueous-phase adsorption and desorption of toluene in activated carbon fixed beds: Experiments and model. *Chem. Eng. Sci.* **1995**, *50*, 127–141.
- Chiang, Y.; Chiang, P.; Huang, C. Effects of pore structure and temperature on VOC adsorption on activated carbon. *Carbon* **2001**, *39*, 523–534.
- Chiang, H.L.; Huang, C.P.; Chiang, P.C. The surface characteristics of activated carbon as affected by ozone and alkaline treatment. *Chemosphere* **2002**, *47*, 257–265.
- Compressed Air Best Practices, The Energy Costs Associated with Nitrogen Specifications. <http://www.airbestpractices.com/system-assessments/air-treatment/n2/energy-costs-associated-nitrogen-specifications>.
- Cooney, D.; Xi, Z. Activated carbon catalyzes reactions of phenolics during liquid-phase adsorption. *AIChE J.* **1994**, *40*, 341–344.
- Costa, E.; Calleja, G.; Marijuan, L. Comparative adsorption of phenol, *p*-nitrophenol and *p*-hydroxybenzoic acid on activated carbon. *Adsorpt. Sci. Technol.* **1989**, *5*, 213–228.
- Coughlin, R.W.; Ezra, F.S. Role of surface acidity in the adsorption of organic pollutants on the surface of carbon. *Environ. Sci. Technol.*, **1968**, *2*, 291–297.
- Dabrowski, A.; Podkoscielny, P.; Hubicki, Z.; Barczak, M. Adsorption of phenolic compounds by activated carbon-A critical review. *Chemosphere* **2005**, *58*, 1049–1070.
- Das, D.; Gaur, V.; Verma, N. Removal of volatile organic compound by activated carbon fiber. *Carbon* **2004**, *42*, 2949–2962.
- Dehdashti, A.; Khavanin, A.; Rezaee, A.; Assilian, H.; Motalebi, M. Application of microwave irradiation for the treatment of adsorbed volatile organic compounds on granular activated carbon. *Iran. J. Environ. Health. Sci. Eng.* **2011**, *8*, 85–94.
- de Jonge, R.J.; Breure, A.M.; van Andel, J.G. Bioregeneration of powdered activated carbon (PAC) loaded with aromatic compound. *Water Res.* **1996a**, *30*, 875–882.

- de Jonge, R.J.; Breure, A.M.; van Andel, J.G. Reversibility of adsorption of aromatic compounds onto powdered activated carbon. *Water Res.* **1996b**, *30*, 883–892.
- de la Puente, G.; Pis, J. J.; Menendez, J. A.; Grange, P. Thermal stability of oxygenated functions in activated carbons. *J. Anal. Appl. Pyrol.* **1997**, *43*, 125–138.
- Delmas, H.; Creanga, C.; Julcour-Lebigue, C.; Wilhelm, A.M. AD–OX: a sequential oxidative process for water treatment—adsorption and batch CWAO regeneration of activated carbon. *Chem. Eng. J.* **2009**, *152*, 189–194.
- Dubinin, M.M.; Radushkevich, L.V. The equation of the characteristic curve of the activated charcoal. *Proc. Acad. Sci. USSR Phys. Chem. Sect.* **1947**, *55*, 331–337.
- Duchowicz, P.R.; Castaneta, H.; Castro, E.A.; Fernandez, F.M.; Vicente, J.L. QSPR prediction of the Dubinin-Radushkevich's k parameter for the adsorption of organic vapors on BPL carbon. *Atmos. Environ.* **2006**, *40*, 2929–2934.
- Efremenko, I.; Sheintuch, M. Predicting solute adsorption on activated carbon: phenol. *Langmuir* **2006**, *22*, 3614–3621.
- El-Khaiary, M.I. Least-squares regression of adsorption equilibrium data: comparing the options, *J. Hazard. Mater.* **2008**, *158*, 73–87.
- Emamipour, H.; Hashisho, Z.; Cevallos, D.; Rood, M.J.; Thurston, D.L.; Hay, K.J.; Kim, B.J.; Sullivan, P. D. Steady-state and dynamic desorption of organic vapor from activated carbon with electrothermal swing adsorption. *Environ. Sci. Technol.* **2007**, *41*, 5063–5069.
- Environment Canada (2015); Volatile organic compound emissions; www.ec.gc.ca/indicateurs-indicators/default.asp?lang=en&n=64B9E95D-1.
- Fayaz, M.; Wang, H.; Jahandar Lashaki, M.; Hashisho, Z.; Phillips, J.H.; Anderson, J.E. Accumulation of adsorbed organic vapors from automobile painting operations on bead activated carbon. In *proceedings of 104th Air and Waste Management Association's Annual Conference and Exhibition*, Orlando, FL, 2011.
- Fayaz, M.; Shariaty, P.; Atkinson, J.D.; Hashisho, Z.; Phillips, J.H.; Anderson, J.E.; Nichols, M. The effect of microwave heating on regeneration of beaded activated carbon and a polymeric adsorbent. In *proceedings of 107th Air and Waste Management Association's Annual Conference and Exhibition*. Long Beach, CA, 2014.

- Fayaz, M.; Shariaty, P.; Hashisho, Z.; Phillips, J.H.; Anderson, J.E.; Nichols, M. Using microwave heating to improve the desorption efficiency of high molecular weight VOC from beaded activated carbon. *Environ. Sci. Technol.* **2015a**, *49*, 4536–4542.
- Fayaz, M.; Niknaddaf, S.; Jahandar Lashaki, M.; Shariaty, P.; Hashisho, Z.; Phillips, J.H.; Anderson, J.E.; Nichols, M. The effect of regeneration temperature and heating rate on heel build-up during microwave regeneration. *In Proceedings of the American Institute of Chemical Engineers' Annual Meeting*, Salt Lake City, UT, 2015b.
- Ferro-Garcia, M.A.; Utrera-Hidalgo, E.; Rivera-Utrilla, J.; Moreno-Castilla, C.; Joly, J.P. Regeneration of activated carbons exhausted with chlorophenols. *Carbon* **1993**, *31*, 857–863.
- Ferro-Garcia, M.A.; Joly, J.P.; Rivera-Utrilla, J.; Moreno-Castilla, C. Thermal desorption of chlorophenols from activated carbons with different porosity. *Langmuir* **1995**, *11*, 2648–2651.
- Ferro-Garcia, M. A.; Rivera-Utrilla, J.; Bautista-Toledo, I.; Moreno-Castilla, C., Chemical and thermal regeneration of an activated carbon saturated with chlorophenols. *J. Chem. Technol. Biotechnol.* **1996**, *67*, 183–189.
- Foo, K.Y.; Hameed, B.H. Insights into the modeling of adsorption isotherm systems. *Chem. Eng. J.* **2010**, *156*, 2–10.
- Franz, M.; Arafat, H.A.; Pinto, N.G. Effect of chemical surface heterogeneity on the adsorption mechanism of dissolved aromatics on activated carbon. *Carbon* **2000**, *38*, 1807–1819.
- Freundlich, H.M.F. Over the adsorption in solution. *J. Phys. Chem.* **1906**, *57*, 385–471.
- Fuentes, A.B.; Marban, G.; Nevskaja, D.M. Adsorption of volatile organic compounds by means of activated carbon fiber-based monoliths. *Carbon* **2003**, *41*, 87–96.
- Garcia-Araya, J.F.; Beltran, F.J.; Alvarez, P.A.; Masa, F.J. Activated carbon adsorption of some phenolic compounds present in agroindustrial wastewater. *Adsorption* **2003**, *9*, 107–115.
- Garner, I.A.; Watson-Craik, I.A.; Kirkwood, R.; Senior, E. Dual solute adsorption of 2,4,6-trichlorophenol and N-(2-(2,4,6-trichlorophenoxy) propyl) amine on to activated carbon. *J. Chem. Technol. Biotechnol.* **2001**, *76*, 932–940.
- Golovoy, A.; Braslaw, J. Adsorption of automotive paint solvents on activated carbon: Equilibrium adsorption of single vapors. *Air Pollution Control Assoc.* **1981**, *31*, 861–865.

- Goto, M.; Hayaeh, N.; Goto, S. Adsorption and desorption of phenol on anion-exchange resin and activated carbon. *Environ. Sci. Technol.* **1986**, *20*, 463–467.
- Grant, T.M.; King, C.J. Mechanism of irreversible adsorption of phenolic compounds by activated carbons. *Ind. Eng. Chem. Res.* **1990**, *29*, 264–271.
- Gregg, S.J.; Sing, K.S.W. *Adsorption, Surface Area, and Porosity*; Academic Press: London, U.K., 1982.
- Guo, G.Q.; Chen, H.; Long, Y.C. Separation of p-xylene from C-8 aromatics on binder-free hydrophobic adsorbent of MFI zeolite. I. Studies on static equilibrium. *Micropor. Mesopor. Mater.* **2000**, *39*, 149–161.
- Gupta, V. K.; Verma, N. Removal of volatile organic compounds by cryogenic condensation followed by adsorption. *Chem. Eng. Sci.* **2002**, *57*, 2679–96.
- Ha, S.R.; Vinitnantharat, S. Competitive removal of phenol and 2, 4-dichlorophenol in biological activated carbon system. *Environ. Technol.* **2000**, *21*, 387–396.
- Haghseresht, F.; Lu, G. Adsorption characteristics of phenolic compounds onto coal-reject-derived adsorbents. *Energ. Fuel.* **1998**, *12*, 1100–1107.
- Hashisho, Z.; Rood, M.J.; Botich, L. Microwave-swing adsorption to capture and recover vapors from air streams with activated carbon fiber cloth. *Environ. Sci. Technol.* **2005**, *39*, 6851–6859.
- Hashisho, Z.; Emamipour, H.; Cevallos D.; Rood, M.J.; Hay, K.J.; Kim, B.J. Rapid response concentration-controlled desorption of activated carbon to dampen concentration fluctuations. *Environ. Sci. Technol.* **2007**, *41*, 1753–1758.
- Hashisho, Z.; Emamipour, H.; Rood, M.J.; Hay, K.J.; Kim, B.J.; Thurston, D. Concomitant adsorption and desorption of organic vapor in dry and humid air streams using microwave and direct electrothermal swing adsorption. *Environ. Sci. Technol.* **2008**, *42*, 9317–9322.
- Hashisho, Z.; Rood, M.J.; Barot, S.; Bernhard, J. Role of functional groups on the microwave attenuation and electric resistivity of activated carbon fiber cloth. *Carbon* **2009**, *47*, 1814–1823.
- Henning, K.D.; Bongartz, W.; Degel, J. Adsorptive recovery of problematic solvents. *In proceedings of Biennial Conference on Carbon*, Pennsylvania State University, USA, 1989.

- Humayun, R.; Karakas, G.; Dahlstrom, P.R.; Ozkan, U.S.; Tomasko, D.L. Supercritical fluid extraction and temperature-programmed desorption of phenol and its oxidative coupling products from activated carbon. *Ind. Eng. Chem. Res.* **1998**, *37*, 3089–3097.
- Hung, H.; Lin, T. Prediction of the adsorption capacity for volatile organic compounds onto activated carbons by the Dubinin–Radushkevich–Langmuir model. *J. Air Waste Manage. Assoc.* **2007**, *57*, 497–506.
- Hung, C.; Bai, H. Adsorption behaviors of organic vapors using mesoporous silica particles made by evaporation induced self-assembly method. *Chem. Eng. Sci.* **2008**, *63*, 1997–2005.
- Hunter, P.; and Oyama, S.T. *Control of Volatile Organic Compound Emissions: Conventional and Emerging Technologies*; John Wiley: New York, USA, 2002.
- Hutson, N.D.; Yang, R.T. Theoretical basis for the Dubinin-Radushkevitch (D-R) adsorption isotherm equation. *Adsorption* **1997**, *3*, 189–195.
- Jahandar Lashaki, M.; Fayaz, M.; Wang, H.; Hashisho, Z.; Phillips, J.H.; Anderson, J.E.; Nichols, M. Effect of adsorption and regeneration temperature on irreversible adsorption of organic vapors on beaded activated carbon. *Environ. Sci. Technol.* **2012a**, *46*, 4083–4090.
- Jahandar Lashaki, M.; Fayaz, M.; Niknaddaf, S.; Hashisho, Z. Effect of the adsorbate kinetic diameter on the accuracy of the Dubinin-Radushkevich equation for modeling adsorption of organic vapors on activated carbon. *J. Hazard. Mater.* **2012b**, *241–242*, 154–163.
- Jahandar Lashaki, M.; Fayaz, M.; Wang, H.; Hashisho, Z.; Phillips, J.H.; Anderson, J.E.; Nichols, M. Effect of adsorption and regeneration temperature on the irreversible adsorption of a mixture of organic vapors. *In proceedings of 105th Air and Waste Management Association's Annual Conference and Exhibition*, San Antonio, TX, 2012c.
- Jahandar Lashaki, Niknaddaf, S.; Fayaz, M.; Hashisho, Z. The accuracy of the Dubinin-Radushkevich equation for modeling adsorption of organic vapors on activated carbon: Effect of the adsorbate kinetic diameter. *In proceedings of 106th Air and Waste Management Association's Annual Conference and Exhibition*, Chicago, IL, 2013a.
- Jahandar Lashaki, M.; Shariaty, P.; Kamravaei, S.; Fayaz, M.; Hashisho, Z.; Phillips, J.H.; Anderson, J.E.; Nichols, M. Effect of adsorption carrier gas on the irreversible adsorption

- of a mixture of organic vapors. *In proceedings of 106th Air and Waste Management Association's Annual Conference and Exhibition*, Chicago, IL, 2013b.
- Jahandar Lashaki, M.; Atkinson, J.D.; Hashisho, Z.; Phillips, J.H.; Anderson, J.E.; Nichols, M. Effect of surface oxygen groups on the irreversible adsorption of organic vapors. *In proceedings of 107th Air and Waste Management Association's Annual Conference and Exhibition*, Long Beach, CA, 2014.
- Jahandar Lashaki, M.; Atkinson, J.D.; Hashisho, Z.; Phillips, J.H.; Anderson, J.E.; Nichols, M. Misovski, T. Effect of desorption purge gas impurities on irreversible adsorption of organic vapors. *In proceedings of the American Institute of Chemical Engineers' Annual Meeting*, Salt Lake City, UT, 2015a.
- Jahandar Lashaki, M.; Atkinson, J.D.; Hashisho, Z.; Phillips, J.H.; Anderson, J.E.; Nichols, M. The impact of activated carbon's pore size distribution on heel formation during adsorption of organic vapors. *In proceedings of the American Institute of Chemical Engineers' Annual Meeting*, Salt Lake City, UT, 2015b.
- Jahandar Lashaki, M.; Atkinson, J.D.; Hashisho, Z.; Phillips, J.H.; Anderson, J.E.; Nichols, M.; Misovski, T. Effect of desorption purge gas oxygen impurity on irreversible adsorption of organic vapors. *Carbon* **2015**, doi:10.1016/j.carbon.2015.12.037.
- Jelinek, L.; Kovats, E.S. True surface areas from nitrogen adsorption experiments. *Langmuir* **1994**, *10*, 4225–4231.
- Jiun-Horng, T.; Hsiu-Mei, C.; Guan-Yinag, H.; Hung-Lung, C. Adsorption characteristics of acetone, chloroform and acetonitrile on sludge-derived adsorbent, commercial granular activated carbon and activated carbon fibers. *J. Hazard. Mater.* **2008**, *154*, 1183–1191.
- Johnsen, D.L.; Mallouk, K.E.; Rood, M.J. Control of electrothermal heating during regeneration of activated carbon fiber cloth. *Environ. Sci. Technol.* **2011**, *45*, 738–743.
- Jones, D.P. *Biomedical Sensors*; Momentum Press: New York, 2010.
- Kampa, M.; Castanas, E. Human health effects of air pollution. *Environ. Pollut.* **2008**, *151*, 362–367.
- Karsli, H.; Culfaz, A.; Yucel, H. Sorption properties of synthetic ferrierite. *Chem. Eng. Comm.* **2003**, *190*, 693–704.

- Kawasaki, N.; Kinoshita, H.; Oue, T.; Nakamura, T.; Tanada, S. Study on adsorption kinetic of aromatic hydrocarbons onto activated carbon in gaseous flow method. *J. Colloid Interface Sci.* **2004**, *275*, 40–43.
- Khan, F.I.; Ghoshal, A.K. Removal of volatile organic compounds from polluted air. *J. Loss Prev. Process Ind.* **2000**, *13*, 527–545.
- Kilduff, J.E.; King, C.J. Effect of carbon adsorbent surface properties on the uptake and solvent regeneration of phenol. *Ind. Eng. Chem. Res.* **1997**, *36*, 1603–1613.
- Kim, K.J.; Kang, C.S.; You, Y.J.; Chung, M.C.; Jeong, S.W.; Jeong, W.J.; Woo, M.W.; Ahn, H.G. Adsorption-desorption characteristics of modified activated carbons for volatile organic compounds. *Stud. Surf. Sci. Catal.* **2006**, *159*, 457–460.
- Kim, B.R. VOC emissions from automotive painting and their control: A review. *Environ. Eng. Res.* **2011**, *16*, 1–9.
- Knovel Critical Tables (2nd Edition). (2008);
http://www.knovel.com/web/portal/browse/display?_EXT_KNOVEL_DISPLAY_bookid=761&VerticalID=0
- Koh, M.; Nakajima, T.; Adsorption of aromatic compounds on C_xN-coated activated Carbon. *Carbon* **2000**, *38*, 1947–1954.
- Kotdawala, R.R.; Kazantzis, N.; Thompson, R.W. Molecular simulation studies of adsorption of hydrogen cyanide and methyl ethyl ketone on zeolite NaX and activated carbon. *J. Hazard. Mater.* **2008**, *159*, 169–176.
- Kureha Corporation Website; <http://www.kureha.com/pdfs/Kureha-BAC-Bead-Activated-Carbon.pdf>.
- Langmuir, I. The constitution and fundamental properties of solids and liquids. *J. Am. Chem. Soc.* **1916**, *38*, 2221–2295.
- Langmuir, I. The Adsorption of gases on plane surfaces of glass, mica, and platinum. *J. Am. Chem. Soc.* **1918**, *40*, 1361–1403.
- Lapkin, A.; Joyce, L.; and Crittenden, B. Framework for evaluating the “Greenness” of chemical processes: Case studies for a novel VOC recovery technology. *Environ. Sci. Technol.* **2004**, *38*, 5815–5823.

- Lee, J.Y.; Yun, T.S.; Santamarina, J.C.; Ruppel, C. Observations related to tetrahydrofuran and methane hydrates for laboratory studies of hydrate-bearing sediments. *Geochem. Geophys. Geosyst.* **2007**, *8*, Q06003, doi:10.1029/2006GC001531.
- Leethochawalit, M.; Bustard, M.T.; Wright, P.C.; Meeyoo, V. Novel vapor-phase biofiltration and catalytic combustion of volatile organic compounds. *Ind. Eng. Chem. Res.*, **2001**, *40*, 5334–5341.
- Leng, C.C.; Pinto, N.G. Effects of surface properties of activated carbons on adsorption behavior of selected aromatics. *Carbon* **1997**, *35*, 1375–1385.
- Leslie, G.B. Health risks from indoor air pollutants: Public alarm and toxicological reality. *Indoor Built Environ.* **2000**, *9*, 5–16.
- Li, P.; Xiu, G.H.; Jiang, L. Adsorption and desorption of phenol on activated carbon fibers in a fixed bed. *Sep. Sci. Technol.* **2001**, *36*, 2147–2163.
- Li, C.; Moe, W.M. Activated carbon load equalization of discontinuously generated acetone and toluene mixtures treated by biofiltration. *Environ. Sci. Technol.* **2005**, *39*, 2349–2356.
- Li, L.; Liu, S.; Liu, J. Surface modification of coconut shell based activated carbon for the improvement of hydrophobic VOC removal. *J. Hazard. Mater.* **2011**, *192*, 683–690.
- Lillo-Rodenas, M.A.; Cazorla-Amoros, D.; Linares-Solano, A. Behaviour of activated carbons with different pore size distributions and oxygen groups for benzene and toluene adsorption at low concentrations. *Carbon* **2005**, *43*, 1758–1767.
- Liu, P.K.T.; Feltch, S.M.; Wagner, N.J. Thermal desorption behavior of aliphatic and aromatic hydrocarbons loaded on activated carbon. *Ind. Eng. Chem. Res.* **1987**, *26*, 1540–1545.
- Liu, W.; Vidic, R.D. Optimization of sulfur impregnation protocol for fixed-bed application of activated carbon-based sorbents for gas-phase mercury removal. *Environ. Sci. Technol.* **1998**, *32*, 531–538.
- Liu, P.K.T.; Feltch, S.M.F.; Merchan, M.D. Regeneration of ortho-chlorophenol-exhausted activated carbons with liquid water at high pressure and temperature. *Water Res.* **2003**, *37*, 1905–1911.
- Long, C.; Lu, J. D.; Li, A.; Hu, D.; Liu, F.; Zhang, Q. Adsorption of naphthalene onto the carbon adsorbent from waste ion exchange resin: Equilibrium and kinetic characteristics. *J. Hazard. Mater.* **2008**, *150*, 656–661.

- Long, C.; Li, Y.; Yu, W.; Li, A. Removal of benzene and methyl ethyl ketone vapor: Comparison of hypercrosslinked polymeric adsorbent with activated carbon. *J. Hazard. Mater.* **2012**, 203–204, 251–256.
- Lowell, S.; Shields, J.E. *Powder Surface Area and Porosity*; Chapman & Hall: London, New York, USA, 1991.
- Lu, Q.; Sorial, G.A. The role of adsorbent pore size distribution in multicomponent adsorption on activated carbon. *Carbon* **2004a**, 42, 3133–3142.
- Lu, Q.; Sorial, G.A. Adsorption of phenolics on activated carbon- impact of pore size and molecular oxygen. *Chemosphere* **2004b**, 55, 671–679.
- Lu, Q.; Sorial, G.A. Impact of pore size on competitive adsorption of phenolic compounds. *Water Sci. Technol.* **2004c**, 4, 1–7.
- Lu, Q.; Sorial, G.A. The effect of functional groups on oligomerization of phenolics on activated carbon. *J. Hazard. Mater.* **2007**, 148, 436–445.
- Lu, Q.; Sorial, G.A. A comparative study of multicomponent adsorption of phenolic compounds on GAC and ACFC. *J. Hazard. Mater.* **2009**, 167, 89–96.
- Lukomskaya, A.Y.; Tarkovskaya, I.A.; Strelko, V.V. Chemisorption of o-xylene on activated carbons. *Theor. Exp. Chem.* **1986**, 22, 357–360.
- Magalhaes, F.D.; Laurence, R.L.; Conner, W.C. Diffusion of cyclohexane and alkylcyclohexanes in silicalite. *J. Phys. Chem. B* **1998**, 102, 2317–2324.
- Mahajan, O. P.; Moreno-Castilla, C.; Walker Jr., P.L. Surface-treated activated carbon for removal of phenol from water. *Sep. Sci. Technol.* **1980**, 15, 1733–1752.
- Magne, P.; Walker Jr., P.L. Phenol adsorption on activated carbons: application to the regeneration of activated carbons polluted with phenol. *Carbon* **1986**, 24, 101–107.
- Mallouk, K.E.; Johnsen, D.L.; Rood, M.J. Capture and recovery of isobutane by electrothermal swing adsorption with post-desorption liquefaction. *Environ. Sci. Technol.* **2010**, 44, 7070–7075.
- Maroto-Valer, M.M.; Dranca, I.; Clifford, D.; Lupascu, T.; Nastas, R.; Leon y Leon, C.A. Thermal regeneration of activated carbons saturated with ortho- and meta-chlorophenols. *Thermochimica Acta* **2006**, 444, 148–156.
- Matatov-Meytal, Y.I.; Sheintuch, M. Abatement of pollutants by adsorption and oxidative catalytic regeneration. *Ind. Eng. Chem. Res.* **1997**, 36, 4374–4380.

- Matatov-Meytal, Y.I.; Sheintuch, M. Catalytic abatement of water pollutants. *Ind. Eng. Chem. Res.* **1998**, *37*, 309–326.
- Mattson, J.S.; Mark, H.B.; Malbin, M.D.; Weber, W.J.; Crittenden, J.C. Surface chemistry of active carbon. Specific adsorption of phenols. *J. Colloid Interface Sci.* **1969**, *31*, 116–130.
- Menendez, J.A.; Phillips, J.; Xia, B.; Radovic, L.R. On the modification and characterization of chemical surface properties of activated carbon: In the search of carbons with stable basic properties. *Langmuir* **1996**, *12*, 4404–4410.
- Monneyron, P.; Manero, M.H.; Foussard, J.N. Measurement and modeling of single- and multi-component adsorption equilibria of VOC on high-silica zeolites. *Environ. Sci. Technol.* **2003**, *37*, 2410–2414.
- Moreno-Castilla, C.; Rivera-Utrilla, J.; Joly, J.P.; Lopez-Ramon, M.V.; Ferro-Garcia, M.A.; Carrasco-Marin, F. Thermal regeneration of an activated carbon exhausted with different substituted phenols. *Carbon* **1995**, *33*, 1417–1423.
- Moreno-Castilla C.; Carrasco-Marin F.; Mueden A. The creation of acid carbon surfaces by treatment with $(\text{NH}_4)_2\text{S}_2\text{O}_8$. *Carbon* **1997**, *35*, 1619–1626.
- Nakhla, G.F.; Abuzaid, N.; Farooq, S.; Ala'ama, S. Oxygen-induced enhancement of the adsorptive capacity of activated charcoal. *Environ. Technol.* **1992**, *13*, 181–188.
- Nakhla, G.; Abuzaid, N.; Farooq, S. Activated carbon adsorption of phenolics in oxic systems: Effect of pH and temperature variations. *Water Environ. Res.* **1994**, *66*, 842–850.
- Nevskaia, D.M.; Santianes, A.; Munoz, V.; Guerrero-Ruiz, A. Interaction of aqueous solutions of phenol with commercial activated carbons: an adsorption and kinetic study. *Carbon* **1999**, *37*, 1065–1074.
- Niknaddaf, S.; Jahandar Lashaki, M.; Shariaty, P.; Hashisho, Z.; Phillips, J.H.; Anderson, J.E.; Nichols, M. Effect of pore size distribution of activated carbon fiber cloth on irreversible adsorption of organic vapors. In *proceedings of 107th Air and Waste Management Association's Annual Conference and Exhibition*, Long Beach, CA, 2014.
- Niknaddaf, S.; Atkinson, J.D.; Shariaty, P.; Jahandar Lashaki, M.; Hashisho, Z.; Phillips, J.H.; Anderson, J.E.; Nichols, M. Heel formation during volatile organic compound desorption from activated carbon fiber cloth. *Carbon* **2016**, *96*, 131–138.

- Nirmalakhandan, N.N.; Speece, R.E. Prediction of activated carbon adsorption capacities for organic vapors using quantitative structure-activity relationship methods. *Environ. Sci. Technol.* **1983**, *27*, 1512–1516.
- Noll, K.E.; Wang, D.; Shen, T. Comparison of three methods to predict adsorption isotherms for organic vapors from similar polarity and nonsimilar polarity reference vapors. *Carbon* **1989**, *27*, 239–245.
- Olivier, J.P. Improving the models used for calculating the size distribution of micropore volume of activated carbons from adsorption data. *Carbon* **1998**, *36*, 1469–1472.
- Osei-Twum, E.Y.; Abuzaid, N.S.; Nahkla, G. Carbon-catalyzed oxidative coupling of phenolic compounds. *B. Environ. Contam. Tox.* **1996**, *56*, 513–519.
- Otake, Y.; Jenkins, R.G. Characterization of oxygen-containing surface complexes created on a microporous carbon by air and nitric acid treatment. *Carbon* **1993**, *31*, 109–121.
- Papasavva, S.; Kia, S.; Claya, J.; Gunther, R. Characterization of automotive paints: An environmental impact analysis. *Prog. Org. Coat.* **2001**, *43*, 193–206.
- Park, S.W.; Lee, W.K. Adsorption and desorption of gaseous methyl iodide in a triethylenediamine impregnated activated carbon bed. *Sep. Technol.* **1993**, *3*, 133–142.
- Parmar, G.R.; Rao, N.N. Emerging control technologies for volatile organic compounds. *Cri. Rev. Environ. Sci. Technol.* **2009**, *39*, 41–78.
- Pelekani, C.; Snoeyink, V.L. Competitive adsorption in natural water: Role of activated carbon pore size. *Water Res.* **1999**, *33*, 1209–1219.
- Perrard, A.; Retailleau, L.; Berjoan, R.; Joly, J.P. Liquid phase oxidation kinetics of an ex-cellulose activated carbon cloth by NaOCl. *Carbon* **2012**, *50*, 2226–2234.
- Popescu, M.; Joly, J. P.; Carre, J.; Danatoiu, C. Dynamical adsorption and temperature-programmed desorption of VOCs (toluene, butyl acetate and butanol) on activated carbons. *Carbon* **2003**, *41*, 739–748.
- Qi, S.; Hay, K.J.; Rood, M.J.; Cal, M.P. Carbon fiber adsorption using quantitative structure-activity relationship. *J. Environ. Eng.* **2000**, *126*, 865–868.
- Qiao, W.M.; Korai, Y.; Mochida, I.; Hori, Y.; Maeda, T. Preparation of an activated carbon artifact: Oxidative modification of coconut shell-based carbon to improve the strength. *Carbon* **2002**, *40*, 351–358.

- Qin, W.; Xiao-yi, L.; Rui, Z.; Chao-jun, L.; Xiao-jun, L.; Wen-ming, Q.; Liang, Z.; Li-cheng, L. Preparation of polystyrene-based activated carbon spheres and their adsorption of dibenzothiophene. *New Carbon Mater.* **2009**, *24*, 55–60.
- Quantachrome Autosorb 1 Operating Manual; **2006**.
- Radovic, L.R.; Moreno-Castilla, C.; Rivera-Utrilla, J. Carbon materials as adsorbents in aqueous solutions. *Chem. Phys. Carbon* **2001**, *27*, 227–405.
- Ramirez, D.; Sullivan, P.D.; Rood, M.J.; Hay, K.J. Equilibrium adsorption of phenol-, tire-, and coal-derived activated carbons for organic vapors. *J. Environ. Eng.* **2004**, *130*, 231–241.
- Ramirez, D.; Qi, S.Y.; Rood, M.J. Equilibrium and heat of adsorption for organic vapors and activated carbons. *Environ. Sci. Technol.* **2005**, *39*, 5864–5871.
- Ramos, M.E.; Bonelli, P.R.; Cukierman, A.L.; Ribeiro Carrott, M.M.L.; Carrott, P.J.M. Adsorption of volatile organic compounds onto activated carbon cloths derived from a novel regenerated cellulosic precursor. *J. Hazard. Mater.* **2010**, *177*, 175–182.
- Ravi, V.P.; Jasra, R.V.; Bhat, T.S.G. Adsorption of phenol, cresol isomers and benzyl alcohol from aqueous solution on activated carbon at 278, 298 and 323 K. *J. Chem. Technol. Biotechnol.* **1998**, *71*, 173–179.
- Reucroft, P.J.; Simpson, W.H.; Jonas, L.A. Sorption properties of activated carbon. *J. Phys. Chem.* **1971**, *75*, 3526–3531.
- Rivera-Utrilla, J.; Ferro-Garcia, M.A.; Bautista-Toledo, I.; Sanchez-Jimenez, C.; Salvador, F.; Merchan, M.D. Regeneration of ortho-chlorophenol-exhausted activated carbons with liquid water at high pressure and temperature. *Water Res.* **2003**, *37*, 1905–1911.
- Rivera-Utrilla, J.; Sanchez-Polo, M.; Gomez-Serrano, V.; Alvarez, P.M. Alvim-Ferraz, M.C.M.; Dias, J.M. Activated carbon modifications to enhance its water treatment applications: An overview. *J. Hazard. Mater.* **2011**, *187*, 1–23.
- Ruthven, D.M. *Principles of Adsorption Processes*; John Wiley: New York, NY, USA, 1984.
- Salvador, F.; Merchan, M.D. Study of the desorption of phenol and phenolic compounds from activated carbon by liquid-phase temperature-programmed desorption. *Carbon* **1996**, *34*, 1543–1551.
- Salvador, F.; Martin-Sanchez, N.; Sanchez-Hernandez, R.; Sanchez-Montero, M.J.; Izquierdo, C. Regeneration of carbonaceous adsorbents. Part I: Thermal regeneration. *Micropor. Mesopor. Mat.* **2015**, *202*, 259–276.

- Schnelle, K.B.; Brown, C.A. *Air Pollution Control Technology Handbook*; CRC Press: Florida, USA, 2002.
- Sheintuch, M.; Matatov-Meytal, Y.I. Comparison of catalytic processes with other regeneration methods of activated carbon. *Catal. Today* **1999**, *53*, 73–80.
- Shonnard, D.R.; Hiew, D.S. Comparative environmental assessments of VOC recovery and recycle design alternatives for a gaseous waste stream. *Environ. Sci. Technol.* **2000**, *34*, 5222–5228.
- Sorial, G.A.; Suidan, M.T.; Vidic, R.D.; Brenner, R.C. Effect of GAC characteristics on adsorption of organic pollutants. *Water Environ. Res.* **1993**, *65*, 53–57.
- Soto, M.L.; Moure, A.; Dominguez, H.; Parajo, J.C. Recovery, concentration and purification of phenolic compounds by adsorption: A review. *J. Food Eng.* **2011**, *105*, 1–27.
- Stavropoulos, G.G.; Samaras, P.; Sakellariopoulos, G.P. Effect of activated carbons modification on porosity, surface structure and phenol adsorption. *J. Hazard. Mater.* **2008**, *151*, 414–421.
- Sullivan, P.D.; Rood, M.J.; Grevillot, G.; Wander, J.D.; Hay, K.J. Activated carbon fiber cloth electrothermal swing adsorption system. *Environ. Sci. Technol.* **2004**, *38*, 4865–4877.
- Sullivan, P.D.; Stone, B.R.; Hashisho, Z.; Rood, M.J. Water adsorption with hysteresis effect onto microporous activated carbon fabrics. *Adsorption* **2007**, *13*, 173–189.
- Suzuki, M.; Misic, D.M.; Koyama, O.; Kawazoe, K. Study of thermal regeneration of spent activated carbons: thermogravimetric measurement of various single component organics loaded on activated carbons. *Chem. Eng. Sci.* **1978**, *33*, 271–279.
- Tamon, H.; Saito, T.; Kishimura, M.; Okazaki, M.; Toei, R. Solvent regeneration of spent activated carbon in wastewater treatment. *J. Chem. Eng. Japan* **1990**, *23*, 426–432.
- Tamon, H.; Atsushi, M.; Okazaki, M. On irreversible adsorption of electron-donating compounds in aqueous solution. *J. Colloid Interface Sci.* **1996**, *177*, 384–390.
- Tamon, H.; Okazaki, M. Desorption characteristics of aromatic compounds in aqueous solution on solid adsorbents. *J. Colloid Interface Sci.* **1996**, *179*, 181–187.
- Tanthapanichakoon, W.; Ariyadejwanich, P.; Japthong, P.; Nakagawa, K.; Mukai, S.R.; Tamon, H. Adsorption-desorption characteristics of phenol and reactive dyes from aqueous solution on mesoporous activated carbon prepared from waste tires. *Water Res.* **2005**, *39*, 1347–1353.

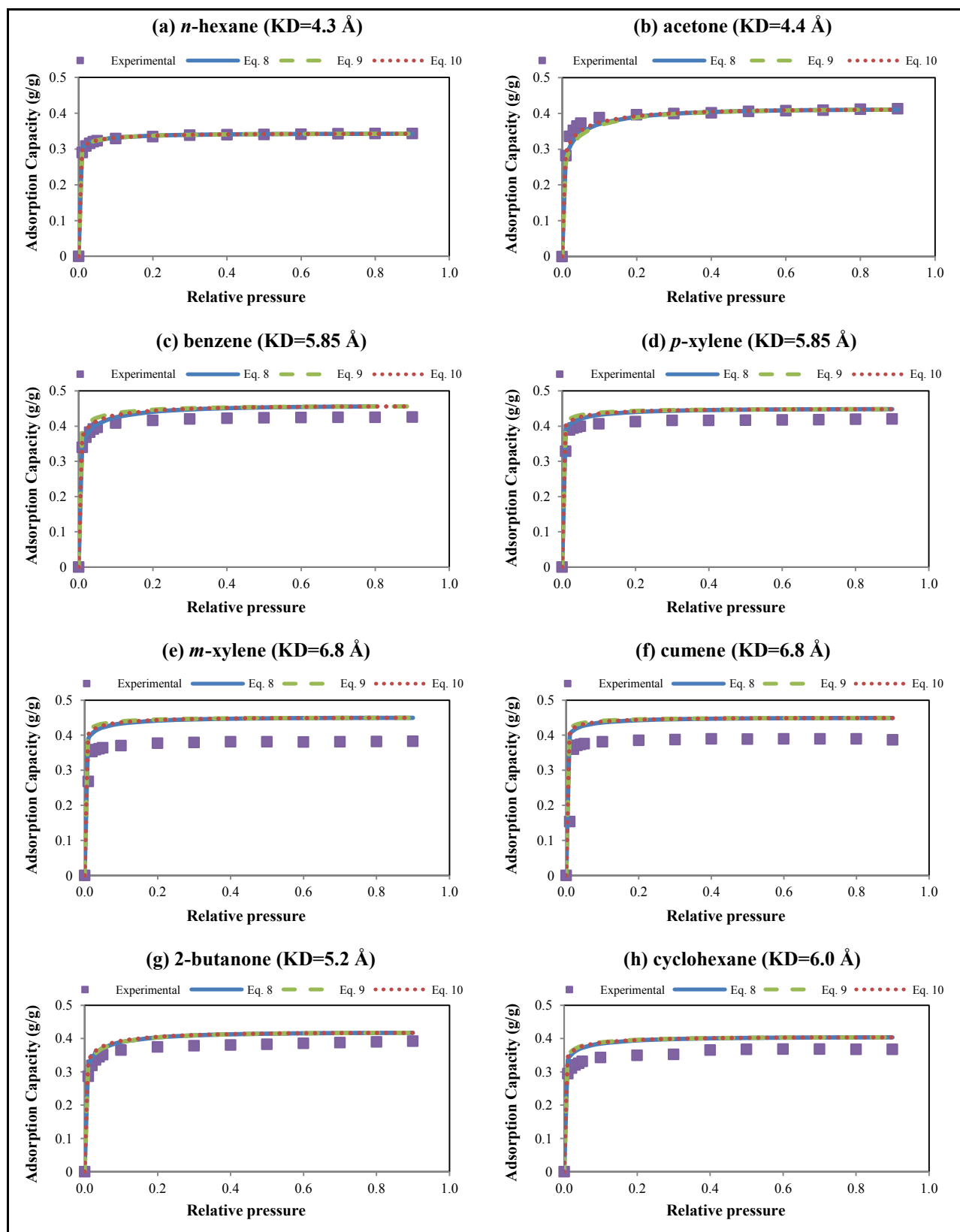
- Tefera, D.T.; Jahandar Lashaki, M.; Fayaz, M.; Hashisho, Z.; Phillips, J.H.; Anderson, J.E.; Nichols, M. Two-dimensional modelling of temperature swing adsorption of volatile organic compounds using beaded activated carbon. *Environ. Sci. Technol.* **2013a**, *47*, 11700–11710.
- Tefera, D.T.; Jahandar Lashaki, M.; Fayaz, M.; Hashisho, Z.; Phillips, J.H.; Anderson, J.E.; Nichols, M. Two-dimensional modelling of temperature swing adsorption of volatile organic compounds using beaded activated carbon. *In proceedings of 106th Air and Waste Management Association's Annual Conference and Exhibition*, Chicago, IL, 2013b.
- Tefera, D.T.; Hashisho, Z.; Phillips, J.H.; Anderson, J.E.; Nichols, M. Modeling competitive adsorption of mixtures of volatile organic compounds in a fixed-bed of beaded activated carbon. *Environ. Sci. Technol.* **2014**, *48*, 5108–5117.
- Terzyk, A.P. Further insights into the role of carbon surface functionalities in the mechanism of phenol adsorption. *J. Colloid Interface Sci.* **2003**, *268*, 301–329.
- Terzyk, A.P. The impact of carbon surface chemical composition on the adsorption of phenol determined at the real oxic and anoxic conditions. *Appl. Surf. Sci.* **2007**, *253*, 5752–5755.
- Terzyk, A.P.; Wisniewski, M.; Gauden, P.A.; Rychlicki, G.; Furmaniak, S. Carbon surface chemical composition in para-nitrophenol adsorption determined under real oxic and anoxic conditions. *J. Colloid Interface Sci.* **2008**, *320*, 40–51.
- Tessmer, C.H.; Vidic, R.D.; Uranowski, L.J. Impact of oxygen-containing surface functional groups on activated carbon adsorption of phenols. *Environ. Sci. Technol.* **1997**, *31*, 1872–1878.
- Thommes, M.; Guillet-Nicolas, R.; Cychosz, K.A. Physical adsorption characterization of mesoporous zeolites. In *Mesoporous Zeolites: Preparation, Characterization and Applications*; Garica-Martinez, J., Li, K., Eds.; Wiley-VCH Verlag GmbH & Co. KGaA: Weinheim, Germany, 2015; pp 349–383.
- Tobias. H.; Soffer, A. Chemisorption of halogen on carbons—I. Stepwise chlorination and exchange of C-Cl with C-H bonds. *Carbon* **1985**, *23*, 281–289.
- Tuan, V.A.; Li, S.; Falconer, J.L.; Noble, R.D. In situ crystallization of beta zeolite membranes and their permeation and separation properties. *Chem. Mater.* **2002**, *14*, 489–492.

- Tung, C.; Wu, L.; Zhang, L.; Li, H.; Yi, X.; Song, K.; Xu, M.; Yuan, Z.; Guan, J.; Wang, H.; Ying, Y.; Xu, X. Microreactor-controlled selectivity in organic photochemical reactions. *Pure Appl. Chem.* **2000**, *72*, 2289–2298.
- Urano, K.; Omori, S.; Yamamoto, E. Prediction method for adsorption capacities of commercial activated carbons in removal of organic vapors. *Environ. Sci. Technol.* **1982**, *16*, 10–14.
- Uranowski, L.J.; Tessmer, C.H.; Vidic, R.D. The effect of surface metal oxides on activated carbon adsorption of phenolics. *Water Res.* **1998**, *32*, 1841–1851.
- United States Naval Research Laboratory (1984); The reaction of oxygen-nitrogen mixtures with granular activated carbons below the spontaneous ignition temperature; <http://www.dtic.mil/dtic/tr/fulltext/u2/a149041.pdf>.
- US Environmental Protection Agency (2009); Definition of volatile organic compounds (VOC); www.epa.gov/ttn/naaqs/ozone/ozonetech/def_voc.htm.
- Vidic, R.D.; Suidan, M.T.; Traegner, U.K.; Nakhla, G.F. Adsorption isotherms: illusive capacity and role of oxygen. *Water Res.* **1990**, *24*, 1187–1195.
- Vidic, R.D.; Suidan, M.T. Role of dissolved oxygen on the adsorptive capacity of activated carbon for synthetic and natural organic matter. *Environ. Sci. Technol.* **1991**, *25*, 1612–1618.
- Vidic, R.D.; Sorial, G.A.; Papadimas, S.P.; Suidan, M.T.; Speth, T.F. Effect of molecular oxygen on the scale-up of GAC adsorbents. *J. Am. Water Works Assoc.* **1992**, *84*, 98–105.
- Vidic, R.D.; Suidan, M.T.; Brenner, R.C. Oxidative coupling of phenols on activated carbon: impact on adsorption equilibrium. *Environ. Sci. Technol.* **1993**, *27*, 2079–2085.
- Vidic, R.D.; Suidan, M.T.; Brenner, R.C. Impact of oxygen mediated oxidative coupling on adsorption kinetics. *Water Res.* **1994a**, *28*, 263–268.
- Vidic, R.D.; Suidan, M.T.; Sorial, G.A.; Brenner, R.C. Effect of molecular oxygen on adsorptive capacity and extraction efficiency of granulated activated carbon for three ortho-substituted phenols. *J. Hazard. Mater.* **1994b**, *38*, 373–388.
- Vidic, R.D.; Tessmer, C.H.; Uranowski, L.J. Impact of surface properties of activated carbons on oxidative coupling of phenolic compounds. *Carbon* **1997**, *35*, 1349–1359.
- Vinitnantharat, S.; Baral, A.; Ishibashi, Y.; Ha, S.R. Quantitative bioregeneration of granular activated carbon loaded with phenol and 2,4-dichlorophenol. *Environ. Technol.* **2001**, *22*, 339–344.

- Wang, H.; Jahandar Lashaki, M.; Fayaz, M.; Hashisho, Z.; Phillips, J.H.; Anderson, J.E.; Nichols, M. Adsorption and desorption of mixtures of organic vapors on beaded activated carbon. *Environ. Sci. Technol.* **2012**, *46*, 8341–8350.
- Wark, K.; Warner, C.F.; Davis, W.T. *Air Pollution: Its Origin and Control*; Addison-Wesley: 1998.
- Wood, G.O. Activated carbon adsorption capacities for vapors. *Carbon* **1992**, *30*, 593–599.
- Wood, G.O. Affinity coefficients of the Polanyi /Dubinin adsorption isotherm equations: A review with compilations and correlations. *Carbon* **2001**, *39*, 343–356.
- Wood, G.O. Review and comparisons of D/R models of equilibrium adsorption of binary mixtures of organic vapors on activated carbons. *Carbon* **2002**, *40*, 231–239.
- Wu, J.; Stromqvist, E.; Claesson, O.; Fangmark, I.E.; Hammarstrom, L.G. A systematic approach for modeling the affinity coefficient in the Dubinin–Radushkevich equation. *Carbon* **2002**, *40*, 2587–2596.
- Yan, L.; Sorial, G.A. Chemical activation of bituminous coal for hampering oligomerization of organic contaminants. *J. Hazard. Mater.* **2011**, *197*, 311–319.
- Yang, R.T., *Adsorbents: Fundamentals and Application*. John Wiley & Sons, Inc.: Hoboken, NJ, USA, 2003.
- Yang, K.; Sun, Q.; Xue, F.; Liu, D. Adsorption of volatile organic compounds by metal–organic frameworks MIL-101: Influence of molecular size and shape. *J. Hazard. Mater.* **2011**, *195*, 124–131.
- Yao, M.; Zhang, Q.; Hand, D.W.; Perram, D.L. Investigation of the treatability of the primary indoor volatile organic compounds on activated carbon fiber clothes at typical indoor concentrations. *J. Air Waste Manage.* **2009**, *59*, 882–890.
- Yonge, D.R.; Keinath, T.M.; Poznanska, K.; Jiang, Z.P. Single-solute irreversible adsorption on granular activated carbon. *Environ. Sci. Technol.* **1985**, *19*, 690–694.
- Yun, J.H.; Choi, D.K.; Moon, H. Benzene adsorption and hot purge regeneration in activated carbon beds. *Chem. Eng. Sci.* **2000**, *55*, 5857–5872.
- Zerbonia, R.A.; Brockmann, C.M.; Peterson, P.R. Carbon bed fires and the use of carbon canisters for air emissions control on fixed-roof tanks. *J. Air Waste Manage. Assoc.* **2001**, *51*, 1617–1627.

Zhu, D.; Pignatello, J.J. A concentration-dependent multi-term linear free energy relationship for sorption of organic compounds to soils based on the hexadecane dilute-solution reference state. *Environ. Sci. Technol.* **2005**, *39*, 2033–2041.

APPENDIX A: SUPPLEMENTARY DATA FOR CHAPTER 3



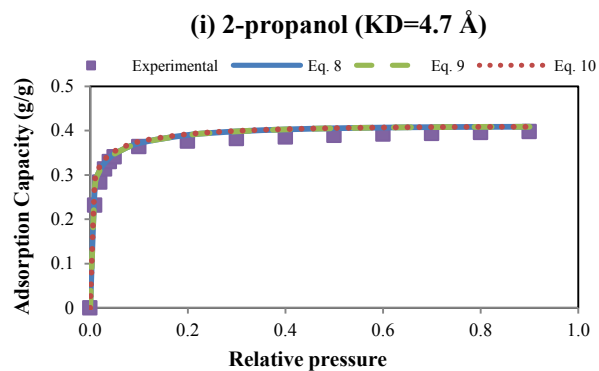
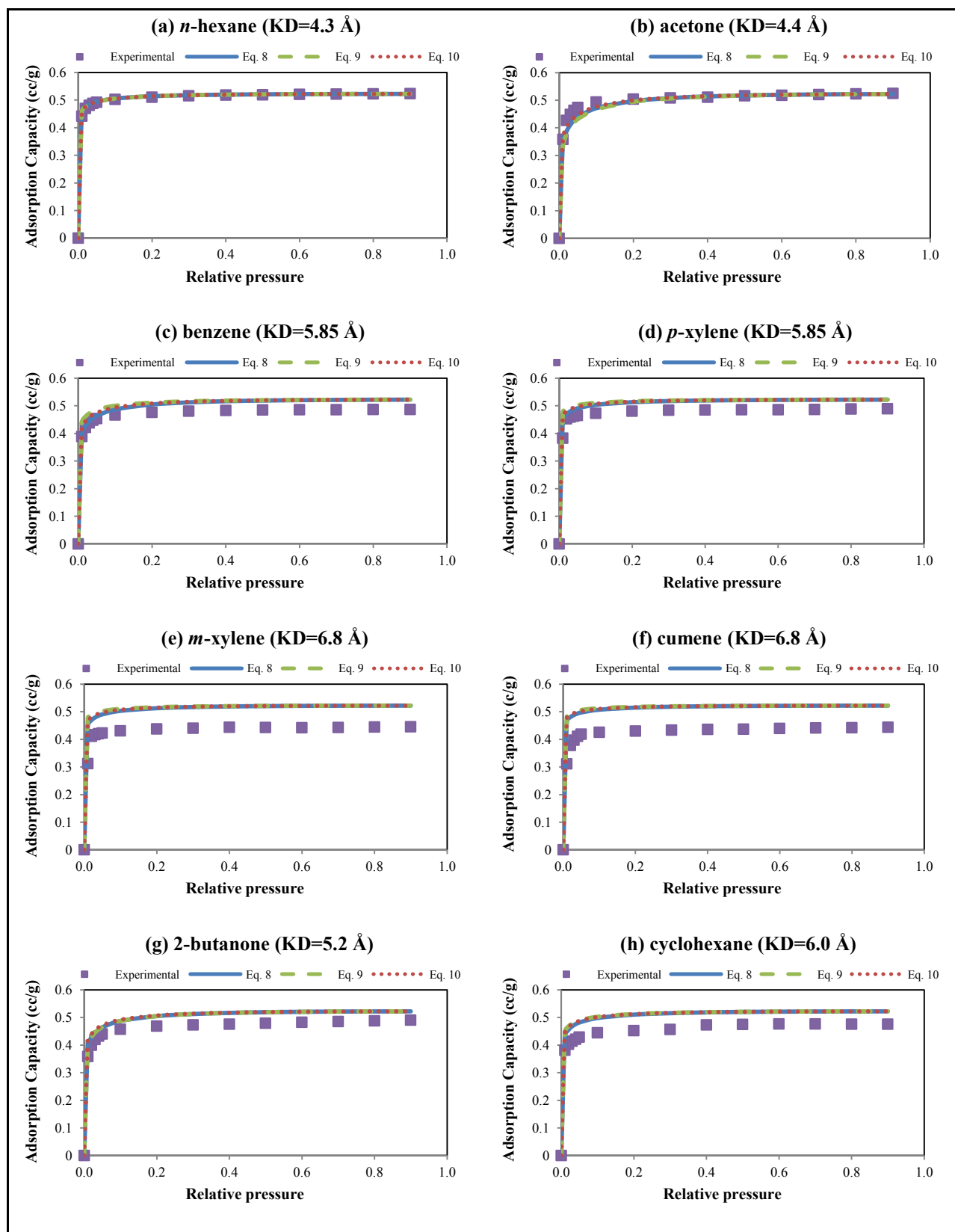


Figure A1. Measured and predicted, gravimetric adsorption isotherms for (a) *n*-hexane, (b) acetone (c) benzene, (d) *p*-xylene, (e) *m*-xylene, (f) cumene, (g) 2-butanone, (h) cyclohexane, and (i) 2-propanol using *n*-hexane (KD=4.3 Å) as reference adsorbate.



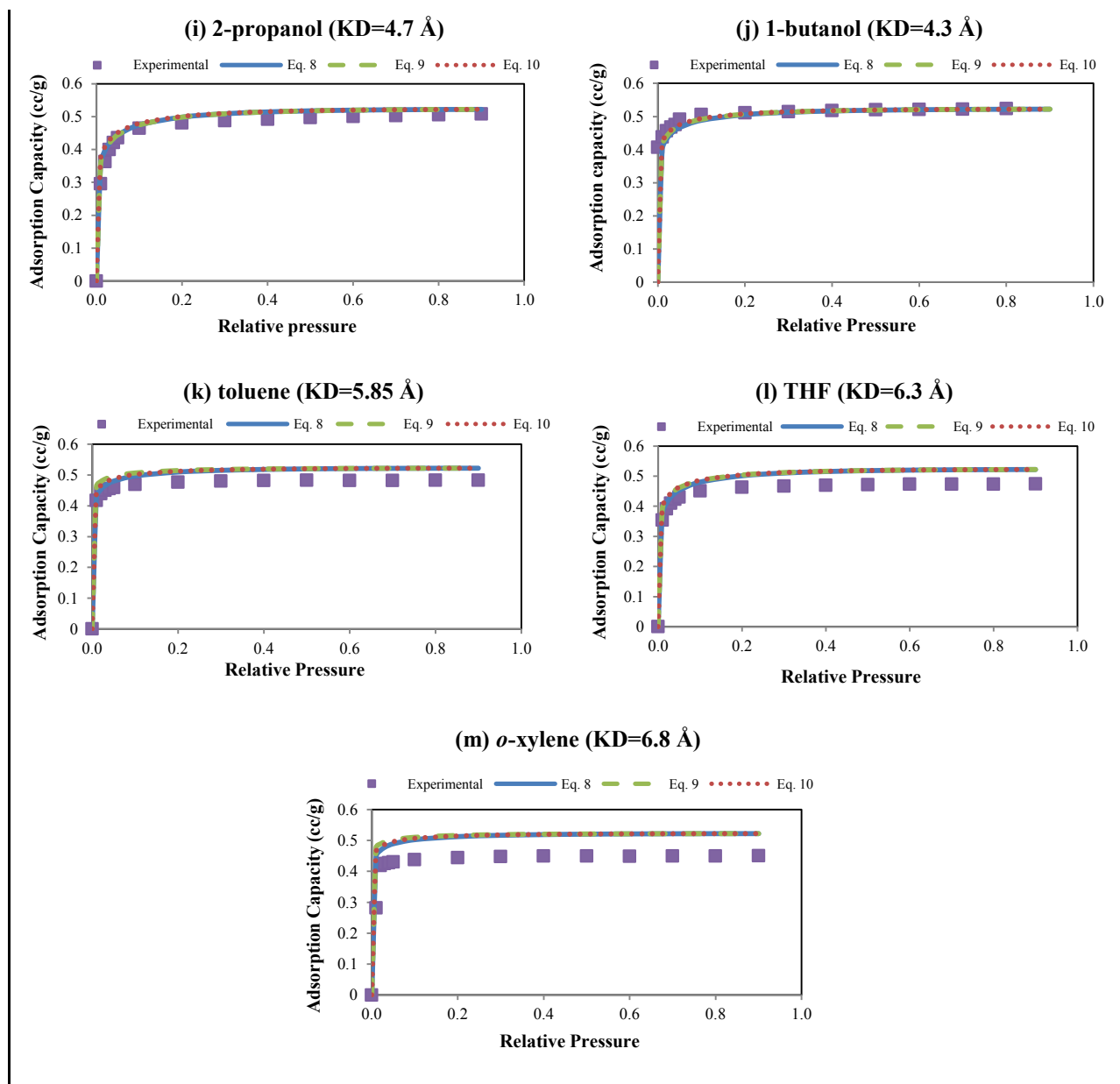
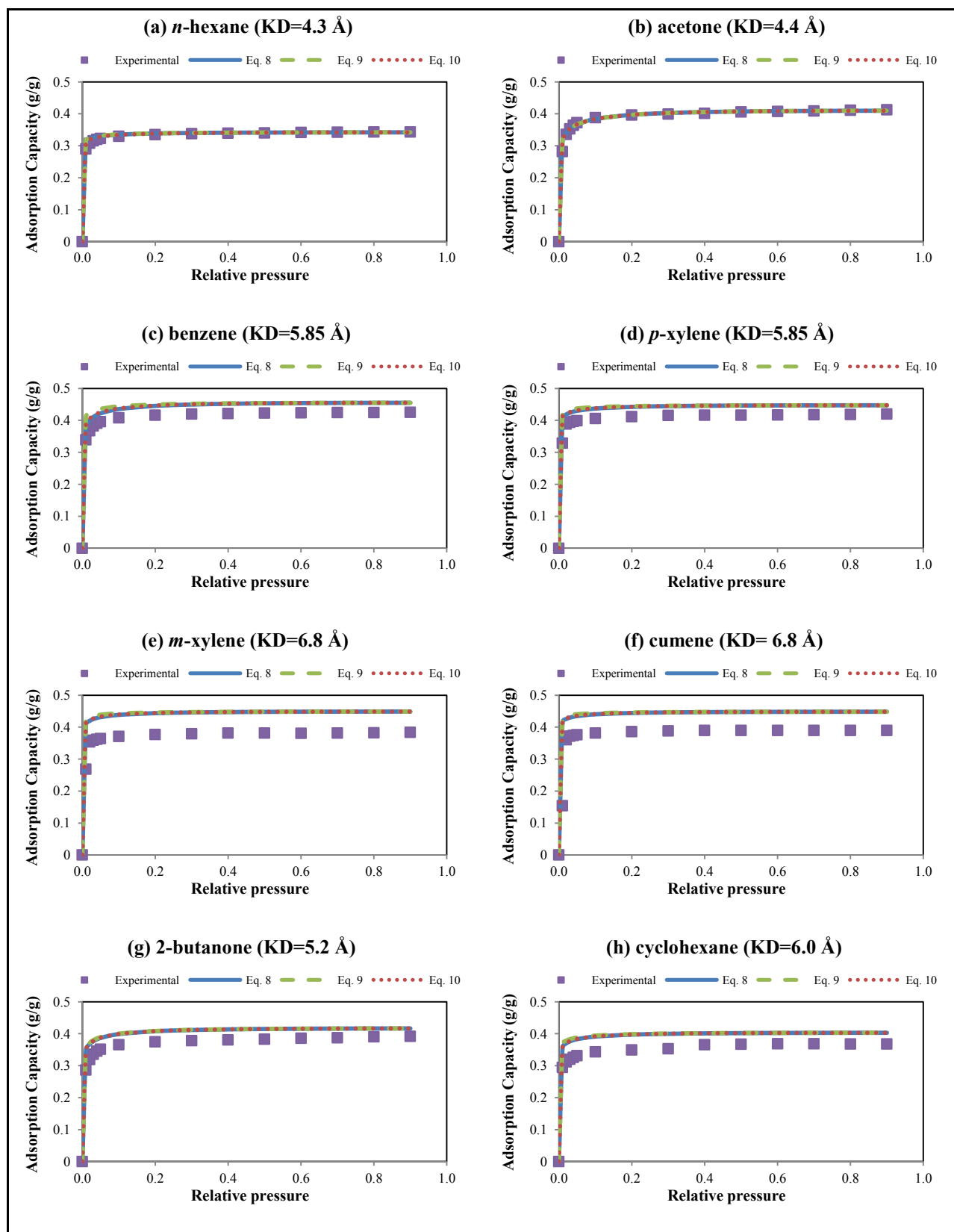


Figure A2. Measured and predicted, volumetric adsorption isotherms for (a) *n*-hexane, (b) acetone (c) benzene, (d) *p*-xylene, (e) *m*-xylene, (f) cumene, (g) 2-butanone, (h) cyclohexane, (i) 2-propanol, (j) 1-butanol, (k) toluene, (l) THF, and (m) *o*-xylene using *n*-hexane (KD=4.3 Å) as reference adsorbate.



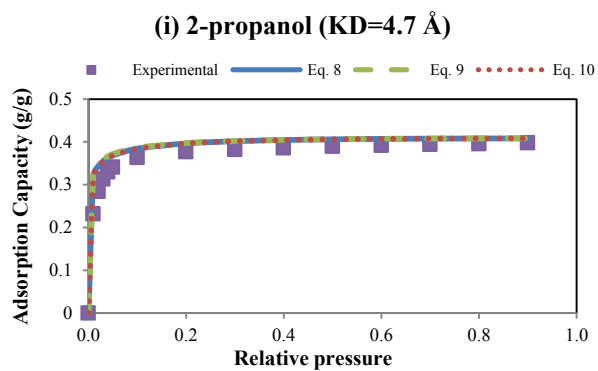
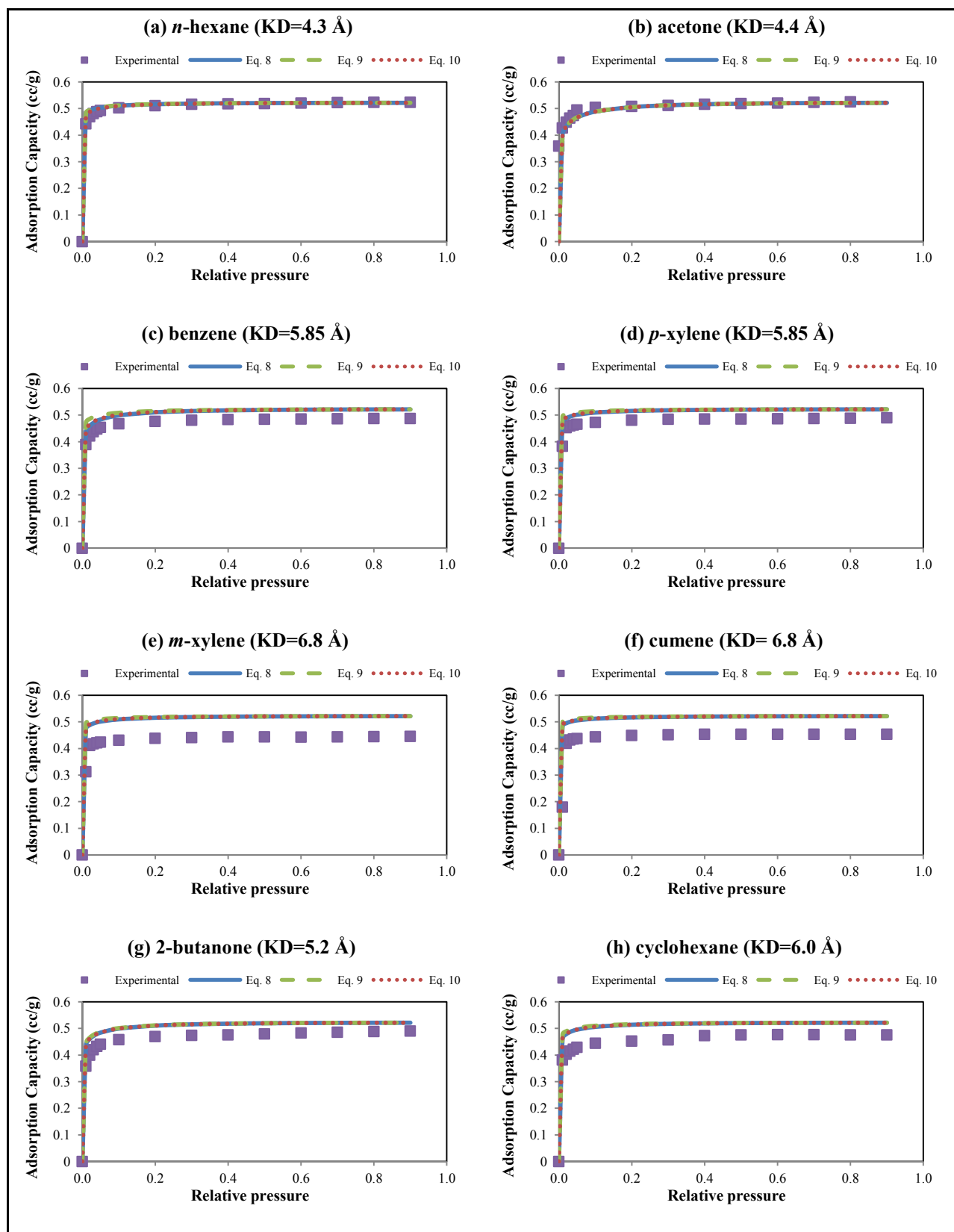


Figure A3. Measured and predicted, gravimetric adsorption isotherms for (a) *n*-hexane, (b) acetone (c) benzene, (d) *p*-xylene, (e) *m*-xylene, (f) cumene, (g) 2-butanone, (h) cyclohexane, and (i) 2-propanol using acetone (KD=4.4 Å) as reference adsorbate.



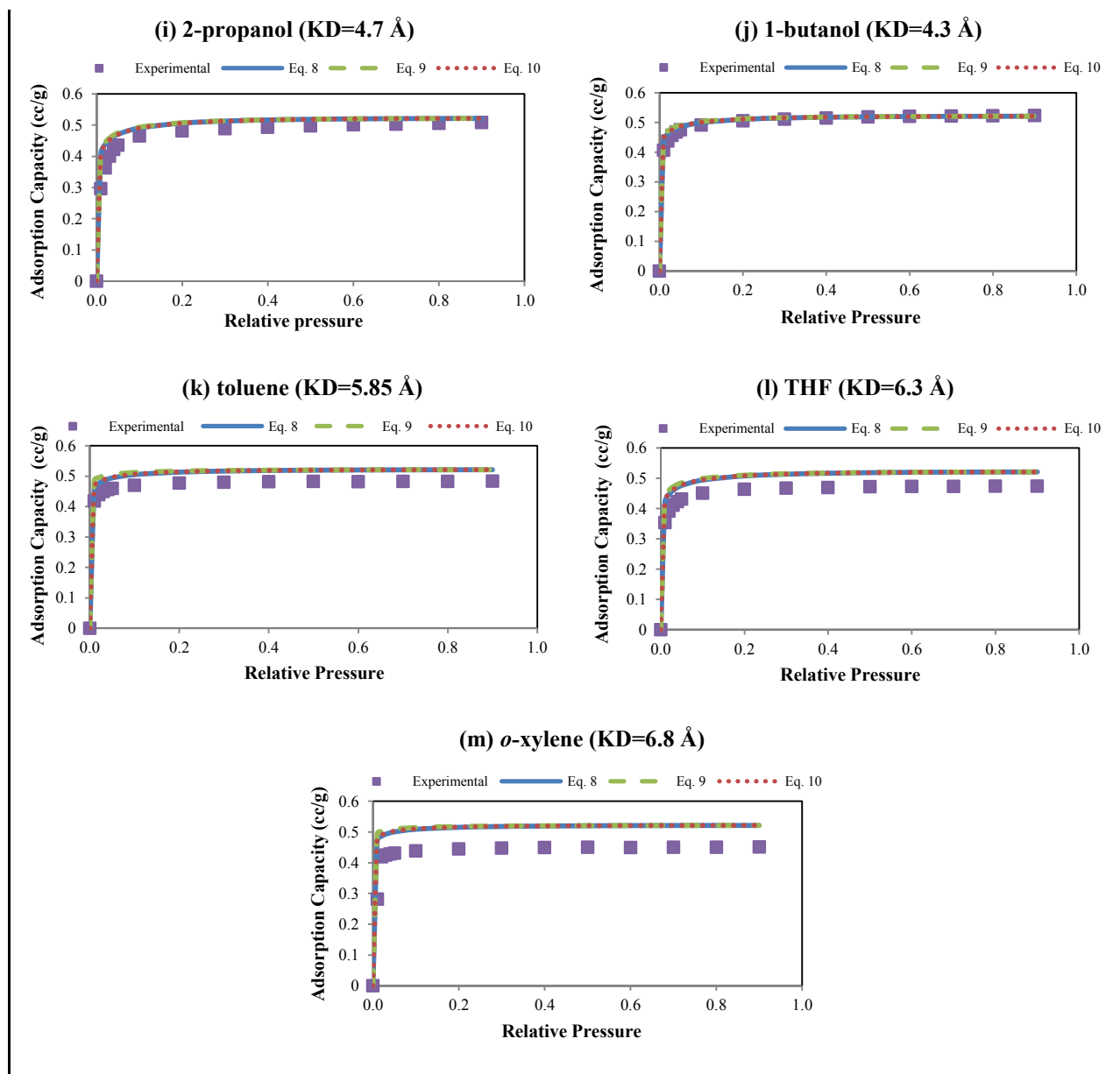
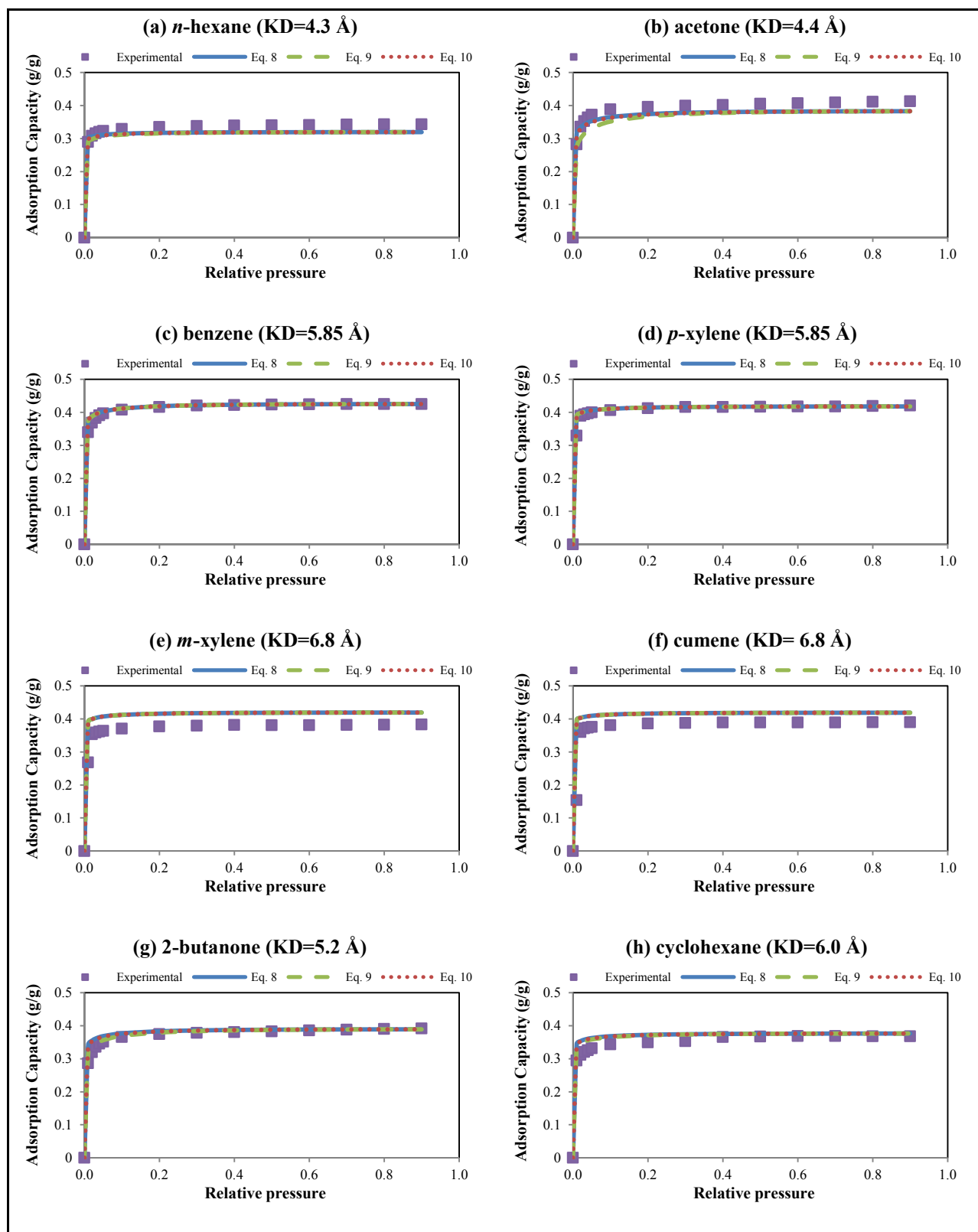


Figure A4. Measured and predicted, volumetric adsorption isotherms for (a) *n*-hexane, (b) acetone (c) benzene, (d) *p*-xylene, (e) *m*-xylene, (f) cumene, (g) 2-butanone, (h) cyclohexane, (i) 2-propanol, (j) 1-butanol, (k) toluene, (l) THF, and (m) *o*-xylene using acetone (KD=4.4 Å) as reference adsorbate.



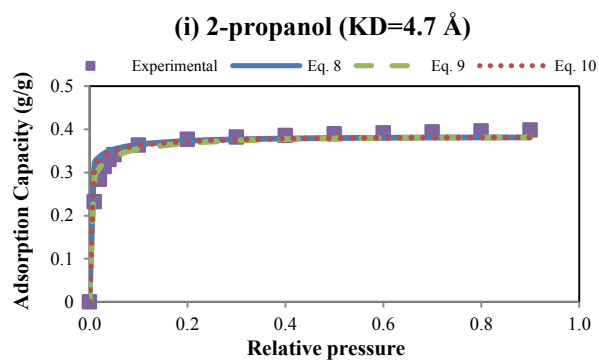
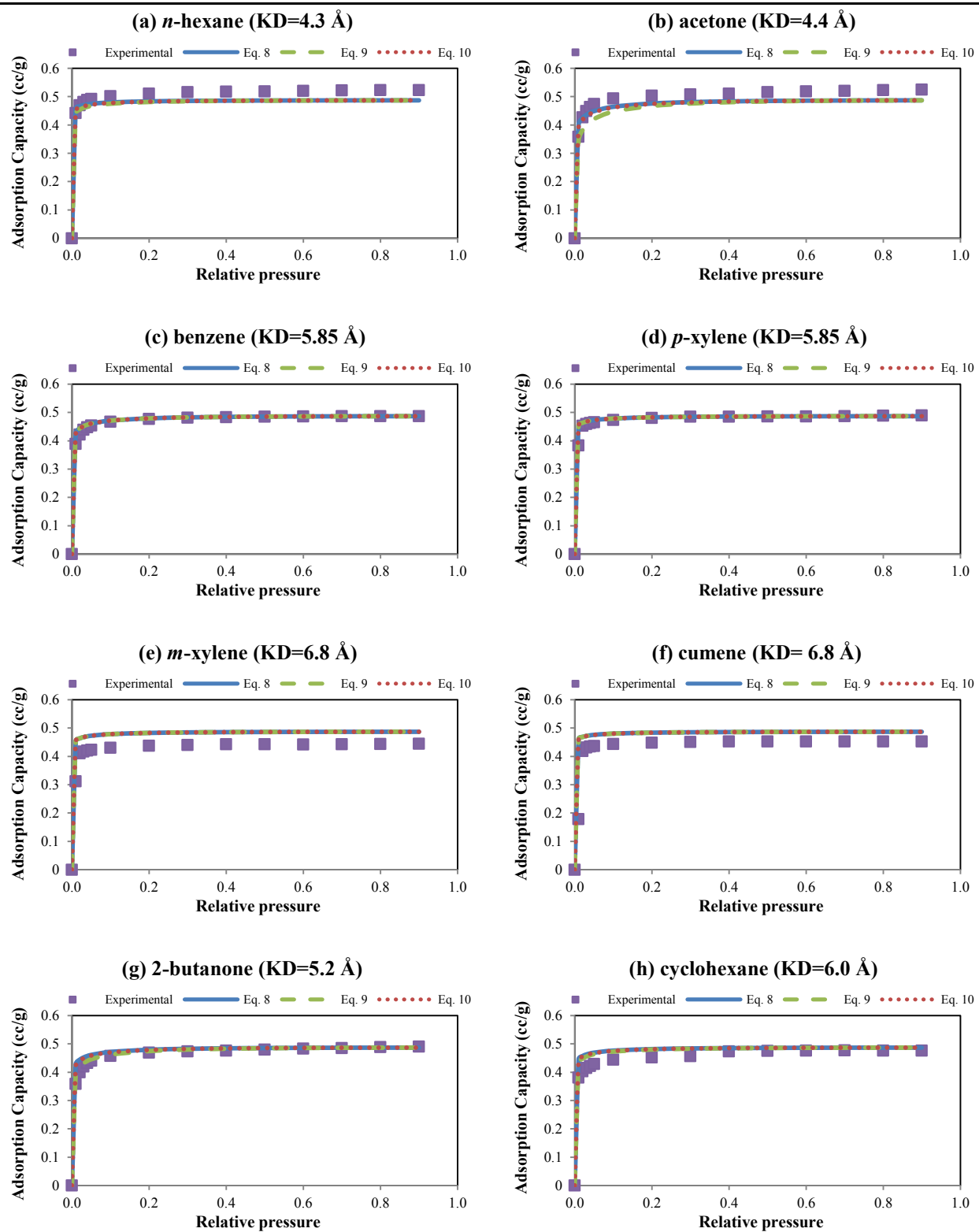


Figure A5. Measured and predicted, gravimetric adsorption isotherms for (a) *n*-hexane, (b) acetone (c) benzene, (d) *p*-xylene, (e) *m*-xylene, (f) cumene, (g) 2-butanone, (h) cyclohexane, and (i) 2-propanol using benzene (KD=5.85 Å) as reference adsorbate.



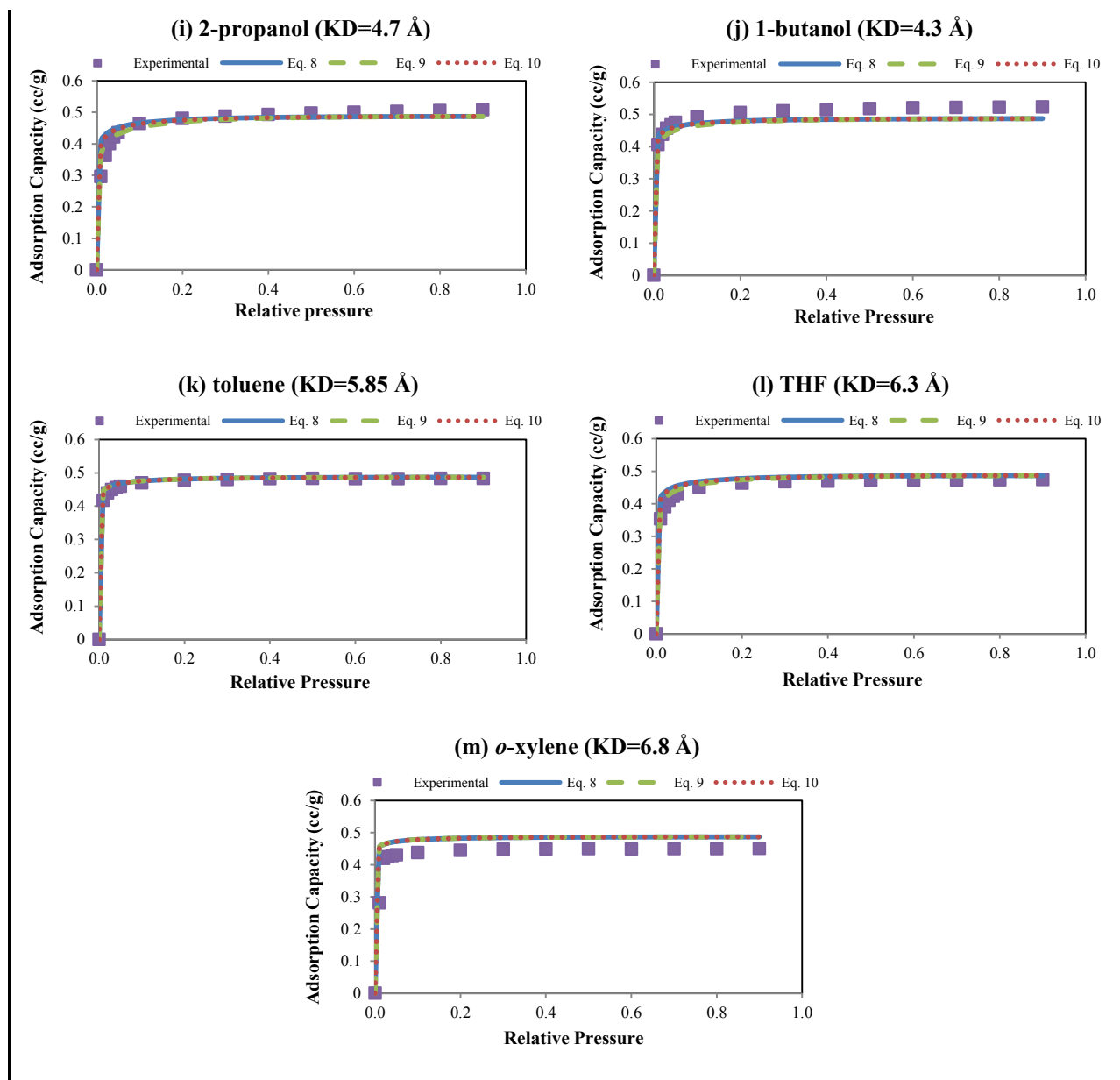
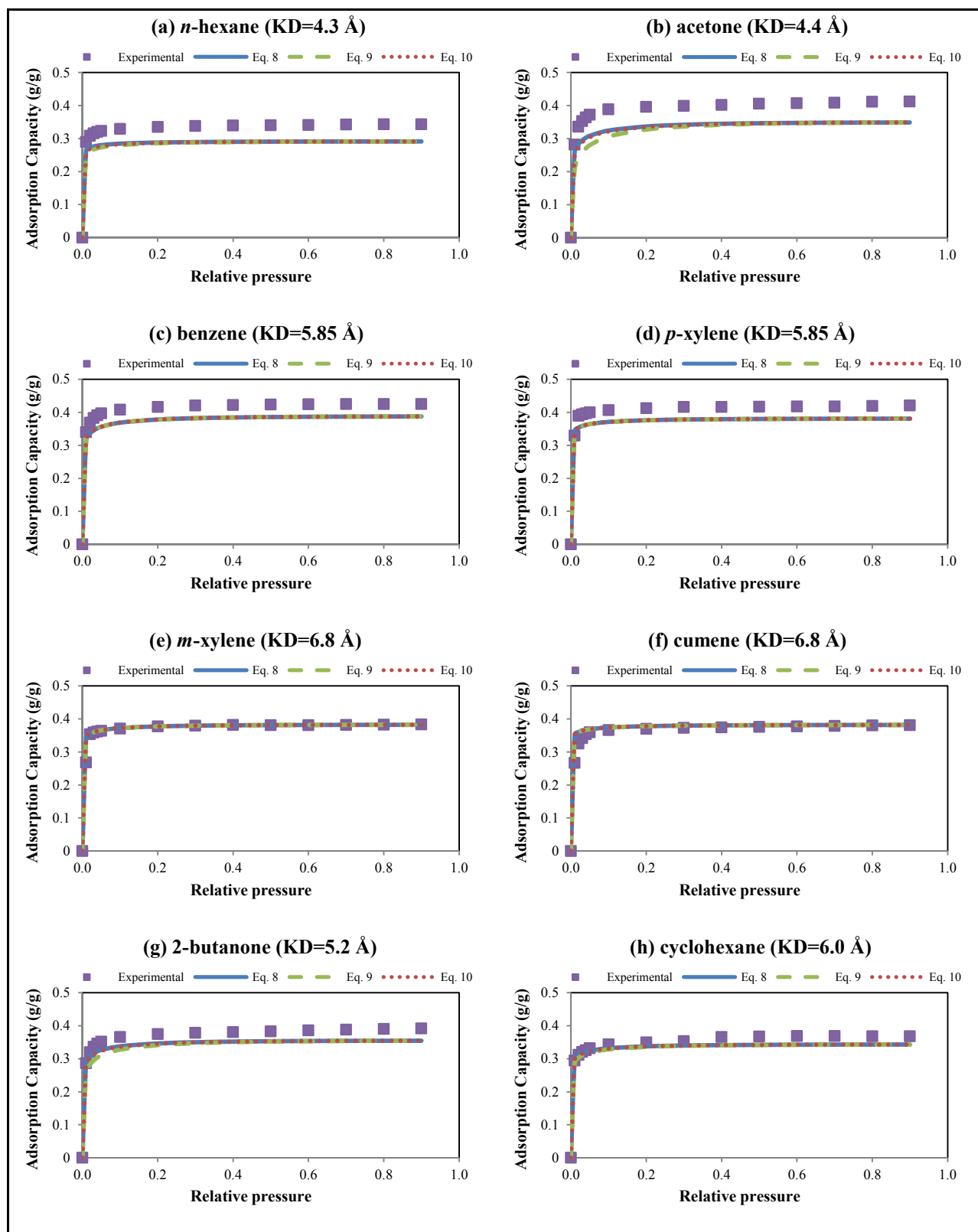


Figure A6. Measured and predicted, volumetric adsorption isotherms for (a) *n*-hexane, (b) acetone (c) benzene, (d) *p*-xylene, (e) *m*-xylene, (f) cumene, (g) 2-butanone, (h) cyclohexane, (i) 2-propanol, (j) 1-butanol, (k) toluene, (l) THF, and (m) *o*-xylene using benzene (KD=5.85 Å) as reference adsorbate.



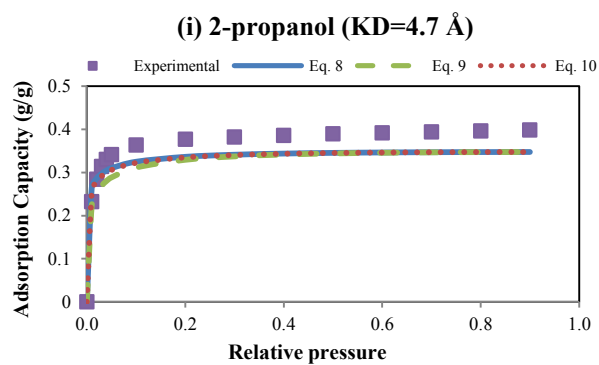
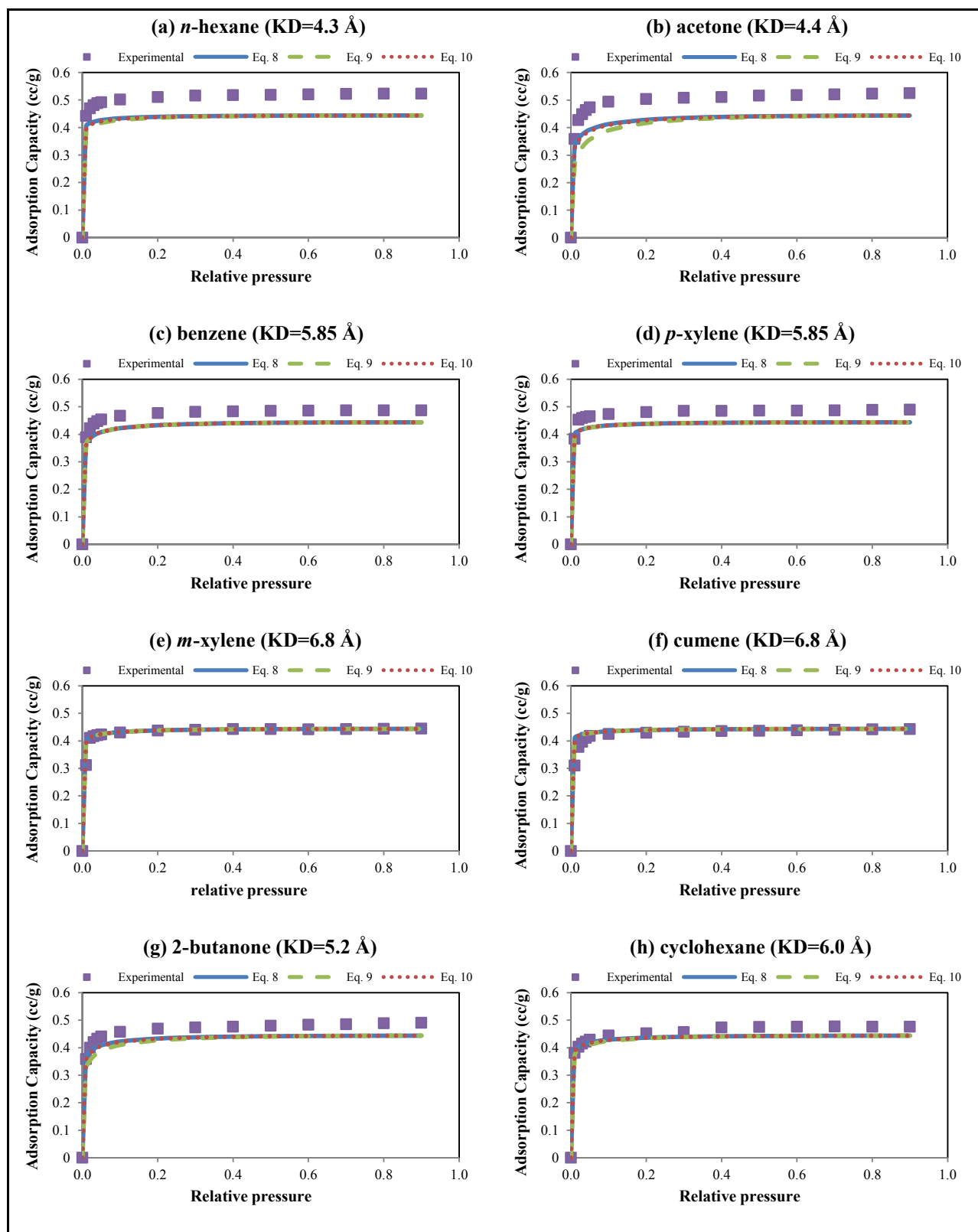


Figure A7. Measured and predicted, gravimetric adsorption isotherms for (a) *n*-hexane, (b) acetone (c) benzene, (d) *p*-xylene, (e) *m*-xylene, (f) cumene, (g) 2-butanone, (h) cyclohexane, and (i) 2-propanol using *m*-xylene (KD=6.8 Å) as reference adsorbate.



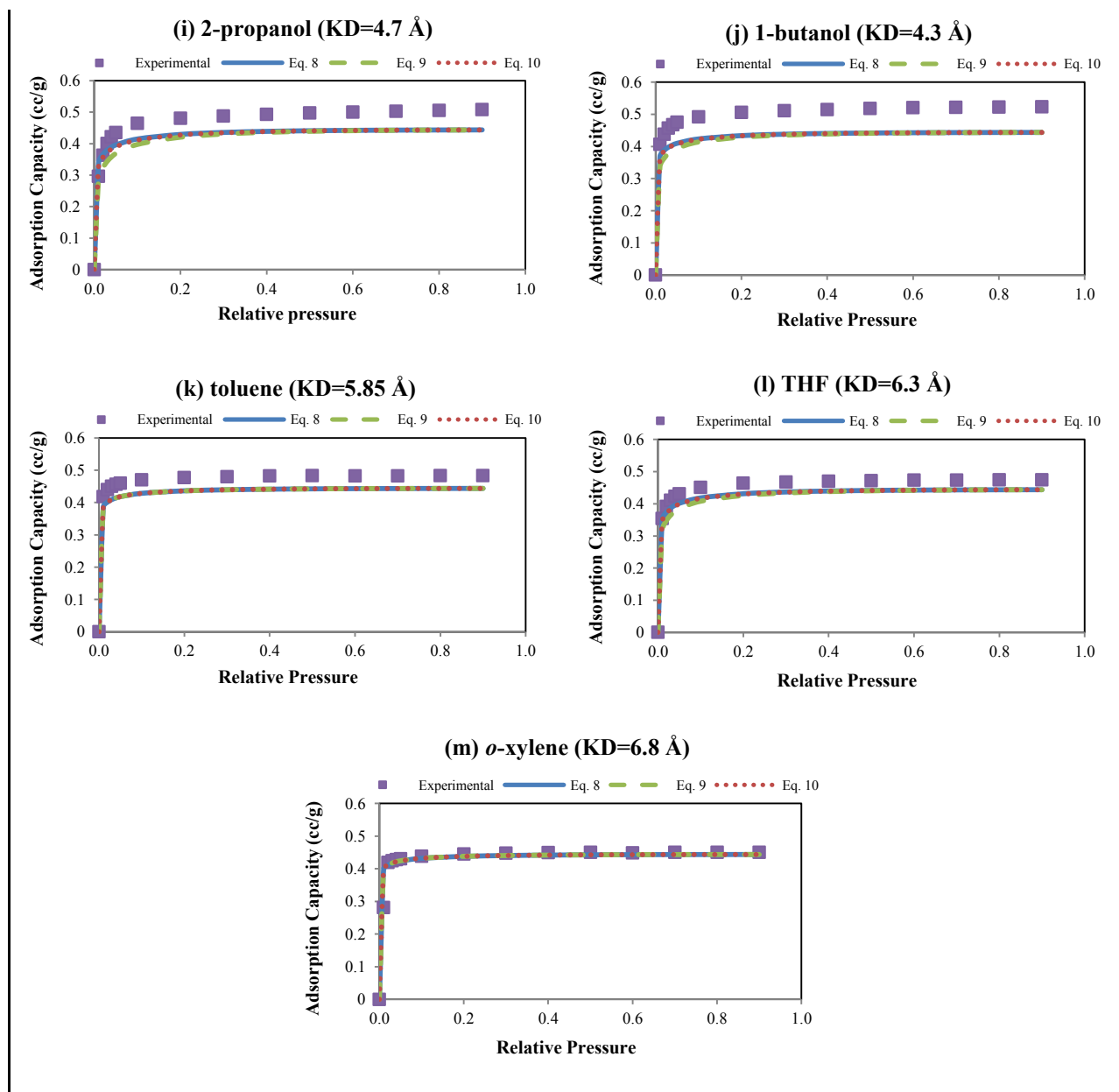


Figure A8. Measured and predicted, volumetric adsorption isotherms for (a) *n*-hexane, (b) acetone (c) benzene, (d) *p*-xylene, (e) *m*-xylene, (f) cumene, (g) 2-butanone, (h) cyclohexane, (i) 2-propanol, (j) 1-butanol, (k) toluene, (l) THF, and (m) *o*-xylene using *m*-xylene (KD=6.8 Å) as reference adsorbate.

APPENDIX B: SUPPLEMENTARY DATA FOR CHAPTERS 4 TO 7



Figure B1. Adsorption/regeneration experimental setup

Table B1. Sample mass balance calculations (virgin BAC weight of 4.1 g)

Cycle	Amount adsorbed (g)	Amount adsorbed (g/g BAC)	Heel (g)	Cumulative heel (g/g BAC)	Cumulative heel (%)
#1	2.403	0.586	0.226	0.226	5.5
#2	2.157	0.526	0.185	0.445	10.9
#3	1.952	0.476	0.148	0.593	14.5
#4	1.788	0.436	0.127	0.720	17.6
#5	1.648	0.402	0.098	0.818	19.9

Table B2. Sample DTG analysis calculations (heating rate of 2 °C/min)

Time (s)	T _{sample} (°C)	T _{reference} (°C)	Mass loss (%)	dm/dt (% loss/s)
0	27.98	25.00	100.0000	0.00000
88	29.79	27.93	99.9706	0.00033
176	32.62	30.87	99.9321	0.00044
264	35.42	33.80	99.8792	0.00060
352	38.19	36.73	99.8428	0.00041
440	40.95	39.67	99.8006	0.00048
528	43.71	42.60	99.7701	0.00035
616	46.49	45.53	99.7339	0.00041
704	49.27	48.47	99.7049	0.00033
792	52.05	51.40	99.6784	0.00030
880	54.84	54.33	99.6524	0.00030
968	57.64	57.27	99.6256	0.00030
1056	60.44	60.20	99.6100	0.00018
1144	63.27	63.13	99.5864	0.00027
1232	66.10	66.07	99.5636	0.00026
1320	68.91	69.00	99.5451	0.00021
1408	71.76	71.93	99.5303	0.00017
1496	74.60	74.87	99.5159	0.00016
1584	77.43	77.80	99.4944	0.00024
1672	80.29	80.73	99.4800	0.00016
1760	83.17	83.67	99.4691	0.00012
1848	86.04	86.60	99.4588	0.00012
1936	88.92	89.53	99.4463	0.00014
2024	91.79	92.47	99.4374	0.00010
2112	94.67	95.40	99.4239	0.00015
2200	97.55	98.33	99.4143	0.00011
2288	100.46	101.27	99.4062	0.00009
2376	103.36	104.20	99.3981	0.00009
2464	106.27	107.13	99.3891	0.00010
2552	109.19	110.07	99.3814	0.00009
2640	112.11	113.00	99.3726	0.00010
2728	115.02	115.93	99.3658	0.00008
2816	117.95	118.87	99.3587	0.00008
2904	120.87	121.80	99.3476	0.00013
2992	123.79	124.73	99.3444	0.00004
3080	126.73	127.67	99.3347	0.00011

3168	129.67	130.60	99.3281	0.00008
3256	132.61	133.53	99.3270	0.00001
3344	135.54	136.47	99.3199	0.00008
3432	138.50	139.40	99.3192	0.00001
3520	141.44	142.33	99.3105	0.00010
3608	144.38	145.27	99.3097	0.00001
3696	147.33	148.20	99.3064	0.00004
3784	150.27	151.13	99.3059	0.00001
3872	153.23	154.07	99.2952	0.00012
3960	156.17	157.00	99.2925	0.00003
4048	159.13	159.93	99.2886	0.00004
4136	162.09	162.87	99.2805	0.00009
4224	165.04	165.80	99.2786	0.00002
4312	168.01	168.73	99.2773	0.00002
4400	170.97	171.67	99.2705	0.00008
4488	173.94	174.60	99.2709	-0.00001
4576	176.90	177.53	99.2711	0.00000
4664	179.86	180.47	99.2626	0.00010
4752	182.84	183.40	99.2641	-0.00002
4840	185.80	186.33	99.2589	0.00006
4928	188.76	189.27	99.2616	-0.00003
5016	191.74	192.20	99.2572	0.00005
5104	194.72	195.13	99.2545	0.00003
5192	197.66	198.07	99.2526	0.00002
5280	200.64	201.00	99.2536	-0.00001
5368	203.60	203.93	99.2467	0.00008
5456	206.57	206.87	99.2486	-0.00002
5544	209.54	209.80	99.2465	0.00002
5632	212.51	212.73	99.2438	0.00003
5720	215.46	215.67	99.2462	-0.00003
5808	218.45	218.60	99.2465	0.00000
5896	221.41	221.53	99.2411	0.00006
5984	224.40	224.47	99.2423	-0.00001
6072	227.37	227.40	99.2465	-0.00005
6160	230.32	230.33	99.2395	0.00008
6248	233.31	233.27	99.2464	-0.00008
6336	236.27	236.20	99.2464	0.00000
6424	239.23	239.13	99.2431	0.00004
6512	242.20	242.07	99.2386	0.00005

6600	245.15	245.00	99.2448	-0.00007
6688	248.14	247.93	99.2465	-0.00002
6776	251.11	250.87	99.2465	0.00000
6864	254.08	253.80	99.2460	0.00001
6952	257.02	256.73	99.2443	0.00002
7040	259.99	259.67	99.2438	0.00001
7128	262.95	262.60	99.2456	-0.00002
7216	265.92	265.53	99.2465	-0.00001
7304	268.89	268.47	99.2465	0.00000
7392	271.84	271.40	99.2465	0.00000
7480	274.81	274.33	99.2440	0.00003
7568	277.76	277.27	99.2442	0.00000
7656	280.71	280.20	99.2422	0.00002
7744	283.68	283.13	99.2406	0.00002
7832	286.65	286.07	99.2386	0.00002
7920	289.60	289.00	99.2388	0.00000
8008	292.55	291.93	99.2424	-0.00004
8096	295.51	294.87	99.2444	-0.00002
8184	298.46	297.80	99.2462	-0.00002
8272	301.42	300.73	99.2465	0.00000
8360	304.37	303.67	99.2465	0.00000
8448	307.32	306.60	99.2464	0.00000
8536	310.27	309.53	99.2446	0.00002
8624	313.23	312.47	99.2463	-0.00002
8712	316.17	315.40	99.2454	0.00001
8800	319.12	318.33	99.2465	-0.00001
8888	322.05	321.27	99.2465	0.00000
8976	325.01	324.20	99.2465	0.00000
9064	327.95	327.13	99.2465	0.00000
9152	330.90	330.07	99.2450	0.00002
9240	333.84	333.00	99.2475	-0.00003
9328	336.78	335.93	99.2488	-0.00001
9416	339.72	338.87	99.2472	0.00002
9504	342.67	341.80	99.2464	0.00001
9592	345.61	344.73	99.2471	-0.00001
9680	348.55	347.67	99.2456	0.00002
9768	351.50	350.60	99.2466	-0.00001
9856	354.43	353.53	99.2465	0.00000
9944	357.37	356.47	99.2465	0.00000

10032	360.30	359.40	99.2474	-0.00001
10120	363.25	362.33	99.2451	0.00003
10208	366.17	365.27	99.2404	0.00005
10296	369.11	368.20	99.2460	-0.00006
10384	372.04	371.13	99.2465	-0.00001
10472	374.97	374.07	99.2464	0.00000
10560	377.91	377.00	99.2388	0.00009
10648	380.84	379.93	99.2393	-0.00001
10736	383.77	382.87	99.2414	-0.00002
10824	386.70	385.80	99.2463	-0.00006
10912	389.64	388.73	99.2436	0.00003
11000	392.55	391.67	99.2388	0.00006
11088	395.48	394.60	99.2465	-0.00009
11176	398.40	397.53	99.2421	0.00005
11264	401.32	400.47	99.2386	0.00004
11352	404.25	403.40	99.2402	-0.00002
11440	407.18	406.33	99.2436	-0.00004
11528	410.09	409.27	99.2393	0.00005
11616	413.00	412.20	99.2347	0.00005
11704	415.92	415.13	99.2391	-0.00005
11792	418.85	418.07	99.2377	0.00002
11880	421.76	421.00	99.2388	-0.00001
11968	424.68	423.93	99.2377	0.00001
12056	427.61	426.87	99.2386	-0.00001
12144	430.53	429.80	99.2315	0.00008
12232	433.43	432.73	99.2394	-0.00009
12320	436.34	435.67	99.2386	0.00001
12408	439.25	438.60	99.2342	0.00005
12496	442.16	441.53	99.2386	-0.00005
12584	445.06	444.47	99.2344	0.00005
12672	447.96	447.40	99.2338	0.00001
12760	450.87	450.33	99.2324	0.00002
12848	453.78	453.27	99.2305	0.00002
12936	456.69	456.20	99.2368	-0.00007
13024	459.59	459.13	99.2313	0.00006
13112	462.50	462.07	99.2322	-0.00001
13200	465.40	465.00	99.2305	0.00002
13288	468.31	467.93	99.2300	0.00001
13376	471.21	470.87	99.2213	0.00010

13464	474.10	473.80	99.2226	-0.00001
13552	477.00	476.73	99.2226	0.00000
13640	479.90	479.67	99.2248	-0.00003
13728	482.79	482.60	99.2218	0.00003
13816	485.69	485.53	99.2238	-0.00002
13904	488.58	488.47	99.2233	0.00001
13992	491.48	491.40	99.2166	0.00008
14080	494.38	494.33	99.2225	-0.00007
14168	497.27	497.27	99.2162	0.00007
14256	500.17	500.20	99.2210	-0.00005
14344	503.08	503.13	99.2161	0.00006
14432	505.97	506.07	99.2159	0.00000
14520	508.88	509.00	99.2159	0.00000
14608	511.77	511.93	99.2138	0.00002
14696	514.65	514.87	99.2145	-0.00001
14784	517.54	517.80	99.2098	0.00005
14872	520.44	520.73	99.2146	-0.00005
14960	523.35	523.67	99.2079	0.00008
15048	526.25	526.60	99.2146	-0.00008
15136	529.14	529.53	99.2096	0.00006
15224	532.04	532.47	99.2095	0.00000
15312	534.94	535.40	99.2067	0.00003
15400	537.83	538.33	99.2067	0.00000
15488	540.73	541.27	99.2070	0.00000
15576	543.62	544.20	99.2067	0.00000
15664	546.52	547.13	99.1986	0.00009
15752	549.41	550.07	99.2022	-0.00004
15840	552.30	553.00	99.1994	0.00003
15928	555.20	555.93	99.1909	0.00010
16016	558.09	558.87	99.1985	-0.00009
16104	560.99	561.80	99.1923	0.00007
16192	563.88	564.73	99.1923	0.00000
16280	566.78	567.67	99.1962	-0.00004
16368	569.67	570.60	99.1894	0.00008
16456	572.58	573.53	99.1875	0.00002
16544	575.47	576.47	99.1819	0.00006
16632	578.37	579.40	99.1833	-0.00002
16720	581.25	582.33	99.1826	0.00001
16808	584.16	585.27	99.1745	0.00009

16896	587.05	588.20	99.1747	0.00000
16984	589.93	591.13	99.1747	0.00000
17072	592.83	594.07	99.1727	0.00002
17160	595.72	597.00	99.1701	0.00003
17248	598.60	599.93	99.1677	0.00003
17336	601.51	602.87	99.1700	-0.00003
17424	604.40	605.80	99.1667	0.00004
17512	607.29	608.73	99.1589	0.00009
17600	610.17	611.67	99.1533	0.00006
17688	613.07	614.60	99.1507	0.00003
17776	615.96	617.53	99.1507	0.00000
17864	618.84	620.47	99.1439	0.00008
17952	621.72	623.40	99.1443	-0.00001
18040	624.62	626.33	99.1427	0.00002
18128	627.52	629.27	99.1370	0.00007
18216	630.40	632.20	99.1366	0.00000
18304	633.29	635.13	99.1298	0.00008
18392	636.17	638.07	99.1259	0.00004
18480	639.04	641.00	99.1259	0.00000
18568	641.94	643.93	99.1259	0.00000
18656	644.82	646.87	99.1179	0.00009
18744	647.71	649.80	99.1179	0.00000
18832	650.58	652.73	99.1101	0.00009
18920	653.47	655.67	99.1099	0.00000
19008	656.36	658.60	99.0956	0.00016
19096	659.23	661.53	99.0948	0.00001
19184	662.12	664.47	99.0869	0.00009
19272	665.02	667.40	99.0789	0.00009
19360	667.90	670.33	99.0789	0.00000
19448	670.78	673.27	99.0708	0.00009
19536	673.67	676.20	99.0708	0.00000
19624	676.56	679.13	99.0688	0.00002
19712	679.43	682.07	99.0628	0.00007
19800	682.31	685.00	99.0556	0.00008
19888	685.19	687.93	99.0469	0.00010
19976	688.08	690.87	99.0435	0.00004
20064	690.96	693.80	99.0312	0.00014
20152	693.83	696.73	99.0293	0.00002
20240	696.71	699.67	99.0230	0.00007

20328	699.59	702.60	99.0140	0.00010
20416	702.47	705.53	99.0070	0.00008
20504	705.35	708.47	99.0070	0.00000
20592	708.23	711.40	98.9996	0.00008
20680	711.10	714.33	98.9991	0.00001
20768	713.98	717.27	98.9911	0.00009
20856	716.86	720.20	98.9829	0.00009
20944	719.72	723.13	98.9744	0.00010
21032	722.61	726.07	98.9663	0.00009
21120	725.50	729.00	98.9591	0.00008
21208	728.38	731.93	98.9510	0.00009
21296	731.26	734.87	98.9417	0.00011
21384	734.13	737.80	98.9350	0.00008
21472	737.01	740.73	98.9251	0.00011
21560	739.90	743.67	98.9191	0.00007
21648	742.78	746.60	98.9082	0.00012
21736	745.65	749.53	98.8952	0.00015
21824	748.54	752.47	98.8821	0.00015
21912	751.41	755.40	98.8705	0.00013
22000	754.29	758.33	98.8576	0.00015
22088	757.17	761.27	98.8495	0.00009
22176	760.04	764.20	98.8436	0.00007
22264	762.92	767.13	98.8268	0.00019
22352	765.77	770.07	98.8213	0.00006
22440	768.65	773.00	98.8033	0.00020
22528	771.54	775.93	98.7914	0.00014
22616	774.43	778.87	98.7835	0.00009
22704	777.33	781.80	98.7674	0.00018
22792	780.22	784.73	98.7515	0.00018
22880	783.10	787.67	98.7361	0.00017
22968	785.99	790.60	98.7163	0.00022
23056	788.86	793.53	98.7034	0.00015
23144	791.74	796.47	98.6720	0.00036
23232	794.60	799.40	98.6564	0.00018
23320	797.46	802.33	98.6391	0.00020
23408	800.34	805.27	98.6117	0.00031
23496	803.21	808.20	98.5895	0.00025
23584	806.10	811.13	98.5596	0.00034
23672	808.97	814.07	98.5290	0.00035

23760	811.86	817.00	98.4961	0.00037
23848	814.75	819.93	98.4716	0.00028
23936	817.63	822.87	98.4401	0.00036
24024	820.52	825.80	98.4082	0.00036
24112	823.41	828.73	98.3734	0.00040
24200	826.30	831.67	98.3363	0.00042
24288	829.16	834.60	98.2999	0.00041
24376	832.05	837.53	98.2567	0.00049
24464	834.93	840.47	98.2166	0.00046
24552	837.81	843.40	98.1707	0.00052
24640	840.70	846.33	98.1219	0.00055
24728	843.61	849.27	98.0808	0.00047
24816	846.50	852.20	98.0338	0.00053
24904	849.39	855.13	97.9827	0.00058
24992	852.28	858.07	97.9292	0.00061
25080	855.17	861.00	97.8773	0.00059
25168	858.08	863.93	97.8226	0.00062
25256	860.99	866.87	97.7623	0.00069
25344	863.87	869.80	97.7004	0.00070
25432	866.78	872.73	97.6413	0.00067
25520	869.68	875.67	97.5762	0.00074
25608	872.56	878.60	97.5037	0.00082
25696	875.47	881.53	97.4403	0.00072
25784	878.37	884.47	97.3703	0.00080
25872	881.27	887.40	97.2980	0.00082
25960	884.18	890.33	97.2200	0.00089
26048	887.08	893.27	97.1442	0.00086
26136	889.99	896.20	97.0654	0.00090
26224	892.89	899.13	96.9848	0.00092

Table B3. Sample PSD analysis (QSDFT)

Half pore width (Å)	Pore width (Å)	Cumulative Pore Volume (cm³/g)	Cumulative Surface Area (m²/g)	dV(r) (cm³/Å/g)	dS(r) (m²/Å/g)
2.62	5.24	0.10351	429.99	0.19107	729.27
2.835	5.67	0.13483	540.46	0.14566	513.8
3.07	6.14	0.15406	603.12	0.08186	266.64
3.33	6.66	0.17108	654.23	0.06545	196.56
3.615	7.23	0.19842	729.85	0.09592	265.33
3.925	7.85	0.23654	826.96	0.12296	313.27
4.26	8.52	0.2704	906.47	0.1011	237.33
4.63	9.26	0.29445	958.4	0.06499	140.37
5.035	10.07	0.31965	1008.5	0.06222	123.58
5.48	10.96	0.356	1074.8	0.08167	149.03
5.965	11.93	0.39656	1142.8	0.08364	140.21
6.495	12.99	0.42929	1193.2	0.06175	95.073
7.08	14.16	0.46183	1239.1	0.05563	78.579
7.715	15.43	0.49109	1277.1	0.04608	59.729
8.41	16.82	0.5094	1298.8	0.02634	31.324
9.17	18.34	0.52168	1312.2	0.01615	17.615
10	20	0.52767	1318.2	0.00722	7.2157
10.915	21.83	0.53086	1321.1	0.00349	3.196
11.91	23.82	0.53356	1323.4	0.00271	2.275
13	26	0.53599	1325.3	0.00223	1.7186
14.19	28.38	0.53831	1326.9	0.00195	1.3742
15.495	30.99	0.54051	1328.3	0.00168	1.0874
16.925	33.85	0.54272	1329.6	0.00155	0.91382
18.49	36.98	0.54465	1330.7	0.00123	0.66503
20.195	40.39	0.54641	1331.5	0.00103	0.51205
22.065	44.13	0.54801	1332.3	0.00086	0.38847
24.115	48.23	0.54935	1332.8	0.00065	0.26975
26.35	52.7	0.55064	1333.3	0.00058	0.21962
28.8	57.6	0.55183	1333.7	0.00049	0.1691
31.48	62.96	0.5529	1334.1	0.0004	0.12594
34.415	68.83	0.55466	1334.6	0.0006	0.17456
37.62	75.24	0.55609	1335	0.00045	0.1191
41.135	82.27	0.55707	1335.2	0.00028	0.06772
44.975	89.95	0.55782	1335.4	0.0002	0.04346
49.175	98.35	0.55853	1335.5	0.00017	0.03424

53.775	107.55	0.55931	1335.7	0.00017	0.03147
58.805	117.61	0.56025	1335.8	0.00019	0.03179
64.305	128.61	0.56103	1335.9	0.00014	0.02204
70.33	140.66	0.56175	1336	0.00012	0.01698
76.915	153.83	0.56275	1336.2	0.00015	0.01976
84.125	168.25	0.56325	1336.2	6.9E-05	0.00821
92.01	184.02	0.56399	1336.3	9.4E-05	0.01026
100.64	201.28	0.56532	1336.4	0.00015	0.01532
110.08	220.16	0.56601	1336.5	7.3E-05	0.00663
120.41	240.82	0.56686	1336.6	8.2E-05	0.00683
131.715	263.43	0.5679	1336.7	9.2E-05	0.00695
144.08	288.16	0.56856	1336.7	5.4E-05	0.00373
157.61	315.22	0.56935	1336.7	5.8E-05	0.00368
172.41	344.82	0.57044	1336.8	7.4E-05	0.0043